Imperial College London

ATR-FTIR Spectroscopic Imaging to Study Drug Release and Tablet Dissolution

Andrew Vincent Ewing

January 2016

Supervised by Professor Sergei G. Kazarian

Department of Chemical Engineering
Imperial College London
South Kensington Campus
London, SW7 2AZ

Submitted to Imperial College London in part fulfilment of the requirements for the degree of Doctor of Philosophy in Chemical Engineering and the Diploma of Imperial College London

I would like to dedicate this thesis to my Family to acknowledge all of their support throughout my education.

Declaration

The work and results presented in this thesis was carried out in the Department of Chemical Engineering at Imperial College London between October 2012 and December 2015. Except where acknowledged, the material is original work by the author and no part of this thesis has been submitted for a degree at any other academic institution.

Copyright

The copyright of this thesis rests with the author and is made available under a Creative Commons Attribution Non-Commercial No Derivatives licence. Researchers are free to copy, distribute or transmit the thesis on the condition that they attribute it, that they do not use it for commercial purposes and that they do not alter, transform or build upon it. For any reuse or redistribution, researchers must make clear to others the licence terms of this work.

Abstract

The active pharmaceutical ingredient (API) and excipients are vital for determining the behaviour of drug release from tablet compacts. Macro attenuated total reflection-Fourier transform infrared (ATR-FTIR) spectroscopic imaging can be employed for *in situ* studies of dissolving tablets. This thesis describes new developments that applied macro ATR-FTIR spectroscopic imaging to investigate the stability and dissolution of amorphous APIs, the effect of carriers for improving drug release, the stability of ionised drug candidates and the behaviour of multiple formulations in microfluidic devices.

Solid dispersions containing an amorphous drug formulated with different polymers were investigated using ATR-FTIR spectroscopy and spectroscopic imaging. Crystallisation of the amorphous drug was detected during stability and tablet dissolution experiments. The implications of this form change inhibited dissolution of the drug into solution.

ATR-FTIR spectroscopic imaging was also used in combination with ultraviolet detection to study the release of a drug formulated with selected carriers. Hydrogen bonded interactions between the drug and carrier were characterised and resulted in an increased rate of drug release. When these interactions were not present in the tablet, a slower rate of dissolution was observed.

Disproportionation of an ionised drug was investigated by ATR-FTIR spectroscopic imaging and Raman mapping. During dissolution experiments in acidic solution, chemical changes of the ionised API were detected in real time that resulted in the formation of the less soluble form of the drug.

Exciting results were obtained by simultaneously screening the behaviour of multiple formulations in microfluidic channels using macro ATR-FTIR spectroscopic imaging. Moreover, the precipitation of a dissolved drug that crystallised upon contact with an acidic solution was investigated.

Overall, the research in this thesis has demonstrated that macro ATR-FTIR spectroscopic imaging can address the challenges of studying a range of innovative delivery systems that can ultimately lead to the development of more efficient pharmaceutical formulations.

Acknowledgements

I would like to thank my supervisor Professor Sergei Kazarian for his guidance and support throughout my PhD project. His knowledge and enthusiasm for advanced vibrational spectroscopy have inspired me to explore new and exciting areas of research. All that I have achieved during this project would not have been possible without his encouragement and advice. I am grateful for the opportunities to present my research at conferences and other meetings, and I will always remember the enjoyment I felt when our papers were accepted. His dedication to our group has, and will continue, to motivate me to strive for a career in research in the future.

I owe much gratitude to my industrial sponsor Bristol-Myers Squibb for providing a CASE award for this project. Particularly, to my industrial supervisor Dr Graham Clarke and his colleague Dr Patrick Wray who have provided me with valuable insight throughout my project and have always welcomed me during visits to Bristol-Myers Squibb. I would also like to thank the EPSRC for funding my DTA.

I have really enjoyed the experience at Imperial College London which is largely due to meeting new friends and colleagues (past and present) in our research group and the department. I would like to thank Alessandra Vichi, Ben Turner, Stefanie Glassford, Dr Anton Gabrienko, Dr Jennifer Dougan, Dr Kirsty Gibson and Dr Maxime Boulet-Audet for all of the scientific, and non-scientific, discussions. A special thanks goes to Dr James Kimber who has been in our group for the duration of my project, we have shared many good times and helpful research ideas.

I have been fortunate enough to have had the opportunity to work with final year project students, MSc students and visitors in the lab. I am grateful for their hard work and ideas that were helpful for the progress of my own project.

Thank you to Rebecca Groves, who has always been there to talk to about my studies. I have really enjoyed our adventures together that have benefitted my work by recharging me so I am ready to continue when we return. I would like to thank my best friend and brother, James, for always being there for me and I wish you all the best in your future.

Finally, and most importantly, I would like to acknowledge my parents for all of their advice throughout my entire education. This would not have been possible without you always being there to support and encourage me, and for that I cannot thank you enough.

Table of Contents

Declaration **3**

Copyright **4**

Abstract **5**

Acknowledgements **6**

Table of Contents **7**

List of Figures **11**

List of Tables **17**

Nomenclature **18**

List of Abbreviations **18**

List of symbols **20**

Publications and Conferences **22**

1 Introduction **24**

1.1 Aims and objectives **25**

2 Literature Review **27**

2.1 Overview of pharmaceutical formulations **27**

2.1.1 Preparation of pharmaceutical formulations 28

2.1.2 Compaction into solid tablet dosage forms 30

2.1.3 Properties of active pharmaceutical ingredients 31

2.2 Methods of improving the release and bioavailability of drugs **32**

2.3 Controlling drug release **34**

2.3.1 Drug release mechanisms 36

2.4 Monitoring drug release from tablet compacts **38**

2.4.1 Assessment of pharmaceutical formulations using imaging approaches 39

2.5 Fourier transform infrared spectroscopy: principles and applications **40**

2.5.1 Fundamental background 42

2.5.2 Transmission mode 45

2.5.3 Attenuated total reflection mode 46

2.5.4 External reflection mode 48

2.5.5 General principles of quantitative analysis 49

2.5.6 FTIR spectroscopy to study pharmaceutical systems 50
2.6 Fourier transform infrared spectroscopic imaging 51
2.6.1 Macro ATR-FTIR spectroscopic imaging 52
2.6.2 Micro FTIR spectroscopic imaging 55
2.6.3 General applications of ATR-FTIR spectroscopic imaging 56
2.7 Applications of macro FTIR spectroscopic imaging of pharmaceutical systems 57
2.7.1 Transmission-FTIR spectroscopic imaging 57
2.7.2 ATR-FTIR spectroscopic imaging of drug release 58
2.7.3 Recent development of ATR-FTIR spectroscopic imaging for samples under flow 60
2.7.4 Alternative spectroscopic imaging techniques for pharmaceutical analysis 62
2.8 Summary 65

3 Experimental Methods 67
3.1 ATR-FTIR spectroscopy 67
3.2 Macro FTIR spectroscopic imaging 67
3.2.1 ATR imaging accessories 68
3.3 Tablet compaction and flow cells 69
3.4 UV Detection 71
3.5 Microdrop system 72

4 Stability of Indomethacin with Relevance to the Release from Amorphous Solid Dispersions Studied with ATR-FTIR Spectroscopic Imaging 74
4.1 Motivation and scientific background 74
4.2 Materials and methodology 76
4.2.1 Sample preparation 76
4.2.2 Macro ATR-FTIR spectroscopic imaging 77
4.2.3 Dissolution methodology 78
4.3 Structural forms of indomethacin 78
4.4 Stability of amorphous solid dispersions 81
4.4.1 Conventional ATR-FTIR spectroscopy 81
4.4.2 *In situ* Macro ATR-FTIR spectroscopic imaging 83
4.5 Macro ATR-FTIR spectroscopic imaging of drug release 84
4.6 Conclusions 90

5 Comparison of Pharmaceutical Formulations: ATR-FTIR spectroscopic Imaging to Study Drug-Carrier Interactions 91
5.1 Background 91

5.2 Materials and methods 95
5.2.1 Preparation of formulations 95
5.2.2 ATR-FTIR spectroscopy and spectroscopic imaging approach 96
5.2.3 Experimental setup for drug release investigations 97
5.2.4 Calibration of UV detector to quantify release of indomethacin 98
5.3 Macro ATR-FTIR spectroscopic imaging of indomethacin/nicotinamide formulations 99
5.3.1 Analysis of ATR-FTIR spectroscopy and spectroscopic imaging results 101
5.3.2 Monitoring the amount of indomethacin dissolved using UV detection 104
5.3.3 Combined analysis of macro ATR-FTIR spectroscopic imaging with parallel UV detection 106
5.4 Macro ATR-FTIR spectroscopic imaging of indomethacin with other pharmaceutical excipients 110
5.5 Conclusions 114

6 Evaluating Drug Delivery with Salt Formation: Drug Disproportionation Studied *In Situ* by ATR-FTIR Imaging and Raman Mapping 116
6.1 Introduction 116
6.2 Materials and methods 120
6.2.1 Materials 120
6.2.2 Macro ATR-FTIR spectroscopic imaging approach 121
6.2.3 Raman mapping and video imaging approach 122
6.2.4 Dissolution methodologies 123
6.3 Results and discussion 124
6.3.1 Detecting disproportionation of the ionised form of the drug 124
6.3.2 Monitoring the stability and behaviour of tablets containing an ionised drug dissolution in neutral solution 127
6.3.3 Assessing the stability and behaviour of tablets containing an ionised drug during dissolution in acidic solution 130
6.4 Conclusions 135

7 ATR-FTIR Spectroscopic Imaging of Pharmaceutical Systems in Microfluidic Devices 137
7.1 Motivation 137
7.1.1 Main developments of this work 140

7.2 Development of microfluidic devices for use with macro ATR-FTIR spectroscopic imaging 140
7.2.1 Initial methodology for the preparation of microfluidic devices 140
7.2.2 Microfluidic devices prepared with 3D printed moulds 144
7.2.3 Functionalising PDMS devices for more efficient flow 146
7.3 Simultaneous screening of the dissolution of micro-formulations 147
7.3.1 Materials 147
7.3.2 ATR-FTIR spectroscopy and spectroscopic imaging 148
7.3.3 Preparation of the pharmaceutical micro-formulations 148
7.3.4 High-throughput screening of micro-formulations under the same flowing conditions 149
7.3.5 Simultaneous screening of multiple formulations under flowing conditions in different pH environments 152
7.4 Crystallisation of a dissolved drug in changing pH environments 154
7.4.1 Preparation of sodium ibuprofen solutions 154
7.4.2 ATR-FTIR spectroscopy and spectroscopic imaging 154
7.4.3 Results of dissolved drug in changing pH conditions 155
7.5 Conclusions 159

8 Conclusions and Future Work 160
8.1 Overall summary 160
8.1.1 Drug release from tablet compacts monitored by macro ATR-FTIR spectroscopic imaging 160
8.1.2 Development of microfluidic devices for screening dissolution of pharmaceutical formulations with macro ATR-FTIR spectroscopic imaging 162
8.2 Recommendations for future work 164

References 166

List of Figures

Figure 1.1 – The research and development process of a new drug in the pharmaceutical industry. Adapted from (IFPMA, 2015). 24

Figure 2.1 – Biopharmaceutics classification system including some example essential drug candidates as listed by the World Health Organisation. 31

Figure 2.2 – An example of drug release profiles typically recorded from immediate (red line), burst (green plot) and sustained (blue plot) release delivery systems. 35

Figure 2.3 – Schematic diagram of different stages of polymeric disentanglement during dissolution in aqueous solution. Adapted from Siepmann et al. (1999). 37

Figure 2.4 – Schematic representation of United States Pharmacopeia (USP) tests. (A) Shows an example of the basket method known as USP I and (B) the paddle method known as USP II. 38

Figure 2.5 – (A) Schematic diagram of the Michelson interferometer. (B) and (C) show an example of a measured interferogram and single beam spectrum recorded using an FTIR spectrometer, respectively. 41

Figure 2.6 – Diagram of the electromagnetic spectrum. 43

Figure 2.7 – Schematic diagram of the four different molecular vibrations of carbon dioxide. The "+" and "-" represent the atoms moving forwards and backwards perpendicular to the plane of the diagram of the out-of-plane bending mode. 45

Figure 2.8 – Schematic representation of transmission mode experimental setup for FTIR measurements. 45

Figure 2.9 – Schematic diagram showing the principle of attenuated total reflection mode 47

Figure 2.10 – Schematic diagram of the external reflection measurement setup. 49

Figure 2.11 – Schematic diagram of an ATR-FTIR spectroscopic imaging setup. 52

Figure 2.12 – Schematic diagram of the Imaging Golden Gate ATR-FTIR accessory showing the direction of the IR beam that is focused onto the ATR crystal by mirrors and lenses. 53

Figure 2.13 – Schematic diagram of the metal compaction and dissolution cell that can be attached to an Imaging Golden Gate ATR accessory for *in situ* measurements. 60

Figure 3.1 – Photograph of an FTIR spectroscopic imaging system that includes: (A) Bruker Equinox 55 FTIR spectrometer, (B) ATR accessory and (C) IMAC macrochamber. 68

Figure 3.2 – Photograph of (A) Imaging Golden Gate accessory positioned in the IMAC macrochamber of the FTIR spectroscopic imaging system and (B) VeeMax II variable angle accessory. 69

Figure 3.3 – Photograph of (A) dissembled metal flow cell showing the individual component for *in situ* compaction and (B) metal flow cell in the closed position after compaction of the tablet. 70

Figure 3.4 – Schematic diagrams of the experimental setup using the Perspex flow cell for tablet dissolution experiments. (A) Shows the position of the tablet offset from the centre of the diamond crystal on the Imaging Golden Gate accessory. (B) Shows a

cross-sectional view of the tablet dissolution experiment measured using the VeeMax accessory where the tablet is positioned in the centre of the measuring surface on the ZnSe crystal. 71

Figure 3.5 – Photographs of the microdrop system. (A) The complete arrangement of the microdrop system including the dispensing stage, computer and heating system. (B) The dispensing unit with the sample vessel chamber and nozzle highlighted. (C) The dispensing stage upon which the substrate was placed before deposition of the samples. 73

Figure 4.1 – Chemical structures of (A) indomethacin, (B) polyethylene glycol (PEG) and (C) hydroxypropyl methylcellulose (HPMC). 76

Figure 4.2 – ATR-FTIR spectra recorded for the pure γ, α and amorphous forms of indomethacin. The spectral region between 1800–1500 cm^{-1} is displayed highlighting the C=O vibrations of the indomethacin forms. 79

Figure 4.3 – ATR-FTIR spectra measured during the stability studies of the indomethacin/PEG (A) and the indomethacin/HPMC (B) formulations over a 96 hr period. The blue and red labels in (A) highlight the appearance of the peaks of the spectral bands that indicate the presence of α and γ indomethacin, respectively. 82

Figure 4.4 – ATR-FTIR spectroscopic images showing the distribution of PEG (top row) and indomethacin (bottom row) during the *in situ* stability experiment. The accompanying extracted spectra displayed confirm a change in structural form, from amorphous to γ form, via the α form, during the experiment. The dimension of each spectroscopic image is ~0.64 × 0.53 mm^2. 83

Figure 4.5 – ATR-FTIR spectroscopic images revealing the distribution of indomethacin (top row), PEG (middle row) and phosphate buffer (bottom row) during the *in situ* drug release experiment of the indomethacin/PEG ASD. The dimension of each spectroscopic image is ~0.64 × 0.53 mm^2. 86

Figure 4.6 – ATR-FTIR spectroscopic images that reveal the spatial distribution of indomethacin (top row), HPMC (middle row) and phosphate buffer (bottom row) during the *in situ* drug release experiment of the indomethacin/HPMC ASD. The dimension of each spectroscopic image is ~0.64 × 0.53 mm^2. 86

Figure 4.7 – ATR-FTIR spectroscopic images of indomethacin/PEG ASD tablet before exposure to the buffer solution (Dry) and during the experiment (60 min). Extracted spectra from the points labelled (A, B and C) on the spectroscopic images show evidence of the crystallisation of amorphous indomethacin during the experiment. The dimension of each spectroscopic image is ~0.64 × 0.53 mm^2. 88

Figure 5.1 – Schematic diagram of the *in situ* experimental setup. The tablet sample is positioned between a flow cell and ZnSe crystal, and the flowing dissolution medium (in the direction of the arrows) was cycled around the closed experimental system. The experiment is monitored using macro ATR-FTIR spectroscopic imaging simultaneously with parallel UV detection. 94

Figure 5.2 – Chemical structures of the pharmaceutical materials studied in this work. (A) Indomethacin, (B) nicotinamide, (C) mannitol and (D) urea. 95

Figure 5.3 – Calibration plot showing the concentration of dissolved indomethacin vs. absorbance at 320 nm, recorded for indomethacin dissolved in ethanol. The

calibration plot was used to quantify the release of indomethacin from the different compacted tablets. 98

Figure 5.4 – Potential H-bonded interactions between certain functional groups in indomethacin and nicotinamide. The parent molecules of each functional group in this scheme are labelled as Indo and Nico, respectively. 100

Figure 5.5 – ATR-FTIR spectra of (A) pure amorphous indomethacin, (B) pure nicotinamide and (C) the 25:75 (weight ratio) indomethacin/nicotinamide formulation (Tablet C, Table 5.2) after preparation. The specific shifts in peak positions that indicate formation H-bond interactions between indomethacin and nicotinamide are highlighted by the red labels. 101

Figure 5.6 – Representative ATR-FTIR spectroscopic images recorded from the *in situ* dissolution experiments (the image size is approximately 7.75 × 6.05 mm^2). The distributions of indomethacin, nicotinamide and the phosphate buffer are shown during the dissolution of (A) Tablet A, (B) Tablet C and (C) Tablet D. 102

Figure 5.7 – ATR-FTIR spectroscopic images showing the dissolution of Tablet A (the image size is approximately 7.75 × 6.05 mm^2). The distribution of indomethacin, nicotinamide and the phosphate buffer are shown. The spectra are extracted from the same pixel of the FPA detector but from images recorded at different times. The dashed lines highlight the spectral peaks indicative of H-bonded interactions. The broadening of the spectral region between 1675–1615 cm^{-1} in the extracted spectra for (B) and (C) are a result of water vibrations from the solution. 103

Figure 5.8 – Dissolution profiles obtained using UV detection that show the percentage of indomethacin dissolved from the tablet as a function of time for the different tablets studied (Table 5.2). Tablets A–E contained indomethacin and nicotinamide in varying weight loadings. Tablets F and G are pure indomethacin in its γ and amorphous form, respectively. 104

Figure 5.9 – Dissolution profiles showing the percentage of indomethacin dissolved from the tablet during 24 hr for Tablets F and G, made from pure γ and amorphous indomethacin, respectively. The linear trend of the data provides evidence of zero-order drug release from these tablets. 105

Figure 5.10 – Data recorded from the dissolution experiments of Tablet C. (A) UV drug dissolution profiles, (B) ATR-FTIR spectroscopic images (the image size is approximately 7.75 × 6.05 mm^2) and (C) accompanying spectra from the images extracted from the pixel marked "X". The distribution of indomethacin, nicotinamide and the phosphate buffer are shown in the spectroscopic images. 107

Figure 5.11 – ATR-FTIR spectroscopic images recorded during the dissolution experiments for (A) Tablet D and (B) Tablet E (image size is approximately 7.75 × 6.05 mm^2). The distribution of indomethacin, nicotinamide and the phosphate buffer as the experiment progressed are shown. 109

Figure 5.12 – Potential H-bonded intermolecular interactions between (A) indomethacin and urea, and (B) indomethacin and mannitol. 110

Figure 5.13 – UV drug dissolution profiles recorded for the indomethacin/mannitol (Red line with square markers) and indomethacin/urea (Green line with circle markers) compacted tablets (25:75 weight ratio). The UV drug dissolution profiles of pure amorphous indomethacin (black line, square markers) and indomethacin/nicotinamide

(blue line, circle markers) in 25:75 weight ratio (Tablet C, Table 5.2) have been shown for comparison. 111

Figure 5.14 – (A) ATR-FTIR spectroscopic images recorded for the dissolution of the indomethacin/urea tablets. The spatial distribution of urea, amorphous indomethacin and α form of indomethacin are shown. Extracted spectra confirm the conversion of the amorphous form (dashed line) to α form ("Crystalline", solid line) which is most easily distinguished by the appearance of the band with a peak at 1649 cm^{-1}. (B) Shows the spectroscopic images recorded during the indomethacin/mannitol tablet dissolution experiments. The distribution of mannitol and indomethacin are shown. 112

Figure 6.1 – Chemical structures of N-[[4-fluoro-2-(5-methyl-1H-1,2,4-triazol-1-yl)phenyl]methyl]-4,6,7,9-tetrahydro-3-hydroxy-9,9-dimethyl-4-oxopyrimido[2,1-c][1,4]oxazine-2-carboxamide, in its (A) monohydrate free acid form and (B) ionised monosodium salt form. 118

Figure 6.2 – Schematic overview of the different analytical approaches used to study the dissolving tablets *in situ*. 119

Figure 6.3 – Schematic diagrams showing the flow cells used to study the dissolving tablets using the different analytical approaches. (A) The Perspex flow cell used for ATR-FTIR spectroscopic imaging measurements and (B) the flow cell used for Raman mapping and collection of video data. 123

Figure 6.4 – (A) ATR-FTIR spectra and (B) Raman spectra of the two different forms of drug, pure ionised form is shown by the solid line and pure free acid form by the dashed lines. 125

Figure 6.5 – (A) ATR-FTIR spectra and (B) Raman spectra of the drug after filtration from the acidic medium. The solid lines show the recorded spectra and confirm that conversion of the ionised form to the free acid form of the API occurred. Reference spectra of the pure free acid drug form (dashed line) are included for comparison. . 126

Figure 6.6 – Recorded video data that show the swelling behaviour of a 7 mm formulated tablet containing the ionised drug. Images are shown every 2.5 hr during dissolution in the neutral solution. The image size of these images is ~10.8 × 4.9 mm^2. 127

Figure 6.7 – ATR-FTIR spectroscopic images recorded during the first 10 min of the experiment in neutral solution. The VeeMax II accessory was used for these experiments which meant the whole tablet could be measured. The image size is approximately 7.75 × 6.05 mm^2 and the tablets were 3 mm in diameter. The distribution of the ionised form of the drug (top row), polymer (middle row) and dissolution medium (bottom row) are presented. 129

Figure 6.8 – ATR-FTIR spectroscopic images recorded every 0.5 hr for the duration of the experiment in water. The VeeMax II accessory was used for these experiments allowing an image size of ~7.75 × 6.05 mm^2 to be measured. The tablets studied here are 3 mm in diameter. The distribution of the ionised form of the drug (top row), polymer (middle row) and free acid form of the drug (bottom row) are presented. .. 129

Figure 6.9 – Raman mapping results recorded during the dissolution experiment of the 7 mm formulated tablet in the neutral solution. (A) shows the spatial distribution of the ionised API and (B) the spatial distribution of the free acid form of the drug during the experiment. 130

Figure 6.10 – Images recorded from the video imaging approach that shows the behaviour of the 7 mm tablet containing the ionised drug form during dissolution in the acidic solution. The images show clear fracturing of the matrix of the tablet. Each image is ~10.8 × 4.9 mm^2 where the data recorded every 2.5 hr are presented. 131

Figure 6.11 – ATR-FTIR spectroscopic images showing the behaviour of the 3 mm tablet during the initial 10 min of the experiment in the acid solution. The experiment was setup on the Imaging Golden Gate accessory to provide information from the edge of the tablet. Each image is ~0.64 × 0.53 mm^2. The distribution of ionised form of the drug (top row), free acid form (middle row) and polymer (bottom row) are presented. 132

Figure 6.12 – ATR-FTIR spectroscopic images of the 3 mm tablets recorded from the dissolution experiment of the tablet in the acidic solution. The spectroscopic images recorded at different times during the first 120 min of the experiment. A VeeMax II accessory was used which allowed measurement of the whole tablet since the image size is ~7.75 × 6.05 mm^2. The distribution of ionised form of the drug (top row), free acid form of the drug (middle row) and acidic medium (bottom row) are presented. 132

Figure 6.13 – ATR-FTIR spectroscopic images recorded using (A) the Imaging Golden Gate and (B) VeeMax II accessories. These confirm the presence of disproportionation to the free acid form of the drug. Images measured after 10 min from the two separate experiments in the acidic solution are presented. The accompanying ATR-FTIR spectra are extracted from a selected pixel within regions of high free acid drug form concentration (red areas) in the spectroscopic images. Spectrum (A) is extracted from the Imaging Golden Gate accessory measurement and (B) the experiment recorded on the VeeMax II accessory (solid lines). The reference ATR-FTIR spectrum of the free acid form has also been included for comparison purposes (dashed line).....133

Figure 6.14 – Raman mapping results from measurement of the 7 mm tablet in the acidic solution. The conversion from the ionised form of the drug (top) to the free acid form of the drug (bottom) is presented in the maps.....135

Figure 7.1 – The initial designs for the microfluidic channels to be moulded into PDMS substrate along with visible images of the printed paraffin wax (A) and (C) show the single channel device and (B) and (E) show the T-junction design. (D) A visible image of the channel showing the arrangement of the deposited wax. 142

Figure 7.2 – Schematic diagram of the preparation of PDMS microfluidic devices. (A) Deposition of paraffin wax onto the glass substrate. (B) Covered with PDMS and allowed to cure. (C) Device peeled from the substrate to reveal the channels. (D) The microfluidic device placed on the measuring surface of the ZnSe crystal and solution passed through channels using a syringe. 143

Figure 7.3 – Visible images of the 3D printed moulds for creating devices that can study the dissolution of micro-formulations.....144

Figure 7.4 – Visible images showing the disassembled (top left) and assembled (top right) setup of the microfluidic device for ATR-FTIR spectroscopic imaging measurements using a ZnSe crystal. Below, is a schematic representation of the experimental setup. 145

Figure 7.5 – Visible images of the four PDMS microfluidic devices that were used for the experiments in this work.....145

Figure 7.6 – ATR-FTIR spectroscopic images showing the results from the dissolution of PEG in (A) pure PDMS devices and (B) modified PDMS devices. The distribution of the PDMS, water and PEG have been shown as a function of time and the spectroscopic images were generated based on the integration of the unique bands between 1295–1240, 3600–3000 and 975–910 cm^{-1}, respectively. The image size is ~11.5 × 8 mm^2.....147

Figure 7.7 – ATR-FTIR spectra of the ibuprofen/PEG (1:3 weight ratio) formulation, polyethylene glycol (mw: 1000 $g.mol^{-1}$) and ibuprofen in the crystalline state.....149

Figure 7.8 – ATR-FTIR spectroscopic images showing the simultaneous dissolution of four ibuprofen/PEG (1:3 weight ratio) formulations in neutral solution. The spatial distribution of PEG (top row), ibuprofen (middle row) and the aqueous solution (bottom row) have been presented. The dimensions of the images are ~11.5 × 8 mm^2. 150

Figure 7.9 – (A) ATR-FTIR spectroscopic images showing the simultaneous dissolution of two ibuprofen/PEG formulations in acidic medium. The spatial distribution of, ibuprofen (top row) PEG (middle row) and the aqueous solution (bottom row) have been presented. The dimensions of the images are ~11.5 × 8 mm^2. (B) Extracted ATR-FTIR spectra taken from the centre of the formulation at 0 min (Black) and 20 min (Red). 151

Figure 7.10 – (A) ATR-FTIR spectroscopic images showing the behaviour of ibuprofen during the simultaneous dissolution of two ibuprofen/PEG formulations (1:3 weight ratio) in different pH media. The size of the spectroscopic images is ~7.75 × 6 mm^2. Any structural changes of ibuprofen in the media during the experiment were shown in the extracted ATR-FTIR spectra, from the centre of the tablet in the pH 7 (B) and pH 1 (C) solution. 153

Figure 7.11 – ATR-FTIR spectroscopic images showing the precipitation of crystalline ibuprofen crystals upon contact and mixing of a sodium ibuprofen solution (2 $mg.mL^{-1}$) with a pH 1 solution. The spatial distribution of sodium ibuprofen (top row), crystalline ibuprofen (middle row) and aqueous solution (bottom row) are presented. The size of the image is ~11.5 × 8 mm^2. 155

Figure 7.12 – (A) ATR-FTIR spectra recorded for the pure 2 $mg.mL^{-1}$ sodium ibuprofen solution, sodium ibuprofen and crystalline ibuprofen. (B) Extracted spectra from the 2 $mg.mL^{-1}$ sodium ibuprofen solution experiment. The spectra were extracted from a bend in the serpentine channel as the experiment proceeded. 157

Figure 7.13 – ATR-FTIR spectroscopic images showing the precipitation of crystalline ibuprofen crystals from sodium ibuprofen solutions with different concentrations upon mixing with a pH 1 solution. The spatial distribution of crystalline ibuprofen is shown in the 2 $mg.mL^{-1}$ (top row), 1 $mg.mL^{-1}$ (middle row) and 0.5 $mg.mL^{-1}$ (bottom row) experiments. The size of the images is ~11.5 × 8 mm^2.....158

List of Tables

Table 2.1 – Properties of the different ATR-FTIR spectroscopic imaging accessories. 55

Table 4.1 – The spectral range that was integrated to produce spectroscopic images showing the spatial distribution of the different chemical species in this study. 78

Table 4.2 – Position of the ATR-FTIR bands assigned to the carbonyl stretching vibrations of the different indomethacin structural forms (Taylor and Zografi, 1997b).....80

Table 5.1 – The specific absorption band ranges that were used to generate the ATR-FTIR spectroscopic images for the different species in this study. 97

Table 5.2 – Different formulations studied using the ATR-FTIR spectroscopic imaging approach with parallel UV detection. 99

Table 6.1 – List components in the formulated tablets and their respective weight loadings (%).....120

Table 6.2 – Spectral bands integrated to generate the false colour ATR-FTIR spectroscopic images and Raman maps, and the respective position of the peak of the spectral band is indicated. 122

Nomenclature

List of Abbreviations

Abbreviation	Definition
a.u.	Arbitrary unit
AFM	Atomic force microscopy
API	Active pharmaceutical ingredient
ASD	Amorphous solid dispersion
ATR	Attenuated total reflection
BCS	Biopharmaceutics classification system
C=O	Carbonyl group
CaF_2	Calcium fluoride
CO_2	Carbon dioxide
COOH	Carboxylic acid group
D_2O	Deuterated water
FPA	Focal plane array
FTIR	Fourier transform infrared
H_2O	Water
H-Bond	Hydrogen bond
HCl	Hydrochloric acid
HPMC	Hydroxypropyl methylcellulose
hr	Hour
IFPMA	International Federation of Pharmaceutical Manufacturers & Associations
IR	Infrared
min	Minute
mp	Melting point
MRI	Magnetic resonance imaging
mw	Molecular weight
NA	Numerical aperture
NSAID	Non-steroidal anti-inflammatory
PDMS	Polydimethylsiloxane
PDMS-b-PEO	poly(dimethylsiloxane-b-ethylene oxide polymeric)

PEG	Polyethylene glycol
s	Second
SEM	Scanning electron microscopy
SNR	Signal-to-noise ratio
USP	United States Pharmacopeia
UV	Ultraviolet
Vis	Visible
ZnSe	Zinc selenide

List of symbols

Symbol	Description	Units
μ	Reduced mass	kg
A	Absorbance	–
C	Concentration of dissolved drug	$mg.L^{-1}$
c	Molar concentration	$mol.L^{-1}$
c	Speed of light	$m.s^{-1}$
Cs	Saturated solubility of the drug	$mg.cm^{-3}$
C_t	Concentration of dissolved drug at a particular time	$mg.cm^{-3}$
D	Diffusion coefficient	$cm^2.s^{-1}$
d_e	Effective pathlength	m
d_p	Depth of penetration	m
E	Energy	J
h	Thickness of diffusion layer	cm
h	Plank's constant	$J.s^{-1}$
I	Transmitted intensity	–
I_0	Incident intensity	–
k	Bond force constant	N/m
l	Pathlength	m
m	Mass of an atom in a diatomic molecule	kg
n	Refractive index	–
N	Number of atoms	–
r	Distance between two resolved points	m
t	Time	s
T	Transmittance	–
ε	Molar absorptivity	$L.mol^{-1}.cm^{-1}$
θ	Angle of incidence	Radians
λ	Wavelength of light	m

ν	Frequency	Hertz
$\bar{\nu}$	Wavenumber	cm^{-1}

Publications and Conferences

Publications from the reported work undertaken in this thesis:

1. KAZARIAN S. G. and EWING A. V. **2013** Applications of Fourier transform infrared spectroscopic imaging to tablet dissolution and drug release, *Expert Opinion on Drug Delivery*, 10, 1207–1221.

2. EWING A. V., CLARKE G. S., and KAZARIAN S. G., **2014** Stability of indomethacin with relevance to the release from amorphous solid dispersions studied with ATR-FTIR spectroscopic imaging, *European Journal of Pharmaceutical Sciences*, 60, 64–71.

3. EWING A. V., WRAY P. S., CLARKE G. S. and KAZARIAN S.G. **2015** Evaluating drug delivery with salt formation: drug disproportionation studied *in situ* by ATR-FTIR imaging and Raman mapping, *Journal of Pharmaceutical and Biomedical Analysis*, 111, 248–256.

4. EWING A. V., BIGGART G. D., HALE C. R., CLARKE G. S. and KAZARIAN S. G. **2015** Comparison of pharmaceutical formulations: ATR-FTIR spectroscopic imaging to study drug-carrier interactions, *International Journal of Pharmaceutics*, 495, 112–121.

Other publications:

5. WOODWARD R. T., STEVENS L. A., DAWSON R., VIJAYARAGHAVAN M., HASELL T., SILVERWOOD I. P., EWING A. V., RATVIJITVECH T., EXLEY J. D., CHONG S. Y., BLANC F., ADAMS D. J., KAZARIAN S. G., SNAPE C. E., DRAGE T. C., and COOPER A. I. **2014** Swellable, water- and acid-tolerant polymer sponges for chemoselective carbon dioxide capture", *Journal of the American Chemical Society,* 136, 9028–9035.

6. EWING A. V., GABRIENKO A. A., SEMIKOLENOV S. V., DUBKOV K. A. and KAZARIAN S. G. **2015** How do intermolecular interactions affect swelling of polyketones with a differing number of carbonyl groups? An *in situ* ATR-FTIR spectroscopic study of CO_2 sorption in polymers, *Journal of Physical Chemistry C*, 119, 431–440.

7. PUNČOCHOVÁ K., EWING A. V., GAJDOŠOVÁ M., SARVAŠOVÁ N., KAZARIAN S. G., BERÁNEK J. and ŠTĚPÁNEK F. **2015** Identifying the mechanisms of drug release from amorphous solid dispersions using MRI and ATR-FTIR spectroscopic imaging, *International Journal of Pharmaceutics*, 483, 256–267.

8. EWING A. V. and KAZARIAN S. G. **2015** Chapter 19: Interaction of supercritical carbon dioxide with polymers studied by vibrational spectroscopy in *Supercritical Fluid*

Nanotechnology: Advances and Applications in Composites and Hybrid Nanomaterials, C. Domingo and P. Subra (eds.), Pan Stanford Publishing Pte Ltd.

9. GABRIENKO A. A., EWING A. V., CHIBIRYAEV A. M., AGAFONTSEV A. M., DUBKOV K. A. and KAZARIAN S. G., **2016** New insights into the mechanism of interaction between CO2 and polymers from thermodynamic parameters obtained by *in situ* ATR-FTIR spectroscopy, *Physical Chemistry Chemical Physics*, Accepted in press.

Conferences

This work has been selected for presentation at the following conferences and meetings:

1. Centre for Process Analytics and Control Technology (CPACT) Research Day, Glasgow, UK. **2015**. Oral presentation: Aiding pharmaceutical formulation design: ATR-FTIR spectroscopic imaging to study drug release and tablet dissolution. (Awarded Malcolm McIvor CPACT Prize 2015).

2. The Federation of Analytical Chemistry and Spectroscopy Societies (FACSS) The Great Scientific Exchange (SciX), Providence, USA. **2015**. Oral presentation: Design of pharmaceutical formulations: ATR-FTIR spectroscopic imaging to study drug release and tablet dissolution.

3. Department of Chemical Engineering Research Symposium, Imperial College, London UK. **2015**. Oral presentation: Aiding pharmaceutical formulation design: ATR-FTIR spectroscopic imaging for drug release studies.

4. Institution of Chemical Engineers (IChemE) ChemEngDay, Sheffield, UK. **2014**. Poster presentation: Design of pharmaceutical formulations: ATR-FTIR spectroscopic imaging to study drug release and tablet dissolution.

5. Infrared and Raman Discussion Group (IRDG) Annual Meeting, London, UK. **2013**. Poster presentation: ATR-FTIR spectroscopic imaging of the release of indomethacin from polymer matrices.

6. American Association of Pharmaceutical Sciences (AAPS) Annual Meeting, San Antonio, USA. **2013**. Poster presentation: ATR-FTIR spectroscopic imaging of the release of indomethacin from polymer matrices.

1 Introduction

The cost of bringing a newly developed medicine to market continues to rise. It was reported by the International Federation of Pharmaceutical Manufacturers and Associations (IFPMA) in 2015, that the pharmaceutical industry spends approximately USD 141.6 billion per year on the research and development of drugs for specific health problems such as cancer, diabetes and cardiovascular disease (IFPMA, 2015). In fact, 50 % of the leading global research firms across all industrial sectors are companies that develop pharmaceutical products for drug delivery. Research and development of a single new active pharmaceutical ingredient (API) begin by identifying a candidate from, on average, 5,000–10,000 screened chemicals (Figure 1.1). Furthermore, developments can take as long as 10 to 15 years to ensure that the drug is safe and used to its optimum efficiency. Therefore, it comes as little surprise that the pharmaceutical companies are under constant pressure to innovate new drug delivery systems.

Drug delivery from tablet compacts remains as one of the most commonly used and popular methods to administer drugs. They are facile to manufacture, easy to package and have a high patient compliance. However, many of the suitable drug candidates are poorly soluble in aqueous media and thus have a low bioavailability. For improved solubility, it is usually more economical, in terms of cost and time, to develop novel formulations using existing APIs that can be achieved by modifying the drug candidate or adding specific excipients (Sastry et al., 2000). As a result, there is a great interest in the design of novel

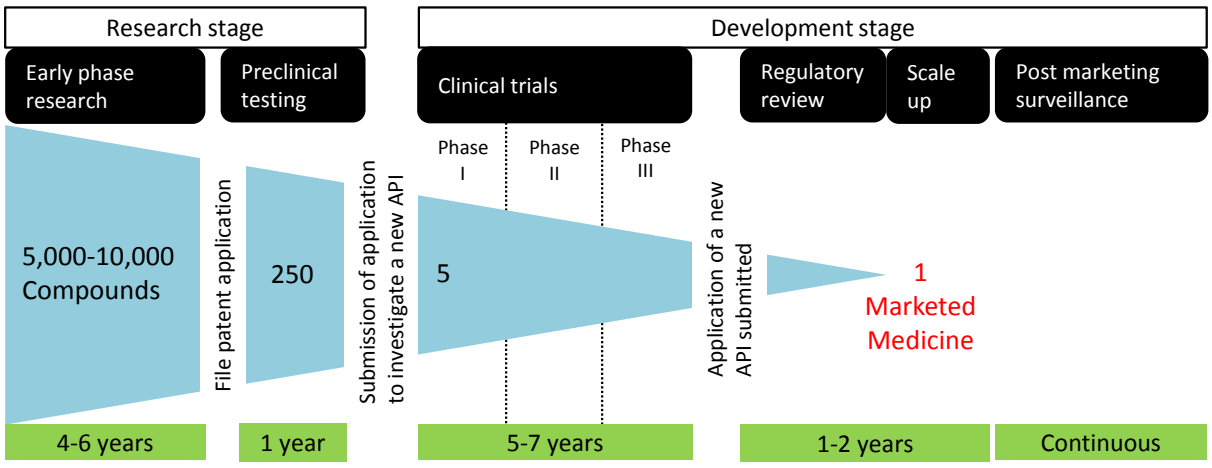


Figure 1.1 – The research and development process of a new drug in the pharmaceutical industry. Adapted from (IFPMA, 2015).

pharmaceutical formulations for tablet compacts that are efficient in delivering the drug to patients. To achieve reliable medicines, the role of the different materials within the formulation needs to be understood. Moreover, revealing the stability and behaviour of the drug during preparation, storage and delivery can aid in the development of delivery systems with high efficacy.

In this project, a specific focus is on the release of the drug from tablet compacts of novel formulations. Conventional dissolutions tests often utilise high performance liquid chromatography or ultraviolet (UV) detection to monitor the amount of drug dissolved into the surrounding solution as a function of time. While these methods are highly sensitive, they do not usually determine chemical changes or mechanistic information about the dissolving tablets. The ability to detect these changes can be particularly useful if a tablet compact is not behaving as expected, for example, the complete release of the drug is not achieved. Therefore, applying alternative analytical approaches to assess drug delivery is needed.

Macro attenuated total reflection-Fourier transform infrared (ATR-FTIR) spectroscopic imaging is a robust approach that has been developed to investigate tablets during *in situ* dissolution experiments (van der Weerd et al., 2004, Kazarian and Chan, 2003). Significantly, this spectroscopic imaging approach reveals the spatial distribution of the individual components in the measured area. Recording separate measurements of a dissolving tablet as a function of time means that the behaviour of the drug and polymer can be assessed. Macro ATR-FTIR spectroscopic imaging has proven to be effective for investigating the dissolution of tablet compacts over recent years (Wray et al., 2014, Wray et al., 2011, van der Weerd et al., 2004). These studies have provided a platform for the use of this spectroscopic imaging approach to be further developed for the study of novel pharmaceutical systems.

1.1 Aims and objectives

The main aim of this work is to demonstrate that macro ATR-FTIR spectroscopic imaging can be utilised as a reliable and robust approach to investigate the stability and behaviour of drugs in pharmaceutical formulations. The specific objectives of this project are:

- To understand the stability and dissolution behaviour of a model amorphous drug, indomethacin, in solid dispersion formulations. Amorphous solid dispersions containing indomethacin formulated with different polymers prepared by a hot melt method will be studied using macro ATR-FTIR spectroscopic imaging. The objective

is to assess the stability of the amorphous form of the drug within the formulation before delivery and during *in situ* tablet dissolution experiments.

- To investigate the influence of excipients that act as carriers to improve the rate of dissolution of a poorly water-soluble drug released from tablet compacts. Macro ATR-FTIR spectroscopic imaging can be used with parallel UV detection to reveal hydrogen bonded interactions and quantify the amount of drug dissolved as a function of time.

- To rationalise the stability of ionised drugs in solutions with different pH values. Ionised drugs are a common method to increase the rate of dissolution and disproportionation to the free acid form of the drug during dissolution in pH 7 and pH 1 media will be monitored.

- To develop microfluidic devices that can be studied using macro ATR-FTIR spectroscopic imaging. The objective is to screen several pharmaceutical formulations simultaneously in flowing conditions.

- To determine the behaviour of a drug after it has been dissolved into solution. Microfluidic channels will be designed and measured with macro ATR-FTIR spectroscopic imaging to seek evidence of crystallisation or precipitation of a dissolved drug solution that is mixed with an aqueous medium of different pH.

2 Literature Review

The main motivation of the thesis is to use macro ATR-FTIR spectroscopic imaging to investigate the stability and behaviour of drugs in pharmaceutical formulations. This literature review aims to summarise the key topics that are relevant to the work undertaken in this thesis.

The first Sections (2.1 to 2.4) of the literature review seek to provide context for the need to develop novel formulations for more efficient drug delivery. These Sections will focus on some of the problems that the pharmaceutical industry faces in the development of new drug delivery systems. These include the need to improve the rate of dissolution of poorly aqueous soluble drugs, the importance of controlling drug release and the analytical approaches currently used to assess the dissolution of drugs.

The second part of this Chapter, Section 2.5 onwards, introduces the principles of infrared (IR) spectroscopy. Furthermore, the development of ATR-FTIR spectroscopic imaging and the applications of this approach are also described. Finally, the progress of using this imaging approach for the study of drug release and tablet dissolution has been reviewed and the opportunities for further work carried out and reported in this thesis are identified and summarised in Section 2.8.

2.1 Overview of pharmaceutical formulations

Solid tablet compacts designed for oral administration are the most common method for the delivery of APIs to patients (Sastry et al., 2000). Their popularity from a patient's perspective stems from the fact that tablets are easy to take, can be self-administered and do not cause discomfort or pain during delivery. Moreover, tablet compacts are favourable during the development and manufacturing stages, hence, making them desirable for the pharmaceutical companies. These drug delivery systems are very versatile in the range of API candidates that can be accommodated, are easy to package and do not require sterile environments during preparation, therefore, they are also economical in terms of cost.

Tablet compacts are defined as individual units of solid medicaments that are prepared by compaction (Kottke and Rudnic, 2002). It is very rare that tablets are made from the pure drug in its concentrated form. Commonly, solid tablet compacts contain formulations made from a mixture of the API and pharmaceutically approved excipients. Excipients are often pharmaceutically inactive compounds that act as fillers to bulk up the size of the formulation

since the amount of drug administered is not very high. However, the careful selection of these added excipients can be used to influence the delivery of a drug, for example, by aiding the disintegration of tablets or prolonging the release of the API in the system (Pifferi et al., 1999). Other intended excipients can simply be used as lubricants, to improve the flavour of the tablet, e.g. sugars, or for colouring that can be important for the branding of certain medicines. Ultimately, the choice of excipient used is intended to control and improve the bioavailability of the drug.

2.1.1 Preparation of pharmaceutical formulations

In addition to the materials included in the tablet dosage forms, the method of preparation is also of great importance to the delivery of the APIs. The manufacturing approaches are stringently regulated and must comply with Good Manufacturing Practices. There are a range of methodologies employed to prepare the formulations that can subsequently be compacted into tablet dosage forms that will be introduced here (Kottke and Rudnic, 2002).

One of the simplest methods is the physical mixing of powders. However, achieving good homogeneity of the ingredients can be difficult due to the cohesion of solid particles which means movement and equal distribution within the final product can take a long time. Thus, there is a chance that there will be segregation of the different materials in the tablets after compaction, arising from variations in the particle size and density (Chowhan and Chi, 1986). Therefore, sufficient energy must be supplied to facilitate effective mixing of the powders and overcome these effects. Original powder mixers were intended to process the entire batch at the same time. However, more recent developments have produced mixers that process portions of the batch in a number of different stages (Kottke and Rudnic, 2002).

The preparation of the formulations by wet granulation is perhaps the most popular method for processing precursors for compaction into tablet dosage forms because it can be used for almost any API (Faure et al., 2001). This method works by combining the dry powdered ingredients followed by wet massing and then drying in a fluidised bed (Kristensen and Schaefer, 1987). However, this approach can be time-consuming and involve the use of expensive solvents. Nevertheless, the resulting granulated formulation will be of a consistent size that will lead to more reproducible tablets after compaction. Though, during solubilisation, movement of the ingredients in the formulation can result in loss of uniformity in the final product (Zelkó et al., 1999).

The solvent evaporation method for the production of formulations involves dissolving the drug and excipients in a common solvent that is subsequently removed (Bates, 1969).

Isolation of the co-evaporated material can be achieved by removal of the solvent using a number of approaches that include: heating, vacuum conditions, freeze drying or spray drying (Leuner and Dressman, 2000). For preparation using this method, it is essential that all of the solvents are removed from the final product due to the inherent toxicity of many organic solvents. The method of solvent removal could also potentially lead to structural changes in the ingredients which can have an adverse impact on the intended delivery properties. Nonetheless, due to the advent of improved procedures, this approach is used to process a range of novel formulations, such as those with very high melting points.

One viable alternative to the use of volatile organic solvents is impregnation of an API into a polymer by using high-pressure or supercritical carbon dioxide (CO_2) (López-Periago et al., 2008, Kazarian and Martirosyan, 2002, Kazarian, 2000). Processing pharmaceutical materials with high-pressure or supercritical CO_2 is not yet widely applied for preparing formulations. This method works by dissolving the drug in pressurised CO_2 and subjecting a polymer to these conditions. In the high-pressure environment, the polymer will swell allowing the drug to be carried into the sample before the whole system is depressurised. The significant advantages of this approach are that CO_2 is widely available, non-toxic and easy to remove from the final products. However, the main prerequisite for processing formulations with CO_2 is that the API must be soluble in high-pressure or supercritical CO_2.

Finally, the production of solid pharmaceutical tablets using a hot melt method has been reported for a number of systems (Leuner and Dressman, 2000). The different ingredients are melted together and subsequently cooled to form a solid product. Different rates of cooling can be used to isolate the formulation in different structural states, for example, liquid nitrogen can be used to rapidly cool the melt and "freeze" the drug in the amorphous form (Chiou and Riegelman, 1969, Kanig, 1964). For the preparation of pharmaceutical formulations using this method, it is important to understand the miscibility of the API and excipients in the molten mixture. Furthermore, consideration has to be made to avoid evaporation, sublimation or thermal degradation of the materials. Hot melt methods have had an impact on the industrial processing of formulations over recent years. Namely, hot melt extrusion has been applied for pharmaceutical purposes (Crowley et al., 2007, Repka et al., 2007, Breitenbach, 2002). This approach utilises a two-screw extruder mechanism that simultaneously melts and mixes the ingredients producing granules that can be compacted.

2.1.2 Compaction into solid tablet dosage forms

Compaction of the powered formulations after preparation involves filling a tablet mould or die and compressing with a punch. A range of physical changes to the formulation can occur during compression (Cunningham et al., 2004, Kottke and Rudnic, 2002). Firstly, the particles rearrange to fill any empty voids in the die, causing the volume to decrease as the force from the punch is applied. Next, after complete rearrangement the force causes some particles to deform and change physical shape. Upon impact during pressing, deformation of the particles can occur that can affect the stability and dissolution characteristics of the resulting tablet. Deformation is often reversible provided that not too much force is applied. However, in some cases irreversible deformation of the particles occurs that can cause problems with the quality of the final tablets. Finally, depending upon the nature of the components, particles can undergo crushing, fracturing or plasticisation during compaction. All of these processes are irreversible and can affect the stability, longevity and dissolution properties of the formulation (Cunningham et al., 2004, Jivraj et al., 2000).

In order to achieve consistent tablet weights and distributions of the different materials within a formulation, the prepared particle sizes of the powders for compaction should be consistent. The compaction characteristics can be easily changed by varying the particle size. Smaller particles, like those collected from spray drying, are more susceptible to irreversible deformation. The brittleness of the resulting manufactured tablets can also be a direct consequence of the initial particle size (Kottke and Rudnic, 2002).

Another factor that can affect properties of the tablets produced during compaction is the moisture content in the formulation and the environment during preparation (Sun, 2008, Elkhider et al., 2007, Sebhatu et al., 1997). The density of formulation is increased when it is exposed to high humidity conditions that can have both positive and negative effects on the process. For example, moisture can act as a lubricant and result in harder or stronger tablets being produced that could decrease the rate of drug release (Ahlneck and Alderborn, 1989). The purity of the formulation is of the utmost importance. Contaminants can affect the compaction properties of the tablets as well as influencing the overall performance of the therapeutic product. Contaminants are defined as any material that is not intended for use in the product and thus, includes precursors or derivatives from the raw materials. Unwanted moisture can initiate changes to the structural form of the materials. Undesired form changes are particularly problematic for efficient release of an API, especially since some candidates are intended for delivery in a particular form (Elkhider et al., 2007, Ahlneck and Zografi, 1990). The regulatory bodies widely recognise the importance of avoiding contamination in

the final products and there are strict requirements to detect traces of unwanted species in the materials before delivery.

Physical changes to the formulated particles during tablet compaction can drastically affect the strength of the tablet and the dissolution behaviour after it has been delivered. Furthermore, difficulties can arise from unfavourable properties of the formulation during compaction such as the materials sticking to the dies and punches. Consequently, this can lead to the whole production line shutting down. Therefore, selecting suitable excipients is a crucial prerequisite that one has to consider during the design and scale-up of formulations (Pifferi et al., 1999).

2.1.3 Properties of active pharmaceutical ingredients

The development of novel APIs is particularly challenging because many of the newly discovered pharmaceutical candidates are poorly soluble in aqueous conditions. Estimations of the number of new drugs that have a poor aqueous solubility vary in different reports, in general, ranging between 40 to 70 % (Khadka et al., 2014, Savjani et al., 2012, Kawabata et al., 2011). Nevertheless, it is agreed that a large number of new drug candidates possess poor solubility in aqueous solutions. The solubility of a drug has a major influence on its rate of dissolution. Hence, innovative formulations and delivery systems are required to enhance the bioavailability of the drug (Khadka et al., 2014).

The bioavailability of drug candidates can be classified based on their aqueous solubility and intestinal permeability using the biopharmaceutics classification system (BCS), Figure 2.1 (Kasim et al., 2004, Lindenberg et al., 2004, Lobenberg and Amidon, 2000). The

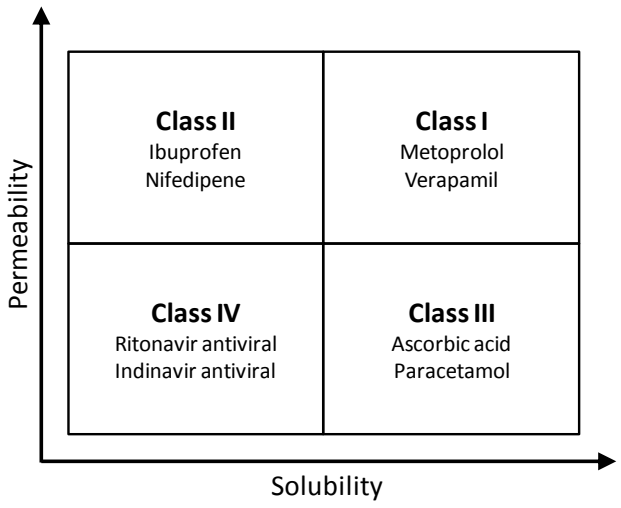


Figure 2.1 – Biopharmaceutics classification system including some example essential drug candidates as listed by the World Health Organisation.

bioavailability of the BCS Class II drugs is of great interest because of the high permeability in the body. Hence, enhancement of the solubility of the API can lead to efficient products. In the case of BCS Class III drugs, it is the permeability of the candidate that needs to be enhanced. Despite the fact that BSC Class IV compounds have low solubility and permeability they should not necessarily be disregarded, instead optimisation of these candidates can be developed.

As a result of the problematic nature of many APIs during drug release and dissolution, there is widespread interest in improving the efficacy of new drug candidates. To further complicate drug delivery, the dissolution rates in real biological systems will depend upon the properties of aqueous solutions in the gastrointestinal tract. For example, whether the stomach is in a fed or fasted state or if the pH of the environment is high or low. Therefore, understanding the mechanisms and processes of drug release is essential for improving the design of pharmaceutical tablets.

2.2 Methods of improving the release and bioavailability of drugs

The characteristic solubility and permeability behaviour of drugs that are formulated for use in solid tablet compacts is a key factor that determines their bioavailability. Since many newly developed APIs are poorly water-soluble, the pharmaceutical industry must develop methods for more efficient drug delivery from these dosage forms. Certain factors can be considered to suggest how the rate of dissolution of the drug (*dC/dt*) can be improved and these are summarised in the Noyes-Witney Equation (Equation 2.1) (Noyes and Whitney, 1897).

$$\frac{dC}{dt} = \frac{SD(C_s - C_t)}{h} \qquad \textbf{Equation 2.1}$$

Where *dC/dt* is the rate of dissolution of the drug, *S* is the surface area available to be dissolved, *D* is the diffusion coefficient, C_s is the maximum solubility of the API in the solution, C_t is the concentration of dissolved drug at time (*t*) and *h* is the thickness of the diffusion boundary layer adjacent to the surface of the dissolving compound.

Hence, by considering Equation 2.1 one of the simplest methods for improving the rate of drug delivery is to increase the surface area (*S*) of the components, i.e. reduce the particle size (Merisko-Liversidge et al., 2003). This can work particularly well for drug delivery from tablet and capsule delivery systems that contain finely ground powders (Rohrs et al., 2006).

Specific formulations for compacted tablets can be designed that may increase the area of the drug available for dissolution. Disintegrants and accelerators can be added to the tablet matrix to break up a compact once it has been consumed (Alanazi, 2007). Moreover, modification of the API or other components of the tablet compacts can result in the increased solubility of the drug.

Applying enteric coatings to tablets is effective in delaying the release of the drug. Enteric materials are insoluble in the acidic conditions of the stomach but will readily dissolve in basic conditions of the small intestine. Hence, enteric coatings prevent dissolution of the tablet until specific local conditions are achieved. Eudragit-S and Eudragit-L dissolve in solutions of pH 7 and 6, respectively, and are examples of enteric polymers that have been used in marketed delivery systems (Friend, 2005).

In solid dispersions, the drug is molecularly dispersed amongst a polymer such that it is present as a solid solution (Leuner and Dressman, 2000). There are several theories as to how solid dispersions influence drug delivery in pharmaceutical tablet formulations. Firstly, the enhanced dissolution rate of the API can arise from the reduced particle size in the solid dispersion. Molecular dispersion of the drug within a polymer matrix theoretically achieves the optimal reduction in the particle size, since one drug molecule is surrounded by solvate molecules in an ideal dispersion (Goldberg et al., 1966). An alternative theory is the fact that the crystalline structure of the drug is removed (Taylor and Zografi, 1997a). As a result, the energy that is usually needed to break down the crystalline structure is no longer required which increases the rate of dissolution.

Characteristic properties of the drugs will arise from the API crystallising in different polymorphic forms (Leuner and Dressman, 2000). These polymorphic forms often have a higher solubility than the most stable crystalline forms of the drug and thus, can lead to improved bioavailability during dissolution (Ford and Rubinstein, 1978). However, it should be realised that many of the polymorphs that show improved bioavailability are metastable so potential conversion to the more thermodynamically stable form is still possible in the tablets before delivery (Zhang et al., 2014, Brits et al., 2010).

Ionising the pharmaceutical candidate is a widely employed method to improve the solubility of APIs and as many as 50 % of emerging drug candidates are synthesised as salts (Guerrieri and Taylor, 2009). The ionised form of the drug can improve the wettability and reduce the toxicity of the materials (Elder et al., 2013, Serajuddin, 2007), but the stability and solubility of these salts is dependent upon the local environment. Hydration of the salt can occur during storage in humid environments or be initiated as a result of the pH of the

solution during delivery (Wray et al., 2015, Christensen et al., 2012). Furthermore, it is not possible to convert all drug candidates into salts.

Prodrugs are defined as biologically inactive compounds that can be converted to an active drug during the metabolic process in the body (Khandare and Minko, 2006). The conversion of the prodrug into an API can be targeted to specific locations within the body, for example, organs, cells or tissues. Polymeric prodrugs can be activated by the cleavage of a molecular bond between a polymeric excipient and a drug. One of the main advantages of prodrugs is that the aqueous solubility of drugs can be easily enhanced which will increase the bioavailability. A successful application of this approach has been demonstrated with amprenavir (Brouwers et al., 2007). Fosamprenavir is the phosphate ester prodrug of amprenavir and has been reported to be up to ten times more soluble than the pure API. The transformation of the active drug is facilitated in the intestine during delivery and amprenavir is subsequently absorbed into the bloodstream.

2.3 Controlling drug release

Controlling the release of the drug from solid tablet compacts is integral to deliver the ideal therapeutic effect to the patient (Williams et al., 2013a, Williams et al., 2013b, Siepmann and Peppas, 2001, Serajuddin, 1999). There is no ideal method of drug delivery that encompasses all of the APIs, so each delivery method should be optimised in such a way that it has the maximum efficiency and effect in treating the diagnosed symptoms. Nevertheless, there is the utmost importance to ensure that the amount of drug released remains below toxic levels during delivery. Several different drug delivery profiles can be achieved by using pharmaceutical tablets. These include sustained release, burst release, and immediate release. Figure 2.2 shows typical profiles of the rate of drug release from the different drug delivery systems.

Sustained release tablets are a common example of controlled release approaches. These involve releasing small quantities of drugs over an extended period by containing the API within an excipient matrix that dissolves slowly (Uhrich et al., 1999). These are often designed for chronically administered tablet, i.e. those that are taken every day. The aim of a sustained release dosage form is to maintain therapeutic levels of the drug in the blood or tissue for an extended period. Optimum therapeutic levels in the body can be achieved by attempting to obtain zero-order release from the dosage form (Langer and Peppas, 1983). Controlled API release systems mean that drug levels are in the therapeutic range for longer periods of time and thus the desirable effect is administered for longer, resulting in a more

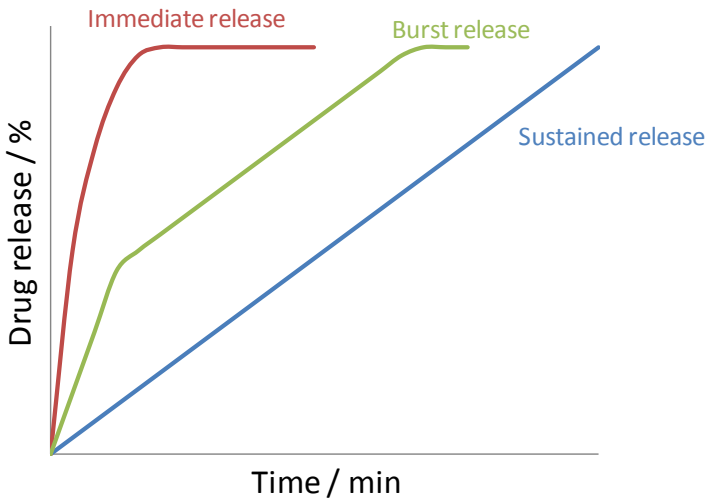


Figure 2.2 – An example of drug release profiles typically recorded from immediate (red line), burst (green plot) and sustained (blue plot) release delivery systems.

suitable and efficient drug delivery method. Alternative sustained release tablet compacts involve designs that are activated by conditions of the local environment. For example, enteric coated tablets delay drug release until in the small intestine where the pH is 6 to 7 by inhibiting dissolution in acidic solutions (Peppas et al., 2000).

As shown in Figure 2.2, the immediate release tablets increase the rate of drug release that can subsequently result in a higher concentration of the drug in the plasma, delivering the therapeutic effect. However, the increased dissolution rate means that there is no sustained effect of the API as the concentration of drug in the plasma will rapidly fall below the minimum therapeutic level. As a result, repeat dosages would be required to maintain sufficient therapeutic levels and this can be inconvenient to the patient. On the other hand, the therapeutic effect will be delivered to the patient much faster that can be particularly desirable, for example, in relieving symptoms of pain.

Finally, burst release essentially delivers the therapeutic effect in two stages: there is a rapid delivery of the drug initially that is followed by a period of sustained release of the API (Huang and Brazel, 2001). Burst release dosage forms have been widely reported to be both positive and negative for drug delivery approaches. However, the ability to control the immediate and sustained release of the drug from tablet compacts is potentially very useful for drug delivery and the development of novel formulations. A burst release dissolution profile of a drug can be achieved by the use of multilayer tablets (Patra et al., 2007) or tablet-in-tablet compacts (Wray et al., 2013) where different polymers and excipients can be used in the different layers.

2.3.1 Drug release mechanisms

Depending upon the dissolution profile that is intended to be delivered, the mechanism by which the drug is released from the tablet compact needs to be identified. Certain excipients can be selected to control the rate of dissolution of the API. However, problems can arise if the release from specific tablet matrices is not understood. For example, if the release is too slow the tablet may not break down and be delivered before it passes through the patient's system.

Common excipients used for controlled drug release tablets are polymers that swell and form a gel upon contact with aqueous solutions (Colombo, 1993, Hogan, 1989). These excipients are often derived from cellulose, such as hydroxypropyl methylcellulose (HPMC) or microcrystalline cellulose. They are particularly desirable as they have favourable compaction properties, do not interact with drug candidates to form ionic salts and are stable over a range of pH conditions (pH 2–13). Furthermore, cellulose derivatives are approved for use in pharmaceutical formulations, non-toxic and metabolically inert (Siepmann and Peppas, 2001). Polymers such as HPMC are also very useful because the molecular structure can easily be modified to gain optimised properties for tablet dissolution and drug release. Specifically, the release properties of HPMC will differ based on the molecular weight, determined by the length of the polymer chain, and the functionality of the methoxy and hydroxypropoxy groups in the polymer. A high molecular weight HPMC polymer will result in a slower rate of water ingress and swelling during a dissolution experiment compared to that of an HPMC polymer with shorter chains (lower molecular weight). It could also be predicted that using longer chain HPMC polymers as excipients may enhance the controlled release properties of the tablets because of more efficient gel layer formation (Siepmann and Peppas, 2001). The reason for the slow ingress of water and hence delayed release properties is that the long chains of the polymers will have a high degree of interaction and entanglement. Therefore, in order for water to penetrate into the sample, the disentanglement of the polymer has to occur. A schematic diagram of a typical disentanglement mechanism during polymer dissolution is shown in Figure 2.3 (Siepmann et al., 1999). This process would be much slower when using polymers with longer chains since there is a higher degree of entanglement within the bulk tablet matrix (Kazarian and van der Weerd, 2008, Colombo et al., 2000). In contrast, the rate of drug release can be increased by modifying the HPMC so that gel formation does not occur, meaning that the aqueous medium penetrates into the centre of the tablet more rapidly, causing the bulk of the tablet to break down.

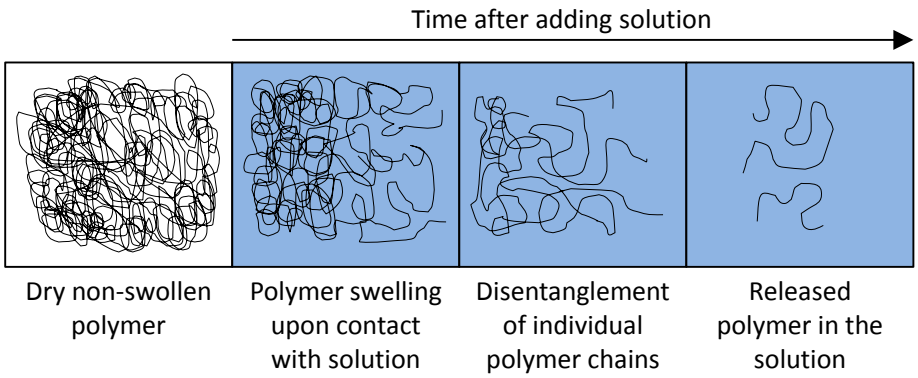


Figure 2.3 – Schematic diagram of different stages of polymeric disentanglement during dissolution in aqueous solution. Adapted from Siepmann et al. (1999).

It should be realised that many other polymers and excipients are used in pharmaceutical formulations for the production of tablet compacts than those derived from cellulose. The final ingredients of many formulations contain a range of excipients that can aid the delivery of the drug. Mixing polymeric excipients can even be a method to increase the rate of drug release from the bulk tablet, for example, combining hydroxypropyl cellulose with HPMC (Vueba et al., 2006).

The excipient or a mixture of excipients used in tablet matrices has a significant influence in controlling the release of the drug from a solid tablet compact. In sustained release tablets using swellable polymers, the drug dissolves out of the bulk matrix and into the surrounding solution. While the degree of swelling is important, it is not the only factor that has to be considered when manufacturing the tablet. Tablet thickness, drug loading and drug solubility can all affect the rate by which the drug is released. The tablet thickness is important since smaller tablets will dissolve faster than larger ones. Therefore, more rapid gel forming excipients will be required to avoid immediate drug release. Varying the drug loading would mean that the dispersion of drug within the matrix would have different homogeneities because the relative concentration of drug and polymer differs. For example, a high drug-loaded tablet may contain more drug particles on the surface of the tablet that will instantly come into contact with the solution and be released (Pham and Lee, 1994). Finally, for highly soluble drugs the mechanism of drug dissolving through the matrix would be quicker than for poorly soluble alternatives, where erosion of the tablet matrix may be required to achieve drug release (Sung et al., 1996).

2.4 Monitoring drug release from tablet compacts

Tablet dissolution is measured using a range of analytical techniques, most commonly UV spectroscopic detection. This approach allows a dissolution profile to be obtained that provides information about the concentration of drug in the surrounding aqueous environment. Typically, UV spectroscopic detection obtains dissolution profiles about the amount of drug dissolved using the United States Pharmacopeia (USP) apparatus (Siewert et al., 2003, Cohen et al., 1990). Examples of the basket and paddle apparatus, also known as USP I and USP II respectively, are shown in Figure 2.4. There is a range of different characteristics that can affect drug release from a tablet, including the solubility of the drug, excipients used and the method of formulation preparation.

The simplicity of these USP tests is what makes these techniques desirable for industrial applications. The tablet is placed in the dissolution medium and stirred, either contained within a bucket or unrestricted within the dissolution vessel, and the concentration of dissolved drug is measured as a function of time. However, problems with such an approach have occurred regarding the consistency of repeat experiments. As a result, there are very strict and stringent guidelines for the calibration of these methods in order to improve the reproducibility of the profiles obtained (Qureshi and Shabnam, 2001).

UV spectroscopic detection is a suitable method to record dissolution profiles of the amount of drug dissolved in the surrounding solution as a function of time. The drug release profiles are shown as graphical plots where the concentration of the API or cumulative drug release is plotted against time. This analytical method is simple and applicable for use with USP tests due to its high sensitivity. UV spectroscopy uses radiation in the region between

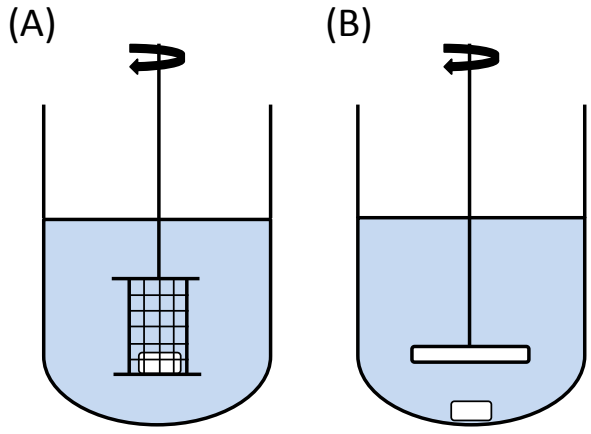


Figure 2.4 – Schematic representation of United States Pharmacopeia (USP) tests. (A) Shows an example of the basket method known as USP I and (B) the paddle method known as USP II.

190 nm and 900 nm of the electromagnetic spectrum and can define the concentration of the subject based on the absorbance at a unique frequency, determined by the Beer-Lambert Law. However, it is important to note that the combination of UV spectroscopy with USP dissolution apparatus often only provides information about the overall amount of drug dissolved and no information about the mechanistic, chemical or physical processes about the dissolving sample are established.

2.4.1 Assessment of pharmaceutical formulations using imaging approaches

Visible imaging using optical photography has been used to study dissolving tablets. However, because many of the drugs and excipients can look similar, usually with the appearance as white powders, added dyes are often needed. Nevertheless, this approach has proven useful for determining different behaviours of the tablet during wetting in aqueous solution. Boundary layers formed during the ingress of the solution can be identified, such as the penetration front, gel formation front and the dissolution front (Gao and Meury, 1996). These allow predictions to be made about the behaviour of the drug in solution which can lead to a more efficient pharmaceutical tablet. Recording visible images of dissolving tablets is an inexpensive and rapid method to screen dissolving tablets but it is not without its limitations. Despite the fact that visible images of dissolving tablets are relatively facile to measure, the interpretation of the different boundaries can be difficult to distinguish. Also, the tablet may need to be removed from the dissolution medium for the images to be recorded. Furthermore, no quantitative information about the individual components in the tablet is revealed. For example, changes in refractive index can cause optical effects that are observed in the captured images.

Visible imaging of the pharmaceutical tablets is much more widely employed to learn about the physical impact of compaction on the powdered formulations, for example cracking and fracturing of the particles after compression. Visible imaging can be used with complementary approaches such as atomic force microscopy (AFM) and scanning electron microscopy (SEM) (De Boer et al., 1978) to provide information about the surface characteristics. AFM is particularly useful for collecting highly spatial resolved information about the topography of the surface of the tablet (Hooton et al., 2004, Danesh et al., 2000). The use of AFM can be challenging for dynamic processes, such as the study of dissolving tablets because of the proximity or contact required between the tip of the AFM and the sample can mean that the tip can potentially be damaged *in situ*.

However, because powders are often visually indistinguishable once mixed, it is challenging to gain any chemical information about the components from visible images. Vibrational spectroscopy is a powerful method to reveal and identify the different components within a pharmaceutical formulation based on the molecular vibrations of the chemical structure. Therefore, a number of spectroscopic imaging approaches that utilise vibration spectroscopy have been applied to monitor dissolving tablets. These include Fourier transform infrared (FTIR) spectroscopic imaging, near-IR imaging and Raman mapping, all of which have been useful for the analysis of pharmaceutical tablets (Šašić and Ozaki, 2010, Clarke et al., 2001). One of the most significant advantages of using these imaging approaches is that spatial information of the different components can be revealed in the samples. Moreover, acquiring data as a function of time allows the behaviour of the materials to be monitored. Hence, physical changes such as crystallisation can be detected.

The aim of this project is to utilise macro FTIR spectroscopic imaging for the investigation of different pharmaceutical formulations. This approach has been proven as a viable tool for studying pharmaceutical tablets in aqueous solutions. The fundamental principles of FTIR spectroscopy and spectroscopic imaging will be introduced and discussed in the following Section.

2.5 Fourier transform infrared spectroscopy: principles and applications

IR spectroscopy has become an integral analytical technique in research and development laboratories today. The versatility of this approach in terms of the range of sampling methodologies possible for data acquisition means that almost any pharmaceutically relevant sample can be studied. Powders, solids, pastes and liquid solutions can all be probed and chemically specific information about the samples will be revealed.

Significant developments in the instrumentation have been realised since the commercialisation of dispersive infrared spectrometers in the 1940s, particularly Fourier-transform instruments. FTIR spectroscopy has allowed faster accumulations of high-quality infrared spectra. An FTIR spectrometer includes a Michelson interferometer that typically contains three components: a fixed mirror, a moving mirror, and a beam splitter. A schematic diagram of an interferometer is shown in Figure 2.5. The infrared radiation is directed towards the beam splitter where it is divided equally. Half of the radiation continues towards the fixed mirror and the other half towards the moving mirror. Upon reflection from the mirrors, which are arranged perpendicular to one another, the radiation recombines at the beam splitter. At this point, an interference pattern is generated due to the varying pathlength

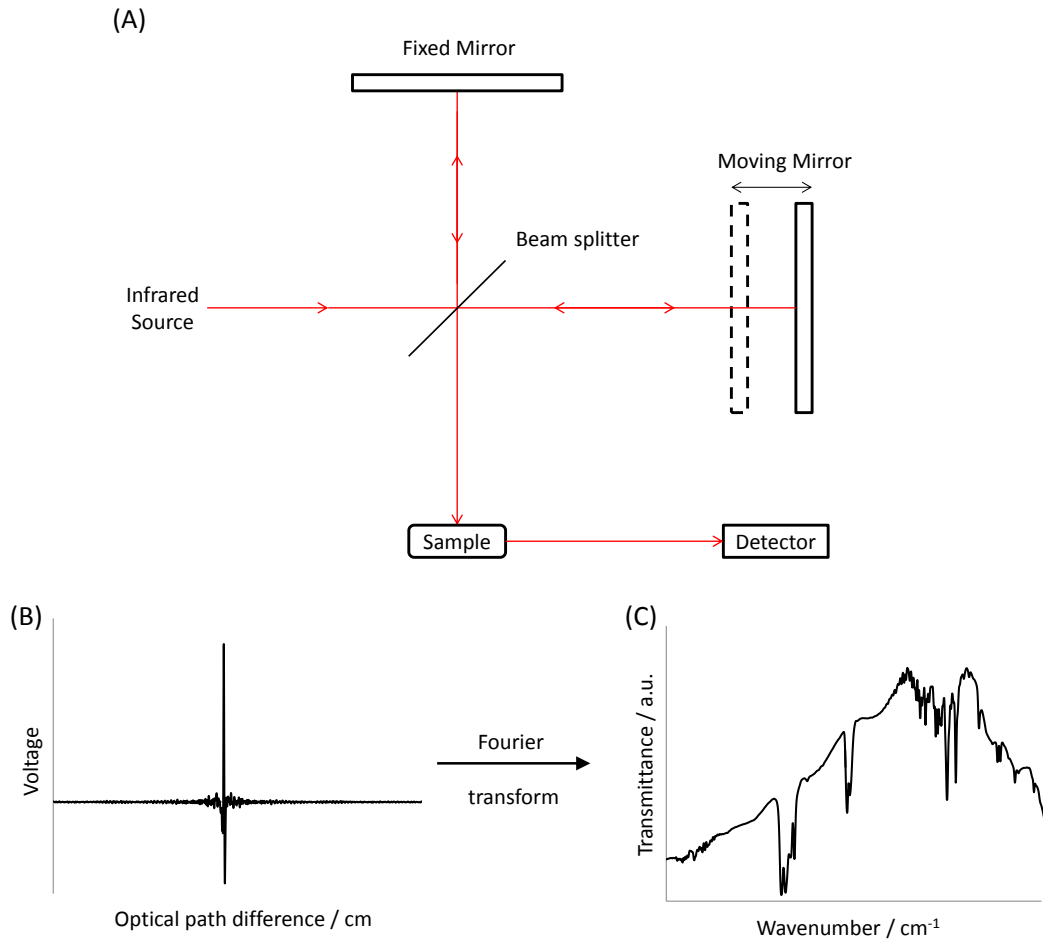


Figure 2.5 – (A) Schematic diagram of the Michelson interferometer. (B) and (C) show an example of a measured interferogram and single beam spectrum recorded using an FTIR spectrometer, respectively.

of the beam, brought about by the moving mirror, where both constructive and destructive manners of interference can be observed. An interferogram will be produced as a plot of beam intensity as a function of pathlength (Figure 2.5). The mathematical process of converting the interferogram into an IR spectrum is obtained by using the Fourier transform algorithm.

FTIR spectrometers use a single beam of radiation. Thus, in order for a spectrum to be produced the recorded sample measurement must be ratioed against a background scan. The background scan is simply used to remove any information and spectral features that result from the instrumentation or the environment e.g. water vapour in the atmosphere. A transmittance (T) spectrum can be calculated by Equation 2.2 where I and I_0 are the intensity of a measurement with and without the sample, respectively.

$$T\ (\%) = \frac{I}{I_0}$$ **Equation 2.2**

It is common for an FTIR spectrum to show the absorbance values instead of transmittance since this is useful for quantitative analysis. The absorbance (A) is the negative log of the transmittance (Equation 2.3). Herein, FTIR absorbance spectra will be presented.

$$A = -\log_{10} T$$ **Equation 2.3**

2.5.1 Fundamental background

Spectroscopy is defined as the analysis of radiation emitted, absorbed or scattered by atoms or molecules. Moreover, IR spectroscopy is the study of the absorption of radiation from the IR region of the electromagnetic spectrum. In absorption spectroscopy, a photon from the incident radiation source excites a molecule to undergo a transition from its ground energy state, E_1, to a higher energy state, E_2. The energy of this absorbed photon is indicative of the frequency, ν, of the radiation and is given by the Bohr frequency condition (Equation 2.4).

$$h\nu = |E_1 - E_2|$$ **Equation 2.4**

Where h is Plank's constant (h = 6.62 × 10^{-34} J.s^{-1}) and E_1 and E_2 are the energies of the two states over which the transition occurs. This relationship is often expressed in terms of wavelength, λ, and is determined by Equation 2.5, where c is the speed of light (c = 2.997 × 10^8 m.s^{-1}).

$$\lambda = \frac{c}{\nu}$$ **Equation 2.5**

Since the frequency is directly proportional to the energy of the photon, it is very common that the units of infrared radiation to be reported and displayed using wavenumber, $\bar{\nu}$. The wavenumber of the radiation is defined by the number of complete wavelengths in a given distance (Equation 2.6) and conventionally reported in reciprocal centimetres (cm^{-1}).

$$\bar{\nu} = \frac{\nu}{c} = \frac{1}{\lambda}$$ **Equation 2.6**

The electromagnetic spectrum is shown in Figure 2.6. The IR region lies between 13000–10 cm^{-1}. IR radiation can be categorised into three different regions in the electromagnetic spectrum: near-IR (13000–4000 cm^{-1}), mid-IR (4000–400 cm^{-1}), and far-IR (400–10 cm^{-1}).

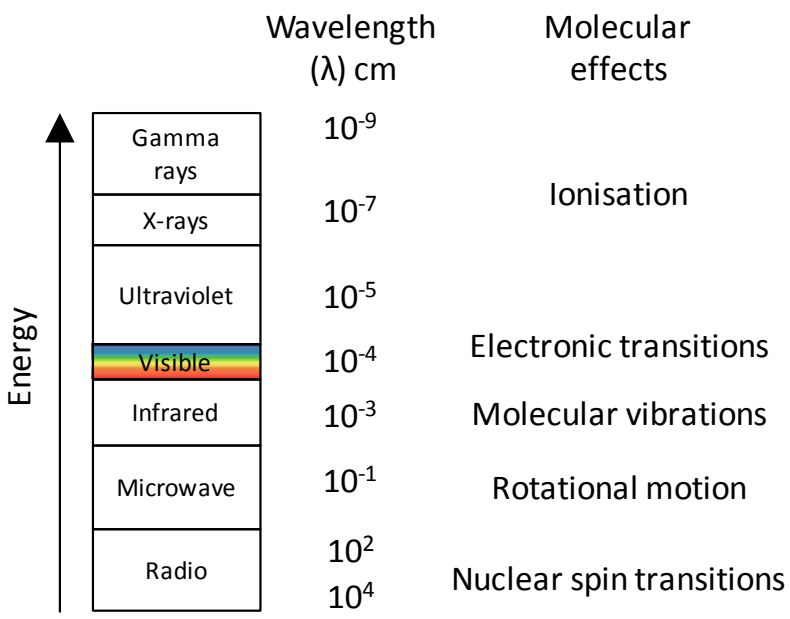


Figure 2.6 – Diagram of the electromagnetic spectrum.

These are named with respect to their proximity to the visible region in the electromagnetic spectrum, i.e. near-IR falls close to the visible region. Each of these regions can be utilised for spectroscopic studies. However, in this work mid-IR spectroscopy was used because it measures the fundamental vibrational transitions of molecules. In comparison, near-IR spectroscopy is used to study the molecular harmonics and overtones and far-IR spectroscopy is employed for the study of rotational modes.

All of the bonds in molecules have the potential to vibrate and excitation of these molecular vibrations can occur upon absorption of mid-IR radiation. Absorption of IR light happens when the frequency of the incident IR radiation corresponds to the frequency at which the chemical bonds are vibrating. Molecules typically of interest to the pharmaceutical field, for example, the APIs and the excipients can have a large number of different vibrational modes. These modes can involve a broad range of different vibrations that include periodic stretching, bending and twisting of the chemical bonds, as well as swelling, shrinking and buckling of aromatic rings if they are present in the molecule. The number of the vibrational degrees of freedom (i.e. vibrational modes) can be determined for linear molecules by $3N - 5$ and for non-linear molecules by $3N - 6$, where N is the number of atoms within the molecules.

The relationship between the type of chemical bond and the frequency of infrared radiation that is absorbed provides information about the chemical structure (Atkins and de

Paula, 2005). Thus, the IR spectrum reveals characteristic group frequency regions that are related to Hooke's law (Equation 2.7).

$$\nu = \frac{1}{2\pi}\left(\frac{k}{\mu}\right)^{\frac{1}{2}} \qquad \left(\mu = \frac{m_A m_B}{m_A + m_B}\right) \qquad \textbf{Equation 2.7}$$

Where v is the vibrational frequency, k is the bond force constant and μ is the reduced mass of a diatomic molecule. The vibrational motion within this bond is quantised and molecules exist as anharmonic oscillators (i.e. bonds can break and cannot be compressed beyond a certain point). Equation 2.7 suggests that the vibrational frequency is dependent upon the atomic mass of the diatomic molecule and the strength of the bond. Therefore, the vibrational frequency (v) of a chemical bond will appear at a characteristic, or 'fingerprint', region in the IR spectrum (Atkins and de Paula, 2005).

Not all vibrational modes within molecules are IR active. The selection rule for vibrational spectroscopy is that there must be a possible change in the dipole moment of the molecule. Thus, homonuclear diatomic molecules, such as N_2 and O_2, are described as IR inactive since the stretching mode of these molecules does not induce a change in dipole moment. If we consider the molecular vibrations for CO_2, it is observed that there are only two bands in the recorded IR spectrum. The appearance of these two spectral bands can be explained by considering the four vibrational modes of CO_2 (Figure 2.7). For the symmetric stretch of CO_2 there is no change in dipole moment and consequently, this does not appear as a band in the IR spectrum. In contrast, the asymmetric stretch (2335 cm^{-1}) and bending modes (667 cm^{-1}) do express a change in dipole moment so are revealed in the spectrum. The two bending modes of CO_2 are degenerate, i.e. absorb at the same frequency, however, this band can be observed to split into two peaks when CO_2 is interacting with other functional groups (Kazarian et al., 1996).

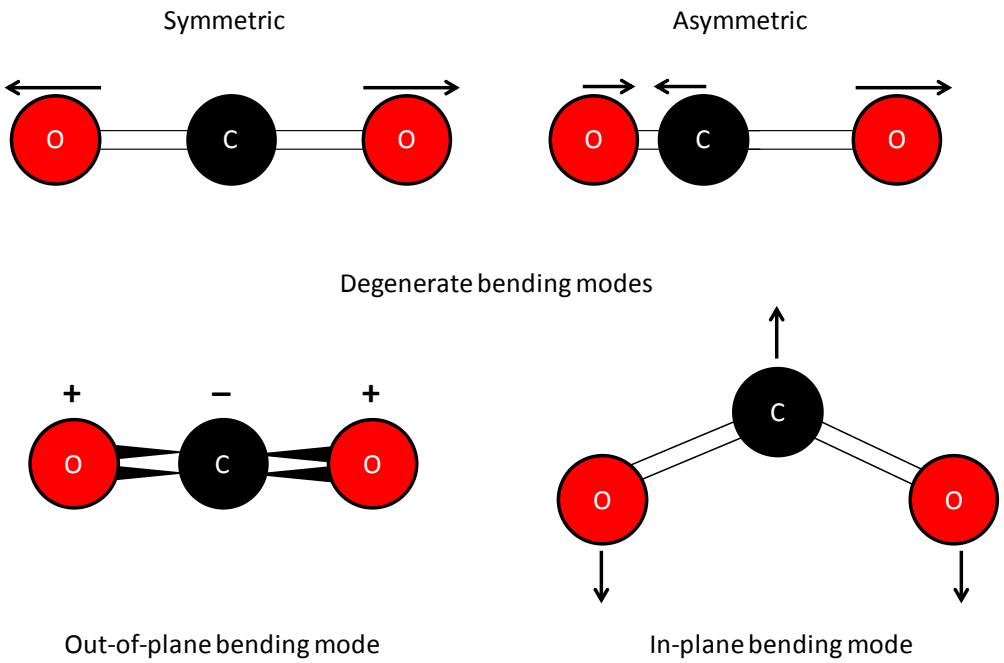


Figure 2.7 – Schematic diagram of the four different molecular vibrations of carbon dioxide. The "+" and "-" represent the atoms moving forwards and backwards perpendicular to the plane of the diagram of the out-of-plane bending mode.

2.5.2 Transmission mode

Transmission mode measurements are based on the absorption of particular wavelengths of IR light as it passes directly through a sample (Figure 2.8). The information is displayed in the IR spectrum, that is, absorbance as a function of frequency that reveals the characteristic bands within the sample. This sampling mode is so widely adopted because the apparatus is relatively inexpensive, straightforward to use and spectra collected have a good signal-to-noise ratio (SNR). Furthermore, it is possible to study solid, liquid or gaseous samples using transmission mode measurements. In this Section, transmission measurements of liquid and solid samples will be discussed as they are relevant to the work undertaken in this thesis.

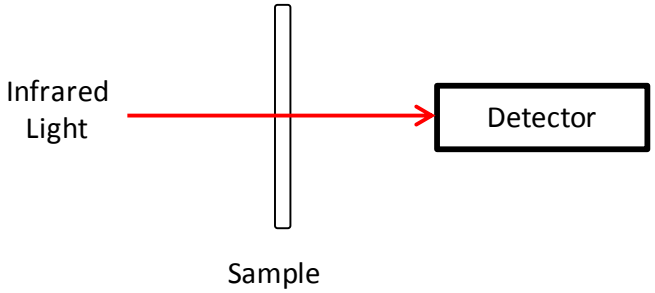


Figure 2.8 – Schematic representation of transmission mode experimental setup for FTIR measurements.

It should be realised that the sample, in any state, has to be prepared so that it is thin enough for the IR radiation to pass through and a typical thickness can range between 5–50 μm. Usually, for liquids and aqueous solutions, transmission cells with a fixed pathlength will be used. These consist of two IR transparent windows that are separated by a spacer of a known pathlength. The cavity between the windows can be filled with the solution and measured. However, careful consideration must be taken when selecting the solvents used to prepare the solutions and the materials for the IR windows. For example, sodium chloride is IR transparent, inexpensive and commonly employed but dissolves in water. Moreover, water has a strong absorbance of IR radiation that can overlap with potential spectral bands of interest in the sample. Hence, a small pathlength is needed to avoid saturation in such measurements.

Several different approaches can be employed for the measurement of solid samples using transmission FTIR spectroscopy. Firstly, the solid sample can be mixed with an IR transparent material in its powdered form and then compacted into pellets. For example, mixing a sample with potassium bromide will result in an IR transparent pellet that can be analysed. Preparing a suspension of the solid in a Nujol mull can also allow one to record IR spectra in transmission mode. Here, a small amount of sample is ground with Nujol (liquid paraffin) to make a paste that is deposited on IR transparent windows. However, when using both of these approaches, it is essential to grind and mix the two materials thoroughly and the measured sample must not be too thick. The spectra recorded can sometimes be distorted by scattering effects that are caused when the solid particles are larger than that of the wavelength radiation. Finally, thin films of the sample can be cast, usually by melting or solvent evaporation. Again, the selection of the solvent has to be carefully considered. Also, if preparing the films using a melting method, then physical effects such as thermal degradation can occur in the sample.

As a result, transmission mode is not the most suitable for the study of dissolving pharmaceutical tablets that have a large thickness and require the use of aqueous solutions. Nevertheless, FTIR spectroscopy in transmission mode has been used to study thin samples such as biological tissues (Kazarian and Chan, 2013a, Colley et al., 2004) and films (Krafft et al., 2006).

2.5.3 Attenuated total reflection mode

Attenuated total reflection (ATR) mode works based on the phenomenon of total internal reflection occurring at the interface between an ATR crystal and sample (Figure 2.9). The

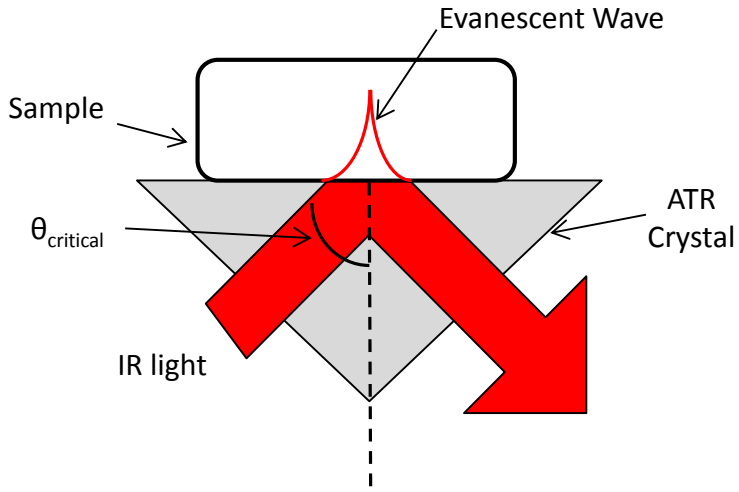


Figure 2.9 – Schematic diagram showing the principle of attenuated total reflection mode.

crystal has to have a higher refractive index than the sample and the IR radiation must enter the crystal at an angle greater than the critical angle (θ_c). When these criteria are fulfilled the IR beam penetrates beyond the surface of the ATR crystal and hence, if in close enough proximity, into the sample. Typically the depth of penetration of the IR light is only a few micrometres and is in the form of an evanescent wave.

The depth of penetration, d_p, of the IR beam beyond the surface of the ATR crystal is defined as the distance the electric field travels into the sample before its amplitude falls to e^{-1} of its original surface value. The value of d_p can be calculated from Equation 2.8. Where, λ is the wavelength of radiation, n_1 and n_2 are the refractive indices of the sample and crystal respectively, and θ is the angle of incidence. The depth of penetration is wavelength dependent.

$$d_p = \frac{\lambda}{2\pi n_1 \left(sin^2\,\theta - \left(\frac{n_2}{n_1}\right)^2 \right)^{0.5}} \qquad \textbf{Equation 2.8}$$

Similarly to transmission mode, samples in their solid, liquid or gaseous states can be recorded. Measurement of a sample in ATR mode does not require any complicated preparation but ensuring that sufficient contact is made between the ATR crystal and sample is a prerequisite to achieve high-quality spectra. Any space or void larger than the depth of penetration can result in no data acquisition in these areas and consequently a low-quality spectrum.

There are a range of materials commonly utilised for making ATR crystals; these include diamond, zinc selenide (ZnSe), germanium, silicon and thallium iodide. The choice of the

crystal is crucial when studying a system by ATR-FTIR spectroscopy as each has unique properties (Stuart, 2004). Both diamond and ZnSe crystals have been used for the experimental work undertaken in this thesis. Hence, the properties of these two crystals will be compared. Diamond is a versatile choice of crystal because it is chemically inert, with respect to most acids and alkalis, can tolerate high temperatures and pressures and is very hard. As a result, a diamond crystal can withstand high compression forces without damage. Thus, diamond is the ideal choice of crystal for *in situ* compaction studies (van der Weerd et al., 2004) and high-pressure investigations (Kazarian and Martirosyan, 2002). One drawback of using a diamond crystal is that they are usually relatively small in size due to the cost and ease of production. The measured area is 2×2 mm^2 that means that only a small amount of sample is studied. In contrast, ZnSe is comparatively inexpensive and can be made into much larger crystals. For example, the measured surface of a ZnSe crystal specifically designed to work with expanded optics for ATR-FTIR spectroscopic imaging is 26×19 mm^2 in size (Chan and Kazarian, 2006b). Despite these advantageous properties, ZnSe is brittle and more easily damaged in the presence of strong acids and bases or by scratching with a hard material.

2.5.4 External reflection mode

Finally, it is possible to record IR measurements by measuring the radiation that is externally reflected from the surface of the sample. Two different modes of external reflection can be used, specular and diffuse reflection. External reflection is most useful for investigating the surfaces of samples (Stuart, 2004).

Specular reflection happens when the reflected angle of the IR beam is coincident with the angle of incidence. Thus, specular reflectance is dependent upon the surface topography and the absorption properties of the sample, as well as the angle of incidence and the refractive index of the materials. In such measurements, the reflected radiation is usually low (less than 10 %) so the signal can appear weak compared to other measurement modes.

Diffuse reflection, widely referred to as DRIFT, measures the intensity of the beam that is reflected in many directions from the sample. Reflection at multiple angles occurs when the IR radiation penetrates beyond one or more of the particles of the sample. DRIFT is useful for the measuring powder samples (Brauns, 2014). The experimental setup of DRIFT employs a cell where reflection across a broad range of angles can be collected (Figure 2.10).

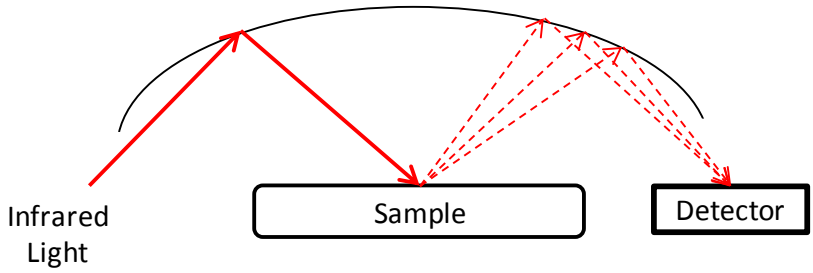


Figure 2.10 – Schematic diagram of the external reflection measurement setup.

2.5.5 General principles of quantitative analysis

One of the great advantages of FTIR spectroscopy is the ability to obtain quantitative data from the spectrum (Wurster et al., 1993, Black and Lovering, 1977). The Beer-Lambert law (Equation 2.9) describes the relationship between the concentration, c, of the sample and the absorbance, A, of the spectral band.

$$A = \varepsilon l c \qquad \textbf{Equation 2.9}$$

Where, A is the absorbance, ε is the molar absorptivity, l is the pathlength through the sample and c is the molar concentration. The absorbance can be determined from the FTIR spectrum by either measuring the height of the peak of the spectral band or calculating the area under the band of interest.

When applying FTIR spectroscopy in transmission mode, the pathlength is simply that given by sample thickness. However, in ATR mode the pathlength (l) can be replaced with the term effective thickness (d_e). The effective thickness is defined as the equivalent thickness of a material that would result in an identical absorbance of the IR beam in a transmission mode measurement to that acquired in ATR mode. In the case of using non-polarised light, the effective thickness is determined from Equation 2.10 (Chan and Kazarian, 2007, Harrick and du Pré, 1966). Where n_1 is the refractive index of the sample, n_2 is the refractive index of the crystal and θ is the angle of incidence of infrared light.

$$\frac{d_e}{\lambda} = \frac{\frac{n_2}{n_1} cos\theta \left[3\, sin^2\,\theta - 2\left(\frac{n_2}{n_1}\right)^2 + \left(\frac{n_2}{n_1}\right)^2 sin^2\theta\right]}{2\pi \left(1 - \left(\frac{n_2}{n_1}\right)^2\right)\left[\left(1 + \left(\frac{n_2}{n_1}\right)^2\right) sin^2\theta - \left(\frac{n_2}{n_1}\right)^2\right]\left(sin^2\theta - \left(\frac{n_2}{n_1}\right)^2\right)^{0.5}}$$

Equation 2.10

2.5.6 FTIR spectroscopy to study pharmaceutical systems

FTIR spectroscopy can be used for the qualitative identification of compounds; hence, it is a powerful approach for determining the physical states of pharmaceutical materials. Assessing the physical properties of new drug candidates and formulations is especially useful during the developmental process. FTIR spectroscopy has proven a valuable tool to characterise polymorphism, differentiate between hydrates and anhydrates, and evaluate the stability of salts in pharmaceutical samples (Van Eerdenbrugh and Taylor, 2011, Bugay and Brittain, 2006a).

The crystalline state of the drug is often undesired as it typically dissolves slower than the amorphous form, a solid that does not exhibit the long-range order of a crystal, and, therefore, can impede dissolution. This phenomenon has been demonstrated using ATR-FTIR spectroscopy (Higuchi et al., 1969) and more recently with ATR-FTIR spectroscopic imaging (Kazarian and Chan, 2003), where dissolution behaviour of the drugs methylprednisolone and ibuprofen were studied, respectively. Features in the absorption bands, for example shifts in the peak to a different wavenumber, are visible in the acquired spectrum. More specifically, the formation of sodium benzoate from benzoic acid can easily be distinguished by the shift in the carbonyl band from 1678 cm^{-1} to 1595 cm^{-1}. In some cases, the changes between molecular structures can be more discreet, such as subtle changes in the intensity of a spectral band that appears at the same wavenumber during transformation (Bugay and Brittain, 2006a).

The widespread use of tablets as drug delivery systems to enhance the administration of poorly water-soluble drugs has led to significant research efforts exploiting the use of FTIR spectroscopy over the past few decades. Solid dispersion preparation methods have become increasingly popular to improve drug release since they maintain the drug in the amorphous state. A combination of vibrational spectroscopic techniques, FTIR and Raman spectroscopy, was used by Taylor and Zografi (1997) to determine the different polymorphs of indomethacin occurring in solid dispersions. The intermolecular interactions of the amorphous form were compared to the hydrogen bonded (H-Bonded) interactions characterised for the different crystalline polymorphs. The use of FTIR spectroscopy determined that amorphous indomethacin contains dimers that arise from H-bonding between the carboxylic acid groups. Coincidently, the crystalline gamma form displayed similar H-bonding characteristics but in different spatial arrangements. A follow-up study comparing amorphous indomethacin with the amorphous sodium form found that the characteristic peak for the carboxylic acid dimers was absent in the amorphous sodium form (Tong and Zografi,

1999). A possible explanation for the elimination of this peak was due to the electrostatic interactions between the ionised carboxylic acid group and the sodium ions. Additionally, it is of the utmost importance to determine all of the different polymorphic forms of drug candidates, particularly from a commercial point of view, since each polymorph form can be patented individually. As a result, companies that develop new APIs have a great interest in discovering all the possible molecular forms of drugs. Cases have been reported where industrial competitors have been able to use the same drug but in different polymorphic forms because of patenting issues (Cabri et al., 2007).

When exposed to certain environmental conditions, i.e. controlled humidity or aqueous environments, structural forms of the drug can exhibit different characteristics. Slower rates of dissolution, short stability times and degradation into other crystalline forms occur and can be detected using FTIR spectroscopy (Elkhider et al., 2007).

2.6 Fourier transform infrared spectroscopic imaging

The information recorded using a conventional FTIR spectrometer, i.e. with a single element detector, results in one spectrum that shows the average absorbance of the IR beam across the measured area. However, this method provides no spatial information about the samples. FTIR spectroscopic imaging has proven to be a valuable tool for the study of a range different samples (Amigo, 2010, Prati et al., 2010, Stavitski and Weckhuysen, 2010, Bhargava et al., 2006, Chan et al., 2003, Kazarian and Chan, 2003). This robust and reliable spectroscopic approach utilises a focal plane array (FPA) that is capable of measuring thousands of spectra from different regions of a sample at the same time. The FPA detector can be used to measure data from different array sizes, up to 128 × 128 pixels, depending upon the nature of the measurements and measurement mode being used. The pixels are arranged in a grid formation that simultaneously collects a full IR spectrum (4000–900 cm^{-1}) from all of the regions in the measured sample (Figure 2.11). For example, a measurement set up to use 64 × 64 pixels records 4096 individual spectra during each scan. The physical size of each pixel in the FPA detector is ~40 × 40 μm^2.

FTIR spectroscopic imaging can reveal the spatial distribution of selected components in the measured area. Spectroscopic images are generated by plotting the distributed absorbance of carefully selected absorption bands across all of the measured pixels. Hence, regions of high and low concentration of the components can be determined in the resulting images. The schematic diagram shown in Figure 2.11 shows an example of a compacted tablet where spectroscopic images of the drug and the polymer have been generated. One of the initial

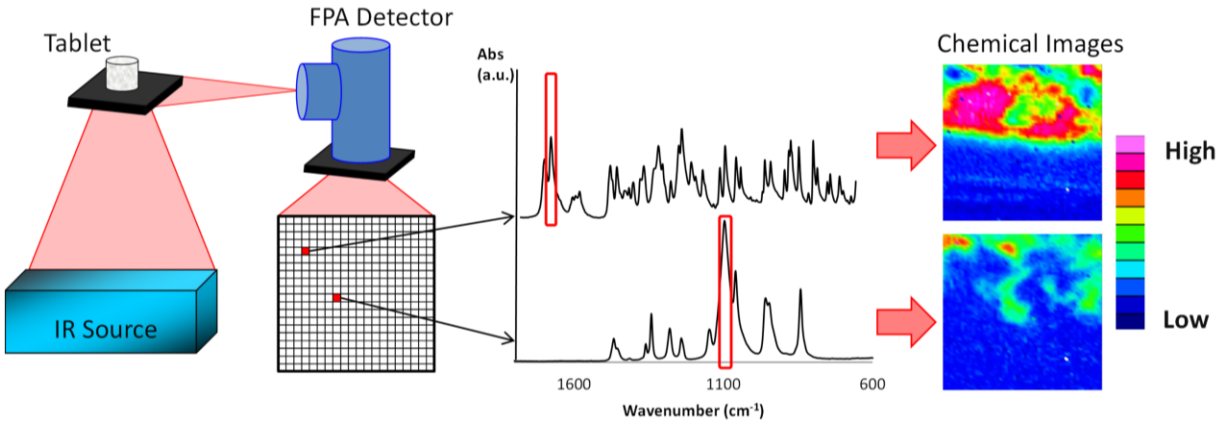


Figure 2.11 – Schematic diagram of an ATR-FTIR spectroscopic imaging setup.

pioneering research articles demonstrating the use of FTIR spectroscopic imaging investigated the release of an API from pharmaceutical formulations (Chan et al., 2003). This work utilised ATR mode that allowed aqueous samples and thick tablets to be studied.

Before the advent of FTIR spectroscopic imaging, mapping approaches using single element or linear array detectors were used for collecting spectral data from different locations in a sample. Mapping using a single element detector requires the use of an aperture and a movable stage. However, this method is a very slow and laborious process and thus not applicable for assessing systems where changes occur rapidly. IR mapping using a linear array detector has proven much more efficient for collecting spatial information. There are both advantages and drawbacks of using this approach compared to imaging with an FPA detector, which are discussed in detail in the published articles (Kazarian and Chan, 2013a, Patterson and Havrilla, 2006).

2.6.1 Macro ATR-FTIR spectroscopic imaging

Macro ATR-FTIR spectroscopic imaging refers to an approach that records imaging data but without the use of microscope optics. Instead, the imaging accessories are placed in a large sample compartment that is attached to an FTIR spectrometer. The IR beam is directed through the spectroscopic imaging setup by a series of mirrors before data is recorded by the FPA detector. This Section focuses on the macro ATR-FTIR spectroscopic imaging since all of the experiments carried out in this work were acquired using this approach.

Two ATR accessories designed for FTIR spectroscopic imaging applications were used to obtain the data presented in this thesis: an Imaging Golden Gate accessory (Specac Ltd.) that was fitted with a diamond crystal and a VeeMax II variable angle accessory (PIKE

Technologies) that measured samples on a ZnSe crystal. The properties of these two accessories will be described in further detail.

Firstly, the Imaging Golden Gate accessory has been developed by Specac Ltd for specific use with an ATR-FTIR spectroscopic imaging system to record measurements in macro mode (Everall et al., 2009, Kazarian et al., 2009). The internal optics of the Imaging Golden Gate accessory are shown in Figure 2.12. This accessory measures a diamond crystal that is shaped like an inverted prism, where the top measuring surface is 2×2 mm^2. The results presented in this thesis when using the Imaging Golden Gate accessory, measured 64×64 pixels of the FPA detector. Spectroscopic images with dimensions of 0.64×0.53 mm^2 and a spatial resolution between 10 to 15 µm were recorded when using this accessory. This ATR accessory was shown to be useful to obtain information from the edge of tablets in contact with aqueous solutions.

It is realised that pharmaceutical tablets are often much larger than the image size recorded using the Imaging Golden Gate accessory. Therefore, when information about the whole tablet was required a VeeMax II ATR accessory was employed. This accessory used a crystal with a diameter of 20 mm. In this work, only the ZnSe crystal was used but this accessory also allows silicon and germanium crystals also to be used. The VeeMax II ATR accessory provides a much larger measuring area as the IR beam is not focused using a lens. Another, advantage of using this approach is that a larger pixel array size can be measured, for example, 96×96 or 128×128 pixels. However, this does come at an expense to spatial resolution. Hence, the image size in these measurements when using an array size of 96×96 and 128×128 is ~7.75×6.05 mm^2 and ~11.5×8 mm^2 respectively, but the spatial resolution

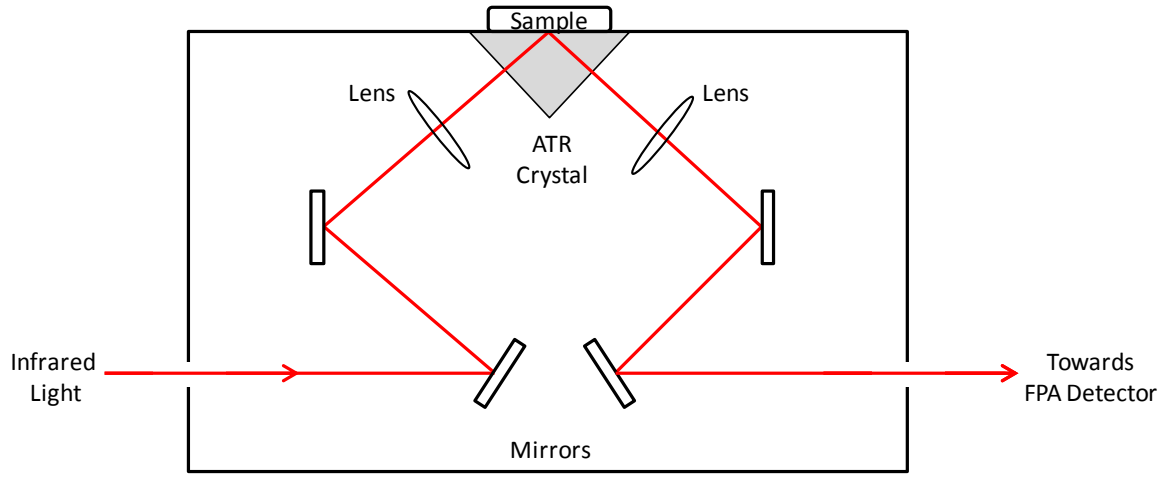


Figure 2.12 – Schematic diagram of the Imaging Golden Gate ATR-FTIR accessory showing the direction of the IR beam that is focused onto the ATR crystal by mirrors and lenses.

is 100 to 150 μm. Nevertheless, this ATR-FTIR spectroscopic imaging accessory is capable of measuring whole tablets (3 mm diameter) simultaneously (van der Weerd and Kazarian, 2004c, Kazarian and Chan, 2003).

From an experimental perspective, it is integral to obtain reliable information in the spectroscopic imaging data to avoid misinterpretation of the results. Due to the nature of the evanescent field generated using ATR-FTIR spectroscopic imaging, i.e. the relationship between the depth of penetration and the angle of incidence, there is the possibility of image artefacts appearing in the form of concentration gradients across the images (Kazarian and Chan, 2013a). Gradients can occur as a result of the angle of incidence not being uniform across the entire measured area caused by unaligned optics. Thus, because of subsequent effects to the absorbance, quantitative analysis is not consistent throughout the measured area. An example of a concentration gradient has been presented by Wessel et al. when measuring homogenous paraffin using an accessory with fixed mirrors (Wessel et al., 2009). However, a study of the same system, conducted by Kazarian et al., using a different imaging accessory showed that when the mirrors were adjustable and the optics could be aligned, no such gradient was observed (Kazarian and Chan, 2013a, Kazarian et al., 2009). Hence, aligning the optics before collection of data is essential to ensure that consistent and reliable quantitative information is collected (Chan et al., 2008a). It is realised that other accessories can be used to collect spectroscopic imaging data and the key information of these is summarised in Table 2.1.

Table 2.1 – Properties of the different ATR-FTIR spectroscopic imaging accessories.

Imaging accessory	Spatial resolution / µm (estimated)	Image size / mm × mm (using 64 × 64 pixel array)	Crystal material
Imaging Golden Gate (Specac Ltd)	10–15	0.64 × 0.53	Diamond
VeeMax II (PIKE Technologies)	100–150	5.5 × 4	ZnSe Germanium Silicon
Expanded field of view	500	21.5 × 15.4	ZnSe
Oil Analyser (Specac Ltd)	40	2.6 × 3.6	ZnSe Germanium Silicon

2.6.2 Micro FTIR spectroscopic imaging

Micro ATR-FTIR spectroscopic enables imaging studies from microscopic domains in the sample by combining the FTIR spectrometer with an IR microscope. Most of the ATR measurements recorded using a microscope use a hemispherical crystal. The spatial resolution can be improved up to four times by the use of a germanium crystal. The high refractive index of the crystal increases the numerical aperture (NA) and, as a result, the spatial resolution.

The NA is a determining factor for spatial resolution of the system and is described by the Rayleigh criterion (Equation 2.11). Where r is the distance required to resolve two points, λ is the wavelength of radiation and NA is the numerical aperture.

$$r = \frac{1.22\lambda}{2NA} \qquad \textbf{Equation 2.11}$$

Chan and Kazarian reported that the use of a germanium crystal combined with an IR microscope improves the spatial resolution of the system, demonstrated by obtaining a resolution of at least 4 µm when using IR light with a wavelength of 6 µm (Chan and Kazarian, 2003).

The fact that micro ATR-FTIR imaging has a higher spatial resolution comes at an expense to the field of view. The size of the recorded images using this approach is

~0.06 × 0.06 mm^2 (or 60 × 60 μm^2). The small image size is a consequence of the effects on the NA of the system. That is, when focusing the IR beam in a microscope, the NA is increased since the area recorded from each pixel of the FPA detector is reduced (Chan and Kazarian, 2006b). The relatively small imaging area results in images with a higher spatial resolution when using micro ATR-FTIR spectroscopic imaging that has been successfully applied to a range of different samples. For example, to study human hair (Chan et al., 2005b, Sommer et al., 2001), live and dead cells (Chan and Kazarian, 2013a) and tissue diagnostics (Baker et al., 2014, Walsh et al., 2012).

2.6.3 General applications of ATR-FTIR spectroscopic imaging

ATR-FTIR spectroscopic imaging has been used to study a variety of different samples across a range of fields (Lewis et al., 1995). Polymeric materials have been extensively investigated with an interest in the stability and degradation, *in situ* dissolution studies, diffusion and release of individual components from these formulations (Koenig and Bobiak, 2007, Gupper and Kazarian, 2005, Gupper et al., 2002, Koenig, 1998). Research and development of polymers are of great importance due to the vast amount of materials that use polymer technologies. Polymeric materials are also used in many pharmaceutical products, whether they are used for the packaging or as added excipients. In the work presented here, there is interest in polymers that are added to pharmaceutical delivery methods, namely compacted tablets. The polymeric substances can also be modified to change and influence the release of a drug from the formulation, for example, varying the molecular weight, adding chemical branches or substituting functional groups can change the properties and subsequently affect drug release. ATR-FTIR spectroscopic imaging has been used as a tool to study the effects of polymer on drug release for many different formulated tablets over recent years (Kimber et al., 2013, Wray et al., 2011).

Furthermore, ATR-FTIR spectroscopic imaging has also been applied to study a range of systems that are outside the scope of this project. These include biological samples (Sroka-Bartnicka et al., 2015, Kazarian and Chan, 2013a, Kazarian and Chan, 2006a) such as skin cells (Zhang et al., 2011, Chan et al., 2008b, Chan and Kazarian, 2003), arteries (Palombo et al., 2009, Colley et al., 2004), cancer cells (Kuimova et al., 2009) and proteins (Boulet-Audet et al., 2015, Glassford et al., 2012b, Glassford et al., 2012a). As well as applying ATR-FTIR spectroscopic imaging to investigate latent fingerprints (Ricci et al., 2007a), artwork (Spring et al., 2008) and photograph (Ricci et al., 2007b) conservation, petroleum heat-exchanger

disposition (Gabrienko et al., 2015b, Gabrienko et al., 2015a, Tay and Kazarian, 2009) and the effect of high pressure CO_2 on polymers (Fleming et al., 2004).

2.7 Applications of macro FTIR spectroscopic imaging of pharmaceutical systems

This Section will review previous work that has provided a platform for the research undertaken in this thesis. The macro FTIR spectroscopic imaging system setup for measurements in both transmission and ATR sampling mode for the study of pharmaceutical systems will be discussed. Also, the use of macro ATR-FTIR spectroscopic imaging for *in situ* studies of dissolving tablets and drug release will be introduced. The ability of using this spectroscopic imaging approach to resolve the spatial distribution of the different species in tablet compacts has provided new insight into the behaviour of drug release from dissolving tablets.

2.7.1 Transmission-FTIR spectroscopic imaging

As described in Section 2.5.2, the IR beam has to pass through the whole sample for transmission measurements to be recorded. Hence, the thickness of the sample is a major factor that has to be considered before using this approach and during sample preparation. In addition, when measuring samples by transmission-FTIR spectroscopic imaging, the images generated will represent the average information from the entire thickness of a sample. The possibility exists that this can result in misleading images (Kazarian and Chan, 2006b). For example, two overlapping particles could give the impression of one larger particle in the spectroscopic images. As a result, careful preparation of the sample, i.e. thickness must be no larger than the particle size, would be needed to ensure that such problems are avoided. The high absorptivity of water (H_2O) was also highlighted to be problematic for the study of drug release systems by transmission-FTIR spectroscopic imaging (Coutts-Lendon et al., 2003). For successful dissolution experiments, deuterated, or "heavy", water (D_2O) had to be used as an alternative solvent. Thus, transmission-FTIR spectroscopic imaging has limited applications for the study of real tablet systems because samples may have to be microtomed and also aqueous media may disrupt the quality of the spectral data recorded. In contrast, ATR-FTIR spectroscopic imaging has proven effective to study aqueous systems. The relatively shallow depth of penetration of the evanescent wave into the sample means that aqueous species or thick samples can be measured without saturation of the IR light.

Nevertheless, transmission-FTIR spectroscopic imaging has successfully been used for investigation of a range of pharmaceutical applications (Chan et al., 2007a). The effect of temperature and humidity on drug polymorphism was studied in a high-throughput manner where many formulations were monitored simultaneously. The model pharmaceutical formulations were composed of nifedipine and nitrendipine in different weight ratios. Spectroscopic images were recorded as a function of time to analyse the behaviour of the different samples subjected to a controlled environment. The results showed that the onset of crystallisation of the nifedipine occurred faster in certain molar ratios when exposed to conditions of 40 °C and 90 % relative humidity (Chan et al., 2007a). This work was one of the first articles to report an approach that studied many samples at the same time using macro FTIR spectroscopic imaging. Other research groups later adopted a similar approach for studies of tablets using near-IR imaging (Shinzawa et al., 2011, Shinzawa et al., 2009b).

More recently, microfluidic devices have been studied using transmission-FTIR spectroscopic imaging (Kazarian, 2007). These work by creating channels by depositing wax droplets on an IR transparent window and enclosing using a second window. A spacer is used to separate the windows. Microfluidic devices prepared in this way have been demonstrated to be able to study laminar flows of two liquids, H_2O and PEG (mw: 200 $g.mol^{-1}$), within the channels (Chan et al., 2010). Significantly, spectroscopic images can be recorded with rapid acquisition times have been used to generate “chemical movies” of segmented flows (Chan et al., 2011).

2.7.2 ATR-FTIR spectroscopic imaging of drug release

The use of ATR-FTIR spectroscopic imaging to study tablet dissolution and drug release was reported for the first time over a decade ago (Chan et al., 2003, Kazarian and Chan, 2003). Kazarian and Chan presented pioneering results upon which many studies of different pharmaceutical systems have been developed. A ZnSe crystal was employed for imaging formulations containing PEG and ibuprofen. In order to achieve good contact between the sample and the measuring surface of the crystal, the materials were melted together and applied directly as a film onto the crystal. To investigate drug release, a chamber capable of containing water was prepared by covering the crystal with a glass slide separated by a rubber spacer. This dissolution cell was filled with water and ATR-FTIR spectroscopic data were recorded during the experiment. This research produced a number of key results, such as characterising simultaneous release of the polymer and a model water-soluble drug in solution. This result is indicative of a mechanism where the API is released via polymer

dissolution as opposed to diffusion through the swelling polymer. Furthermore, structural changes of ibuprofen from the molecularly dispersed form to a crystalline structure were determined which subsequently reduced the rate of drug release.

Molecular dispersions of the drug within the polymer matrix were of interest for the preliminary studies using this spectroscopic approach since it is believed that formulations of this type facilitate dissolution of poorly soluble drugs (Kazarian and Chan, 2003, Chiou and Riegelman, 1971). The model ibuprofen/PEG formulations investigated were prepared to utilise a supercritical fluid impregnation approach (Kazarian and Martirosyan, 2002, Kazarian, 2002, Cooper et al., 1993). Initially, the spectroscopic images showed that there was no presence of crystalline ibuprofen detected in the measured formulation. However, when water was added to start the dissolution process, accumulation of drug was observed around the edges of the tablet (Kazarian and Chan, 2003). During the experiment, it was determined that crystallisation of the drug continued to occur and dissolution of the drug was prevented.

The behaviour of the release of a drug from materials where the API has been entrapped within cyclodextrins has also been investigated (Kazarian and Chan, 2003). ATR-FTIR spectroscopic imaging was applied to study the dissolution of ibuprofen/cyclodextrin formulations in differing weight ratios of the components. Crystallisation of ibuprofen was not observed in any of the formulations below a 1:1 weight ratio of components.

Overall, the preliminary investigations of pharmaceutical systems using ATR-FTIR spectroscopic imaging opened up opportunities to research drug release from a range of model systems (van der Weerd and Kazarian, 2004b, van der Weerd and Kazarian, 2004c, Chan and Kazarian, 2005, Chan et al., 2005a, van der Weerd and Kazarian, 2005). Subsequent research was conducted that validated ATR-FTIR imaging as a novel approach to study drug release from a polymer matrix, including under flowing conditions (van der Weerd and Kazarian, 2004b, van der Weerd and Kazarian, 2004c).

Furthermore, macro ATR-FTIR spectroscopic imaging has been reported in the application of high-throughput screening studies. Investigation of the stability of ibuprofen in many different formulated samples in a single experiment have been assessed under humid conditions (Chan and Kazarian, 2005). Also, drug crystallisation was detected in the different model formulations of nifedipine and PEG (Chan and Kazarian, 2004). On addition of water to the system, crystallisation of the nifedipine was characterised in the spectroscopic images. Interestingly, in this experiment, there was some evidence of crystallisation occurring in

regions where water had not been added. It was suggested that water vapour present in this experimental chamber initiated this crystallisation.

2.7.3 Recent development of ATR-FTIR spectroscopic imaging for samples under flow

The initial developments of ATR-FTIR spectroscopic imaging for studying drug release have been discussed. However, these experimental setups have focused on the behaviour in static conditions. Hence, there was an avenue for developing an experimental setup that allowed for flowing conditions to be investigated. A custom designed compaction and dissolution cell was manufactured to study tablet compacts (van der Weerd et al., 2004). This innovative cell, shown in Figure 2.13, was intended to be used directly with an Imaging Golden Gate ATR accessory (van der Weerd et al., 2004). This demonstrated the use of this cell for *in situ* compaction and dissolution of HPMC formulated with caffeine, used as a model API. For the first time, the effect of the continuous flow of solution during the experiment was investigated. The properties of HPMC are that swelling will occur upon contact with the solution, thus, the mechanism of drug release when using this polymer was determined to be one of diffusion of caffeine through the polymer matrix.

Moreover, the introduction of the flow-through cell not only prevented saturation of dissolved species in the cell but also meant that additional information could be collected in parallel. For example, data were collected simultaneously using a combination of ATR-FTIR

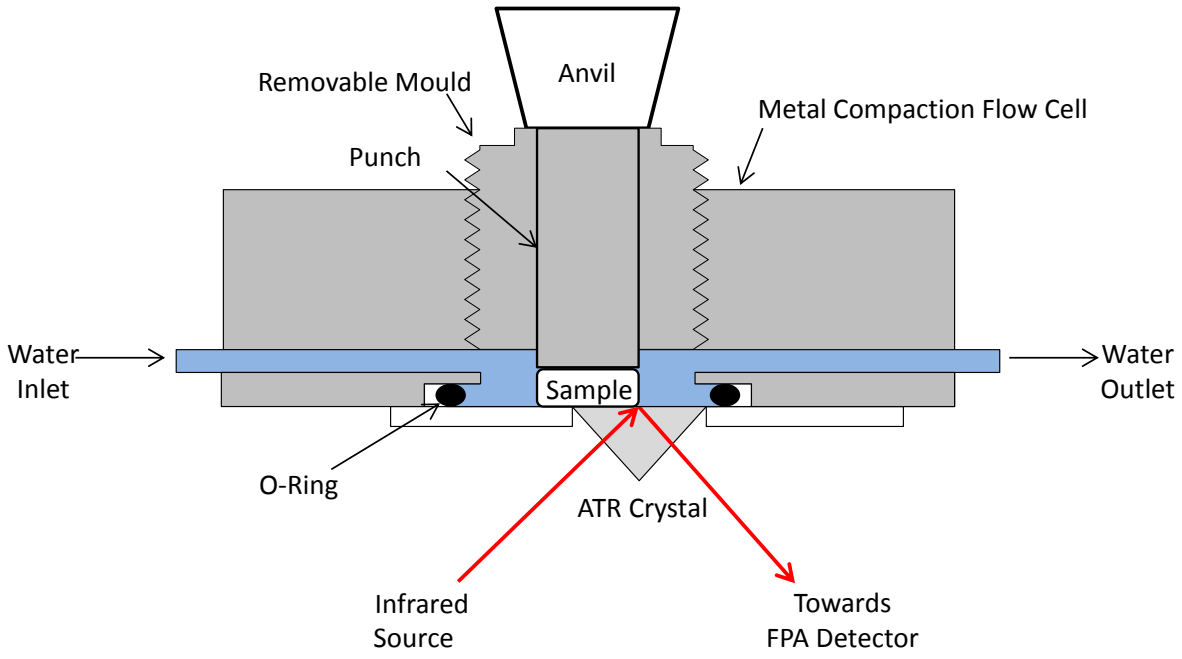


Figure 2.13 – Schematic diagram of the metal compaction and dissolution cell that can be attached to an Imaging Golden Gate ATR accessory for *in situ* measurements.

spectroscopic imaging and UV detection. Hence, the amount of drug dissolved as a function of time was recorded by UV as well as spatial profiles from the imaging data (van der Weerd and Kazarian, 2004b). Correlations were established based on the observed trends between the concentration profiles of nicotinamide in both the ATR-FTIR spectroscopic images and UV dissolution profiles. In addition, the UV data recorded were compared with conventional USP testing apparatus, again showing similar dissolution rates of the drugs. One of the main advantages of using ATR-FTIR spectroscopic imaging was demonstrated in subsequent work (van der Weerd and Kazarian, 2005). Detection of the drug in different structural forms and precipitation of the dissolving tablets was observed in the ATR-FTIR spectroscopic images. However, it is not possible to characterise these changes directly when using UV methods, including USP testing.

The drug release can be predicted by simulating tablet dissolution behaviour with mathematical modelling. Validation of modelling data for predicting drug release has been experimentally tested with the use of ATR-FTIR spectroscopic imaging (Kimber et al., 2013). The dissolution of pharmaceutical tablets was investigated using ATR-FTIR imaging with UV detection. These results were compared with those from the simulations. It was possible to extract physical properties of components such as diffusion coefficients that were used to optimise the design of formulations by predicting drug release.

Developments of the metal flow cell have been made that allow further insight about the dissolution and subsequent drug release from tablets. It is possible to collect visible images of the tablet at the same time as ATR-FTIR spectroscopic images and UV dissolution profiles (Kazarian and van der Weerd, 2008). A transparent Perspex flow cell was constructed that could be attached to the imaging accessories. Assignment of the dissolution front using visible imaging alone is not a highly informative way to study dissolution and ingress of the solution. Due to optical effects, the possibility exists for information to be misinterpreted (Kazarian and van der Weerd, 2008). For example, changes in the refractive index of the samples can result in different scattering properties that will be reflected in the visible images obtained. As a result of these investigations, three dissolution fronts were determined: true water, total gelification of the polymer and the erosion front. These were somewhat different to those initially estimated by Bettini et al. (2001) but consistent with the estimations by Gao and Meury (1996).

The pH microenvironments can affect the dissolution rate of pharmaceutical systems. Depending upon the nature of the materials, acidic or basic conditions can either facilitate or inhibit drug release (Velasco et al., 2011, Wray et al., 2011). There are cases where there is

crystallisation of the drug during dissolution that can cause irritation to the digestive system of a patient and in extreme cases cause stomach ulcers (Lanza et al., 1979). Hence, the necessity for this research is to find viable methods of avoiding crystallisation once administered to the patient. Wray et al. (2011) studied the dissolution of ibuprofen from HPMC polymer matrices and reported that it can be influenced by the addition of pH modifiers. This is due to the inherent weak acidity of ibuprofen, thus, adding basic compounds to the tablet matrix was expected to increase the solubility (Levis et al., 2003). Experiments confirmed that this was indeed the case because slow drug dissolution in acidic solution was observed. Conversely, when a buffer solution containing sodium carbonate was used the solubilisation of ibuprofen increased due to the formation of sodium salts *in situ*. This research was the first time that ATR-FTIR spectroscopic imaging had been used to characterise the formation of sodium salts during the dissolution process, arising from the changing the pH microenvironment (Wray et al., 2011). Effects of pH-sensitive hydrogels on crystallisation of ibuprofen during dissolution of formulations were also studied by ATR-FTIR spectroscopic imaging, where successful prevention of ibuprofen crystallites has been demonstrated (Velasco et al., 2011).

Finally, the most recent developments utilising this spectroscopic approach have focused on the study of tablets that contain more than one API. Novel formulations of bilayer tablets (Wray et al., 2014) and tablet-in-tablet (Wray et al., 2013) compacts have been studied. Tablet-in-tablet compacts were successfully designed for the delayed release of drugs in different pH environments.

2.7.4 Alternative spectroscopic imaging techniques for pharmaceutical analysis

It is realised that there several other spectroscopic imaging approaches that have been used to investigate drug release that includes: Raman mapping, near-IR imaging, UV imaging and magnetic resonance imaging (MRI). Applications of these approaches will be briefly introduced on studies of drug release. It should be noted that with the exception of Raman mapping, these are outside of the scope of this thesis but further information can be found in the articles cited in this Section.

Raman spectroscopy reveals complementary information to FTIR spectroscopy since both techniques investigate the vibrations of molecules. Over recent years, Raman spectroscopy and mapping have been increasingly used to study pharmaceutical materials (Gordon and McGoverin, 2011, Bugay and Brittain, 2006b). In many cases, drug candidates are strong Raman scatterers that make this approach desirable to elucidate the chemical

structures and characterise materials in formulations. Raman mapping works by recording spectra from different areas of a sample that is mounted on a movable stage. Hence, this approach can be used to identify domains of certain species within the sample, for example, the API within a tablet (Windbergs et al., 2009). The distribution of the API after preparation and granulation has been reported (Fujimaki et al., 2009). The ability to differentiate between amorphous and crystalline domains in the mapped sample is also of great use when using solid dispersion technologies. Characterisation of the distribution, polymorphism and stability of nimodipine in its solid dispersions in polyethylene glycol (PEG) have been determined by micro-Raman spectroscopy and X-ray powder diffraction (Docoslis et al., 2007). In addition to just characterising the distribution of APIs, the spatial domains of all constituents in bilayer tablets have been determined (Zhang et al., 2005). Employing confocal Raman mapping experiments also allow further understanding of compacted formulations as a function of depth into the sample by the use of magnifying optics (Breitenbach et al., 1999).

Near-IR imaging detects transitions corresponding to the overtones and combinational vibrations that appear in this region of the electromagnetic spectrum, 13000–4000 cm^{-1}. Measurements using this approach usually use diffuse reflectance mode. Hence, near-IR reflection spectroscopy can be used as a non-destructive method to determine the content of drugs in batches of pharmaceutical formulations or tablets (Trafford et al., 1999). Furthermore, the depth of penetration of the near-IR radiation can be used to reveal information about the size of the samples measured (Clarke et al., 2002). One of the most significant advantages of near-IR imaging is that almost no sample preparation is required because the beam can penetrate much further into the material compared to mid-IR spectroscopy (Šašić and Ozaki, 2010). The combination of a near-IR spectrometer with an FPA detector means that images can be generated in a similar way to those from FTIR spectroscopic imaging data in the mid-IR region. Near-IR chemical imaging has proven to be a powerful approach for assessing the quality of materials during the formulation process (Lyon et al., 2002) and investigating counterfeit products (Puchert et al., 2010). Similarly to ATR-FTIR spectroscopic imaging, near-IR images can be taken as a function of time to study dissolving tablets under flowing conditions. Release profiles of drugs and changes in structural forms in the experiments have been detected using this approach most recently (Wray et al., 2015).

UV imaging records and generates spatially resolved images as a function of time, based on the detection of specific UV absorbances from the selected analyte. The intensity of the UV light that passes through a quartz UV sample chamber can be measured and quantified.

UV imaging systems are relatively small and have the potential to be used for *in situ* studies of drug release. For such applications, the UV absorbance is recorded around a dissolving drug delivery system, hence, quantifying the amount of drug dissolved during the experiment from concentration gradients. Several studies of UV imaging for the release of drug from different delivery systems have been reported. Investigating the release of nicotine from transdermal patches using this approach was one of the first examples to demonstrate the potential of UV imaging for *in vitro* drug release studies (Østergaard et al., 2010a). The diffusion of the drug from HPMC compacts (Pajander et al., 2012) and Pluronic F127 hydrogels (Ye et al., 2011) has since been reported. However, to date, there are very few articles that use UV imaging to study compacted tablets.

Finally, a particularly important alternative imaging approach to ATR-FTIR spectroscopic imaging is MRI. MRI has been applied to study drug release both *in vitro* and *in vivo* (Richardson et al., 2005). An early *in vitro* approach related to drug delivery was the effect of water on a swellable polymer (Rajabi-Siahboomi et al., 1994). MRI was used to non-invasively image the ingress of the solution and swelling of the polymer (Mikac et al., 2011), similar to the studies that have been carried out using ATR-FTIR spectroscopic imaging (van der Weerd and Kazarian, 2005). The advantage of MRI is that it represents chemical information from the whole tablet as opposed to the surface layer, thus, 3D images can be collected. MRI has been employed to investigate flowing conditions, where flow-through dissolution apparatus was mounted within an MRI magnet (Fyfe et al., 2000). One slight drawback of using MRI is the fact that large magnets are needed to obtain high spatial resolution measurement and liquid cryogens are needed to cool the system. The acquisition time of MRI is also significantly longer than that of ATR-FTIR imaging where 3D images can take as long as 30 min to be obtained. However, it is realised that "ultra-fast" measurement of tablets that contain a polymer with gel-forming capabilities, HPMC, have been recorded in ~3 min (Chen et al., 2010). Nonetheless, this is still longer than FTIR spectroscopic imaging measurements that are recorded in the order of seconds. Furthermore, the hydrodynamics in USP dissolution testing equipment have been investigated using MRI (Shiko et al., 2011). The first example of combining ATR-FTIR spectroscopic imaging and MRI to study dissolving tablets to validate the results of the release of a model drug has recently been reported (Punčochová et al., 2015).

2.8 Summary

The aim of this literature review Chapter has been to summarise key aspects from previous research and development that have provided a platform for the work undertaken in this project. The motivation of this thesis is to seek further understanding of the stability and behaviour of poorly aqueous soluble APIs using macro ATR-FTIR spectroscopic imaging.

The first Section of this Chapter introduced some of the common problems that need to be overcome for the successful development of new pharmaceutical formulations. Methods that are currently used to improve the rate of dissolution of poorly aqueous soluble drugs have also been summarised. These include delivery of the API in solid dispersion formulations and ionising the drug candidate, which have both been studied in this work. Furthermore, methods to control the release of the drug from tablet compacts have been described, which is relevant since the use of excipients as carriers for drugs has been presented in this thesis.

The principles and applications of macro ATR-FTIR spectroscopic imaging for drug release studies have been introduced and the development of this approach to study pharmaceutical systems has been reviewed. As a result, novel opportunities have been identified and subsequently investigated in this work. For example, miniaturised systems are becoming a more common delivery method for administering drugs to patients. In fact, the combination of macro ATR-FTIR spectroscopic imaging and microfluidic technologies is still relatively unexplored and thus the versatility of this approach for pharmaceutical applications is yet to be realised. The potential to develop microfluidic devices that can be studied using macro ATR-FTIR spectroscopic imaging could allow the rapid screening of micro-formulations under flowing conditions.

It is clear from reviewing the literature that macro ATR-FTIR spectroscopic imaging has had a large impact on the investigation of model pharmaceutical systems. Nevertheless, there is still much research needed to aid the development of more efficient pharmaceutical formulations where this spectroscopic imaging approach can be particularly useful. The aim of this project is to use macro ATR-FTIR spectroscopic imaging to reveal valuable information about formulations that could ultimately establish this approach as a powerful analytical tool for research and development in industry.

Assessment of the literature has provided motivation for new research to be undertaken in this work. Four different areas of research will be investigated in this project that are summarised as the following:

1. The study of the stability and behaviour of indomethacin in amorphous solid dispersions formulated with different polymeric excipients before and during *in situ* dissolution experiments.

2. The effect of different carriers on the dissolution rate of a poorly water-soluble drug, indomethacin, assessed by macro ATR-FTIR spectroscopic imaging and UV detection.

3. The investigation of disproportionation of an ionised drug in different aqueous pH conditions monitored by macro ATR-FTIR spectroscopic imaging and Raman mapping.

4. The development of macro ATR-FTIR spectroscopic imaging for screening pharmaceutical systems in microfluidic devices.

3 Experimental Methods

3.1 ATR-FTIR spectroscopy

As a means to record conventional FTIR spectra of the materials studied in this project a Bruker Alpha-P spectrometer was used. This spectrometer utilised a single element deuterated triglycine sulphate (DTGS) detector to record spectral information in the mid-IR region across 4000–500 cm^{-1}. In all measurements presented in this thesis, the Alpha-P spectrometer was set up to record in ATR mode. The ATR accessory contained a diamond crystal, shaped like an inverted prism, where the area of the measuring surface of the crystal was 2 × 2 mm^2. A spectral resolution of 8 cm^{-1} was measured for all of the presented FTIR spectra while the number of co-added scans varied from 16 to 128 scans depending upon the sample measured. It should be noted that the specific measurement parameters used in the different investigations have been stated in each Chapter.

The Alpha-P FTIR instrument was especially helpful for recording spectra of the pure samples for preliminary investigation of the different species of interest. Moreover, the pure component spectra were used to identify unique absorption bands that were later used for generation of the spectroscopic images.

3.2 Macro FTIR spectroscopic imaging

The macro FTIR spectroscopic imaging system was the most extensively used analytical approach employed in the work undertaken in this thesis (Figure 3.1). A Bruker Equinox 55 infrared spectrometer aligned with an IMAC macrochamber and an FPA detector was employed for the collection of spectroscopic images. The IMAC macrochamber (Figure 3.1C) was specifically designed for macro FTIR spectroscopic imaging measurements and was built to accommodate a transmission or ATR imaging accessory and an FPA detector. The FPA detector is an array of Mercury-Cadmium-Telluride (MCT) detectors in a 128 × 128 pixel arrangement, each able to record an IR spectrum across 4000–900 cm^{-1}. The physical size of each pixel in the FPA detector is ~40 × 40 μm^2. The FPA detector requires cooling with liquid nitrogen before use and the system needs to be carefully aligned to ensure that the whole of the measured area of the detector is illuminated.

In the work presented in this thesis, all of the spectroscopic imaging data were acquired in ATR mode. The measurements were recorded at a resolution of 8 cm^{-1}. However, the size of the pixel array (64 × 64, 96 × 96 or 128 × 128) and the number of co-added scans recorded

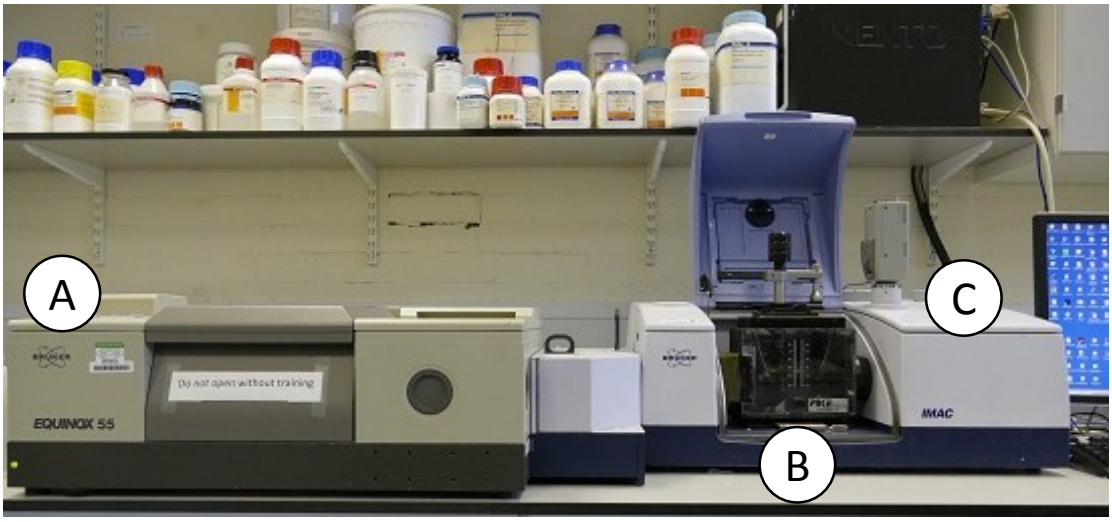


Figure 3.1 – Photograph of an FTIR spectroscopic imaging system that includes: (A) Bruker Equinox 55 FTIR spectrometer, (B) ATR accessory and (C) IMAC macrochamber.

to obtain the data was different depending upon the ATR accessory and/or sample used. These parameters were carefully selected based on the size of the imaged area intended to be recorded and the measurement time needed for the experiments. It should be realised that specific details of the acquisition parameters for the different experiments are reported in each Chapter.

3.2.1 ATR imaging accessories

The macro FTIR spectroscopic imaging measurements were carried out using two different ATR imaging accessories, an Imaging Golden Gate accessory (Specac Ltd.) and VeeMax II variable angle accessory (PIKE Technologies), which are shown in Figure 3.2. The internal optics of these accessories allow for careful alignment that can be achieved with the FPA detector. Comparisons between these two ATR accessories have been described in Section 2.6.1 of this thesis. Nevertheless, a brief summary of how the accessories were employed for the different investigations reported in this work will be described.

The Imaging Golden Gate ATR accessory with a diamond crystal was utilised to record measurements from smaller domains from the measured samples. Due to the relatively small size of the diamond crystal, 2×2 mm^2, a 64×64 pixel array was recorded when using this accessory. As a result, spectroscopic images with dimensions of 0.64×0.53 mm^2 were able to be generated with a spatial resolution of 10–15 μm (Chan and Kazarian, 2003). Thus, the use of this accessory was particularly important for studying the interface between the tablets and dissolution medium, which are presented in Chapters 4 and 6. Furthermore, because the crystal could be directly heated, the Imaging Golden Gate accessory was used for the *in situ*

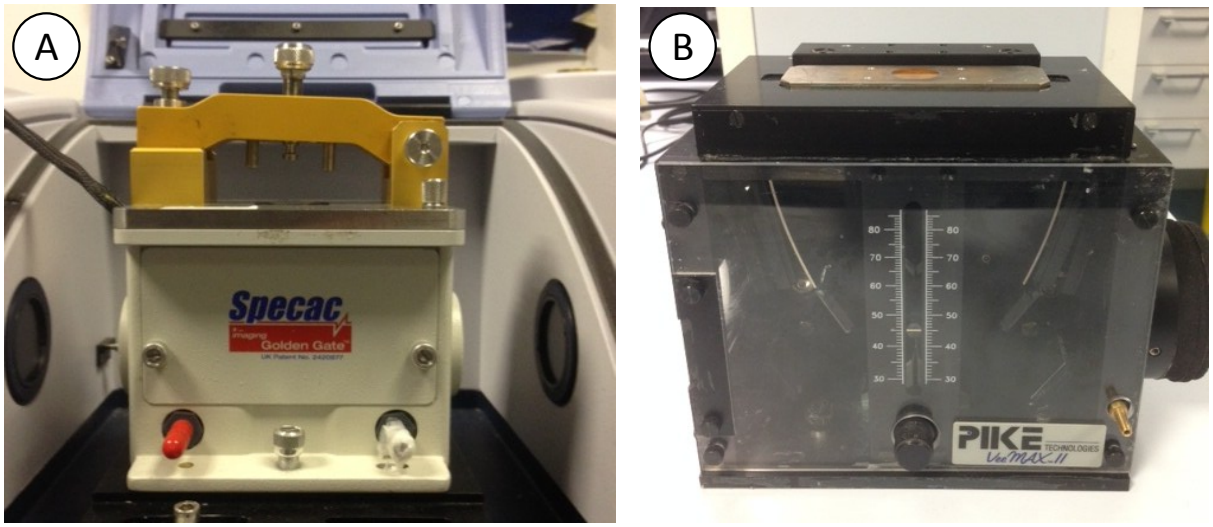


Figure 3.2 – Photograph of (A) Imaging Golden Gate accessory positioned in the IMAC macrochamber of the FTIR spectroscopic imaging system and (B) VeeMax II variable angle accessory.

investigation of the stability of indomethacin mixing with PEG, which is described in Chapter 4.

The VeeMax II accessory was used with a ZnSe crystal that had a larger measuring surface (20 mm in diameter) compared to the diamond crystal. The optics in this accessory allows the IR beam to be focused on more pixels of the FPA detector and hence information from larger domains in the sample can be measured. Measurements were recorded using 96×96 or 128×128 pixels which resulted in ATR-FTIR spectroscopic images with dimensions of 7.75×6.05 mm^2 and 11.5×8 mm^2 to be generated, respectively.

In this work, the VeeMax II accessory was employed to measure the distribution of the different components in a whole tablet (Chapter 5 and 6) and for studying the behaviour of pharmaceutical systems in microfluidic devices (Chapter 7). It should be realised that a lower spatial resolution (~100–150 µm) is recorded in the images at the expense of a larger field of view. Hence, to resolve smaller features (less than 100 µm) the Imaging Golden Gate accessory would be a more suitable choice.

3.3 Tablet compaction and flow cells

Tablet compacts were prepared in this work by using specifically designed compaction and dissolution cells. Tablets with a diameter of 3 mm were compacted using the metal compaction cell which is shown in Figure 3.3. This cell was attached directly to the Imaging Golden Gate accessory. For *in situ* compaction, the threaded mould was screwed into the metal cell until sufficient contact between the diamond crystal and the bottom of the mould

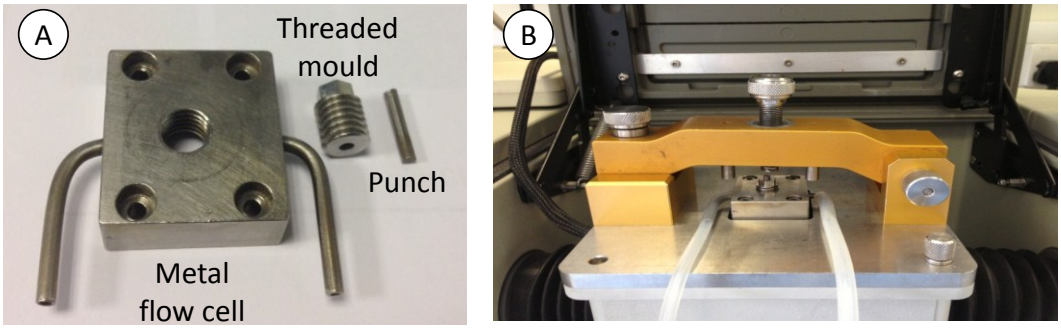


Figure 3.3 – Photograph of (A) dissembled metal flow cell showing the individual component for *in situ* compaction and (B) metal flow cell in the closed position after compaction of the tablet.

was achieved. Powdered samples, ~20 mg, were placed inside the mould. Finally, the punch was positioned and compressed using a torque screwdriver (set to 120 cN/M) to supply consistent compaction force to produce the tablets.

The metal cell can additionally be used for *in situ* tablet dissolution experiments (van der Weerd et al., 2004). However, dissolution studies with this flow cell were not utilised in this work. Instead, the tablet compacts were removed from the cell after compaction and dissolution experiments were performed using a Perspex flow cell. The Perspex cell was the preferred option for all of the tablet dissolution experiments carried out in the presented work because, unlike the metal cell, it could be set up on the Imaging Golden Gate and VeeMax II accessories. Figure 3.4 shows the positioning of the tablet on the measuring surface of the two ATR crystals used in this work. The Imaging Golden Gate accessory was employed to gain high spatial resolution images from the interfacial area of the tablet in contact with the dissolution medium, so, the tablet was placed offset from the centre of the diamond crystal (Figure 3.4A). On the other hand, the tablet was positioned in the centre of the ZnSe crystal meaning that the whole tablet could be measured in a single experiment due to the increased field of view (Figure 3.4B). For both approaches, sufficient contact had to be obtained between the ATR crystal and the tablet for successful measurements during dissolution experiments to be achieved. The tablet was positioned between the ATR crystal and the Perspex flow cell, which were separated by a rubber O-ring. The flow cell was subsequently fastened to the ATR accessory and in doing so pressed the tablet onto the measuring surface of the crystal.

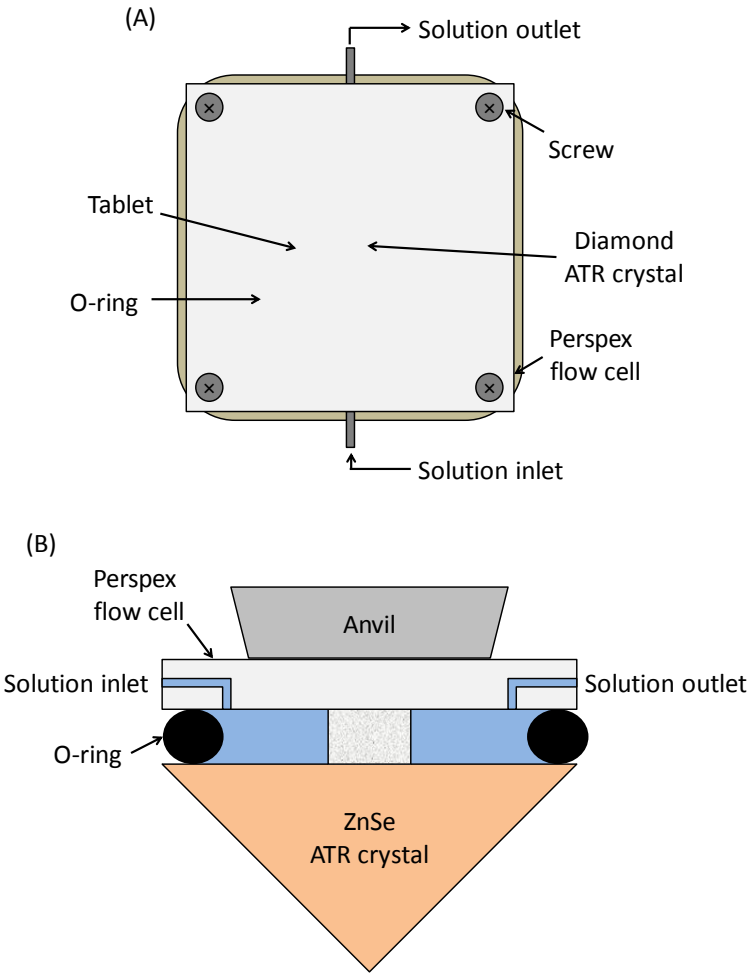


Figure 3.4 – Schematic diagrams of the experimental setup using the Perspex flow cell for tablet dissolution experiments. (A) Shows the position of the tablet offset from the centre of the diamond crystal on the Imaging Golden Gate accessory. (B) Shows a cross-sectional view of the tablet dissolution experiment measured using the VeeMax accessory where the tablet is positioned in the centre of the measuring surface on the ZnSe crystal.

3.4 UV Detection

A UV detector was employed to quantify the amount of drug dissolved in the surrounding solution. A Kontron 332 UV detector was used to determine the change in absorbance at a particular wavelength as a function of time. In this work, the UV detector was specifically used to determine the amount of indomethacin dissolved from the tablet compacts. A unique absorbance for indomethacin was identified at 320 nm as this did not interfere with the UV absorption of any of the other materials used in these formulations. The setup of this approach is described in further detail in Chapter 5 of the thesis.

3.5 Microdrop system

A microdrop system (Autodrop, Germany) was used for the microfluidics work undertaken in this thesis (Chapter 7). This use of this system to deposit samples for FTIR spectroscopic imaging applications has been reported in previous articles from the group (Chan and Kazarian, 2005). Channels made from Paraffin wax have been deposited directly on IR transparent windows for FTIR imaging of microfluidic flows in transmission mode (Chan et al., 2010).

Here, the microdrop system was used to deposit wax channels onto a substrate that were used as 3D moulds to create microfluidic devices for ATR mode measurements. Furthermore, micro-formulations comprised of ibuprofen/PEG were prepared by depositing the samples directly onto the measuring surface of an ATR crystal based on a similar method that has been reported in the literature (Chan and Kazarian, 2006a).

The microdrop system is a computer-controlled dispensing device that is capable of movement in the *XYZ* coordinates (Figure 3.5). The dispensing unit contains a sample vessel that is surrounded by a jacket capable of being heated. Therefore, any materials in the sample vessel can be melted until the viscosity is suitable for deposition (Figure 3.5B). A droplet of the sample is dispensed from a nozzle at the end of the dispensing unit at specified locations on the substrate. The diameter of this nozzle is ~100 μm and the size of the droplets deposited can be controlled by varying the voltage and pulse width using the microdrop software. In this work the size of the droplets was ~60 μm (0.06 mm) in diameter. The patterns of the dispensed sample could be determined by programming the computer to deposit droplets at defined coordinates onto the substrate.

Preparation of the wax droplets was achieved by melting paraffin wax in the sample vessel to 60 °C. Once the entire sample had melted the computer was instructed to dispense wax droplets in the design of the channels. Since the height of the droplets was not large enough for thick channels, the wax was deposited several times to build up sufficient height in the moulds.

Formulations of ibuprofen/PEG were prepared by weighing ibuprofen and PEG in a 1:3 weight ratio and placing them in the sample vessel. The vessel containing the solid materials was heated to 120 °C until both of the species had melted and mixed. Next, droplets were dispensed directly onto the ZnSe crystal at specified locations. The computer was programmed to dispense the droplets in a formation that produced circular formulations with a diameter of 0.5 mm.

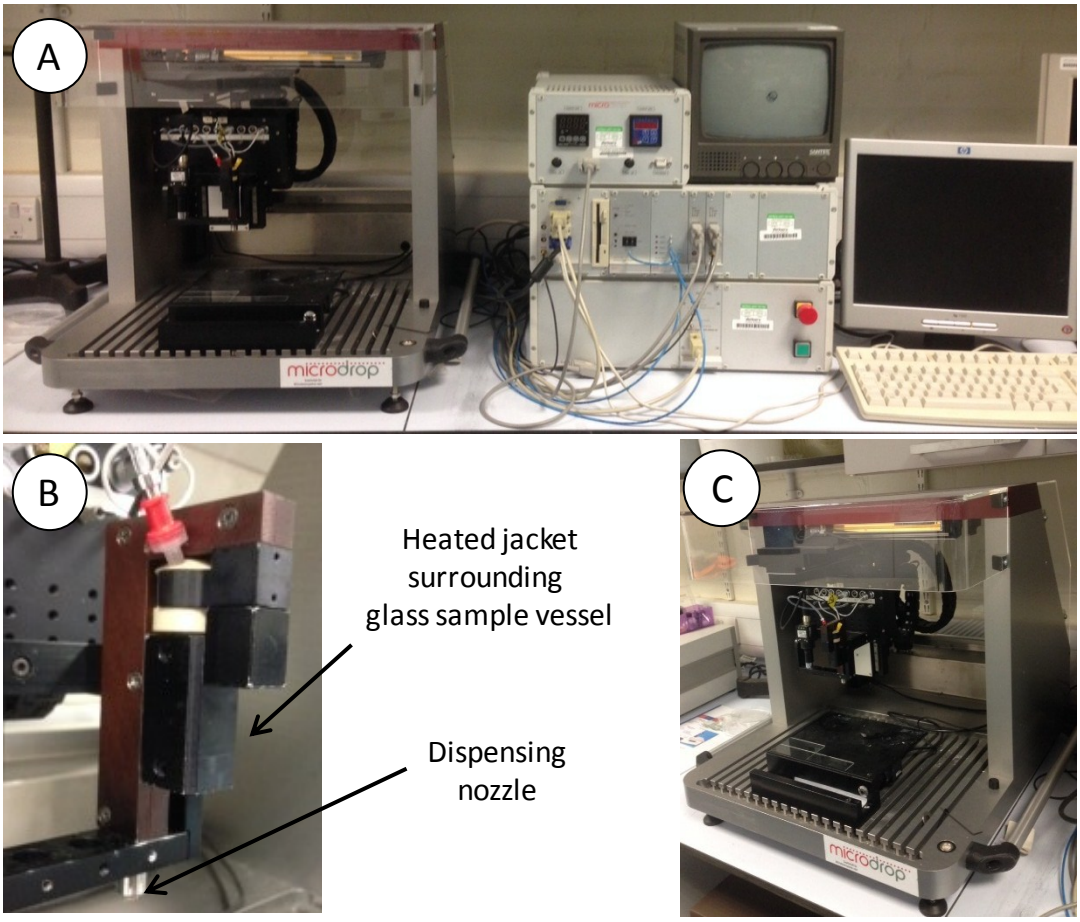


Figure 3.5 – Photographs of the microdrop system. (A) The complete arrangement of the microdrop system including the dispensing stage, computer and heating system. (B) The dispensing unit with the sample vessel chamber and nozzle highlighted. (C) The dispensing stage upon which the substrate was placed before deposition of the samples.

4 Stability of Indomethacin with Relevance to the Release from Amorphous Solid Dispersions Studied with ATR-FTIR Spectroscopic Imaging

This Chapter presents the use of ATR-FTIR spectroscopy and spectroscopic imaging to study the stability and dissolution behaviour of a model drug formulated in two different amorphous solid dispersions (ASDs). This investigation focuses on the importance of selecting appropriate polymeric excipients for use in pharmaceutical tablets which is a crucial step in controlling drug release. Indomethacin was chosen as the model drug in this work since it is inherently poorly soluble in aqueous solutions. Interestingly, the amorphous form has been reported to exhibit improved rates of dissolution compared to the crystalline forms. Therefore, formulated ASDs, where indomethacin is intended to be in its amorphous form, were designed using PEG and HPMC as excipients.

The first part of this Chapter describes the use of conventional ATR-FTIR spectroscopy, using a single element detector, to monitor the short-term stability of the amorphous indomethacin in the two ASDs. This investigation was extended to include the use of macro ATR-FTIR spectroscopic imaging for the *in situ* monitoring of the formulations upon cooling during the preparation stage. The second Section of this Chapter focuses entirely on the application of macro ATR-FTIR spectroscopic imaging to study the dissolution of ASD formulations compacted into tablets. Specific attention was paid to the behaviour of dissolving tablets containing amorphous indomethacin and how any subsequent structural changes affected the release of the drug.

4.1 Motivation and scientific background

Many APIs can exist in different structural forms or polymorphs and each of these forms can have different physical properties that can directly affect the rate of dissolution (Aguiar and Zelmer, 1969). The amorphous form is of particular interest since it lacks long-range order, i.e. has no crystal lattice and, as a result, can have a faster dissolution rate compared to the crystalline structures (Hancock and Parks, 2000, Hancock and Zografi, 1997). However, amorphous solids are not the favourable molecular state as they are thermodynamically metastable. Thus, conversion back to a more stable crystalline form can occur during the production, storage and delivery stages (Kao et al., 2012, Alonzo et al., 2010).

ASDs can play a significant role in stabilising amorphous materials by the introduction of a polymeric excipient. Depending upon the excipient used, the dissolution profile (drug release over time) can be modified to influence and control drug release from the tablets. Intermolecular interactions between the API and polymer can result in effects, such as the reduced molecular mobility of API in the polymer (Aso et al., 2004, Matsumoto and Zografi, 1999), that assist in preventing nucleation within the formulations and inhibiting crystallisation. ASDs are one of the most useful strategies employed to improve the release of poorly aqueous soluble APIs (Vasconcelos et al., 2007, Six et al., 2004, Leuner and Dressman, 2000). During the design and formulation of ASDs, it is of the utmost importance to maintain the amorphous form of the API and the selection of suitable polymers is pivotal to achieving the desired release kinetics. Furthermore, polymeric excipients added to formulations can play an essential role in preventing the crystallisation of drug candidates (Van Eerdenbrugh and Taylor, 2010).

Due to the potential of enhanced drug delivery by employing amorphous APIs in novel formulations, this Chapter investigates the applicability of ATR-FTIR spectroscopy and spectroscopic imaging to observe structural changes of amorphous drugs in different ASDs. Here, indomethacin was used as the model API because the amorphous form exhibits faster rates of dissolution (Heinz et al., 2007); whereas the stable and metastable crystalline forms (γ form and α form, respectively) dissolve at a slower rate in aqueous conditions. In previous work by Priemel et al. (2012), the behaviour of the crystallisation and dissolution of indomethacin were studied and it was reported that ATR-FTIR spectroscopy provided the most reliable assessment of the analytical techniques used. Recent studies also state that the stability of an amorphous drug changes depending upon the polymer used (Priemel et al., 2013, Konno et al., 2008).

The purpose of this Chapter is to investigate the behaviour and stability of amorphous indomethacin in two different ASDs formulated with the following polymers: PEG and HPMC. The chemical structures of the materials studied here are shown in Figure 4.1 and they have been selected since they are widely used in pharmaceutical tablets. Significantly, the polymers chosen as excipients in this study were done so because they have different properties in aqueous solutions. PEG is readily soluble and as a result, the surfaces of tablets containing this polymer in contact with the dissolution medium will erode, exposing the drug to the solution. On the other hand, HPMC has a tendency to swell upon contact with aqueous solutions. Hence, drugs can be released from this polymer either by diffusion through the

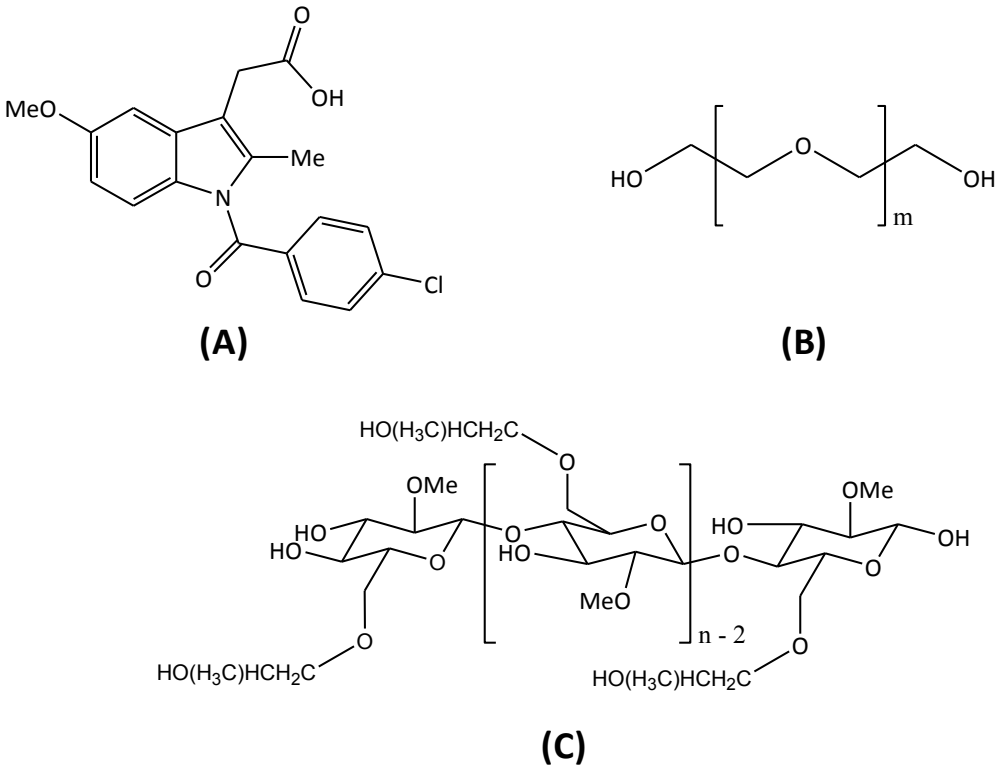


Figure 4.1 – Chemical structures of (A) indomethacin, (B) polyethylene glycol (PEG) and (C) hydroxypropyl methylcellulose (HPMC).

swollen tablet matrix, or by translocation of drug particles moving in the tablet as the polymer swells. The results of this work will highlight the importance of selecting appropriate excipients to maintain the desired structural form of indomethacin in ASDs. Macro ATR-FTIR spectroscopic imaging was employed to monitor the behaviour of amorphous indomethacin during *in situ* dissolution experiments. The release of indomethacin into the surrounding solution was observed and mechanisms of drug release have been proposed from the recorded spectroscopic images and ATR-FTIR spectra of the studied systems.

4.2 Materials and methodology

4.2.1 Sample preparation

Indomethacin (γ form) and PEG (mw: 4000 $g.mol^{-1}$) were purchased from Sigma-Aldrich (UK). HPMC (K100 LV) was supplied from Colorcon (UK). Pure samples of different indomethacin forms were prepared by the following procedures: γ indomethacin was used as received, α indomethacin was prepared using a solvent evaporation method with ethanol

(Kaneniwa et al., 1985) and amorphous indomethacin using the hot melt method described below but without the introduction of any polymer.

ASDs were prepared by a hot melt method followed by quench cooling with liquid nitrogen. Two different tablet formulations containing 25 % (weight loading) loading of indomethacin were prepared: indomethacin with PEG (1:3 weight ratio); and indomethacin with HPMC (1:3 weight ratio). Amorphous indomethacin was heated to 165 °C followed by addition of the polymer. This temperature was maintained for 5 min while the molten formulation was stirred to achieve an even dispersion of both materials in the mixture. The melts were removed from the heat and flash-cooled using liquid nitrogen. After measurements by conventional ATR-FTIR spectroscopy, the resulting ASDs were stored in a closed desiccator, containing a solution of saturated potassium carbonate to control the relative humidity at 43 %, at room temperature until further use.

Model pharmaceutical tablets, 3 mm in diameter, were prepared by grinding the ASDs and sieved to collect particles between 90–125 μm. The resulting powder was compacted using the custom designed metal cell that was designed to be attached to the Imaging Golden Gate accessory as described in Section 3.3 (van der Weerd and Kazarian, 2005, van der Weerd and Kazarian, 2004c).

The dissolution medium used throughout this work was a phosphate buffer solution of pH 7.5. A flow rate of 5 mL/min for the dissolution experiments in this study was used. The phosphate buffer was prepared by mixing a solution of 0.1 M sodium hydroxide solution with 0.1 M potassium dihydrogen phosphate solution in a 0.8:1.0 ratio. Both chemicals were purchased from Sigma-Aldrich (UK).

4.2.2 Macro ATR-FTIR spectroscopic imaging

An FTIR spectrometer (Alpha-P, Bruker, UK) in ATR mode with a single element detector was used to obtain conventional ATR-FTIR spectra presented in this thesis. A spectral resolution of 8 cm^{-1} with 32 co-added scans was used throughout this investigation.

ATR-FTIR spectroscopic images in macro imaging mode (without the use of a microscope) were collected using an FPA detector with an array size of 64 × 64 pixels giving an approximate image size of 638 × 525 μm^2 (0.638 × 0.525 mm^2) with a spatial resolution of ~10 μm. The accessory used was an Imaging Golden Gate (Specac Ltd., UK) fitted within the macrochamber linked to a spectrometer (Equinox 55, Bruker, UK). 8 cm^{-1} spectral resolution and 32 co-added scans were used for collection of the imaging data.

Table 4.1 – The spectral range that was integrated to produce spectroscopic images showing the spatial distribution of the different chemical species in this study.

Chemical species	Integration range (cm^{-1})
Indomethacin (amorphous and γ)	1730–1700
Polyethylene glycol	985–952
Hydroxypropyl methylcellulose	1200–970
Aqueous solution (pH 7.5)	3600–3000

False colour spectroscopic images representing the different components in the ASDs within the imaged area were obtained by selecting unique absorption bands for each of the constituents in the formulation. These are summarised in Table 4.1. Since, the main constituent of the phosphate buffer was deionised water; an absorption band characteristic of this species was selected to generate representative spectroscopic images. The red regions in the images represent areas of high absorbance and blue regions represent areas of low absorbance of the unique spectral band in the colour images.

4.2.3 Dissolution methodology

A specially designed Perspex flow cell was used for the dissolution experiments throughout this investigation (Kazarian and van der Weerd, 2008). As shown in Section 3.3, the tablets were placed on the measuring surface of the diamond crystal and positioned to one side of the crystal to allow data from the interfacial area at the edge of the tablet and the phosphate buffer dissolution medium to be observed. The flow cell provided the necessary contact between the tablet and crystal by gently pressing the top surface of the tablet such that the phosphate buffer could only contact the tablet from the sides. The spectroscopic images presented throughout are from the bottom surface layer of the sample. Each experiment was repeated three times where a separate batch of the ASD was prepared immediately before use to ensure the formulations were of a similar age. Representative spectroscopic images have been selected from these results and shown herein.

4.3 Structural forms of indomethacin

Firstly, it is important to understand that indomethacin is polymorphic and consider how the rate of dissolution can be affected by the crystalline nature of the drug form. Indomethacin has been characterised to exist in eight crystalline structural forms (Surwase et al., 2013). Initially, only five of these forms had been identified, namely, α, β, γ, δ and an additional

unnamed form (Lin, 1992, Borka, 1974). The different polymorphs often occur from the crystallisation of amorphous indomethacin depending upon the preparation method and conditions during storage (Rumondor et al., 2009, Savolainen et al., 2007, Andronis et al., 1997). Recent work, by Surwase et al. (2013) reported the existence of three new polymorphs of indomethacin, the ε, ζ and η forms. Each of these forms was characterised by analysing the crystallisation behaviour of amorphous indomethacin from aqueous solutions. Different temperature and pH conditions were investigated and the stability of all of the forms of indomethacin was assessed using a range of analytical techniques, including FTIR spectroscopy.

However, three different forms of indomethacin were of interest to this particular investigation: the γ, α and amorphous forms. The fundamental reason behind this arises from the fact that the γ form of indomethacin is the most thermodynamically stable form. Furthermore, the α form is the most commonly reported metastable polymorph of indomethacin and is often characterised from conversion of amorphous indomethacin upon contact with aqueous solutions (Andronis et al., 1997). Vibrational spectroscopy is a powerful approach for determining the crystallinity and polymorphic changes in samples and FTIR spectroscopy can determine the different structural forms of indomethacin brought about by changes in the intermolecular interactions within the sample (Surwase et al., 2013, Taylor and Zografi, 1997b). The use of vibrational spectroscopy to study the structure of the different indomethacin forms has previously been reported by Taylor and Zografi (1997b). Here, particular attention was paid to the spectral region between 1800–1500 cm^{-1} which

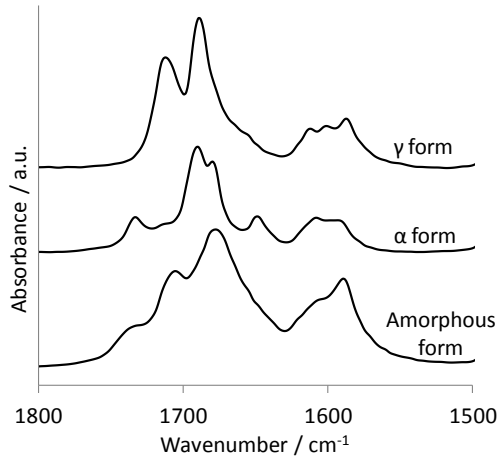


Figure 4.2 – ATR-FTIR spectra recorded for the pure γ, α and amorphous forms of indomethacin. The spectral region between 1800–1500 cm^{-1} is displayed highlighting the C=O vibrations of the indomethacin forms.

includes the region characteristic of the stretching of carbonyl (C=O) bands (Figure 4.2). Indomethacin contains two different C=O groups from the carboxylic acid and benzoyl functional groups (see Figure 4.1). The behaviour of the C=O groups in the individual indomethacin forms accounts for the spectral differences observed in Figure 4.2. The simplest observation that can be made is that the γ, α and amorphous forms have two, four and three spectral bands between 1800–1650 cm^{-1}, respectively. Intermolecular interactions between the molecules of indomethacin are responsible for the observed differences in the FTIR spectra. The assignment of these bands has been summarised in Table 4.2.

The two absorption bands observed in the ATR-FTIR spectrum of γ indomethacin result from the vibrations of the two C=O groups in the molecule (Figure 4.1). The C=O vibration between the benzoyl and amide group can be assigned to the peak at 1690 cm^{-1}. This band is usually observed at a higher wavenumber for a typical amide group (1695–1630 cm^{-1}). It has been described that the reason behind this is mesomerism in the amide group, where nitrogen

Table 4.2 – Position of the ATR-FTIR bands assigned to the carbonyl stretching vibrations of the different indomethacin structural forms (Taylor and Zografi, 1997b).

Structural form of indomethacin	Band position (cm^{-1})	C=O group assignment
γ	1690	Benzoyl
	1712	Carboxylic acid in cyclic dimer
α	1649	Hydrogen bonded carboxylic acid in a chain
	1680	Hydrogen bonded carboxylic acid in a chain
	1688	Benzoyl
	1735	Non-hydrogen bonded carboxylic acid
Amorphous	1680	Benzoyl
	1706	Hydrogen bonded carboxylic acid in a chain
	1735	Non-hydrogen bonded carboxylic acid

can donate its lone pair of electrons. Typically the mesomeric effect will cause a reduction in the bond force constant, reducing the frequency of vibration. However, as has been observed in the case of indole ketones, the contribution of the mesomeric form is reduced in molecules where the nitrogen atom is part of the ring. This effect helps to explain the relatively high wavenumber of the benzoyl C=O group in the γ form. The appearance of the benzoyl C=O bond at a lower wavenumber in the spectra of the α form and amorphous indomethacin, 1688 cm^{-1} and 1680 cm^{-1} respectively, is suggestive of there being fewer conformational restrictions in these forms. The other absorption band observed in the spectrum of the γ form, at 1712 cm^{-1} is a result of the asymmetric stretch of the carboxylic acid C=O bond that is known to exist as a cyclic dimer in this structural arrangement (Taylor and Zografi, 1997b).

The bands characteristic of the carboxylic acid C=O vibration are more complex in the α form than they are in the γ form. These are useful as they provide information about the presence of H-bonding involving these functional groups. In the spectrum of the α form the other three peaks can be assigned to this moiety. The bands at 1680 cm^{-1} and 1649 cm^{-1} suggest H-bonding, but not of a cyclic dimer. Therefore, it is proposed that these result from the formation of H-bonded chains. The band at 1734 cm^{-1} is indicative of a non-H-bonded asymmetric acid C=O stretch and is a result of a terminated chain i.e. a free carboxylic acid C=O bond.

Finally, the spectrum of amorphous indomethacin shows similarities to both of the crystalline structures described above (Figure 4.2). The band at 1706 cm^{-1} suggests the presence of cyclic dimers in the amorphous phase that are also characterised in the γ form. Additionally, there is a peak at 1735 cm^{-1} which is also observed in the α form and characterised as a non-H-bonded carboxylic acid C=O stretch. Therefore, it can be suggested that amorphous indomethacin exists as a mixture of both cyclic dimers and H-bonded chains.

4.4 Stability of amorphous solid dispersions

4.4.1 Conventional ATR-FTIR spectroscopy

This Section reports the use of conventional ATR-FTIR spectroscopy to study the short-term stability of the two ADSs over 96 hr at conditions of 25 °C and 43 % relative humidity. Figure 4.3A presents the ATR-FTIR spectrum recorded of the indomethacin/PEG ASD every 24 hr during this period. It should be noted that the spectra labelled “0 hr” refer to those measured immediately after preparation of the sample by the hot melt method. The ATR-FTIR spectrum at 0 hr confirms that indomethacin is present in the amorphous form,

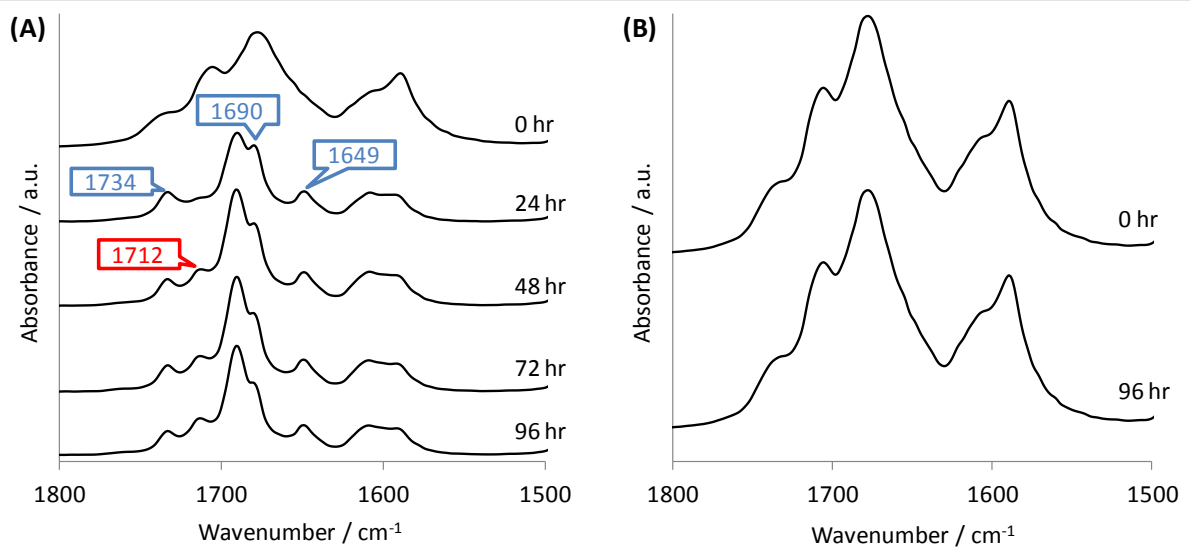


Figure 4.3 – ATR-FTIR spectra measured during the stability studies of the indomethacin/PEG (A) and the indomethacin/HPMC (B) formulations over a 96 hr period. The blue and red labels in (A) highlight the appearance of the peaks of the spectral bands that indicate the presence of α and γ indomethacin, respectively.

determined by the three spectral bands that correspond to the reference spectrum shown in Figure 4.2. However, over time, significant changes to the spectral bands can be observed. After 24 hr a band characteristic of the α form starts to become present, most easily distinguished by the appearance of the spectral bands at 1734, 1690 and 1649 cm^{-1} which are highlighted by the blue labels in Figure 4.3A. Furthermore, between 48–96 hr the spectra show evidence of crystallisation back to the most thermodynamically stable γ form. This change in form can be seen by the band appearing at 1712 cm^{-1} that is specific to the γ form (red label in Figure 4.3A). The relative absorbance of this spectral band can be seen to increase continually, suggesting that there is a greater concentration of the γ form appearing as a function of time. In contrast, the bands corresponding to the α form (1734, 1690 and 1649 cm^{-1}) display a decrease in absorbance as a function of time. Hence, this is strongly indicative of the conversion from the metastable polymorph to the γ form in this particular ASD.

The same measurements were obtained for the ASD containing indomethacin/HPMC. In contrast to the indomethacin/PEG formulations, this ASD was seen to remain stable over the period of 96 hr (Figure 4.3B). The fact that this ASD maintained indomethacin in the amorphous form is very useful as it provided further evidence that the stability of amorphous indomethacin is different depending on the polymer selected. The increased stability of amorphous indomethacin in HPMC has the potential to improve not only the storage time of

tablets but also the dissolution properties and drug release from these solid dosage forms by inhibiting crystallisation to polymorphs that dissolve more slowly.

4.4.2 *In situ* Macro ATR-FTIR spectroscopic imaging

Figure 4.4 shows ATR-FTIR spectroscopic images, with accompanying spectra, to understand the crystallisation process in the indomethacin/PEG ASD by monitoring *in situ*. The spectroscopic images represent the interface between pure amorphous indomethacin and PEG during the cooling stage of the hot melt method. Amorphous indomethacin was deposited directly onto the measuring surface of the diamond crystal to cover approximately half of the imaged area. Using a heated ATR-FTIR accessory, the crystal and amorphous indomethacin were heated to 60 °C. It should be noted this is below the melting point of indomethacin (158 °C) and does not affect the amorphous phase.

After heating to 60 °C, molten PEG was introduced onto the other half of the diamond surface (Figure 4.4). The temperature was then reduced 10 °C every 20 min back to 30 °C, effectively reproducing the cooling stage during preparation, albeit on a much slower time

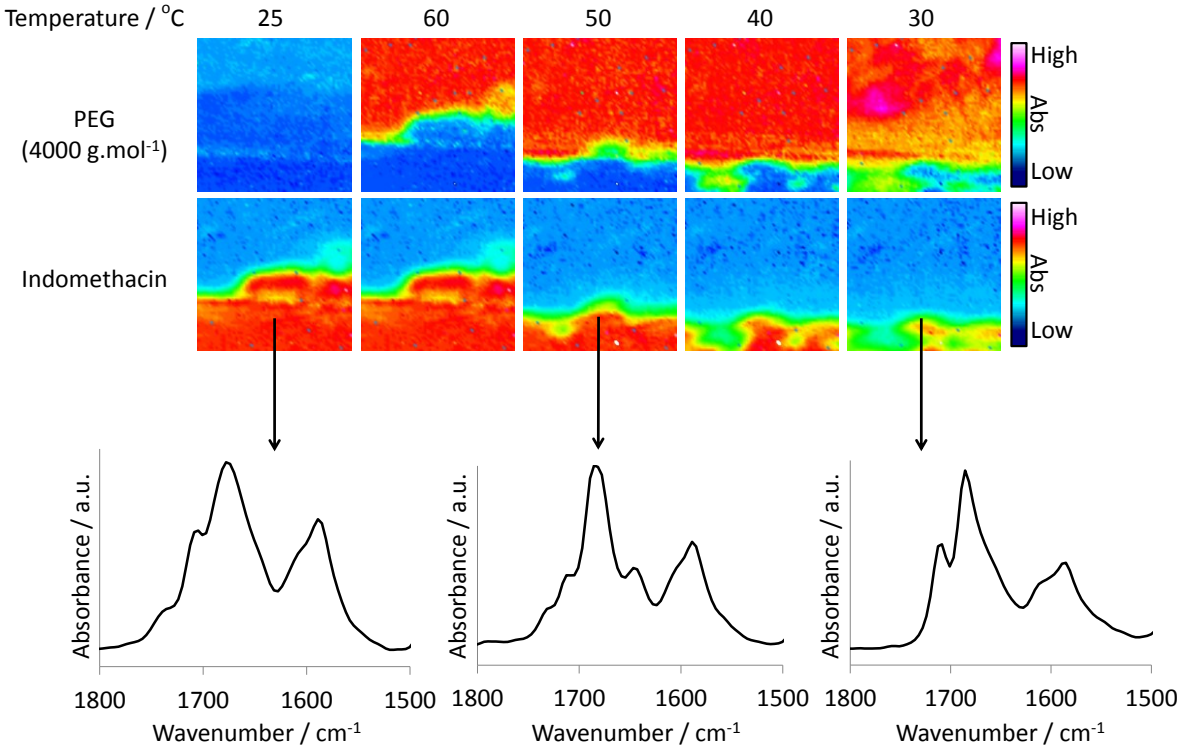


Figure 4.4 – ATR-FTIR spectroscopic images showing the distribution of PEG (top row) and indomethacin (bottom row) during the *in situ* stability experiment. The accompanying extracted spectra displayed confirm a change in structural form, from amorphous to γ form, via the α form, during the experiment. The dimension of each spectroscopic image is ~0.64 × 0.53 mm^2.

frame. It should be noted that the melting point of the PEG (mw: 4000 $g.mol^{-1}$) used for this work is 56 °C, thus at temperatures below 50 °C the PEG began to solidify. The spectroscopic images in Figure 4.4 show the distribution of both PEG and indomethacin at these different temperatures, revealing changes in their spatial distribution within the formulation as PEG mixes with the solid indomethacin sample. Individual spectra from a single pixel located at the interface between the indomethacin and PEG have been extracted and compared. Similarly to the conventional ATR-FTIR study, amorphous indomethacin converts to the stable γ form, via the metastable α form. However, in this experiment the change occurs over a much shorter time frame (~1 hr). This result can be explained since mixing at the interface between the drug and polymer was intended to be investigated in this experiment. This provided information about the mobility and mechanisms of the behaviour of indomethacin within PEG. Figure 4.4 shows that movement of PEG and subsequent mixing occurs upon contact of the two materials, which is most easily observed by the ingress of PEG into the region where indomethacin was initially located. As a result, this indicates that there is some mobility of PEG within the indomethacin region or vice versa. Importantly, this can aid the explanation of why the amorphous indomethacin is crystallising when formulated with PEG. A higher mobility of the drug and polymer in the formulation can result in the formation of favourable intermolecular interactions between the indomethacin molecules that will subsequently convert to the most thermodynamically stable form as a function of time. Hence, this indicates why the appearance of the α form followed by γ polymorph of indomethacin are observed in the ATR-FTIR spectra presented in Figure 4.3 and Figure 4.4.

Despite there being differences with the sample used for the *in situ* imaging experiment and the indomethacin/PEG ASD, this experiment gives valuable information about the behaviour of indomethacin within a PEG matrix. ATR-FTIR spectroscopy and spectroscopic imaging have been shown as powerful approaches to learn about the stability of different ASDs, demonstrating that, in the case of ASDs containing PEG, indomethacin has a preference to return to the stable γ form.

4.5 Macro ATR-FTIR spectroscopic imaging of drug release

In this work, ATR-FTIR spectroscopic imaging has further been applied to study the release of indomethacin during the dissolution of the ASDs compacted into tablets. Immediately after preparation the ASDs were ground and compacted into tablets (3 mm diameter) which were monitored *in situ* under flowing conditions in a pH 7.5 aqueous medium. As described in

Section 4.1, PEG and HPMC behave differently in aqueous solutions, hence allowing the stability of the amorphous drug to be observed from tablets with different drug release properties.

The spectroscopic images in Figure 4.5 show the behaviour of the indomethacin/PEG ASD tablet during the *in situ* dissolution experiment. The first observation of interest is the fact that indomethacin does not appear to be homogeneously distributed throughout the tablet matrix. As can be observed in the spectroscopic image labelled "Dry" in Figure 4.5, there are localised regions where the indomethacin has agglomerated in the tablet. One would expect a much a more even distribution of indomethacin throughout the tablet because of the preparation using the hot melt method. Clear differences in the distribution of the drug can be seen by comparing the distribution of indomethacin in the dry tablets in the two ASD tablets. In the indomethacin/HPMC ASD ("Dry" Figure 4.6) the dispersion of indomethacin is homogenous throughout the bulk of the tablet. Understanding the molecular mobility of indomethacin within the polymer matrices can further provide an explanation for this.

Priemel et al. (2013) have recently reported that the crystallisation of indomethacin with Soluplus and Eudragit during exposure to different relative humidity conditions. Indomethacin/Eudragit mixtures were more stable than indomethacin/Soluplus mixtures. SEM images revealed that this was influenced by the particle size of the polymers. Adhesion of indomethacin was seen to occur with Eudragit particles because of their smaller size thus reducing nucleation in the mixture. In contrast, indomethacin/Soluplus mixtures did not stabilise indomethacin because there was no adhesion between the larger Soluplus particles.

As a result, since similar effects are seen in the spectroscopic images of the two ASDs studied here, the interactions and mobility of indomethacin with the polymers can play a crucial role in stabilising the amorphous form. When one considers the chemical structure of the polymers used for the ASDs (Figure 4.1), it can be seen that HPMC contains more hydroxyl groups per unit in the polymer chain than PEG. The tendency for C=O groups in indomethacin to form H-bonds is evident, hence there may be a tendency for H-bonding to occur between the polymer and indomethacin. Due to the higher proportion of OH groups in HPMC, it is proposed that there is the potential for more indomethacin-HPMC interactions in this ASD. The stability arising from the interaction in these ASDs will result in lower mobility of indomethacin within the bulk of the formulation, confirmed by the homogenous distribution observed in the spectroscopic images. Another possibility is that the molecular chains of HPMC are longer than those of PEG. The longer chain length of the polymer can

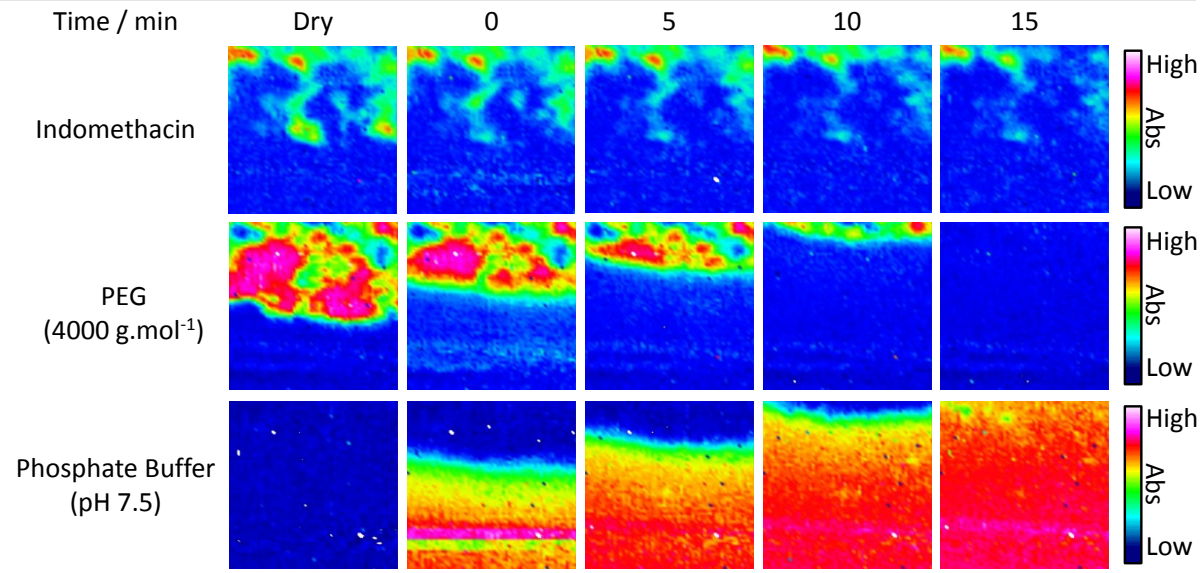


Figure 4.5 – ATR-FTIR spectroscopic images revealing the distribution of indomethacin (top row), PEG (middle row) and phosphate buffer (bottom row) during the *in situ* drug release experiment of the indomethacin/PEG ASD. The dimension of each spectroscopic image is ~0.64 × 0.53 mm^2.

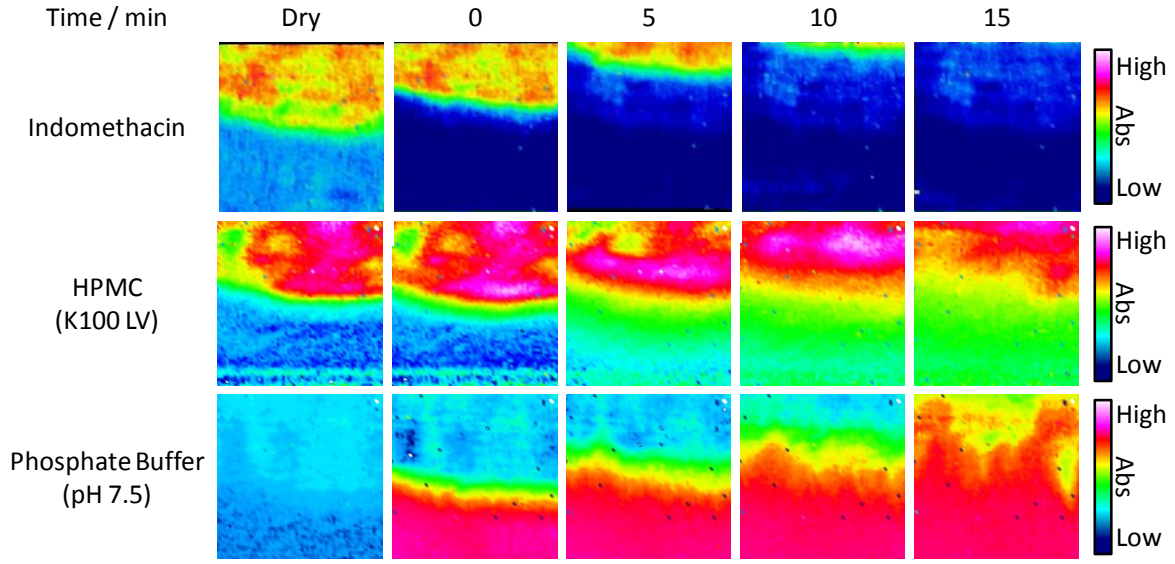


Figure 4.6 – ATR-FTIR spectroscopic images that reveal the spatial distribution of indomethacin (top row), HPMC (middle row) and phosphate buffer (bottom row) during the *in situ* drug release experiment of the indomethacin/HPMC ASD. The dimension of each spectroscopic image is ~0.64 × 0.53 mm^2.

result in greater entanglement of indomethacin within the polymeric chains thus hindering the mobility of the drug within the matrix. In fact, the most likely and logical explanation would involve both of these proposed effects occurring simultaneously in the ASD.

Although it is not known how long the drug takes to agglomerate in the indomethacin/PEG ASD tablets, some factors could influence the rate at which this occurs, most notably during grinding and compaction. Despite the ASDs being prepared immediately before use in the dissolution experiments, the ASDs were ground into a powder and then compacted as part of the tablet preparation process. The mechanical energy that is involved in these steps could have an influence on the stability of the indomethacin. Nevertheless, the ATR-FTIR spectroscopic images obtained from the dry tablets shows that there is an agglomeration of amorphous indomethacin in the PEG ASD (Figure 4.5) which is not apparent with the HPMC ASD (Figure 4.6).

The distribution and mobility of the indomethacin within the ASD has implications for the release behaviour from the tablets. Figure 4.5 shows representative ATR-FTIR spectroscopic images recorded during *in situ* dissolution of the indomethacin/PEG in a phosphate buffer solution (pH 7.5). The spectroscopic images show the spatial distribution of all three components present in this experiment. As time progressed, ingress of the buffer solution into the tablet can be observed. The interface of PEG erodes rapidly on contact with water until there is no presence of PEG in the spectroscopic images after 15 min. The spectroscopic images representing the distribution of indomethacin reveal that the dissolution and drug release was lower than expected during the experiment. This is highlighted by the appearance of the red and green regions in the ATR-FTIR spectroscopic images that shows indomethacin is still present in the imaged area, even when PEG is not. Understanding the effect of mobility and accumulation of indomethacin within the ASD during tablet preparation is important because it has been reported that systems with higher mobility can result in the crystallisation of indomethacin. Similar observations have been reported in the literature where indomethacin crystallises but with different polymers (Priemel et al., 2013).

In contrast, the indomethacin/HPMC ASD have different dissolution properties. HPMC swells to form a gel during tablet dissolution as observed in the ATR-FTIR spectroscopic images (Figure 4.6). As a result, the dissolution mechanism for drug release is different. Indomethacin dissolves in solution before diffusing through the bulk of the tablet matrix and into the surrounding medium. These images show obvious differences compared to the behaviour observed during the indomethacin/PEG dissolution experiments. Firstly, the indomethacin is distributed homogenously over the sample area. As the buffer is introduced to the tablet, the HPMC polymer swells as expected. The buffer is seen to ingress into the tablet and in doing so dissolves the indomethacin. The dissolution of the drug is characterised

by the decreasing absorbance of indomethacin in the images. The ATR-FTIR spectroscopic images also reveal that the indomethacin interface erodes at a very similar rate to the ingression of buffer suggesting that drug dissolves and diffuses through the swollen bulk of the tablet when in contact with the solution. In contrast to Figure 4.5, the chemical image at 15 min in Figure 4.6 shows no presence of indomethacin in the ATR-FTIR spectroscopic images during this experiment indicating that there is complete drug release into the surrounding solution.

One of the advantages of using ATR-FTIR spectroscopic imaging for tablet dissolution is that, in addition to spatial information, chemical information can be obtained at a high sensitivity. Individual spectra can be extracted from specific pixels from areas of interest displayed in the ATR-FTIR spectroscopic images. Extraction of spectra from particular pixels is useful for learning about the behaviour of polymorphic changes within the tablet during dissolution and reveals further understanding about the mechanisms of crystallisation and drug release from the indomethacin/PEG ASD. As already described, during the tablet dissolution experiment there was a tendency for indomethacin to accumulate which later inhibited drug release. Figure 4.5 shows the images collected for the first 15 min during the experiment, however, the experiment was continued beyond this time for up to 60 min.

Figure 4.7 presents the distribution of indomethacin in the dry tablet and after 60 min of

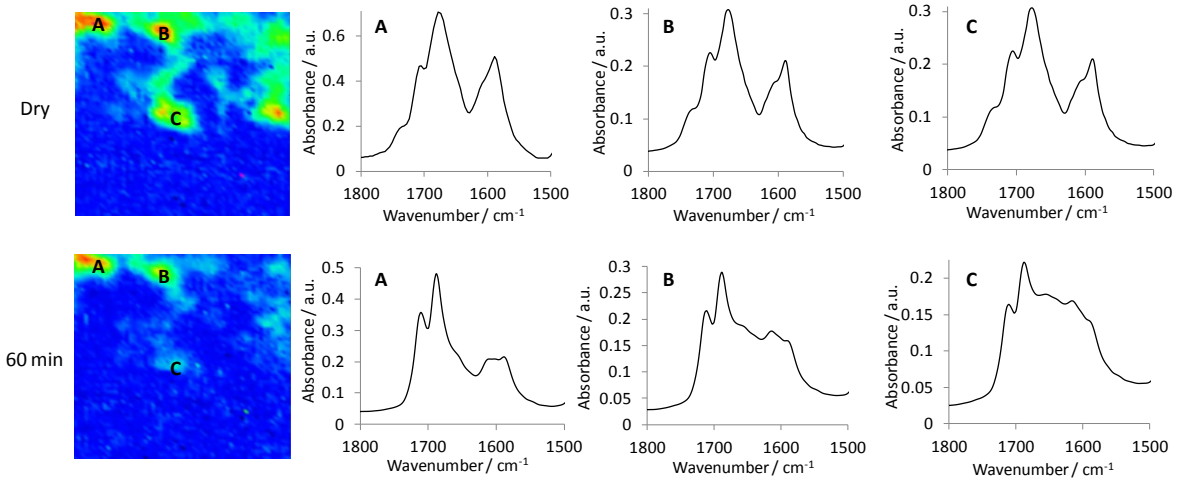


Figure 4.7 – ATR-FTIR spectroscopic images of indomethacin/PEG ASD tablet before exposure to the buffer solution (Dry) and during the experiment (60 min). Extracted spectra from the points labelled (A, B and C) on the spectroscopic images show evidence of the crystallisation of amorphous indomethacin during the experiment. The dimension of each spectroscopic image is ~0.64 × 0.53 mm^2.

the dissolution experiment. It should be noted that there is little difference between the images obtained after 15 min compared to that at 60 min in terms of the distribution of indomethacin in the measured area. However, the absorbance of the spectral band and thus the concentration of the API is slightly lower after 60 min as one would expect as a result of continued drug dissolution. Individual spectra have been extracted from different areas in the tablet where indomethacin is present both at 0 and 60 min. The spectra in the top row are taken from the dry tablet at the positions labelled "A", "B" and "C" respectively. The extracted spectra are similar and show three absorption bands that are consistent with those expected for amorphous indomethacin. However, when the spectrum from the same pixel was extracted from the measurement taken at 60 min, there are obvious differences. A change from the intended amorphous form can be seen, where amorphous indomethacin crystallises to the γ form. Absorption bands characteristic of the γ form, with spectral peaks at 1712 and 1692 cm^{-1}, appear in the extracted spectra where indomethacin is still present in the spectroscopic images recorded after 60 min. It should be noted that the appearance of the band at 1655 cm^{-1} is a result of the bending vibration (ν_2) of water present in the buffer.

Formation of the γ form can be induced as a result of the increased mobility of indomethacin in the indomethacin/PEG ASD. As indomethacin migrates through the polymer, H-bonded cyclic dimers form when two molecules of the drug interact. This dimer is the major component in the γ form and characterised by the band at 1692 cm^{-1} which has the highest absorbance in all of the extracted spectra from the images recorded at 60 min (Figure 4.7). It is proposed, based on the ATR-FTIR spectroscopic imaging experiments that, as PEG dissolves, the remaining indomethacin can accumulate and initiate crystallisation.

In the case of the indomethacin/HPMC ASD, the release of the homogeneously dispersed amorphous indomethacin was readily observed in the spectroscopic images. This result is significant for improving the drug release of poorly water-soluble APIs. In contrast, the indomethacin/PEG ASD showed a tendency for agglomeration and subsequent crystallisation of indomethacin to the γ form that caused problems for drug release. During contact with water, the indomethacin aggregates did not move from the imaged area. Extracting spectra from the regions indicative of high concentrations of indomethacin show the presence of γ form during dissolution. This form is poorly aqueous soluble and thus less effective in releasing the drug into the surrounding solution.

4.6 Conclusions

In this Chapter, the application of ATR-FTIR spectroscopy and spectroscopic imaging to investigate the stability and drug release of indomethacin from different ASDs have been demonstrated. Amorphous indomethacin had longer stability in the ASDs where HPMC was used as the polymeric excipient. The increased stability was proposed to be caused by a reduction in the mobility of indomethacin arising from two plausible mechanisms: (1) the formation of intermolecular interactions between indomethacin-HPMC, and (2) greater entanglement of indomethacin within the polymeric chains of HPMC.

This investigation showed that there is a greater tendency for the mobility of amorphous indomethacin within a PEG polymer matrix that resulted in the formation of H-bonded cyclic dimers characteristic of crystallisation to the most thermodynamically stable γ polymorph. Conventional ATR-FTIR spectroscopy revealed that during crystallisation of indomethacin from amorphous to the γ form, the metastable α form can be observed as an intermediate polymorph. Macro ATR-FTIR spectroscopic imaging was applied to study the interface between amorphous indomethacin and molten PEG during the cooling stage. The crystallisation of amorphous indomethacin was detected at the interface of this formulation upon mixing where obvious structural changes were characterised in the extracted spectra.

Furthermore, macro ATR-FTIR spectroscopic imaging was employed to study tablet dissolution and revealed that crystallisation of indomethacin in solution caused problems for the subsequent drug release from ASD tablets. Indomethacin/PEG tablets were characterised to crystallise to the γ form during *in situ* drug release experiments that inhibited drug release. Conversely, amorphous indomethacin formulated with HPMC did not crystallise and was observed to be readily dissolved from the studied tablets. As this Chapter intended, the results from the macro ATR-FTIR spectroscopic imaging of dissolving tablets have shown that careful selection of the most effective polymeric excipient is integral to enhance the release of indomethacin by impeding crystallisation in the formulations.

Overall, macro ATR-FTIR spectroscopic imaging served as a valuable tool in this Chapter to aid the understanding of mechanisms that control the dissolution behaviour and drug release. This approach has the potential to be applied to study different API/polymer systems where polymorphic changes are suspected or known to be problematic during storage and drug release.

5 Comparison of Pharmaceutical Formulations: ATR-FTIR spectroscopic Imaging to Study Drug-Carrier Interactions

In this Chapter, macro ATR-FTIR spectroscopic imaging has been used in combination with parallel UV detection to study the release of indomethacin when formulated with carefully selected excipients that can potentially act as drug carriers. In the first Section of this work, a series of tablets made from indomethacin (drug) formulated with nicotinamide (carrier) in different weight ratios were studied. This research provided the opportunity to propose mechanisms of the release of indomethacin from the dissolving tablets, which have been explained in this Chapter. Furthermore, the predicted drug release mechanisms have been validated by the study of tablets made of indomethacin formulated with urea and mannitol. Macro ATR-FTIR spectroscopic imaging provided highly chemically specific information as well as revealing the spatial distribution of the components during the dissolution process. Parallel UV detection meant that the rate and amount of indomethacin dissolved could be quantified during the experiment.

5.1 Background

A significant challenge often encountered during the development of innovative pharmaceutical formulations is achieving effective drug delivery since many drug candidates are poorly soluble in aqueous media. Therefore, there is a great drive towards improving the dissolution and release rates of the drug in the system (Kawabata et al., 2011, Vasconcelos et al., 2007, Leuner and Dressman, 2000). Some common examples include the ionisation of drugs to a more readily soluble form (Serajuddin, 2007), milling the drug substance to reduce the particle size (Salazar et al., 2013, Millan et al., 1998) and changing the structural form of the drug, i.e. reducing the crystallinity to form an amorphous state (Song et al., 2015, Newman et al., 2012, Kaushal et al., 2004). Potential caveats of using these approaches exist, for example, the amorphous form is in a thermodynamically unfavourable state so conversion to a more stable (or metastable) crystalline form can occur (Thakral et al., 2015, Patterson et al., 2005). It is also possible for the ionised species to undergo disproportionation, where the salt form converts back to its original acid or base structure. The formation of smaller particles is one of the most common approaches to improve the release of the drug (Merisko-Liversidge et al., 2003, Liversidge and Conzentino, 1995). The solvent free preparations of

microparticles containing a drug, indomethacin, and a polyelectrolyte for inhalatory administration have proven to be stable for long periods of time (Ceschan et al., 2015).

However, one approach that has shown promise to increase the dissolution rate of poorly water-soluble drugs is using an excipient that acts as a drug carrier (Leuner and Dressman, 2000). This method has been demonstrated, by both mathematical models (Ahuja et al., 2007) and experimentally (Jain, 2008, Watanabe et al., 2003), to improve the bioavailability of poorly water-soluble drug candidates. The development and research of drug delivery systems that contain more than one API are becoming more common, for example, in bilayer tablets (Zhang and McGeorge, 2015, Wray et al., 2014, Wardrop et al., 1998), tablet-in-tablet formulations (Wray et al., 2013) and in "polypill" compacts (Khaled et al., 2015, Sanz and Fuster, 2009, Wald and Law, 2003). It is feasible that if multiple drugs are administered within the same tablet then the formation of relatively strong intermolecular interactions, such as H-bonded interactions, can have an influence on the rate of drug release by acting as carriers. For example, some well-known commercial drugs such as Panadol® Extra Advance (GlaxoSmithKline) contain two APIs, paracetamol and caffeine, in the same tablet. Paracetamol acts as a painkiller whereas caffeine is a stimulant. However, caffeine has been shown to enhance the absorption and painkilling effect of paracetamol.

Similarly to Chapter 4, in this work indomethacin was selected as a suitable API in this investigation. Indomethacin is a non-steroidal anti-inflammatory drug (NSAID) which is poorly soluble in aqueous solutions. Indomethacin has been used as a model poorly water-soluble drug in a number of investigations where co-complexes between the drug and carrier have been achieved via H-bonded interactions (Majumder et al., 2013, Maruyoshi et al., 2012). Indomethacin with various hydrotropes such as sodium benzoate, nicotinamide, resorcinol and urea were studied which enhanced the solubility for aqueous injections (Jain, 2008). Ionic interactions and molecular aggregation increased solubilisation of indomethacin in these samples, but the interest for this specific thesis Chapter is the study of solid tablet compacts. Binary systems of indomethacin and nicotinamide in solid dispersions have also been studied for improving the release of the drug (Bogdanova et al., 1998). A range of analytical techniques, including FTIR spectroscopy and UV spectroscopy, were used to assess the dissolution of indomethacin. Bogdanova et al. (1998) reported that although there was an increase in the dissolution of the drug for some indomethacin/nicotinamide formulations, for those with a molar ratio above 1:1 (molar ratio) there was no improvement

in the amount of drug dissolved compared to those measured for pure amorphous indomethacin samples.

The solubilising effects of other potential carriers such as mannitol, PEG and lactose, for solid dosage forms have also been studied (Valizadeh et al., 2004). FTIR spectroscopic analysis showed that there was no conclusive evidence for interactions between indomethacin and some of the carriers used, including mannitol. What is particularly interesting is the fact that indomethacin was characterised to be in its amorphous form. This structural form has been reported to have a faster dissolution rate than the crystalline γ and α forms. Despite the fact that drug-carrier interactions were not identified for all the formulations, there was still an observed enhancement in the dissolution of indomethacin (Valizadeh et al., 2004). As a result, there is further scope to investigate the mechanisms involved in the drug release of indomethacin from formulations with reported drug carriers. A binary mixture of indomethacin and naproxen was studied with relevance to stabilising the two drugs in their amorphous forms (Löbmann et al., 2011). Stabilisation of amorphous naproxen was only achieved in co-amorphous mixtures with indomethacin and naproxen. This had a positive influence on the dissolution of the formulation, where synchronised release of the two drugs was measured.

Macro ATR-FTIR spectroscopic imaging approach has proven a versatile analytical tool for the study of dynamic processes, revealing information about structural changes within the measured samples (Kimber et al., 2014, Chan and Kazarian, 2004). However, the application of this approach could potentially lead to questions as to what is happening to the drug after it leaves the measured area. To complement the information obtained from the spectroscopic imaging approach, UV detection can be used in parallel to quantify the amount of API dissolved from different tablets (Pudlas et al., 2015, van der Weerd and Kazarian, 2004a). The aim of this study is to determine the effectiveness of binary drug tablets containing indomethacin (model drug) and selected excipients that have been reported to act as carriers or dissolution accelerators. Here, evidence and proposed drug release mechanisms were studied using macro ATR-FTIR spectroscopic imaging with parallel UV detection. The experimental setup used for all of the measurements is shown in Figure 5.1.

The first Section of the work undertaken in this Chapter compares the dissolution behaviour of compacted tablets formulated from indomethacin and nicotinamide (Figure 5.2), with different weight loadings. The interest of such formulations stems from the recent development of tablet dosage forms that contain multiple APIs (Wray et al., 2013, Lopes et

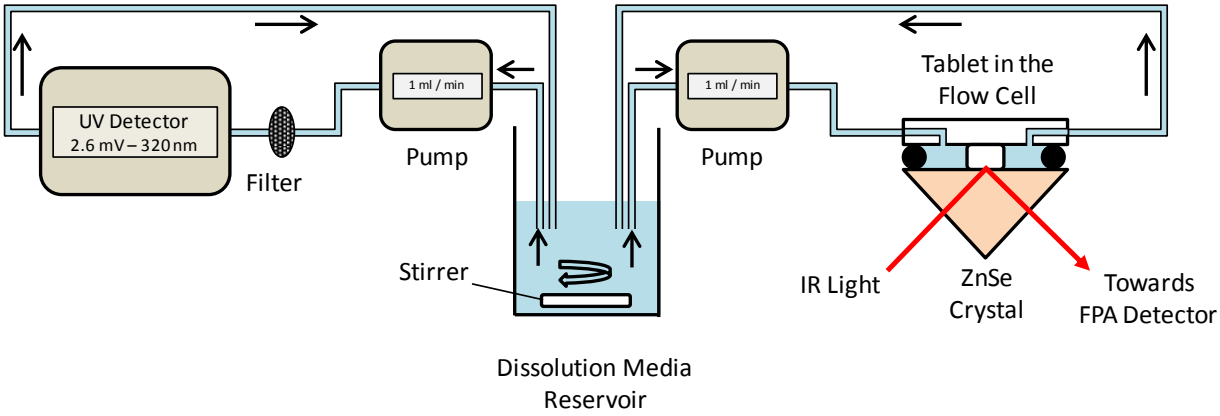


Figure 5.1 – Schematic diagram of the *in situ* experimental setup. The tablet sample is positioned between a flow cell and ZnSe crystal, and the flowing dissolution medium (in the direction of the arrows) was cycled around the closed experimental system. The experiment is monitored using macro ATR-FTIR spectroscopic imaging simultaneously with parallel UV detection.

al., 2007, Conte and Maggi, 1996). There is still a great need for a robust and reliable approach that can reveal how the two components will interact and subsequently influence drug release. In some cases, interaction between the drugs may be undesirable (Shende et al., 2013). Conversely, the dissolution and release of poorly water-soluble drugs can be improved by interactions with a more soluble drug candidate (Bogdanova et al., 1998). The inherent chemical specificity of macro ATR-FTIR spectroscopic imaging, together with parallel UV detection has demonstrated the potential of this combinational setup to reveal valuable mechanistic insight about dissolving tablet compacts. Moreover, the proposed drug release mechanisms were assessed by the investigation of formulations containing indomethacin with added urea and mannitol (Figure 5.2). Such formulations were studied based on their reported behaviour in the literature, where urea is expected to form interactions with indomethacin and mannitol to act as a dissolution accelerator. The results of this investigation have confirmed the mechanisms of drug release for all of the different formulations and thus demonstrate the application of this combined *in situ* approach to aid the design of novel pharmaceutical formulations.

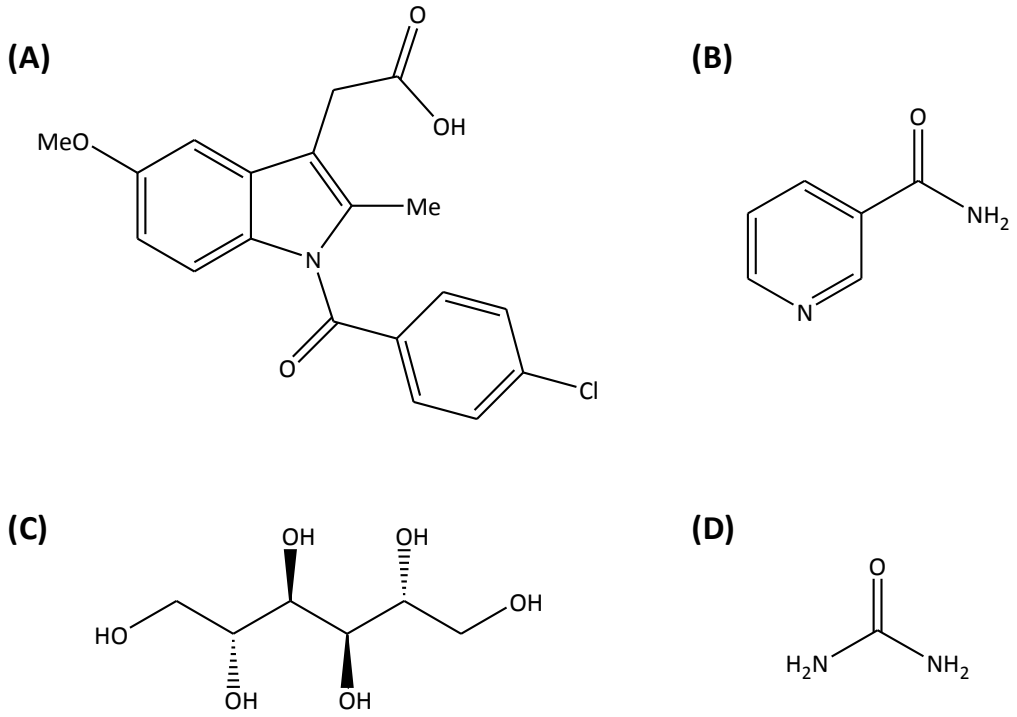


Figure 5.2 – Chemical structures of the pharmaceutical materials studied in this work. (A) Indomethacin, (B) nicotinamide, (C) mannitol and (D) urea.

5.2 Materials and methods

5.2.1 Preparation of formulations

Indomethacin, urea, mannitol and nicotinamide were purchased from Sigma-Aldrich (UK). All of the formulations were prepared using a hot melt method. Different composition mixtures of indomethacin (mp: 155–162 °C) and nicotinamide (mp: 128 °C), varying from 10 % (weight ratio) up to 90 % (weight ratio) of loaded drug were made. These formulations were treated by heating the materials on a temperature controlled hotplate up to 165 °C, ensuring that both powdered samples had melted. The mixture was maintained at this temperature for 5 min while being stirred to ensure that the formulation was homogeneous. The melts were then flash cooled using liquid nitrogen and stored in a desiccator at room temperature until ground and compacted. Treated reference samples of amorphous indomethacin (100 %) were prepared using the same hot melt method. It should be noted that the urea (mp: 132–135 °C) and mannitol (mp: 167–170 °C) formulations with indomethacin were prepared following the same procedure where the formulation was heated and maintained at 165 °C and 175 °C respectively to ensure that both materials had melted. Before compaction into tablet samples suitable for the dissolution setup used in this study, the

formulations were ground using a pestle and mortar. 20 mg of the formulation was compacted into tablets using a custom-designed press with a diameter of 3 mm.

5.2.2 ATR-FTIR spectroscopy and spectroscopic imaging approach

A Bruker Alpha-P FTIR spectrometer with a single element detector was used to measure the initial infrared spectra of the individual components in this investigation. The spectrometer was setup in ATR mode using a diamond crystal. The mid-IR range across 4000–600 cm^{-1} was measured at a resolution of 8 cm^{-1} and 32 co-added scans.

The FTIR spectroscopic imaging approach was utilised in macro ATR mode. This study used a ZnSe crystal, which was aligned for use with a variable angle ATR accessory (PIKE Technologies) to measure spectroscopic images of the whole tablet during the different experiments. The accessory was placed in the macrochamber of the system that is specifically designed for FTIR spectroscopic imaging applications. The macrochamber was fitted to an Equinox 55 FTIR spectrometer (Bruker, Germany) and an FPA detector to record spectroscopic images in the mid-infrared region between 4000–900 cm^{-1}. OPUS software was used to record the spectral data at a resolution of 8 cm^{-1} and 32 co-added scans. A macro was used in OPUS to record the spectroscopic images at regularly defined intervals during the experiments. The pixel array size using a VeeMax II accessory was 96 × 96 pixels resulting in an image size of approximately 7.75 × 6.05 mm^2 and a spatial resolution of ~150 µm (Kazarian and Chan, 2013b).

The ATR-FTIR spectroscopic imaging approach allows the spatial distribution of the different materials in the sample to be generated based on identifying unique infrared absorption bands for each component. Table 5.1 shows the specific range of the unique absorption band that was integrated to generate the spectroscopic images representing the different components in this study. It should be noted that since the different excipients display characteristic absorption bands in the spectrum, careful analysis of the position of the absorption bands to generate the spectroscopic images was carried out to ensure there was no overlap of the spectral bands. For example, indomethacin (nicotinamide) in Table 5.1 represents the integration range used to obtain the distribution of indomethacin in the measurements of the indomethacin/nicotinamide formulations.

Table 5.1 – The specific absorption band ranges that were used to generate the ATR-FTIR spectroscopic images for the different species in this study.

Material	Absorption band range (cm^{-1})
Indomethacin (Nicotinamide)	1338–1295
Indomethacin (Mannitol)	1380–1340
Indomethacin (Urea)	1250–1200
α indomethacin (Urea)	1760–1720
Nicotinamide	1437–1410
Urea	1630–1500
Mannitol	1200–1005
Phosphate buffer	3600–3000

5.2.3 Experimental setup for drug release investigations

A closed system was used to allow collection of both spectroscopic images and quantitative information about the release and dissolution of indomethacin. This system included a 400 mL volume of dissolution medium ensuring sink conditions were maintained (Figure 5.1). For the ATR-FTIR spectroscopic imaging measurements, a custom designed Perspex flow cell was used in a similar manner as has been described in previous dissolution studies using this approach for tablet dissolution experiments (van der Weerd and Kazarian, 2005). As shown in Section 3.3, the tablet was positioned in the centre of the ZnSe crystal and held in place by pressing the Perspex flow cell from the top of the tablet. A seal was formed using a rubber O-ring meaning that sufficient contact between the crystal and the tablet was formed, which was required for collection of spectroscopic images. Since the tablet was sandwiched between the flow cell and the ZnSe crystal, the top and bottom surfaces of the tablet were not in contact with the dissolution medium during the experiments. All of the experiments were carried out at ambient conditions and the dissolution medium, a phosphate buffer (pH 7) solution, was circulated through the system at a rate of 5 mL/min using a Hitachi pump.

400 mL of phosphate buffer (pH 7) was prepared by mixing a solution of 0.1 M sodium hydroxide solution to 0.1 M potassium dihydrogen phosphate solution in a 0.8:1.0 ratio. Both chemicals were products of Sigma-Aldrich (UK).

In this investigation, all of the experiments were repeated three times to ensure that the results were reproducible. Representative spectroscopic images for the experiments are shown in the figures throughout and the error bars, calculated by the standard deviation from

the mean absorbance recorded in the UV data, are displayed in the dissolution profiles obtained by UV detection. As a consequence of the experimental setup used in this work, the tablet is only in contact with the dissolution medium via its circumference. Hence, the dissolution rate is expected to be slower compared to conventional dissolution methodologies such as USP testing.

5.2.4 Calibration of UV detector to quantify release of indomethacin

A Kontron 332 UV detector was used in parallel to the spectroscopic imaging approach to quantify the amount of indomethacin dissolved in the solution during the experiment. The UV detector was setup to measure the change in absorbance at 320 nm that was identified as a suitable UV absorbance peak for indomethacin as this does not overlap with the UV absorbance from any of the other excipients used in this investigation. Quantification was determined by dissolving 10 mg of indomethacin in ethanol and diluting the solution with further known aliquots of ethanol to construct a calibration plot. Figure 5.3 shows the resulting calibration curve that was obtained for indomethacin.

By using the equation of the trend line from this calibration plot (Figure 5.3), it was possible to determine the amount of indomethacin dissolved from the different tablets. This

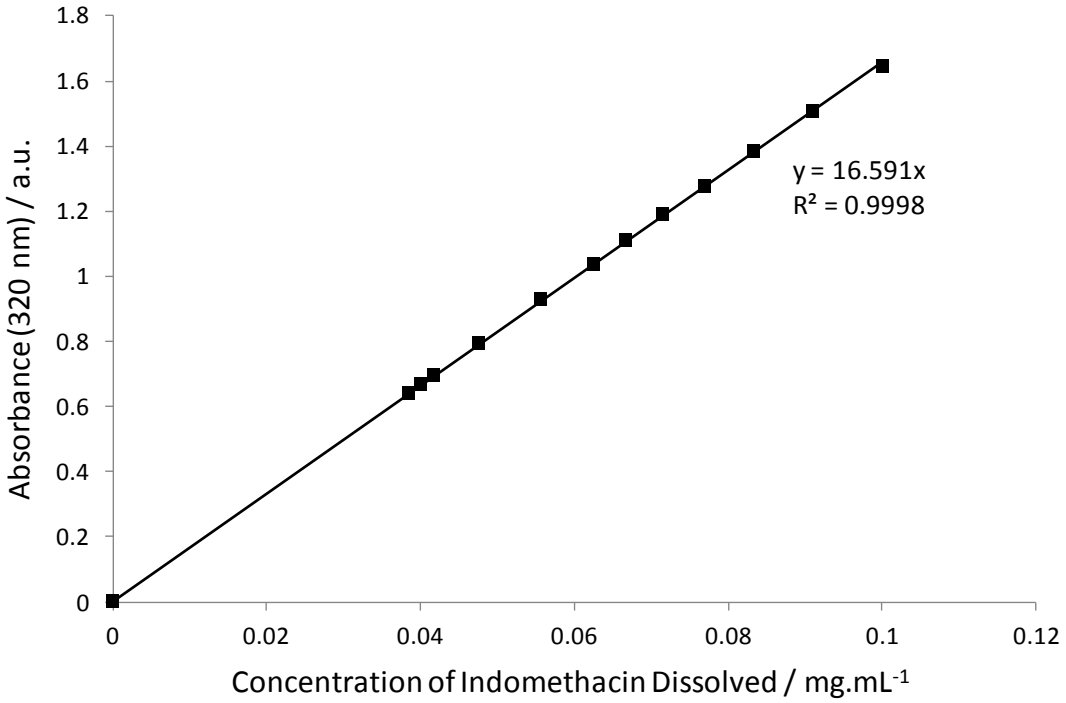


Figure 5.3 – Calibration plot showing the concentration of dissolved indomethacin vs. absorbance at 320 nm, recorded for indomethacin dissolved in ethanol. The calibration plot was used to quantify the release of indomethacin from the different compacted tablets.

method provided the opportunity to compare the different formulations directly. For this to be accurately calculated, the weight of the tablet and the volume of dissolution medium were kept constant for all of the experiments. Each tablet weighed 20 mg, and the volume of phosphate buffer used was 400 mL. The amount of indomethacin in the respective tablets was determined from the weight loadings of the materials within the formulation. As a result, this allowed one to determine the maximum concentration ($mg.mL^{-1}$) of dissolved indomethacin in the solution after complete release. Next, the relationship between the concentration of indomethacin dissolved (x-axis) and absorbance (y-axis) is determined by the equation (y = 16.591x). Hence, analysis of increasing absorbance at 320 nm during the experiments allowed the concentration of dissolved indomethacin and consequently the percentage of indomethacin release from the tablets to be obtained and compared.

5.3 Macro ATR-FTIR spectroscopic imaging of indomethacin/nicotinamide formulations

The first part of this Section focuses on binary formulations comprised of two model drug candidates with different dissolution behaviours in aqueous solution, indomethacin (poorly soluble) and nicotinamide (readily soluble). The weight loading of the indomethacin/ nicotinamide formulations were systematically varied and studied using ATR-FTIR spectroscopic imaging and parallel UV detection. The compositions of the different tablets studied are shown in Table 5.2.

Table 5.2 – Different formulations studied using the ATR-FTIR spectroscopic imaging approach with parallel UV detection.

Compact identification	Weight loading of indomethacin (%)	Weight loading of nicotinamide (%)
Tablet A	10	90
Tablet B	15	85
Tablet C	25	75
Tablet D	50	50
Tablet E	75	25
Tablet F	100[(1)]	0
Tablet G	100[(2)]	0

[(1)] Tablet F contained pure γ indomethacin

[(2)] Tablet G contained pure amorphous indomethacin

Due to the nature of the functional groups within the chemical structures of nicotinamide and indomethacin it is possible to form physicochemical H-bonded interactions between the readily and poorly soluble species (Maruyoshi et al., 2012, Bogdanova et al., 1998). Some of the potential H-bonded interactions have been considered and shown in Figure 5.4. The H-bonding schemes in Figure 5.4 account for the intermolecular interaction between the same species, i.e. indomethacin-indomethacin, as well as between indomethacin-nicotinamide. In fact, during the formulation of these two species, it would be expected that there will be competing interactions in which only the most stable would be favoured. After formation of these intermolecular interactions between the species and provided that these interactions be maintained during the dissolution process, the more readily soluble drug should act as a carrier, thus increasing the release of the poorly water-soluble drug into the solution.

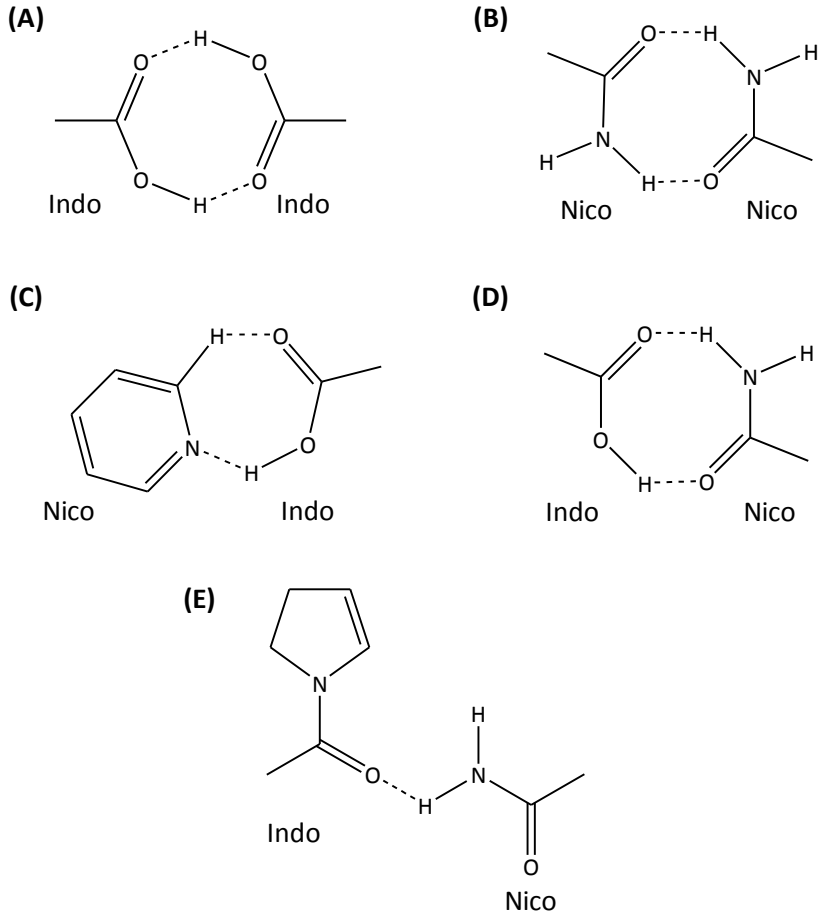


Figure 5.4 – Potential H-bonded interactions between certain functional groups in indomethacin and nicotinamide. The parent molecules of each functional group in this scheme are labelled as Indo and Nico, respectively.

5.3.1 Analysis of ATR-FTIR spectroscopy and spectroscopic imaging results

Figure 5.5 shows ATR-FTIR spectra of pure amorphous indomethacin, pure nicotinamide and the 25:75 (weight ratio) indomethacin/nicotinamide formulation (Tablet C) after preparation by the hot melt method. The shift in the peak of the absorption bands from 1611 and 1124 cm^{-1} to 1624 and 1114 cm^{-1}, respectively (highlighted in Figure 5.5) have been identified as a result of the intermolecular H-bond formation between the two components (Bogdanova et al., 1998). It should be noted that the hot melt procedure was used for preparing the formulation in this investigation such that indomethacin was in the amorphous form. Furthermore, proof that indomethacin is present in its amorphous form after preparation is determined by the appearance of the absorption bands with peaks at 1462, 1315, 1219, 1073, 921 and 749 cm^{-1}.

The ATR-FTIR spectroscopic images presented in Figure 5.6 show the relative amount of indomethacin, nicotinamide and the phosphate buffer solution during the dissolution experiments of Tablets A, C and D. It is clear from the spectroscopic images that there is faster dissolution and release of the indomethacin from the tablets made from the formulations that contained a lower weight loading of indomethacin. These results could

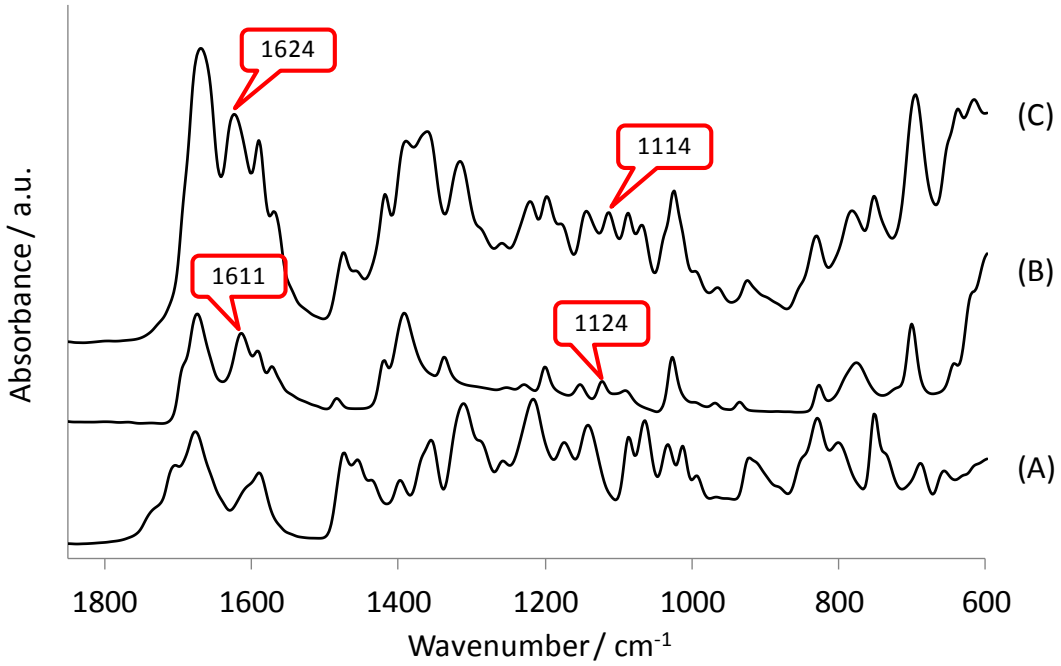


Figure 5.5 – ATR-FTIR spectra of (A) pure amorphous indomethacin, (B) pure nicotinamide and (C) the 25:75 (weight ratio) indomethacin/nicotinamide formulation (Tablet C, Table 5.2) after preparation. The specific shifts in peak positions that indicate formation H-bond interactions between indomethacin and nicotinamide are highlighted by the red labels.

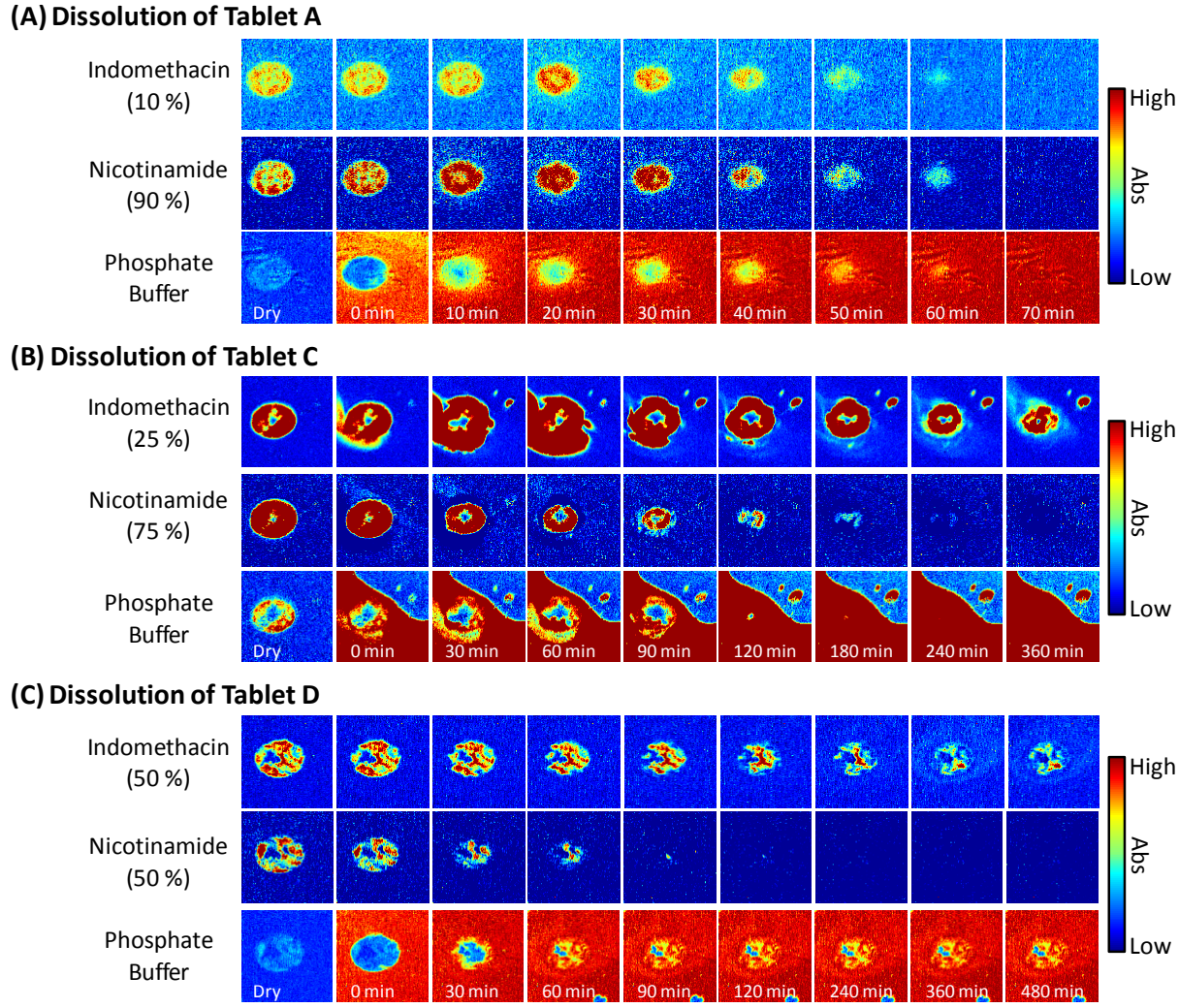


Figure 5.6 – Representative ATR-FTIR spectroscopic images recorded from the *in situ* dissolution experiments (the image size is approximately 7.75 × 6.05 mm^2). The distributions of indomethacin, nicotinamide and the phosphate buffer are shown during the dissolution of (A) Tablet A, (B) Tablet C and (C) Tablet D.

suggest that a carrier is not needed, and the accelerated dissolution is caused simply by the disintegration of the tablet matrix as the more readily soluble species dissolves in the solution, exposing a higher surface area of indomethacin to the solution. Thus, two valid drug release mechanisms can be proposed with respect to the indomethacin in the tablet: (1) that indomethacin is being carried by the nicotinamide via the H-bonded interactions (Bogdanova et al., 1998), or (2) that disintegration is occurring, resulting in a higher surface area of indomethacin exposed to the buffer, resulting in more rapid dissolution (Talukdar and Kinget, 1995, Ford et al., 1987).

ATR-FTIR spectroscopic imaging has proven a powerful approach for such applications over the last decade regarding the *in situ* characterisation of the transformations within the

samples (Kazarian and Ewing, 2013, Chan and Kazarian, 2006b, van der Weerd and Kazarian, 2005, Kazarian and Chan, 2003). As shown in Figure 5.5, the absorption bands with the peaks at 1114 and 1624 cm^{-1} indicate that there are H-bonded interactions forming in the indomethacin/nicotinamide formulations after preparation (Bogdanova et al., 1998). Information revealing the behaviour of these interactions during dissolution experiments is integral to determine the mechanisms of drug release. Figure 5.7 demonstrates the spatial and chemical information that can be obtained from such measurements showing representative spectroscopic images of Tablet A with accompanying extracted spectra from selected pixels within the tablet during the dissolution experiment. It can be seen that throughout the experiments, even in areas where the buffer solution is present within the tablet, there is evidence of the absorption bands indicative of H-bonded interactions.

The rate of indomethacin and nicotinamide dissolution from Tablet A (Figure 5.6A) are synchronised, in so much that, as the nicotinamide concentration decreases so does the concentration of indomethacin. Conversely, for Tablet C and D it appears that nicotinamide dissolves faster than indomethacin. Figure 5.6B and C show that there is no presence of nicotinamide after 180 min and 60 min, respectively. This is important because when there is no nicotinamide remaining in the tablets, it is not possible for there to be interactions between the two components. As a result, any remaining indomethacin will dissolve without the aid of

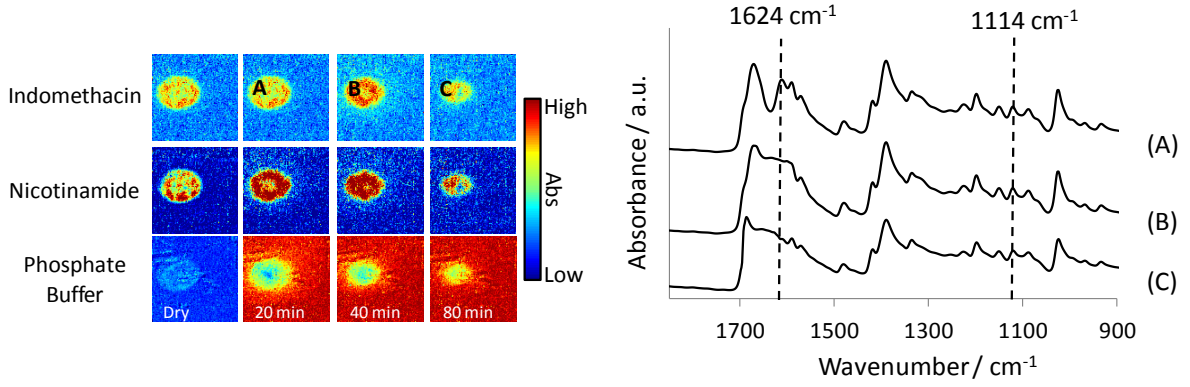


Figure 5.7 – ATR-FTIR spectroscopic images showing the dissolution of Tablet A (the image size is approximately 7.75 × 6.05 mm^2). The distribution of indomethacin, nicotinamide and the phosphate buffer are shown. The spectra are extracted from the same pixel of the FPA detector but from images recorded at different times. The dashed lines highlight the spectral peaks indicative of H-bonded interactions. The broadening of the spectral region between 1675–1615 cm^{-1} in the extracted spectra for (B) and (C) are a result of water vibrations from the solution.

the carrier. However, as shown in Figure 5.7, when both pharmaceutical components are present within the tablet the intermolecular interactions can be maintained and thus the drug can be carried into the solution. Here, the application of ATR-FTIR spectroscopic imaging for the study of such systems allows one to propose different mechanisms of drug release occurring in real time during the experiment.

5.3.2 Monitoring the amount of indomethacin dissolved using UV detection

To provide additional analytical insight, a Kontron 332 UV detector was used in parallel with the ATR-FTIR spectroscopic imaging approach to measure the amount of indomethacin dissolved from the tablets during the experiment. To improve the accuracy of the results a filter was placed in the tubing before the UV detector to prevent any undissolved solid particles from affecting the measurements. Figure 5.8 shows the dissolution profiles for the percentage of indomethacin dissolved from all the tablets (A–G, Table 5.2).

The dissolution experiments were measured for 480 min (8 hr) or until complete dissolution of the indomethacin was achieved. As expected, the dissolution rate of the tablets containing pure amorphous and γ indomethacin displayed slow drug release during this period. However, Tablet G, made from pure amorphous indomethacin did result in a higher

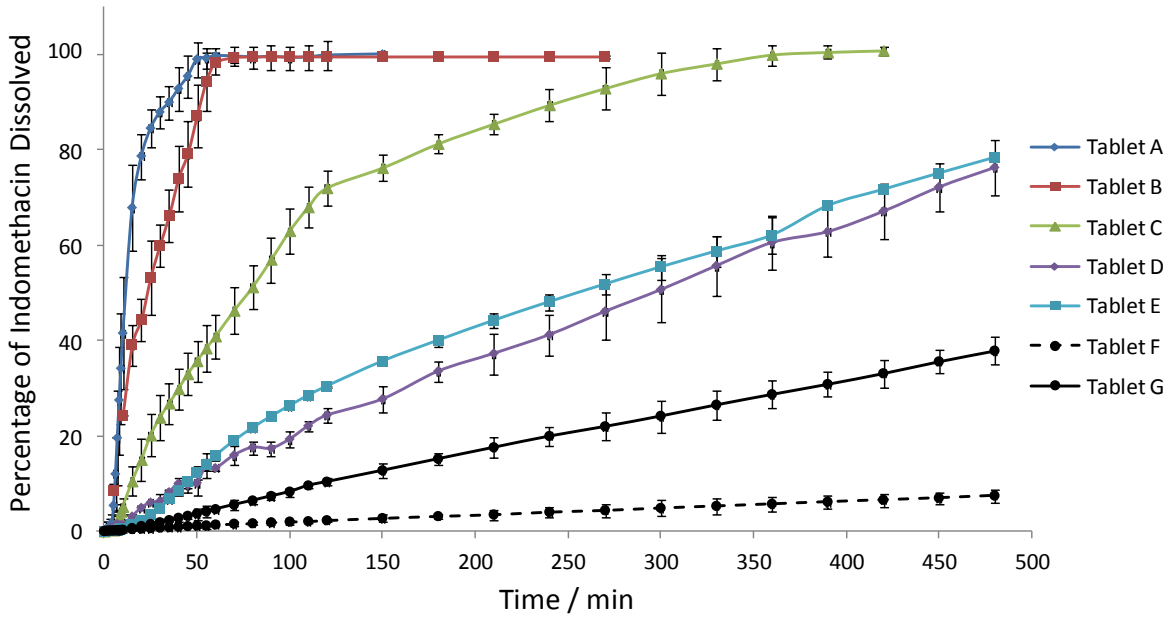


Figure 5.8 – Dissolution profiles obtained using UV detection that show the percentage of indomethacin dissolved from the tablet as a function of time for the different tablets studied (Table 5.2). Tablets A–E contained indomethacin and nicotinamide in varying weight loadings. Tablets F and G are pure indomethacin in its γ and amorphous form, respectively.

dissolution rate compared to the γ indomethacin (Tablet F), where 38 % and 7 % of the indomethacin was dissolved from the 20 mg tablet after 480 min, respectively. Another interesting observation is the linearity of the dissolution profiles measured for Tablets F and G. Such behaviour is typical of a zero-order release curve, defined by the drug dissolving independently of its concentration. In some cases, the zero-order release of a drug can be highly desirable since the rate of dissolution can be accurately predicted. It has been reported that a zero-order release profile can be observed when the change in surface area of the dissolving species is slow (Talukdar and Kinget, 1995, Peppas, 1985). This finding suggests that the area available for dissolution for Tablets F and G in the experimental setup used in this investigation changes very slowly which results in the low release of indomethacin. If the drug candidates are particularly poorly water soluble, as in the case of indomethacin, the release from the tablet may not be fast enough for the drug to be effectively absorbed and have a therapeutic effect on the body before it passes through the system, which is typically around 8 hr. The experiments carried out in this investigation were continued for up to 24 hr in specific cases where complete dissolution of indomethacin was not achieved. The results of the dissolution of indomethacin from Tablet F and G are shown in Figure 5.9 and provide further evidence of a zero-order release from these tablet compacts.

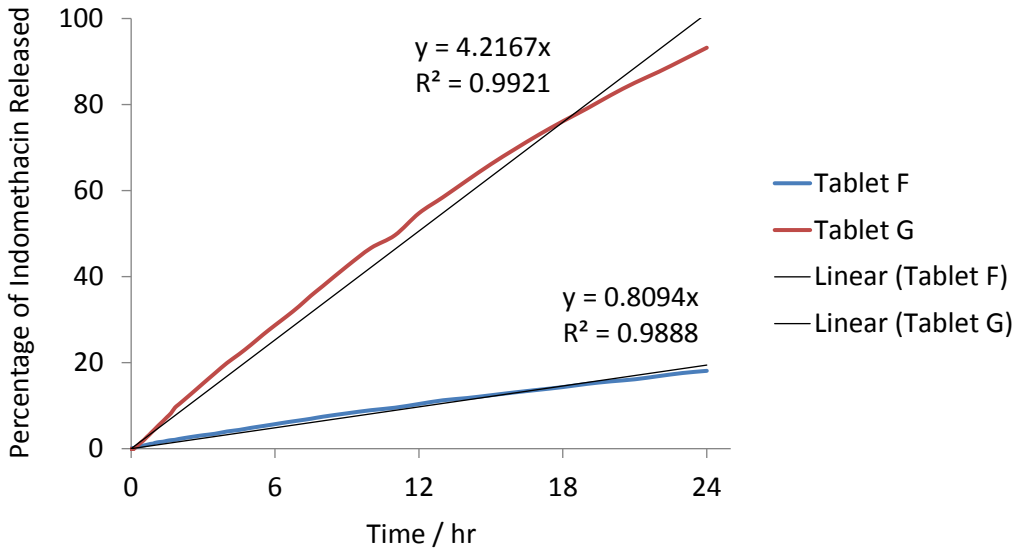


Figure 5.9 – Dissolution profiles showing the percentage of indomethacin dissolved from the tablet during 24 hr for Tablets F and G, made from pure γ and amorphous indomethacin, respectively. The linear trend of the data provides evidence of zero-order drug release from these tablets.

Figure 5.8 confirms that all of the compacted tablets containing nicotinamide did show an improvement in the rates of drug dissolution for indomethacin. The UV dissolution profiles further support the ATR-FTIR spectroscopic images recorded for the experiments which confirm that the drug is dissolving as it is released from the tablet. The use of these combined methodologies means that it is possible to collect a wealth of highly chemically specific information about the different formulations in real time.

5.3.3 Combined analysis of macro ATR-FTIR spectroscopic imaging with parallel UV detection

The spectroscopic images in Figure 5.6A representing the dissolution of Tablet A show that there is a relatively rapid dissolution of the drug, and there is no longer the presence of indomethacin after 60 min. The UV dissolution profile for this formulation (blue line with circle markers in Figure 5.8) shows a remarkably similar time frame to the depletion of indomethacin recorded in the ATR-FTIR spectroscopic images for the release of the drug from Tablet A. Any offset can be attributed to the time taken for the solution to flow from the ATR-FTIR spectroscopic imaging flow cell and reach the UV detector. However, good agreement between the two methods has been demonstrated in terms of determining the time of drug release from the model compacted tablets.

In contrast, Tablet C displayed two different release rates of indomethacin during the experiment. The UV detection shows that there is a burst release between 0–120 min, followed by a slightly slower dissolution rate of the remaining indomethacin until complete release is achieved at 360 min. Figure 5.10 shows selected spectroscopic images recorded during the experiment, along with the dissolution profile for these formulations. The spectroscopic images indicate that there is an initial burst release around the outer surface of the tablet where a higher concentration of both nicotinamide and indomethacin can be observed outside the original tablet diameter. This phenomenon is proposed to have been due to the H-bonded complexes formed between the two components, where proof of the formation of this complex is characterised in Figure 5.10C. However, the core of the tablet remains unaffected during this stage. The ATR-FTIR spectra have been extracted from the pixels marked by the "X" in the spectroscopic images (Figure 5.10B). The spectrum extracted from the image recorded at 120 min shows that the spectral bands for the interactions are no longer present in the formulation. Information revealed in the extracted spectra indicate why two different rates of dissolution of indomethacin were identified in the UV data. The change in dissolution rate was observed around 120 min that is coincident with the time of

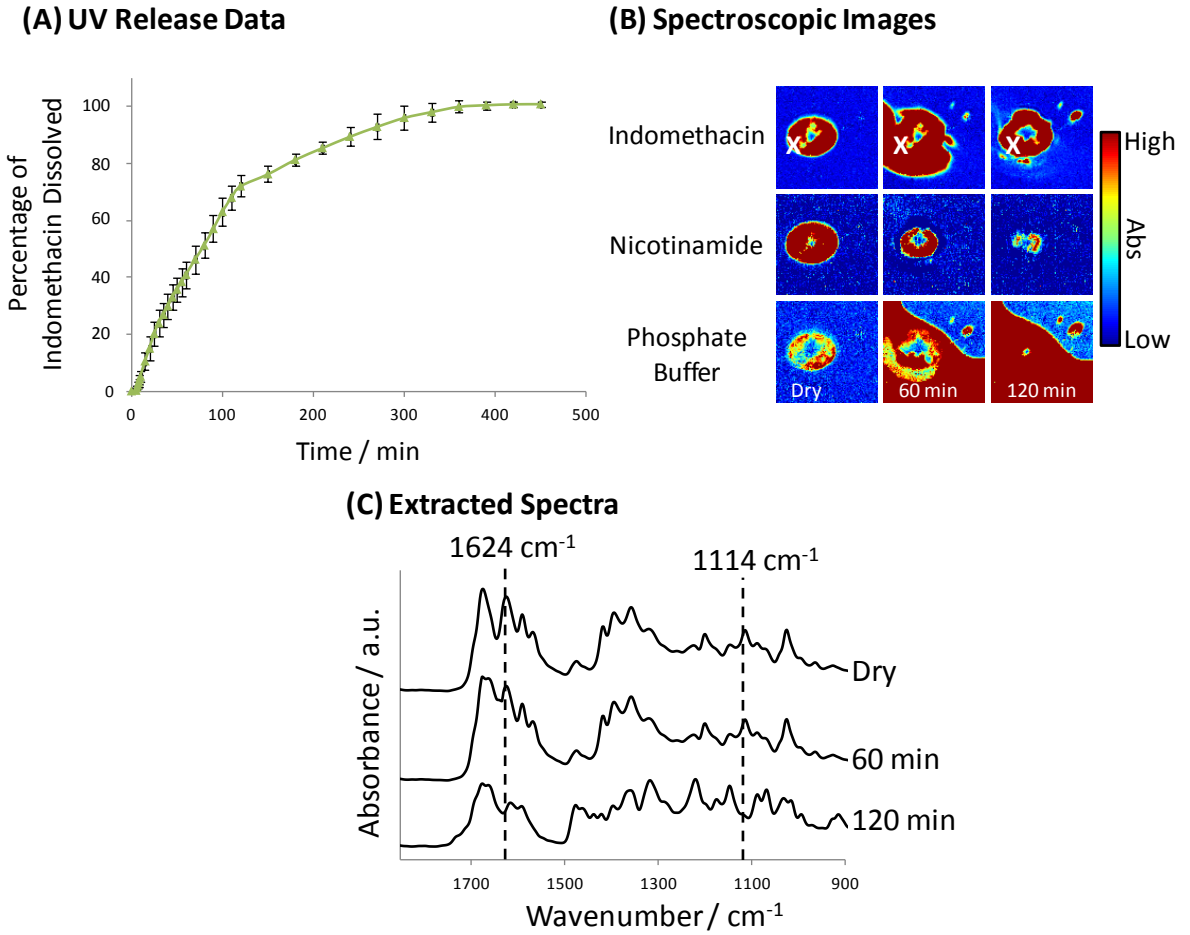


Figure 5.10 – Data recorded from the dissolution experiments of Tablet C. (A) UV drug dissolution profiles, (B) ATR-FTIR spectroscopic images (the image size is approximately 7.75 × 6.05 mm^2) and (C) accompanying spectra from the images extracted from the pixel marked "X". The distribution of indomethacin, nicotinamide and the phosphate buffer are shown in the spectroscopic images.

nicotinamide depletion from the tablet in the spectroscopic imaging data (Figure 5.6B). It is also interesting to note that during this change in the rate of dissolution, the gradient of the release curve is very similar to those obtained for Tablets D and E. As a result, there are two apparent dissolution mechanisms occurring within this tablet during the experiment. Firstly, there is an immediate release where the indomethacin-nicotinamide interactions are present, and increased dissolution of the drug is observed. Secondly, the disintegration of the tablet matrix results in an increased surface area of indomethacin exposed to the dissolution medium. Thus, the dissolution of indomethacin continues, albeit at a slower rate.

Analysis of the UV dissolution profile for Tablets D and E show that there is a faster release of the drug compared to the pure amorphous indomethacin compacted tablets (Figure

5.8). However, it was observed that the rate of drug dissolution for these two compacted tablets was very similar during the different experiments, where the final quantities of dissolved indomethacin recorded at 480 min were 76 % (Tablet D) and 78 % (Tablet E). The similarity in drug release was not expected since the loading of indomethacin in the formulations was different. When comparing all of the dissolution results analysed by the UV detection for the different tablets it appears that there are certain formulations in which indomethacin-nicotinamide interactions will be formed more favourably than others.

Formation of intermolecular interactions can be explained based on consideration of the molecular structures of indomethacin and nicotinamide (Figure 5.2). In certain molar ratios, it is feasible that different intermolecular interactions will compete within the formulation. Some of the possible indomethacin-nicotinamide interactions have been described by Maruyoshi et al. (2012). It has been reported that H-bonds forming between the carbonyl group (COOH) in the indomethacin and the aromatic functional group in the nicotinamide can be characterised. It was also reported that the different structural forms of indomethacin (amorphous, α and γ forms) are also a result of intermolecular interactions between two indomethacin molecules (Taylor and Zografi, 1997a). For example, the γ form is a cyclic dimer of two indomethacin molecules. Thus, as the loading of indomethacin was increased to 50:50 (weight ratio) or higher there is greater competition between the possible intermolecular interactions. The competing interactions may result in an increased concentration of indomethacin-indomethacin complexes instead of indomethacin-nicotinamide H-bonded complexes.

In the case of Tablets D and E, due to the nature of the formulation preparation, it can be expected that there are some indomethacin-nicotinamide interactions occurring but the effect of the carrier is only apparent at the very start of the experiment, rather than maintained during the entire experiment. The UV dissolution profiles collected for Tablets D and E show that there is much less influence of nicotinamide as a carrier in these formulations, displayed by the typical zero-order release in Figure 5.8. Instead, the dissolution mechanism in these tablets is more consistent with a disintegration effect on the tablet. The spectroscopic images in Figure 5.11 suggest that this is a result of the nicotinamide readily dissolving and exposing an increased surface area of the remaining indomethacin to the phosphate buffer. As the nicotinamide dissolves from the tablet it leaves only indomethacin and the phosphate buffer in the imaged area, after 60 and 90 min for Tablet D and E, respectively. The appearance of pores within the tablets suggests that there is an increased surface area of indomethacin that is

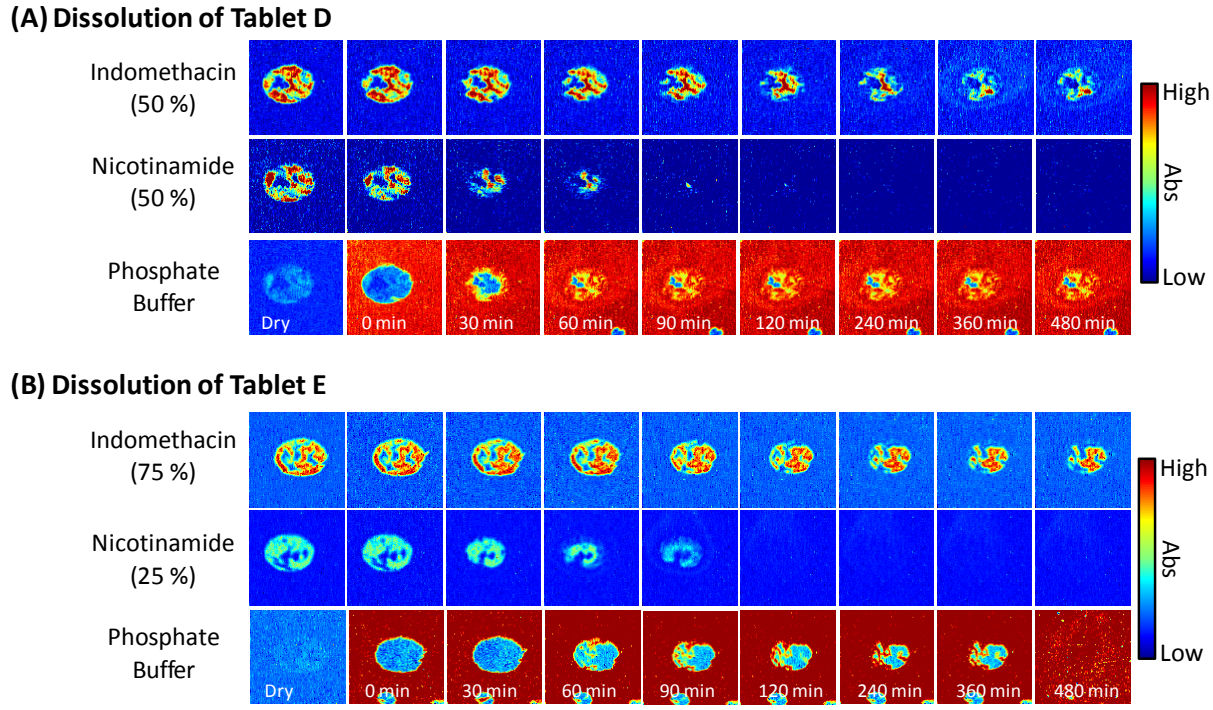


Figure 5.11 – ATR-FTIR spectroscopic images recorded during the dissolution experiments for (A) Tablet D and (B) Tablet E (image size is approximately 7.75 × 6.05 mm^2). The distribution of indomethacin, nicotinamide and the phosphate buffer as the experiment progressed are shown.

available to dissolve in the aqueous medium. When one considers the setup of the tablets in this system such effect can manifest itself in a faster drug dissolution profile.

The first Section of this Chapter has demonstrated the combined experimental setup utilising ATR-FTIR spectroscopic imaging with parallel UV detection. These analytical approaches have proven extremely reliable for the identification of specific interactions between two drug candidates in a model pharmaceutical tablet and assess the effect these have on subsequent dissolution. There is further scope for this setup to be used to reveal vital insight about other samples of interest, including those in the developmental pipeline. The ratio and loading of the drug are very important and can significantly affect the mechanism of drug release due to the nature of competing intermolecular interactions within the formulations. Here, all of the formulations containing nicotinamide resulted in a substantial increase in the dissolution of indomethacin. These results show that by understanding the behaviour of components in a formulation, one can effectively predict and control the dissolution profile of a poorly water-soluble drug by using excipients that can act as a carrier, whether it is for immediate or extended drug delivery.

5.4 Macro ATR-FTIR spectroscopic imaging of indomethacin with other pharmaceutical excipients

To verify the feasibility of the suggested tablet dissolution mechanisms i.e. nicotinamide acting as a carrier for indomethacin in some cases and as a dissolution accelerator in other cases, two additional formulations were studied. Urea was used in a formulation with indomethacin since it has been reported to have carrier properties for this drug (Jain, 2008). Urea was carefully selected over the other carriers reported in this work because of its favourable chemical properties, meaning that it was compatible to be prepared using the hot melt method, in keeping with the indomethacin/nicotinamide formulations. As a way to assess the effect of a disintegrating tablet a readily soluble and commonly used pharmaceutical additive, mannitol, was employed. Mannitol was selected because it was reported to improve the dissolution of indomethacin, but no conclusive interactions have been identified between the compounds (Valizadeh et al., 2004). Possible H-bonded interactions for indomethacin with urea and mannitol are shown in Figure 5.12.

Here, the dissolution of indomethacin from tablet formulations containing 25:75 (weight ratio) of indomethacin and the excipient were studied using ATR-FTIR spectroscopic imaging and parallel UV detection. Figure 5.13 shows the drug dissolution profiles recorded using the UV detector for the different formulations. The dissolution rates from the indomethacin and nicotinamide formulation in Tablet C, which contained the same weight loading (Table 5.2) has been included in the graph. The drug dissolution profiles show that

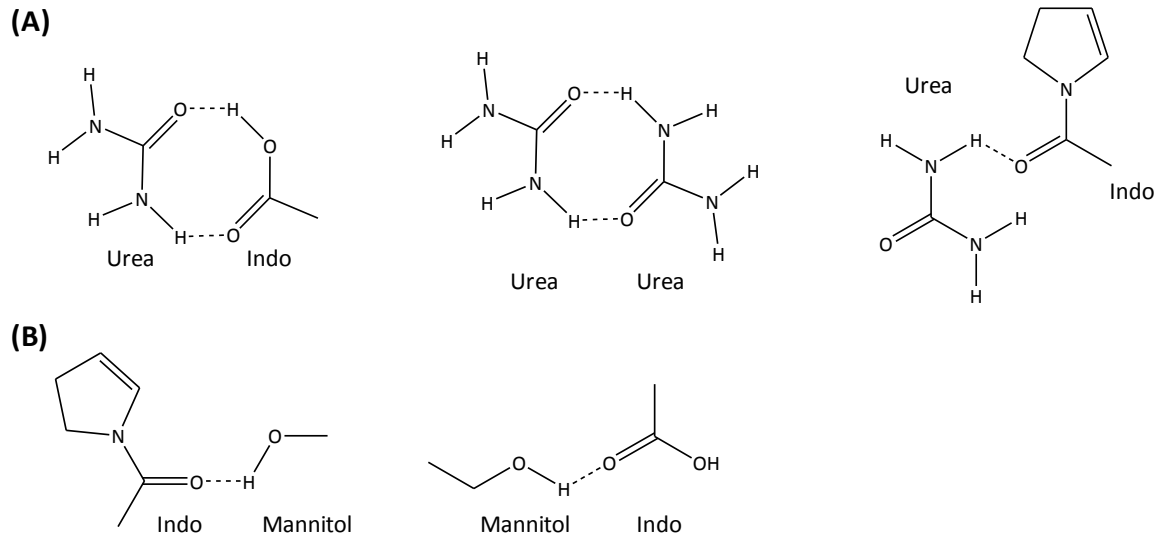


Figure 5.12 – Potential H-bonded intermolecular interactions between (A) indomethacin and urea, and (B) indomethacin and mannitol.

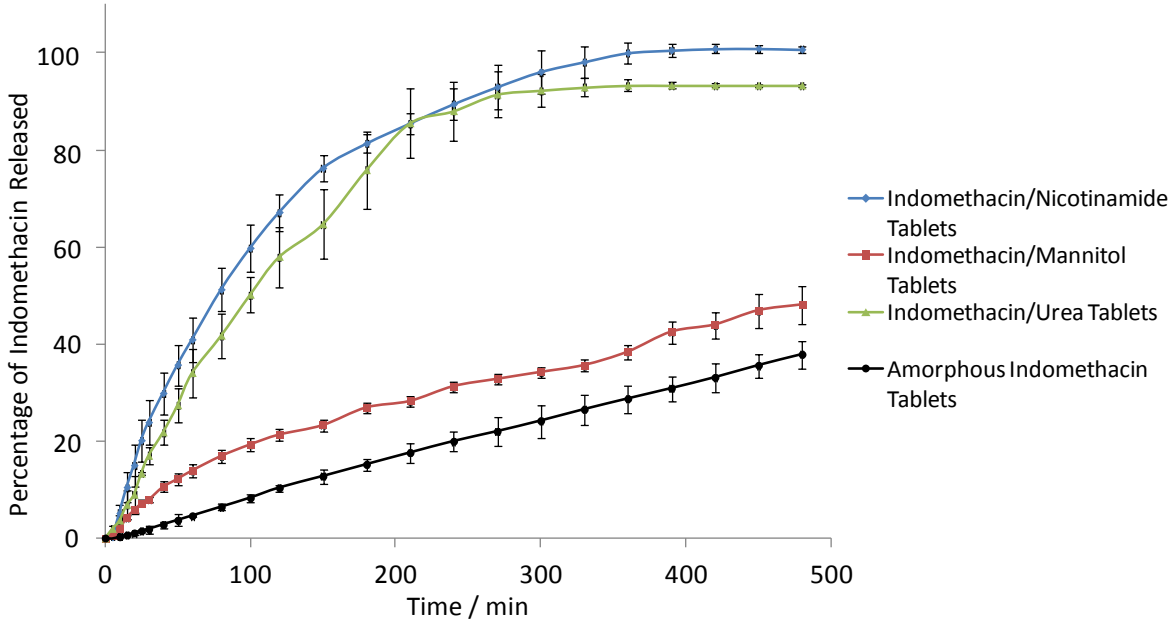


Figure 5.13 – UV drug dissolution profiles recorded for the indomethacin/mannitol (Red line with square markers) and indomethacin/urea (Green line with circle markers) compacted tablets (25:75 weight ratio). The UV drug dissolution profiles of pure amorphous indomethacin (black line, square markers) and indomethacin/nicotinamide (blue line, circle markers) in 25:75 weight ratio (Tablet C, Table 5.2) have been shown for comparison.

there are some similarities between those observed for the release of the indomethacin from the nicotinamide formulations, described in the previous Section.

In general, the drug dissolution profiles indicate that the indomethacin/nicotinamide formulation gives the fastest dissolution of the drug. Urea, the other excipient added as a carrier, initially showed a similar dissolution profile to the indomethacin/nicotinamide tablets (Figure 5.13). However, complete dissolution of the drug was not achieved. Conversely, the indomethacin/mannitol tablets show a much more controlled dissolution of the drug during the experiments, much like Tablets D and E (Table 5.2) containing indomethacin/ nicotinamide. The total amount of drug dissolved after 8 hr is slightly lower than these indomethacin/nicotinamide formulations (Tablets D and E). In these tablets only ~48 % of the indomethacin was dissolved as opposed to 76 % dissolved from Tablet D in the formulations with added nicotinamide. Figure 5.14 shows representative spectroscopic images for the dissolution of urea and mannitol formulations which provides further insight into the behaviour of the components within the tablets during dissolution.

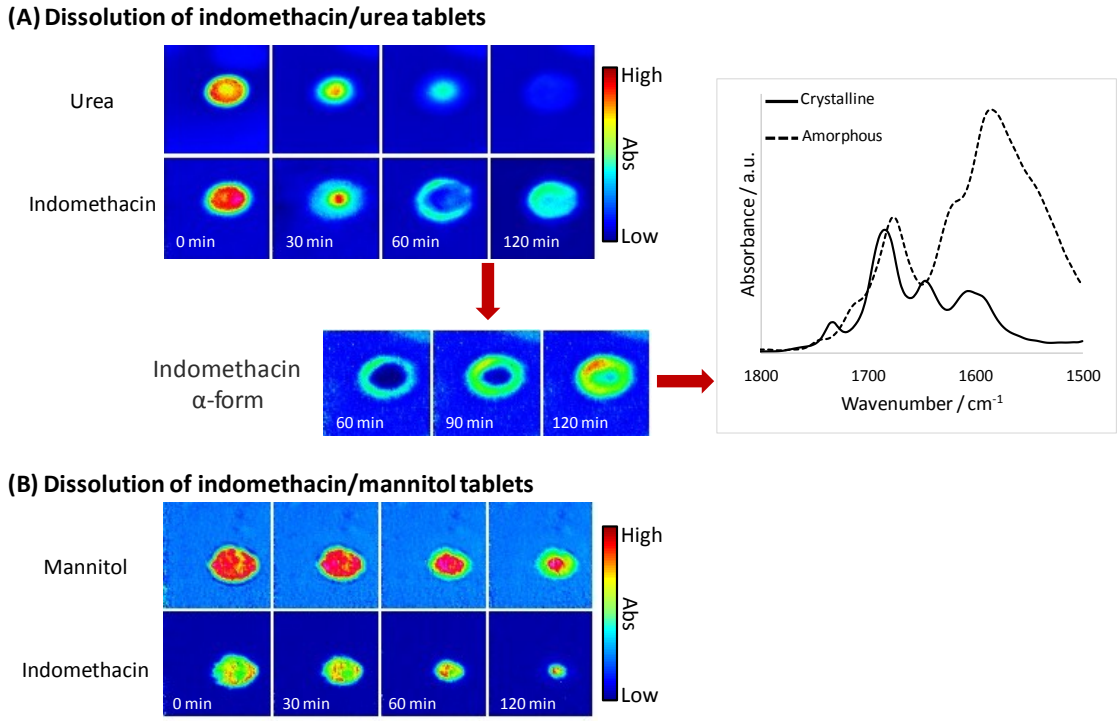


Figure 5.14 – (A) ATR-FTIR spectroscopic images recorded for the dissolution of the indomethacin/urea tablets. The spatial distribution of urea, amorphous indomethacin and α form of indomethacin are shown. Extracted spectra confirm the conversion of the amorphous form (dashed line) to α form ("Crystalline", solid line) which is most easily distinguished by the appearance of the band with a peak at 1649 cm^{-1}. (B) Shows the spectroscopic images recorded during the indomethacin/mannitol tablet dissolution experiments. The distribution of mannitol and indomethacin are shown.

The indomethacin/urea tablets showed that the rate of dissolution was reduced during the experiments. Reasons for this can only be assumed by analysis of the UV profiles. However, the *in situ* spectroscopic images can further explain the observation by providing structural information from the surface layer of the tablet as the experiment progressed. During the experiments, the urea and indomethacin appear to dissolve at a simultaneous rate, i.e. as the urea dissolves so does the indomethacin. The similar rates of release can be attributed to the fact that urea can act as a carrier. The spectroscopic images recorded at 120 min show that there appears to be no distribution of urea, only indomethacin in the measured area. The ability to select individual absorption bands characteristic of the components make the approach particularly powerful for pharmaceutical applications (Table 5.1). For example, the spectral band selected to generate the images for indomethacin is 1250–1200 cm^{-1} which is characteristic of the amorphous form. Under certain experimental conditions, indomethacin can recrystallise to its preferable lower energetic state γ or α form (Ewing et al., 2014). As a

result, an absorption band for the α crystalline form was identified at 1760–1720 cm^{-1}. After 60 min, the spectroscopic images resulting from the integration of this band show that there is an initial onset of the α form that increases in concentration as the experiment proceeds. The fact that it appears in a ring-like formation around the outside of the tablet would indicate that as the urea leaves the tablet, some indomethacin is deposited and crystallises during tablet dissolution.

The effect of the crystallisation of indomethacin is reflected in the UV drug dissolution profiles as a plateau occurring after ~200 min, seemingly preventing any further dissolution of indomethacin into the surrounding system. It is unlikely that the dissolution is prevented but rather inhibited to such a slow rate that is not observed during the remainder of the experiment, i.e. dissolving at a similar rate to pure indomethacin (Tablet F). From the quantitative dissolution profiles, it is determined that approximately 10 % of the indomethacin did not dissolve during the experiment. While this is a relatively small amount, structural changes of drugs can have adverse effects on the body. For example, it is not uncommon for patients on long courses of medication containing NSAIDs, such as indomethacin, to experience aggravations to the lining of the gastrointestinal tract as a result of recrystallisation (Abdallah, 2010).

The drug dissolution profile recorded during the dissolution of the indomethacin/ mannitol tablets show a similar zero-order profile to that recorded for indomethacin/ nicotinamide Tablets D and E. This is a result of tablet disintegration in the indomethacin/nicotinamide formulations. While there are similarities between the two formulations, different rates of dissolution are observed (Figure 5.13). One explanation can be considered based on the solubility of the nicotinamide and mannitol. In the phosphate buffer solution (pH 7), the solubility of nicotinamide and mannitol are 1.0 and 0.18 $g.L^{-1}$, respectively. Hence, it is proposed that nicotinamide will act more effectively as a disintegrant compared to mannitol. The formation of pores in the tablet causes disruption to the initial matrix and leads to an increase in drug release as a consequence. The pores mean that a larger surface area of the tablet can potentially come into contact with the solution and thus is available for dissolution (Talukdar and Kinget, 1995, Ford et al., 1987). The ATR-FTIR spectroscopic images (Figure 5.14B) and the drug dissolution profiles (Figure 5.13) recorded from the experiments further substantiate this claim. The total dissolution of the drug at 480 min was lower from the mannitol tablets (48 %) compared to the nicotinamide tablets (76 %). The lower release of drug was surprising because there was a much higher

drug loading in the tablets with added nicotinamide (50:50 weight ratio) compared to in the mannitol (25:75 weight ratio) formulations. The spectroscopic images for mannitol indicate that there is a slightly slower ingress of the dissolution medium. Nevertheless, much like the nicotinamide formulations, it is observed that the mannitol depletes from the tablet at a slightly faster rate than indomethacin that result in a zero-order rate of dissolution.

5.5 Conclusions

The aim of this Chapter was to demonstrate the potential application of macro ATR-FTIR spectroscopic imaging as a reliable and robust approach to study intermolecular interactions between the components in model pharmaceutical tablets. The use of parallel UV detection provided additional quantitative information about the amount of drug dissolved during the experiments. Furthermore, the indomethacin/nicotinamide tablet compacts studied in this investigation exhibit the first application of ATR-FTIR spectroscopic imaging to study two pharmaceutical drugs in a single tablet, where the chemical specificity of the spectroscopic imaging approach allows mechanistic information of drug release to be revealed. The pharmaceutical sector is developing formulations that contain multiple drugs so an understanding of how intermolecular interactions affect tablet dissolution is becoming increasingly important.

All of the compacted tablets showed an increased dissolution rate of indomethacin compared to the pure drug tablets. The spectroscopic imaging data and dissolution profiles that were obtained from the systematic study of different indomethacin/nicotinamide formulations meant that two different mechanisms for the dissolution of the drug could be identified. Nicotinamide was selected as an excipient for its reported ability to act as a carrier for poorly water-soluble drugs. During this investigation, specific formulations were identified where the effect of the carrier was optimal. The formulations containing 10:90 weight ratio and 15:85 weight ratio of indomethacin and nicotinamide showed a fast dissolution of the entire drug into the surrounding solution. In the spectroscopic images, it was possible to identify characteristic bands in the infrared spectrum that confirmed that H-bonded interactions had been formed and maintained during the experiments. It was concluded that the increased dissolution of indomethacin was a result of these interactions where nicotinamide acted as a carrier. In contrast, the tablets studied which contained a 50 % and 75 % weight loading of indomethacin showed very similar dissolution rates to one another. An alternative mechanism was proposed whereby nicotinamide acts as a disintegrant because of it's relatively high solubility in the aqueous medium thus accelerating dissolution.

The proposed mechanisms were further assessed by studying tablets containing indomethacin with added urea and mannitol. The tablets with added urea showed fast drug dissolution arising from its carrier capabilities. Conversely, the mannitol tablets showed typical zero-order drug release, suggesting that disintegration of the tablet matrix occurred resulting in an increased surface area for dissolution. An increased surface area was determined to have a significant influence for increasing the dissolution of the drug in these formulations. Moreover, the study of all of the pharmaceutical compacts in this investigation demonstrated that a range of carriers can be considered to optimise formulation design. Macro ATR-FTIR spectroscopic imaging provided particularly valuable information allowing mechanisms to be established with respect to interactions between indomethacin and potential carriers. Whereas, chemically specific information could not be identified using the UV drug dissolution profiles. Thus, combining these analytical approaches demonstrates a unique opportunity to study the tablet dissolution mechanisms and quantify the amount of drug dissolved during the experiments.

6 Evaluating Drug Delivery with Salt Formation: Drug Disproportionation Studied *In Situ* by ATR-FTIR Imaging and Raman Mapping

This Chapter presents the application of two vibrational spectroscopic approaches, macro ATR-FTIR spectroscopic imaging and Raman mapping, to determine the behaviour of tablets containing an ionised drug during dissolution experiments *in situ*. The results presented in previous Chapters of this thesis studied model pharmaceutical systems; however, an antiviral drug that is in the developmental pipeline was the focus of this work. The motivation for the work undertaken here stems from the fact that ionised drugs can convert back to their thermodynamically favourable free acid or base forms during the storage or delivery stages. This Chapter contains the experimental results with a specific focus on the structural changes of the drug in different aqueous pH environments.

6.1 Introduction

A widely applied approach to improve the solubility and dissolution rates of poorly soluble drugs in tablet dosage forms is to include the API in the form of an ionised salt derivative (Elder et al., 2013, Serajuddin, 2007). It is reported that up to 50 % of drugs are manufactured as salts and the success of using these ionised species in tablet compacts largely relies on their stability both before and during drug release (Wray et al., 2015). However, under certain conditions, there is a tendency for the salt to convert back to its unionised form via a hydrolysis reaction, known as disproportionation (Stephenson et al., 2011). Disproportionation can have a significant impact on the dissolution behaviour of the API due to unwanted physical and chemical changes occurring in the drug. Thus, the potency and reliability of the API can be compromised as a result of disproportionation (Guerrieri and Taylor, 2009).

When designing new pharmaceutical formulations, it is critical to determine the factors that impact the stability of a drug product and inhibit structural changes occurring in the product. Knowledge of the aqueous solubility and the pK_a of the salt and free acid forms of the API allow predictions to be made about the stability of the ionised form and the potential of this to disproportionate. Mechanistic modelling, with supporting experimental studies, have been used to study the effects of different excipients on disproportionation (Merritt et al., 2013). This information aids the design of new formulations since it allows the

compatibility of drug-excipient combinations to be predicted and provides valuable insight into the stability of the salt form, ultimately leading to a more robust product.

Depending upon the properties of the API, many different factors can initiate and affect the rate of disproportionation. In addition to the selected excipient (Christensen et al., 2012, Guerrieri and Taylor, 2009), the chosen counter ion (David et al., 2012, Guerrieri et al., 2010), method of formulation processing (Christensen et al., 2014, Christensen et al., 2012) and the local conditions during processing (Hsieh and Taylor, 2015, Zannou et al., 2007) can have an effect on the stability of the final product. Spectroscopic approaches have proven useful for characterising chemical changes to the API in such formulations. Model ionised APIs with commonly employed pharmaceutical excipients have been reported to disproportionate under the influence of a number of different factors (Guerrieri and Taylor, 2009). A general trend suggests that the ionised APIs that have a higher solubility exhibit a greater propensity to disproportionate to their respective free base form compared to those that have a lower solubility. The pH value of the aqueous solution and the microenvironment, influenced by the excipients used, as well as the humidity level also have an effect on the extent of conversion (Skrdla and Zhang, 2014, Govindarajan et al., 2006). It should be considered that conversion of an API to the salt form may not always be intended during the production process. Salt formation of acidic drugs was demonstrated during wet granulation preparation (Christensen et al., 2014). Thus, the processing conditions used will also have an effect on the physicochemical properties of the API, which can impact the quality of the final product.

Infrared and Raman spectroscopy are both widely used industrial techniques for analysing pharmaceutical materials. These approaches support the progress of novel products from initial development through to large scale manufacturing. In this Chapter, Raman mapping and macro ATR-FTIR spectroscopic imaging were used as complementary vibrational spectroscopic approaches that allow the spatial distribution of components within the measured sample to be determined. These approaches have been proven as useful tools for pharmaceutical research where the ability to study polymorphic and chemical changes (Larkin et al., 2015, Vajna et al., 2011b, Velasco et al., 2011, Aina et al., 2010, Chan et al., 2004, Taylor and Langkilde, 2000, Taylor and Zografi, 1997a), characterisation of impurities (Vajna et al., 2011a, Ricci et al., 2007c) and dissolution behaviour of solid dosage forms (Ewing et al., 2014, Wray et al., 2011, Savolainen et al., 2009, van der Weerd and Kazarian, 2005) have been demonstrated. However, this is the first time that these spectroscopic

approaches have been applied to compare *in situ* studies of the tablet dissolution process of the same formulation as a function of time.

Raman mapping and macro ATR-FTIR spectroscopic imaging were used to monitor disproportionation in a formulation containing a developmental antiviral drug (Figure 6.1). This API is intended for use in its ionised monosodium form. Here, the behaviour of this species during *in vitro* dissolution experiments in aqueous media with different pH values was assessed. The ability to obtain chemical information from the sample means that the different structural forms of the API can be characterised *in situ*. Moreover, spatially resolved information about any structural changes occurring within the tablet can be obtained (Kazarian and Ewing, 2013, Shinzawa et al., 2009a, Kazarian and Chan, 2003, Clarke et al., 2001).

The Raman mapping approach was based on the measuring an array of specified points from the sample by movement of a motorised stage. Repeating the stage movements continuously during the tablet dissolution experiment allowed chemical maps of the measured points to be recorded. The changes to the functional groups in the molecules that undergo disproportionation are reflected in the measured Raman spectrum by changes in the appearance of absorption bands that allow for chemical identification. A potential limitation of using Raman spectroscopy, depending upon the sample measured, is the appearance of fluorescence in the spectrum. Furthermore, spectral bands for water are not so dominant in the Raman spectrum. Thus, it is difficult for Raman approaches to be used for screening the ingress of the aqueous medium within the samples or for the detection of dissolved species. The Raman microscope that was used in this work was fitted with a video camera that

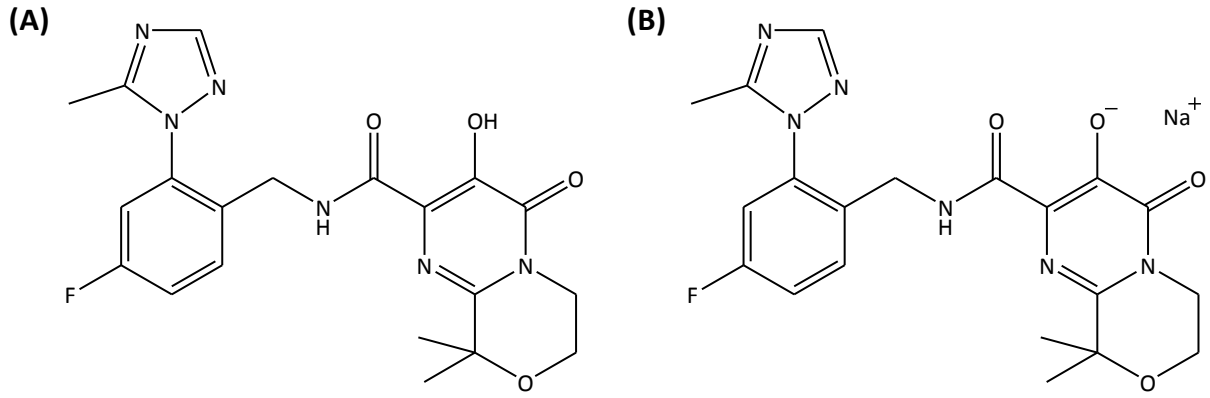


Figure 6.1 – Chemical structures of N-[[4-fluoro-2-(5-methyl-1H-1,2,4-triazol-1-yl)phenyl]methyl]-4,6,7,9-tetrahydro-3-hydroxy-9,9-dimethyl-4-oxopyrimido[2,1-c][1,4]oxazine-2-carboxamide, in its (A) monohydrate free acid form and (B) ionised monosodium salt form.

recorded visible images of the tablet. As a result, ingress of the aqueous medium could be revealed and provided information on the overall behaviour of the tablet structure during the experiments. One advantage of using Raman spectroscopy is that sample preparation is relatively straightforward since both the quartz slide, used as the top window for the flow cell and aqueous medium caused minimal spectral interference.

In this Chapter, macro ATR-FTIR spectroscopic imaging was used to assess tablet dissolution. This approach has been used elsewhere to study systems where the presence of water cannot be avoided, for example, to study drug release (Kazarian and Ewing, 2013, Wray et al., 2011) and for biomedical applications (Kazarian and Chan, 2013b, Kazarian and Chan, 2006a). In fact, unlike in the Raman mapping approach, the distribution of the aqueous medium in the imaged area can be observed and the behaviour of this species monitored during the experiment (Nanubolu and Burley, 2012). Figure 6.2 presents a schematic overview of the different analytical approaches utilised in this work.

Hydration is reported to initiate disproportionation (Rohrs et al., 1999), for example, humid environments can severely affect the state of the tablet before patient consumption. However, the onset and cause of disproportionation have not been investigated in dynamic dissolution experiments under flow in different pH conditions using these imaging approaches. The behaviour of an ionised API has been studied in aqueous solutions with different pH values. The chemical changes from the desired ionised monosodium form to the monohydrate free acid form of the drug have been characterised in the data presented in this Chapter that were recorded by ATR-FTIR spectroscopic imaging and Raman mapping.

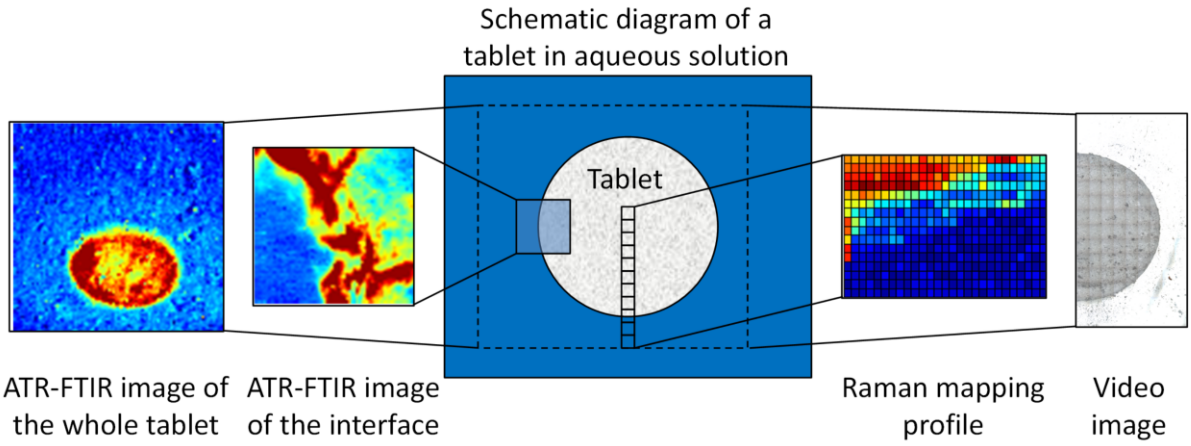


Figure 6.2 – Schematic overview of the different analytical approaches used to study the dissolving tablets *in situ*.

6.2 Materials and methods

6.2.1 Materials

Pure samples and formulated pharmaceutical tablets containing the drug (Figure 6.1, pK_a: 6.6) in its ionised form (37% by weight) and other excipients, listed in Table 6.1, were obtained directly from Bristol-Myers Squibb (Wirral, UK). The formulated pharmaceutical tablets were proprietary tablets prepared at Bristol-Myers Squibb. For the ATR-FTIR spectroscopic imaging experiments, tablets containing the ionised form of the drug were prepared by grinding the received formulation and compacting into tablets that were 3 mm in diameter. The Raman mapping approach used the same tablet compaction procedure but produced larger tablets, 7 mm in diameter. The reason that tablets of different sizes were studied was because they best suited the respective analytical approach. ATR-FTIR spectroscopic imaging measurements were limited by the field of view of the imaging whereas the Raman mapping approach was not.

Two different dissolution media were used in this investigation, deionised water and a 0.1 M hydrochloric acid (HCl) solution. The 0.1 M HCl solution was prepared by diluting 8.30 mL of 12 M HCl in 1 L of deionised water.

Table 6.1 – List components in the formulated tablets and their respective weight loadings (%).

Material	Loading (% by weight)
Drug	37
Lactose anhydrous	34
Silicon Dioxide	4
Sodium lauryl sulphate	2
Croscarmellose sodium	5
Avicel (MCC) PH102	17
Magnesium Stearate	1

6.2.2 Macro ATR-FTIR spectroscopic imaging approach

FTIR spectra of the pure components were measured using an Alpha-P spectrometer (Bruker, UK) in ATR mode. A spectral resolution of 8 cm^{-1} with 64 co-added scans was used for collection of reference spectra over a spectral range of 4000–600 cm^{-1}.

The FTIR spectroscopic imaging approach used two different ATR sampling accessories to obtain images of the dissolving tablets: Imaging Golden Gate (Specac, UK) and VeeMax II (PIKE Technologies) accessories. The accessory was placed within an IMAC macrochamber specifically designed for imaging applications that was attached to an FTIR spectrometer (Equinox 55, Bruker, UK). OPUS software was used to collect the infrared data over the spectral range of 4000–900 cm^{-1} with a resolution of 8 cm^{-1}. The number of co-added scans varied during the experiment; for the first 20 min, 16 co-added scans were recorded every 1 min due to the interest in faster accumulation of data to determine when disproportionation initiated during the experiment. After 20 min, the number of scans was increased to 64 co-added scans and a measurement recorded every 5 min for the duration of the experiment. The ATR-FTIR spectroscopic images were collected using an FPA detector. The array size selected was dependent upon the accessory used. The VeeMax II accessory used an array size of 96 × 96 pixels which resulted in an image size of approximately 7.75 × 6.05 mm^2 and a spatial resolution of 100–150 µm. The measurements on the Imaging Golden Gate accessory used a 64 × 64 pixel array size giving an approximate image size of 0.64 × 0.53 mm^2 with a spatial resolution of ~10–15 µm (Kazarian and Chan, 2013b).

Integration of the absorption bands listed in Table 6.2 were selected to generate the ATR-FTIR spectroscopic images of the different species presented in this thesis. The peak position of these spectral bands has also been indicated in Table 6.2. The red areas in the images relate to high absorbance and the blue areas relate to the low absorbance of the components in the spectroscopic images. The major polymer component characterised by ATR-FTIR spectroscopy in the tablets is Avicel. Hence, a unique absorption band for this component was selected to generated spectroscopic images of the polymer.

Table 6.2 – Spectral bands integrated to generate the false colour ATR-FTIR spectroscopic images and Raman maps, and the respective position of the peak of the spectral band is indicated.

Component	ATR-FTIR spectral band (cm^{-1})	ATR-FTIR spectral band peak (cm^{-1})	Raman spectral band (cm^{-1})	Raman spectral band peak (cm^{-1})
Drug (salt form)	1574–1555	1565	1654–1635	1645
Drug (free acid form)	1700–1650	1679	1695–1674	1685
Polymer (Avicel)	1235–927	1025		
Water	3600–3000	3295		
0.1 HCl solution	3600–3000	3295		

6.2.3 Raman mapping and video imaging approach

The Raman mapping used a dispersive Thermo DXR Raman microscope (Thermo, USA) with a motorised stage. Since this approach has relatively long acquisition times, the region of interest was selected to record data from the middle of the tablet to the edge of the dissolution cell, providing a radial profile of the tablet. Visible video images of half of the tablet were gathered in a 15 × 9 tile grid. The dimension of each tile was 722 × 542 μm^2. During the experiment, a Raman spectrum was collected every 250 μm in a linear pattern. A total of 17 measurements were recorded from the centre of the tablet to the edge. The acquisition time of the 17 Raman spectra, along with the tiled video images, was 10 min. Hence, this was cycled every 10 min for the duration of the experiment. A 780 nm laser was used and the acquisition parameters included a spectral range of 3300–50 cm^{-1}, a laser power of 24 mW where the estimated spot size was 3.1 μm and the aperture was set to a 50 μm slit. Six exposures of 3 s duration were used to record each spectrum. Raman spectra of the pure components were measured by the same Raman spectrometer using the identical settings as the mapping data but with ten exposures of 5 s to improve the SNR in the reference spectra. The Raman maps were generated using the same integration method as the ATR-FTIR spectroscopic images where a spectral band was selected representing the ionised and free acid form of the drug. The spectral ranges used to produce these false colour images are shown in Table 6.2, as is the peak position of the respective integrated band. The integrated peak values were plotted as an intensity map as a function of both position and time. In the

Raman maps, the red areas are indicative of a high scattering and the blue areas of a low scattering from the components of the chemical maps. The maps relate the concentration of scattering species through a similar relationship to the Beer-Lambert law.

6.2.4 Dissolution methodologies

Although two different ATR-FTIR imaging accessories were used, the dissolution experiments were setup in the same way. The tablet compact was placed between a Perspex flow cell (Figure 6.3A) and the ATR crystal. A rubber O-ring was used to form a water-tight seal. For the experiments using the VeeMax II accessory, the tablets were placed in the centre of the crystal to allow the whole tablet to be observed within the measured area. In contrast, for the experiments performed on the diamond crystal, the tablets were positioned offset from the centre of the crystal to allow information from the interface between the edge of the tablet and the dissolution medium to be obtained (see Section 3.3). In both cases, the flow cell provided slight pressure to the top of the tablet which allowed sufficient contact between the sample and the measuring surface of the crystal, which is needed for collection of data using this sampling methodology. The fact that the tablet was sandwiched between the flow cell and the crystal means that during the experiments the dissolution medium only surrounded the tablets from the sides.

For the Raman mapping approach, a custom designed flow cell with a top window of quartz glass and a reflective aluminium backing plate was used as shown in Figure 6.3B. Similarly to the ATR-FTIR dissolution cell, the sample was sandwiched between the window and the backing plate of the cell, separated by an adjustable sealing gasket to account for

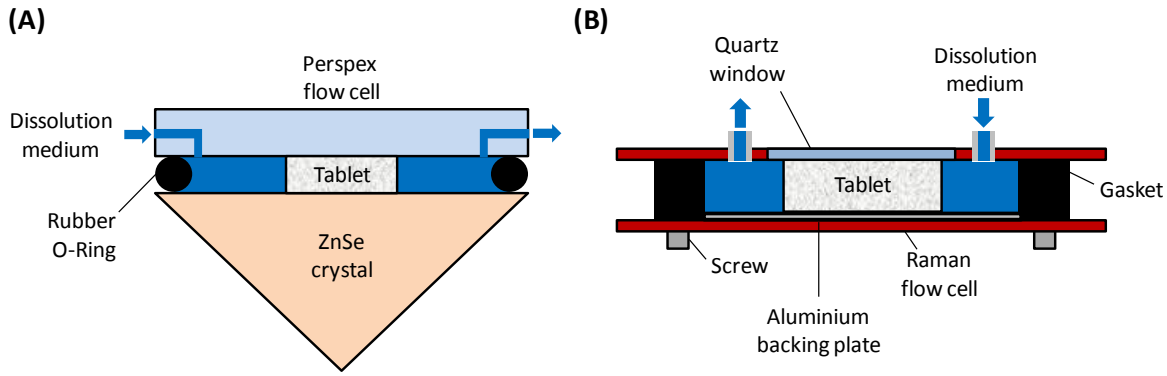


Figure 6.3 – Schematic diagrams showing the flow cells used to study the dissolving tablets using the different analytical approaches. (A) The Perspex flow cell used for ATR-FTIR spectroscopic imaging measurements and (B) the flow cell used for Raman mapping and collection of video data.

variability in the tablet thickness. The cell was positioned such that the microscope optics was able to acquire data from inside the flow cell.

In both of the respective flow cells, the dissolution medium flowed through the system at a rate of 1 mL/min. Fresh dissolution medium was continuously pumped through the flow cells and into a waste container to maintain sink conditions in the dissolution cell at all times, avoiding any cases of supersaturation. Each of the experiments was repeated three times to show reproducibility of the results and representative spectroscopic images and Raman maps have been presented herein.

6.3 Results and discussion

6.3.1 Detecting disproportionation of the ionised form of the drug

The antiviral development drug in the formulated tablets studied in this investigation is intended to be delivered in its ionised salt form (Figure 6.1). The ionised chemical form was predicted to be unstable and have the propensity to convert back to the free acid form in certain conditions and aqueous environments. The free acid form of the drug dissolves at a much slower rate compared to the ionised form and thus, the bioavailability will be affected if disproportionation was to occur during the tablet dissolution process, i.e. after the tablet is administered to a patient.

The spectra shown in Figure 6.4 demonstrate the suitability of ATR-FTIR spectroscopy and Raman spectroscopy to differentiate between the two structural forms, salt and free acid, of the drug. The ATR-FTIR spectra presented in Figure 6.4A show the spectral range of the fingerprint region across 1800–900 cm^{-1}. In the ATR-FTIR spectra of the two pure drug forms, there are some clear differences in the appearance of the absorption bands that enabled one to differentiate the species. For example, the ionised form displays unique bands between 1630–1600, 1574–1555 and 1320–1270 cm^{-1}. In contrast, the carbonyl absorption band at 1700–1650 cm^{-1} is the most obvious absorption band that identified the drug in the free acid form. Figure 6.4B shows Raman spectra of the pure drug forms. Similarly to the ATR-FTIR spectra, there are again also clear spectral differences between the salt and free acid forms. The region over 1850–1400 cm^{-1} has been presented since there are several unique peaks associated with the ionised drug present at 1645, 1622, 1601, 1435 and 1420 cm^{-1}. Whereas, the free acid form of the drug displays a unique peak at 1685 cm^{-1}.

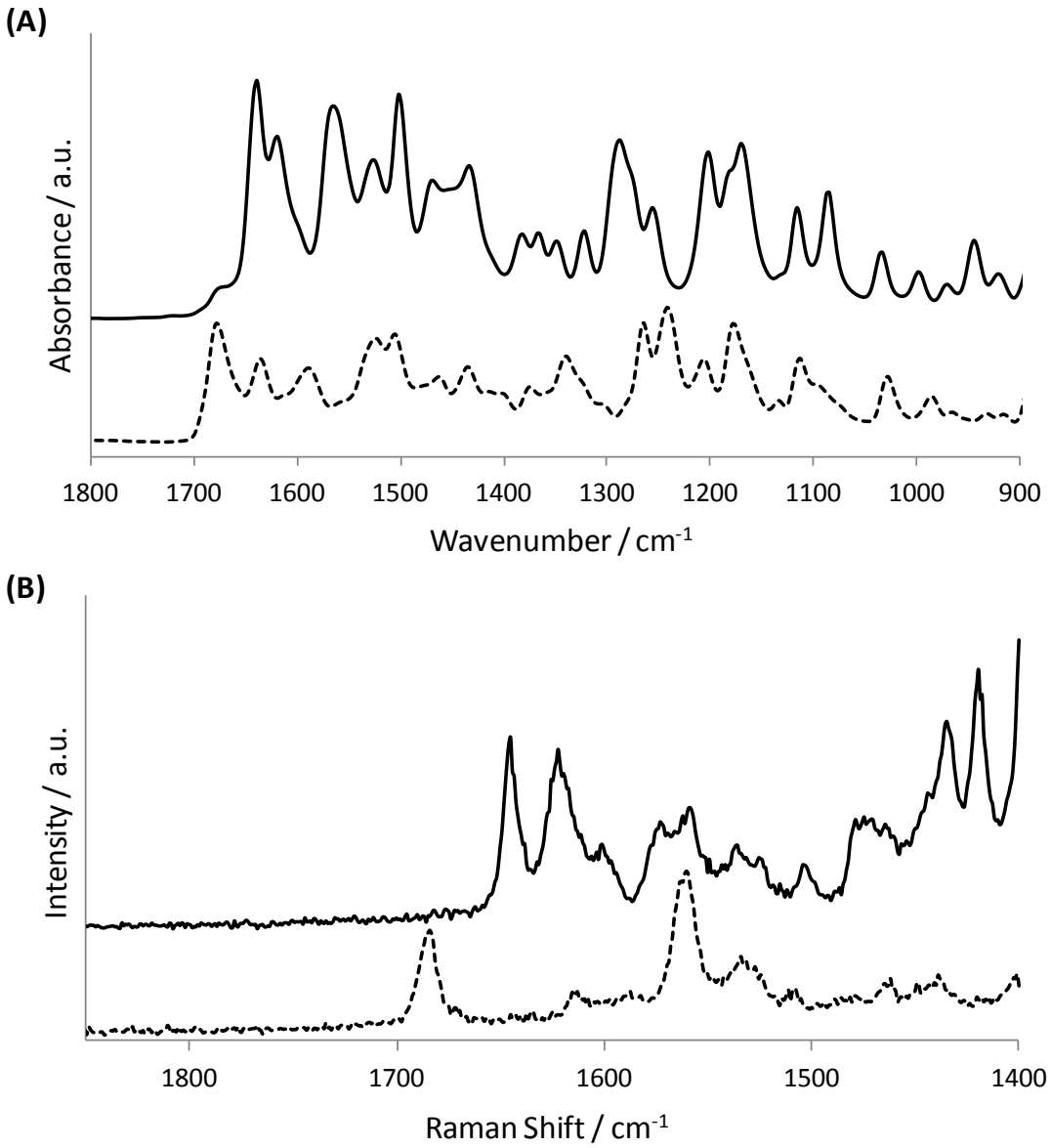


Figure 6.4 – (A) ATR-FTIR spectra and (B) Raman spectra of the two different forms of drug, pure ionised form is shown by the solid line and pure free acid form by the dashed lines.

An initial investigation to monitor the dissolution behaviour of the API in aqueous environments with different pH values, powdered samples of pure ionised drug were stirred in a beaker containing neutral and acidic solutions, respectively. Upon visual inspection of the reaction vessels, the solid precipitates of the drug had dissolved completely in the neutral solution. Conversely, it was apparent that very little dissolution of the drug had occurred in the acidic medium. These remaining particles were filtered and dried before ATR-FTIR and Raman spectra were recorded (Figure 6.5). Based on comparison with the reference spectra of the pure drug forms (shown as dashed lines in Figure 6.5) it was clear that disproportionation from the ionised structure to the free acid form had occurred. Thus, the use

of vibrational spectroscopy has proven effective to determine chemical changes between the two different drug forms. Information such as this is crucial and can explain why the drug did not appear to dissolve in the acidic solution during this experiment.

While visual inspection may suggest that little of the sample was dissolving; it provided no additional information about any chemical changes occurring within the sample. ATR-FTIR and Raman spectroscopy provided specific chemical information about the drug but, so far, only for a dried sample after separation from the dissolution medium. Hence, this does

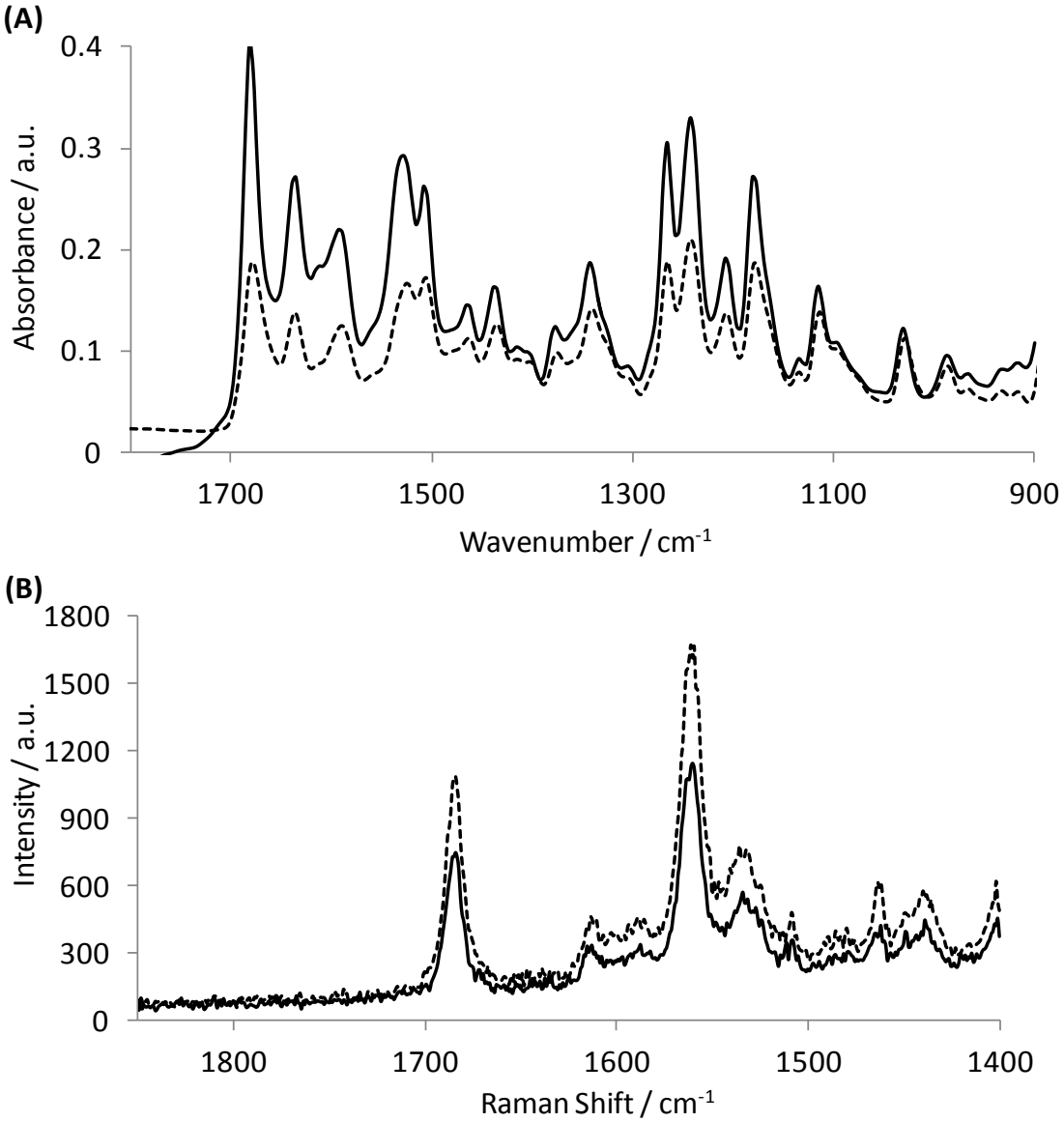


Figure 6.5 – (A) ATR-FTIR spectra and (B) Raman spectra of the drug after filtration from the acidic medium. The solid lines show the recorded spectra and confirm that conversion of the ionised form to the free acid form of the API occurred. Reference spectra of the pure free acid drug form (dashed line) are included for comparison.

not provide conclusive information about the changes occurring in the solution that is ultimately of much more interest for design and development of new pharmaceutical tablets.

6.3.2 Monitoring the stability and behaviour of tablets containing an ionised drug dissolution in neutral solution

In this Section of the Chapter, visible imaging, ATR-FTIR spectroscopic imaging and Raman mapping approaches have been used to study tablet dissolution and drug release from the developmental formulations. During disproportionation, hydrolysis of the ionised drug resulted in a change of its chemical structure where the sodium ion is substituted for a hydrogen atom. ATR-FTIR and Raman spectra could be used to differentiate these two forms by the appearance and shifts of particular absorption bands. Hence, this allowed spatially resolved information from the sample to be measured using the ATR-FTIR spectroscopic imaging and Raman mapping. *In situ* screening of the stability and behaviour of the ionised drug in dissolving tablets was monitored as a function of time. Unique spectral bands can be associated with the individual components of the formulations that allow characterisation of the different species in the sample. The setup of both spectroscopic approaches are well suited to recording video data simultaneously during the dissolution experiments which meant that the spectroscopic images and maps can be compared to visible images.

Figure 6.6 shows visible images recorded for tablet (7 mm diameter) in the neutral aqueous solution. As the solution contacts the tablet the Avicel polymer swells and the diameter of the tablet expands. Figure 6.6 showed that the neutral aqueous medium had ingressed into the core of the tablet after 2.5 hr. As the dissolution medium entered the tablet matrix, the drug contained inside is predicted to dissolve in the solution. However, this is an assumption since the video imaging data alone does not provide information regarding the distribution of the different components throughout the tablets. Both the polymer and drug have the physical appearance as a white powder and thus cannot be distinguished in the images.

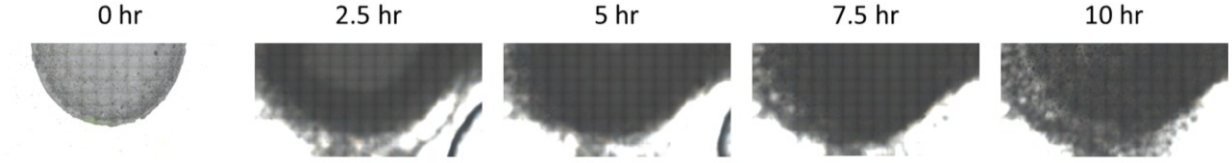


Figure 6.6 – Recorded video data that show the swelling behaviour of a 7 mm formulated tablet containing the ionised drug. Images are shown every 2.5 hr during dissolution in the neutral solution. The image size of these images is ~10.8 × 4.9 mm^2.

The inherent chemical specificity of infrared spectroscopy allowed the identification of unique spectral differences between the two different forms of the drug. By the selection of characteristic bands for each of the components of interest, for example, ionised API (1574–1555 cm^{-1}), free acid form of the drug (1700–1650 cm^{-1}), polymer (1235–927 cm^{-1}) and the dissolution medium (3600–3000 cm^{-1}), the distribution of each component in the measured area was determined. The ATR-FTIR spectroscopic images in Figure 6.7 show the distribution of the ionised drug, polymer and dissolution medium recorded every minute during the first 10 min of the experiment. The results suggest that upon swelling and gel formation of the polymer, water penetrated into the main bulk of the 3 mm tablets after just 3 min and in doing so the concentration of the ionised drug decreases (Figure 6.7). Figure 6.8 shows the ATR-FTIR spectroscopic images recorded every 0.5 hr from the same experiment. There was no spectroscopic evidence of conversion from the ionised API to the free acid form during this experiment in any of the measured data. This result is confirmed by the information in the spectroscopic images showing the distribution of the free acid form of the API. Thus, the data recorded from these experiments suggested that there was complete release of the drug into the neutral solution after just 1.5 hr. Furthermore, the spectroscopic images also show that there is no presence of the ionised API. The imaging data highlighted some interesting behaviour of the polymer during these experiments. The spatial distribution of the polymer appeared to change quite drastically between two measurements in the experiment. In fact, this is due to the quality and consistency of contact between the sample and the ATR crystal. These effects were caused by the swelling of the polymer upon contact with the neutral solution. It could be expected that swelling would improve the contact between the ATR crystal and the tablet. Although, this may not always be true, for example, the penetration time of the solution into the tablet that can initiate swelling of the polymer at different times. As a result, the contact between regions of the tablet and the ATR crystal changed during the experiment which resulted in the appearance of rings in some of the spectroscopic images (e.g. 0.5 hr in Figure 6.8).

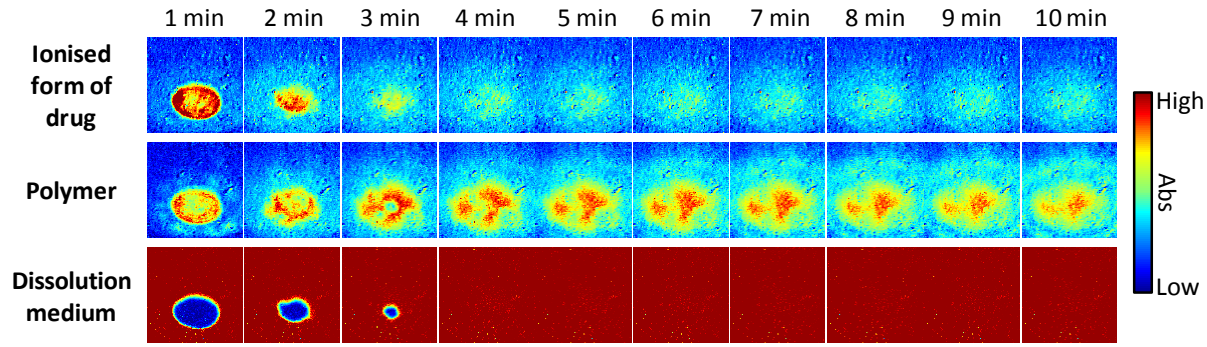


Figure 6.7 – ATR-FTIR spectroscopic images recorded during the first 10 min of the experiment in neutral solution. The VeeMax II accessory was used for these experiments which meant the whole tablet could be measured. The image size is approximately 7.75 × 6.05 mm^2 and the tablets were 3 mm in diameter. The distribution of the ionised form of the drug (top row), polymer (middle row) and dissolution medium (bottom row) are presented.

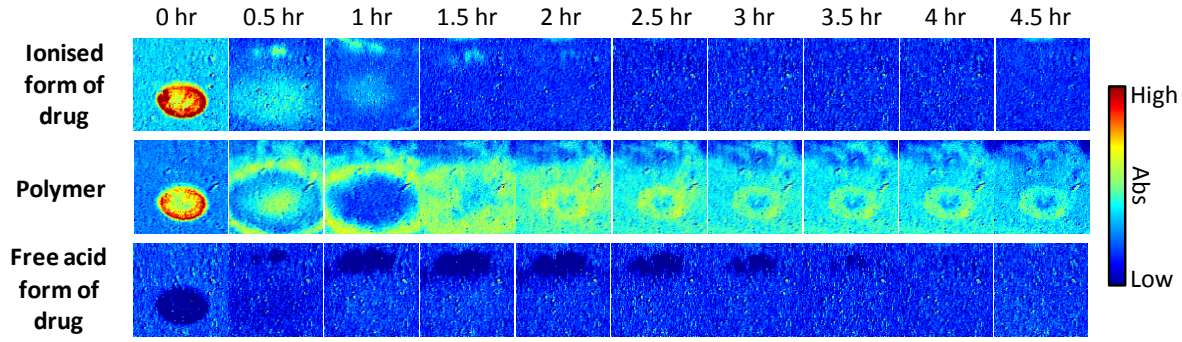


Figure 6.8 – ATR-FTIR spectroscopic images recorded every 0.5 hr for the duration of the experiment in water. The VeeMax II accessory was used for these experiments allowing an image size of ~7.75 × 6.05 mm^2 to be measured. The tablets studied here are 3 mm in diameter. The distribution of the ionised form of the drug (top row), polymer (middle row) and free acid form of the drug (bottom row) are presented.

It is clear from the video data and the ATR-FTIR spectroscopic imaging results that there were discrepancies between the rates of ingress of the solution into the core of the tablet. The difference in the rate of ingress is not entirely surprising because the ATR-FTIR spectroscopic imaging approach measured tablets that were 3 mm in diameter whereas, the video imaging technique measured tablets with a diameter of 7 mm. Further information about the behaviour of the larger 7 mm tablets was collected using the Raman mapping approach. Here, 17 Raman spectra were recorded in a linear formation from the centre of the tablet to the edge of the dissolution cell. The acquisition time for one full cycle was only

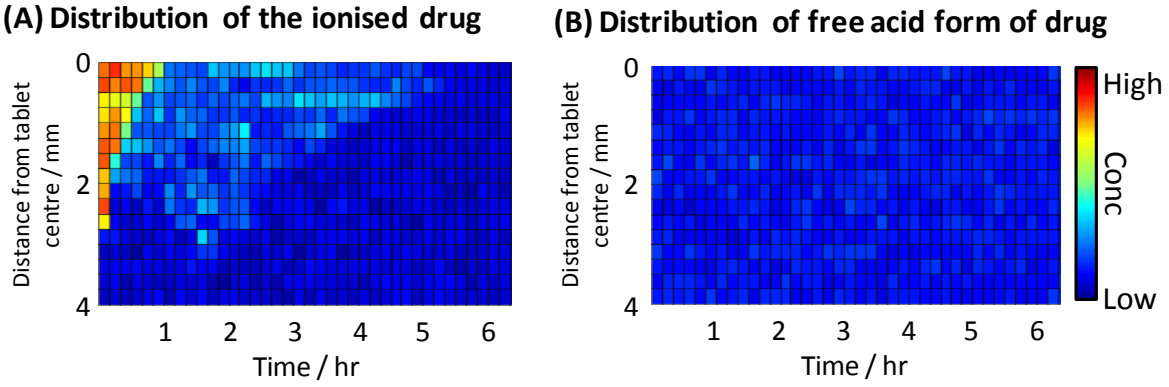


Figure 6.9 – Raman mapping results recorded during the dissolution experiment of the 7 mm formulated tablet in the neutral solution. (A) shows the spatial distribution of the ionised API and (B) the spatial distribution of the free acid form of the drug during the experiment.

10 min, hence, a series of chemically specific radial profiles determining the structure of the drug could be recorded during the experiment. Figure 6.9A shows the distribution of the ionised drug form during a dynamic dissolution experiment of the tablet in a neutral solution. The Raman maps showing the distribution of the salt form indicate that there was a reduction in the concentration of the ionised API as the experiment progressed, i.e. the drug was released into the surrounding solution. At around 5 hr there appears to be no further presence of the ionised API in the recorded Raman maps. This time frame is coincident with the complete ingress of the dissolution medium revealed in the video data (Figure 6.6). Moreover, the distribution of the free acid form of the drug (Figure 6.9B) is consistent with the ATR-FTIR imaging experiment in so much that there is no evidence of this species forming during the entire experiment. The results presented here show a very good correlation between ATR-FTIR spectroscopic imaging and Raman mapping approaches to study drug release and the dissolution of tablets.

6.3.3 Assessing the stability and behaviour of tablets containing an ionised drug during dissolution in acidic solution

The results from the dissolution experiments in the acidic solution (0.1 M HCl) significantly contrast those recorded in the neutral medium. The video data shows that some components in the formulated tablets have different physical behaviour in the acidic medium (Figure 6.10). Instead of the swelling behaviour and gel formation of the tablet that was observed in the neutral medium (Figure 6.6), Figure 6.10 shows that there was cracking and fracturing to the bulk of the tablet. These effects are clearly visible at 2.5 hr in the tablet with a diameter of 7 mm. The acidic medium did continue to penetrate towards the core of the tablet as a

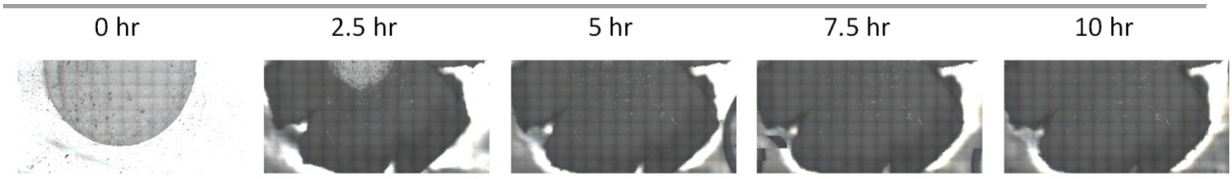


Figure 6.10 – Images recorded from the video imaging approach that shows the behaviour of the 7 mm tablet containing the ionised drug form during dissolution in the acidic solution. The images show clear fracturing of the matrix of the tablet. Each image is ~10.8 × 4.9 mm^2 where the data recorded every 2.5 hr are presented.

function of time. However, even when the tablet is fully wetted, there was still no apparent gel formation. Hence, the information provided by the use of visible imaging suggested that there were changes occurring within the tablet. However, it was not possible to derive any chemically specific explanation as to how the different components of the formulation were affected. Several hypotheses exist that can be attributed to chemical changes in the materials of the formulated tablet. Chemical or structural changes occurring to the materials in the tablet, initiated by the acidic environment, can affect the behaviour of the tablet in solution and alter the dissolution mechanism. For instance, it can be proposed based on the visible images in Figure 6.10, that chemical changes to one or more of the materials in the formulation slows penetration of the aqueous medium into the tablet. These results are a good example of where the spectroscopic imaging approaches can have great potential to reveal further information about the dissolution process and detect chemical changes occurring within tablets.

Representative ATR-FTIR spectroscopic images of the dissolution experiments in the acidic medium are presented in Figure 6.11 and Figure 6.12. Figure 6.11 shows the results recorded during the first 10 min of the experiment setup on the diamond crystal. The changes that occurred between the edge of the tablet and the dissolution medium are displayed. In contrast, the images in Figure 6.12 show the behaviour of the whole tablet every 10 min for the first hour and then every 30 min for the duration of the experiment. These results confirmed that there was the rapid formation of free acid drug form after the acidic medium contacted the tablet. The spectra extracted from individual pixels in Figure 6.13 show that consistent chemical information can be obtained after 10 min in both of the separate experiments. The clear spectral changes indicate that the presence of the ionised API in the formulation converted to the free acid drug. The extracted spectrum from the spectroscopic images recorded using on the diamond crystal (Figure 6.13A) show some slight differences compared to the reference free acid spectrum, specifically in the 1575–1500 cm^{-1} region. The

appearance of the extra bands in this region, at 1565 and 1528 cm^{-1} are attributed to the presence of the ionised form of the drug in the measured tablet (see Figure 6.4). Hence, complete conversion to the free acid from had not occurred throughout the entire tablet by this time. Nevertheless, the most obvious change to determine the formation of freed acid in the measured sample is the appearance of the spectral band at 1702–1659 cm^{-1}, which is highlighted by the arrow in Figure 6.13.

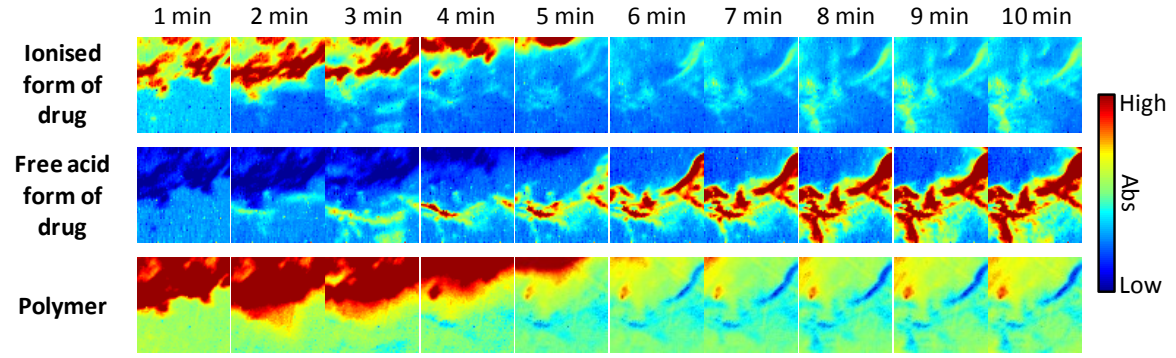


Figure 6.11 – ATR-FTIR spectroscopic images showing the behaviour of the 3 mm tablet during the initial 10 min of the experiment in the acid solution. The experiment was setup on the Imaging Golden Gate accessory to provide information from the edge of the tablet. Each image is ~0.64 × 0.53 mm^2. The distribution of ionised form of the drug (top row), free acid form (middle row) and polymer (bottom row) are presented.

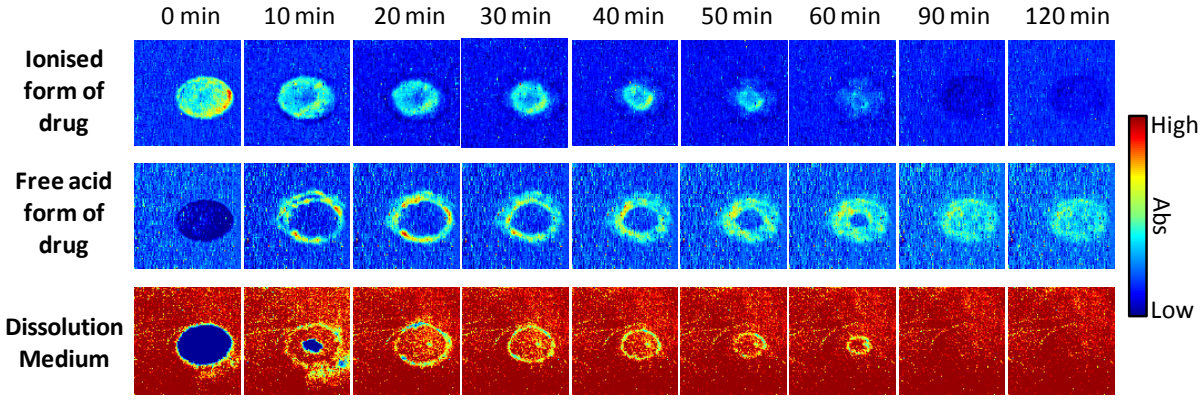


Figure 6.12 – ATR-FTIR spectroscopic images of the 3 mm tablets recorded from the dissolution experiment of the tablet in the acidic solution. The spectroscopic images recorded at different times during the first 120 min of the experiment. A VeeMax II accessory was used which allowed measurement of the whole tablet since the image size is ~7.75 × 6.05 mm^2. The distribution of ionised form of the drug (top row), free acid form of the drug (middle row) and acidic medium (bottom row) are presented.

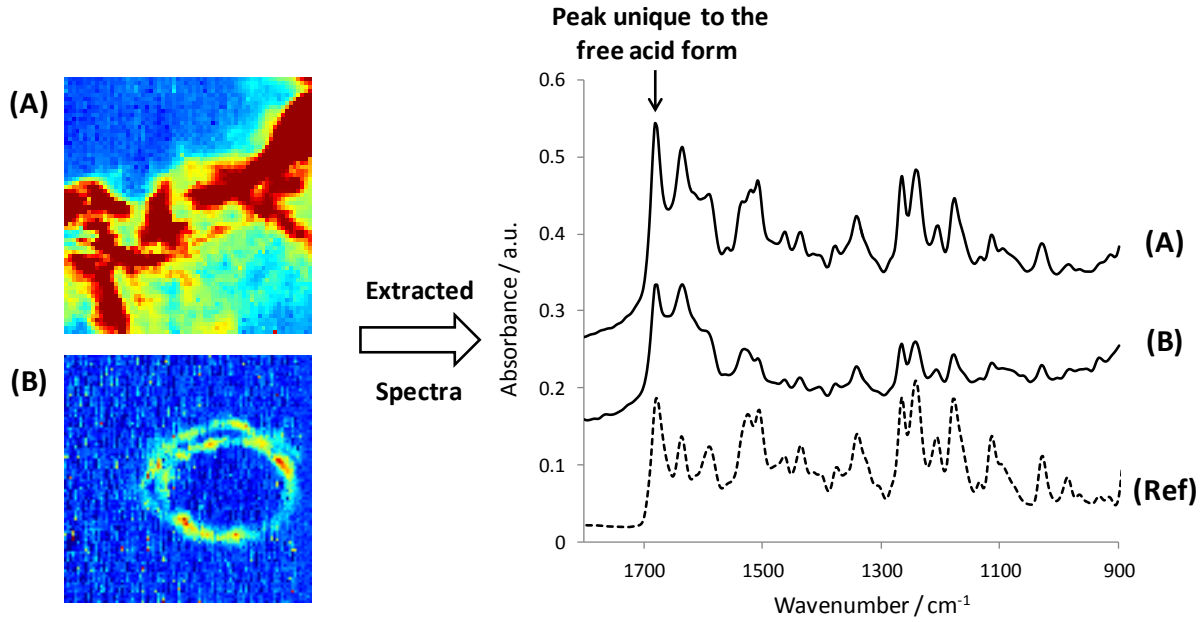


Figure 6.13 – ATR-FTIR spectroscopic images recorded using (A) the Imaging Golden Gate and (B) VeeMax II accessories. These confirm the presence of disproportionation to the free acid form of the drug. Images measured after 10 min from the two separate experiments in the acidic solution are presented. The accompanying ATR-FTIR spectra are extracted from a selected pixel within regions of high free acid drug form concentration (red areas) in the spectroscopic images. Spectrum (A) is extracted from the Imaging Golden Gate accessory measurement and (B) the experiment recorded on the VeeMax II accessory (solid lines). The reference ATR-FTIR spectrum of the free acid form has also been included for comparison purposes (dashed line).

The chemical changes that occurred to the API in the acidic conditions had implications for the overall release of the drug because the free acid form has much lower solubility than the ionised form. The spectroscopic images recorded using the Imaging Golden Gate accessory show that a shell of the free acid form of the drug initiated around the tablet after just 2 min (Figure 6.11). However, it is clear from the distribution of the absorption band from the free acid form that this species continued to appear during the first 10 min of the experiment. Since the Imaging Golden Gate accessory measured a smaller area than that of the tablet, it was difficult to confirm if disproportionation was occurring throughout the entire tablet. Employing the VeeMax II accessory meant that the whole tablet could be imaged, and thus, the penetration of the acidic solution into the core of the tablet could be tracked. Figure 6.12 shows that the dissolution medium did ingress into the whole tablet and in doing so caused further conversion of the free acid form of the drug throughout the bulk of the tablet. Unlike the experiments in the neutral solution (Figure 6.7), where total ingress of the solution into the tablet was observed after just 3 min, the experiments in the acidic medium showed a

much slower rate of penetration. Here, the acidic medium had only reached the core of the tablet after 60 min.

Overall, the ATR-FTIR spectroscopic imaging results of the tablet dissolution experiments in acidic medium confirmed that chemical changes occurred to the API, namely the formation of the free acid form of the drug. This formation was initially observed as a shell around the tablet which slowed the penetration of the acidic medium. Subsequently, full conversion of the API in the main bulk of the tablet was characterised. As a consequence, the API was not released during the experiment.

Using a combination of visible and ATR-FTIR spectroscopic imaging approaches, a mechanism of disproportionation of a developmental ionised drug has been identified. Chemical changes that occurred to the ionised form of the drug in the presence of the acidic medium affected the penetration of solution towards the core of the tablet.

Similarly to the dissolution in neutral medium, the different sizes of the tablets studied can potentially result in some differences with respect to the behaviour of the drug in the acidic solution. For example, the time of onset of the formation of the shell of the free acid surrounding the tablet could be different. These chemical changes can be clearly observed using vibrational spectroscopy as demonstrated in the ATR-FTIR spectra extracted shown in Figure 6.13. Thus, dissolution experiments of the larger tablets were measured using the Raman mapping approach since it is difficult to predict how, and if, these changes occur in the different sized tablets studied. The data obtained using the Raman mapping approach confirmed the presence of disproportionation within the tablet (Figure 6.14). What is most significant in these results, compared to the ATR-FTIR spectroscopic imaging data, is the time frame upon which disproportionation occurred. The visible images indicate that the wetting of the tablet in the acidic solution is slower compared to the tablet dissolved in the neutral solution. The Raman maps provided further evidence that the acidic environment was responsible for the chemical changes since there is conversion to the free acid form of the API, only where the acidic medium had penetrated into the sample. These structural changes caused a cracking of the tablet matrix which resulted in a decreased rate of ingress of the solution into the tablet. After the acidic solution had ingressed into the whole tablet, the free acid form of the drug was detected over the whole measured area and subsequently did not dissolve for the remainder of the experiment (Figure 6.14).

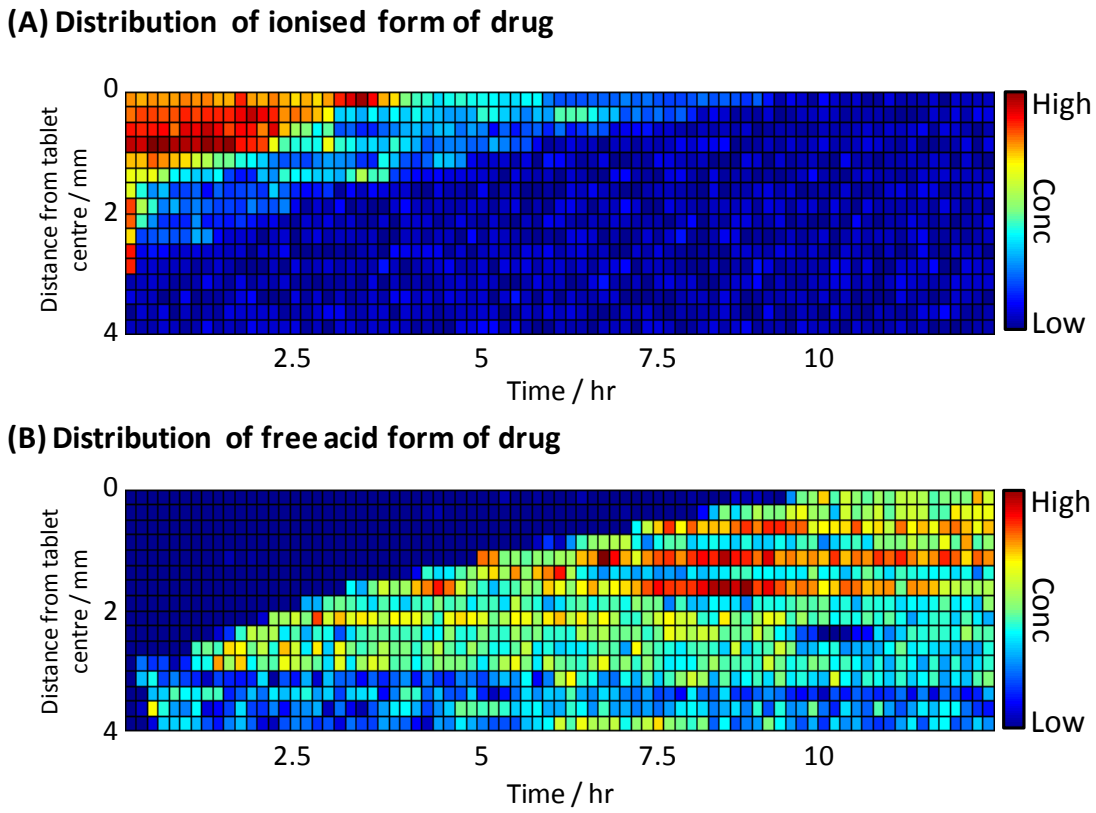


Figure 6.14 – Raman mapping results from measurement of the 7 mm tablet in the acidic solution. The conversion from the ionised form of the drug (top) to the free acid form of the drug (bottom) is presented in the maps.

The imaging and mapping data presented demonstrates that not only is there a conversion to the less soluble form of the drug but these changes have further effects on the behaviour of the tablet in the acidic solution. The behaviour of the tablet during dissolution in the acidic medium was very different to that observed in the neutral solution. Under such conditions, disproportionation resulted in the formation of the free acid form of the drug that initially manifested itself as a shell around the outside of the tablet which inhibited ingress of the dissolution medium. Further measurements of these dissolving tablets highlighted that the structural changes had implications for the release of the API into the surrounding solution.

6.4 Conclusions

Here, macro ATR-FTIR spectroscopic imaging and Raman mapping were used to study the behaviour of an ionised drug during dissolution experiments *in situ*. This study reports the first time that the two vibrational spectroscopic approaches have been used to study the same formulated system. Each approach provided complementary information that allowed detection of chemical changes that produced the undesirable free acid form of the drug.

Formulated tablets that contained the ionised API were measured in different aqueous pH environments; neutral and acidic solutions. Disproportionation was characterised during the experiments in the acidic solution. In contrast, entire drug release of the ionised form into the neutral solution was observed and the spectroscopic approaches detected no chemical changes. The ability to reveal chemically specific information about any changes to the ionised API allowed the effects of disproportionation on drug release to be explained in greater detail. Hydrolysis of the ionised drug occurred upon contact with the acidic dissolution medium which resulted firstly in a shell of the free acid form to encapsulate the tablet. Subsequently, the rate of penetration of the acidic solution into the tablet significantly decreased compared to the tablets studied in the neutral medium. Additionally, as the experiment continued the acidic solution slowly ingressed towards the core of the tablet. The consequence of this was further conversion to the free acid form that was eventually evident throughout the whole tablet.

Utilisation of these complementary vibrational spectroscopic imaging approaches has great potential to investigate further problematic pharmaceutical systems where disproportionation of an ionised drug form occurs. The chemical specificity collected using these approaches can reveal such structural changes in dynamic systems. Ultimately this can help mitigate disproportionation in the tablets and produce more reliable products.

7 ATR-FTIR Spectroscopic Imaging of Pharmaceutical Systems in Microfluidic Devices

The previous Chapters in this thesis have focused on the application of macro ATR-FTIR spectroscopic imaging to study drug release from large tablets. However, here, the motivation is to describe novel experiments that investigate the behaviour of pharmaceutical systems in microfluidic devices using macro ATR-FTIR spectroscopic imaging. Firstly, a reliable and robust method to create microfluidic devices for macro ATR-FTIR spectroscopic imaging applications has been reported, which included the modification of polydimethylsiloxane (PDMS). Devices were designed to allow the drug release from several model formulations to be assessed simultaneously under flowing conditions. These novel imaging studies revealed the behaviour of ibuprofen, formulated with PEG, in different channels under identical flowing conditions. Moreover, microfluidic devices were employed that allowed drug release in different aqueous solutions to be assessed at the same time. The work undertaken here was extended to investigate the behaviour of a drug dissolved in solution upon contact with changing conditions. This study is a relatively unexplored area but the results have implications for drug delivery. Different concentration solutions of sodium ibuprofen dissolved in a neutral aqueous medium were investigated upon contact and mixing with an acidic solution. Precipitation of crystalline ibuprofen and agglomeration of these solid drug particles were detected in the spectroscopic images.

7.1 Motivation

Due to the fact that many active pharmaceutical ingredients are poorly soluble in aqueous conditions (Shah et al., 2014, Williams et al., 2013b, van Hoogevest et al., 2011), there is a great drive to develop reliable and robust approaches to screen novel formulations in a high-throughput manner (Stadler, 2015, Dai, 2010, Dai et al., 2008). The use of high-throughput approaches capable of monitoring systems in real time can have great value and would facilitate identification of the physical changes within the formulations. As a result, this can have significant implications for the research and development stages of formulation design (Kang et al., 2008, Gardner et al., 2004). Recently, there has been much interest in high-throughput studies of pharmaceutical materials in miniaturised vessels or microfluidic devices using a range of analytical approaches (Piletska et al., 2015, Kuentz, 2015, Ding et al., 2015, Heikkila et al., 2008, Dai et al., 2008). The significant advantage of using

microfluidic devices for these types of applications can be of great importance in early drug development (Ding et al., 2015). For example, it may be particularly useful in the study of formulations that contain added materials of high value (i.e. are expensive) since only a small amount of the sample is needed. Hence, the investigation of microparticles that are commonly administered in capsules can be studied (Cheng et al., 2013). Another example considers the potential to test unique 3D printed formulations designed for individual patients; such delivery methods are becoming possible in this industrial sector (Genina et al., 2015, Khaled et al., 2015, Khaled et al., 2014).

Drug release studies are of great importance when it comes to the identification of new candidates (Shah et al., 2014). Common issues that arise in new active pharmaceutical ingredients can include the stability of polymorphs (Gardner et al., 2004), intermolecular interaction with polymers and co-crystal formation (Williams et al., 2013b). Analytical approaches for parallel dissolution studies are currently at different stages of development and one of the most widely employed methods uses UV analysis. UV fibre optic probes are well established for dissolution testing and this approach can be used to determine the dissolution rate of low solubility drugs (Fagerberg et al., 2010, Tsinman et al., 2009). This method also only requires a few milligrams of the sample and multiple experiments in differing dissolution conditions have been carried out in parallel (Avdeef et al., 2009).

It is recognised that imaging approaches provide the opportunity to enhance successful drug discovery and many analytical techniques are being developed and utilised to study miniature delivery systems. Windbergs and Weitz (2011) have reported the design of a microfluidic chip which was used to study small microparticulate formulations. This chip allows visual monitoring of the sample and concentration of the dissolved drug to be determined at the same time. For these studies, the release from the delivery system was analysed using fluorescence microscopy. The assembly of sustained release composites of hydrophobic drugs in nanoparticles using microfluidic devices was recently reported (Hsu et al., 2015). Fluorescence was used to detect the encapsulation of the hydrophobic drugs in the particles that were shown to improve release. UV imaging approaches have also been applied to study the release of APIs from a range of delivery systems. These include investigations into the stability of pure drug forms (Hulse et al., 2012, Østergaard et al., 2011), release from transdermal patches (Østergaard et al., 2010b) and co-crystal stability (Qiao et al., 2013). However, UV imaging has yet to be employed for the study of multiple formulations simultaneously.

Here, for the first time, the simultaneous dissolution of multiple model formulations of ibuprofen/PEG have been investigated *in situ* by macro ATR-FTIR spectroscopic imaging. Furthermore, comparisons of the behaviour of the drug in different solutions under flow with a particular pH were studied by the development and design of microfluidic devices. The potential of macro ATR-FTIR spectroscopic imaging for the high-throughput study of many different formulations under identical conditions has previously been demonstrated (Kazarian, 2007, Chan et al., 2007b, Chan and Kazarian, 2005). ATR-FTIR spectroscopic imaging was used to detect dimerisation of a drug when formulated in different ratios with the excipient (Chan and Kazarian, 2006c). In that study, 40 formulations were investigated simultaneously at a controlled humidity and temperature. Chan and Kazarian (2006a) have also established the use of an expanded field of view accessory for macro ATR-FTIR spectroscopic imaging to investigate the simultaneous dissolution of different formulations in stagnant aqueous conditions. Initial preliminary studies, combining macro ATR-FTIR spectroscopic imaging with microfluidic devices have been reported, where spectroscopic images of flowing systems were recorded (Chan and Kazarian, 2013b, Chan et al., 2011, Chan et al., 2009). The ability to measure these dynamic systems has provided the opportunity to study new physical changes related to drug release.

The behaviour of the drug after it has been released and dissolved from a tablet is still relatively unexplored. Ionising drug molecules is a common method to increase the rate of dissolution from tablet dosage forms (Ewing et al., 2015b, Serajuddin, 2007), however, this can result in areas where there are high concentrations of dissolved drug in the solution. Local areas of saturated and supersaturated concentrations of dissolved drug can initiate precipitation and recrystallisation from the solution and hence inhibit drug delivery (Punčochová et al., 2015, Chandran et al., 2011, Kazarian and Chan, 2003, Leuner and Dressman, 2000). In this work, the behaviour of different concentration solutions of an ionised drug, sodium ibuprofen, has been investigated upon contact with a solution of different pH value.

Previous work conducted using macro ATR-FTIR spectroscopic imaging for high-throughput and microfluidic studies of pharmaceutical formulations has provided a platform for further advancements in this area. This work explores a number of new areas for the use of microfluidic devices with macro ATR-FTIR spectroscopic imaging, with a specific interest in the monitoring of pharmaceutical systems, particularly under flowing conditions.

7.1.1 Main developments of this work

The key developments and findings from the work undertaken in this Chapter are summarised in the following points, which are described herein:

- Design and modification of microfluidic devices suitable for use with macro ATR-FTIR spectroscopic imaging that achieve flow of solutions through multiple channels.
- High-throughput analysis of the dissolution of micro-formulations under the same flowing conditions. Simultaneous screening of micro-formulations in aqueous environments with different pH values under flow.
- Crystallisation and precipitation of drug, from solutions containing different concentrations of a dissolved drug in neutral solutions, upon contact and mixing with an acidic medium.

7.2 Development of microfluidic devices for use with macro ATR-FTIR spectroscopic imaging

7.2.1 Initial methodology for the preparation of microfluidic devices

Novel microfluidics devices that could be used with FTIR spectroscopic imaging in ATR mode were designed to be made from PDMS. PDMS is a widely applied material for microfluidic devices (Whitesides, 2006, Beebe et al., 2002). Furthermore, several previous published articles have reported the combined approach of using PDMS microfluidic devices with ATR-FTIR spectroscopic imaging (Chan et al., 2010, Chan et al., 2009, Chan and Kazarian, 2006a). Due to the nature of the ATR sampling methodology, where the sample has to be in contact with the crystal, it is important to design devices that have the channels on the outside surface of the PDMS. Designing channels that are etched directly into the outside of a PDMS film mean that it can be pressed onto the measured surface of the crystal.

Chan and Kazarian (2006a) prepared a PDMS device that was specifically made to be used with an expanded field of view ATR-FTIR spectroscopic imaging accessory. A multi-channel dissolution grid was prepared by cutting channels into a PDMS film. A scalpel was used for the preparation of the devices where five separate channels were cut through the film. The microfluidic device was then placed directly on the ZnSe crystal of the expanded field of view accessory. The measuring surface of the crystal is 26×19 mm^2 and the size of the recorded spectroscopic images is 21.5×15.4 mm^2. The dissolution of different pure PEG

(differing molecular weights) and PEG/ibuprofen formulations were studied in these channels. This approach successfully demonstrated that the comparison of formulations could be monitored *in situ* using ATR-FTIR spectroscopic imaging. However, since the channels were cut by hand, the smallest features created were ~1 mm (Chan and Kazarian, 2006a). Furthermore, the dissolution experiments were carried out in stagnant conditions, where the solution was dropped into the channels containing the formulation and then covered with a glass slide to prevent evaporation. Nevertheless, this pioneering research has reported that there is great potential to study materials in microfluidic devices using ATR-FTIR spectroscopic imaging.

A further development by Chan et al. studied flows in microfluidic channels by the use of ATR-FTIR spectroscopic imaging and mapping. Isotope exchange between H_2O and D_2O was measured directly using this approach (Chan et al., 2009). Although this is not a pharmaceutical application, similar methods for device fabrication and experimental setups can be applied to the work undertaken in this Chapter. Chan et al. (2009) prepared channels that were moulded into the surface of a PDMS substrate using an SU-8 master and a standard soft lithographic fabrication method (Duffy et al., 1998). Furthermore, for achieving flows, a top plate was made which could be aligned with the microfluidic device and screwed onto the ATR accessory. The inlets and outlets in the PDMS device and top plate allowed the liquids to be flowed through the channels using syringe pumps.

In the work undertaken in this Chapter, it was intended that devices would be prepared so that the behaviour of pharmaceutical systems could be studied under flowing aqueous conditions. Unfortunately, it was not possible to prepare PDMS devices using the soft lithographic method. Hence, a novel approach for preparing channels within the PDMS substrate was needed. Moreover, the microfluidic devices were all designed so that the whole device could be imaged using an ATR accessory (PIKE Technologies), with no expanded field of view optics, in a single measurement so that no mapping is needed.

An idea of creating 3D moulds, over which uncured PDMS could be poured over and subsequently allowed to cure, was explored. A microdrop system (Autodrop, Germany) was used to deposit paraffin wax onto a glass substrate to test the principle and feasibility of this method to create channels in PDMS. The microdrop system consists of a computer-controlled dispensing unit capable of movement in the *XYZ* coordinates. The dispensing unit has a temperature control which means that samples can be melted and deposited at specific locations on a substrate. The use of this system to prepare microfluidic channels for FTIR spectroscopic imaging can be found in the literature (Chan et al., 2010). However, the wax

droplets were dispensed directly onto an IR transparent calcium fluoride (CaF_2) window that was then prepared for transmission measurements by pressing between a second CaF_2 window, separated by a spacer. Therefore, this is the first time that this preparation method has been used to prepare channels in PDMS for use in ATR mode measurements. The two initial designs for this work included a single channel with a serpentine middle section that contains one inlet and outlet and a T-junction with a serpentine middle section that contains two inlets and one outlet. These designs are shown in Figure 7.1 (A and B, respectively) along with the resulting wax printed moulds on a glass substrate. Figure 7.1D also shows a magnified image from a wax channel to displaying the arrangement of the droplets on the glass substrate.

Figure 7.2 presents a schematic of the preparation of the PDMS devices using this approach. Firstly, the paraffin wax was dropped onto the glass substrate. Next, PDMS (Slygard 184, Dow Corning, USA), which was prepared by mixing the elastomer with a crosslinking agent in a 10:1 weight ratio, was cast over the wax mould. Subsequently, the PDMS was allowed to cure in an oven at ~40 °C. After the PDMS had solidified, it was peeled from the glass substrate. As a result, channels moulded into the outside surface of the PDMS were obtained. The PDMS device was pressed directly onto the ZnSe crystal. Initially, a syringe and needle were used to test the flow of water through the channels of the chip

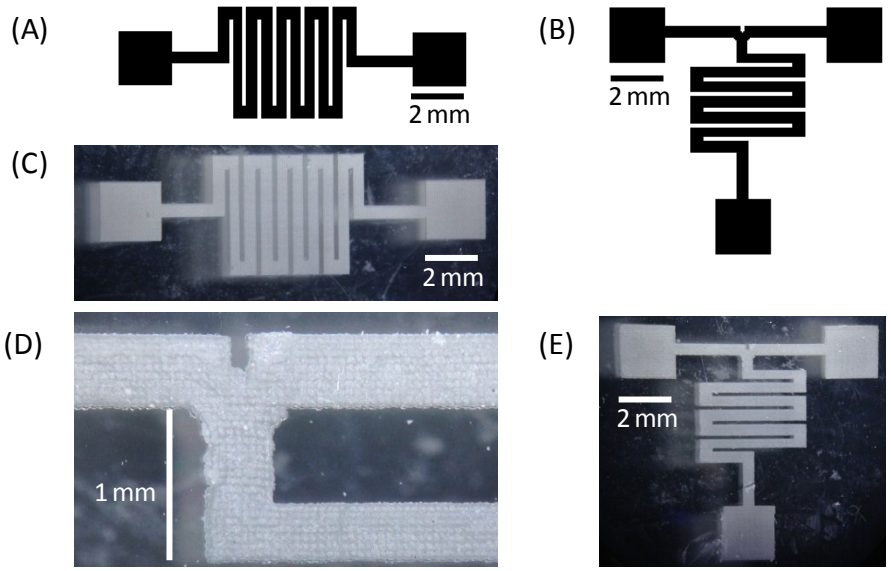


Figure 7.1 – The initial designs for the microfluidic channels to be moulded into PDMS substrate along with visible images of the printed paraffin wax (A) and (C) show the single channel device and (B) and (E) show the T-junction design. (D) A visible image of the channel showing the arrangement of the deposited wax.

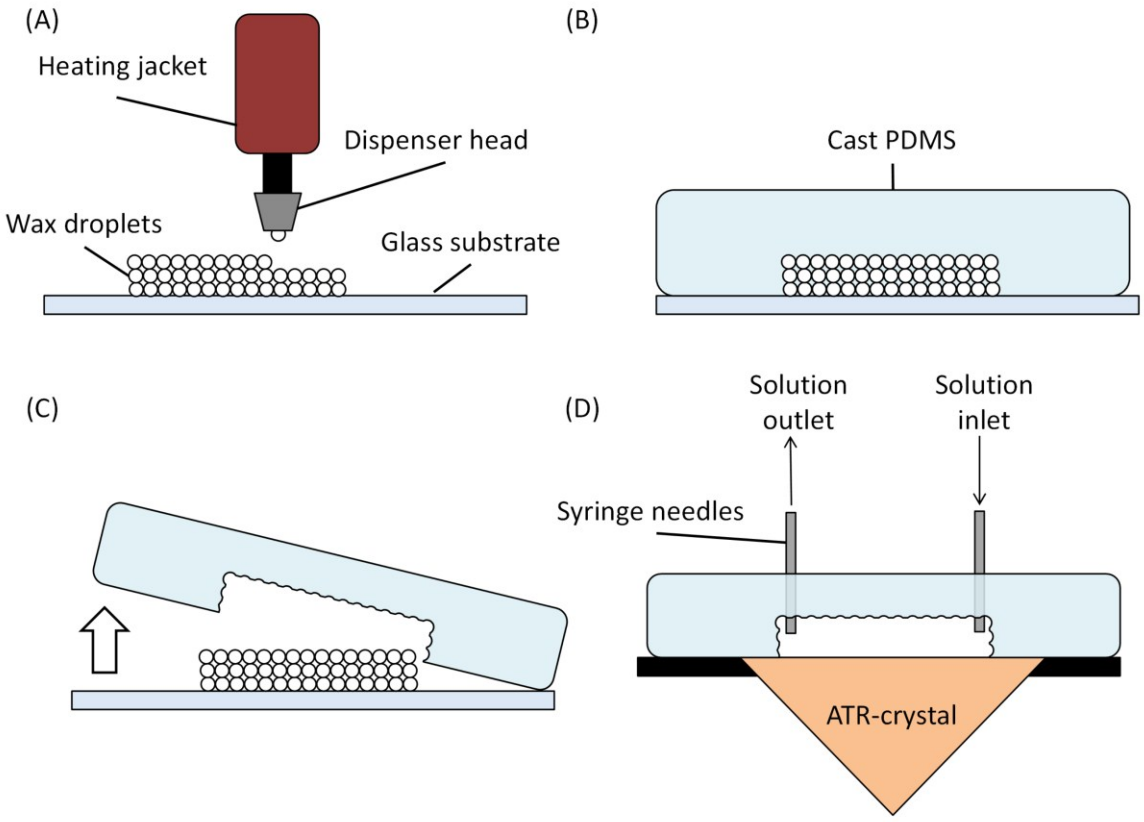


Figure 7.2 – Schematic diagram of the preparation of PDMS microfluidic devices. (A) Deposition of paraffin wax onto the glass substrate. (B) Covered with PDMS and allowed to cure. (C) Device peeled from the substrate to reveal the channels. (D) The microfluidic device placed on the measuring surface of the ZnSe crystal and solution passed through channels using a syringe.

(Figure 7.2D). This approach proved very useful for the design of novel microfluidic devices studied by ATR-FTIR spectroscopic imaging.

The use of the microdrop system to create microfluidic devices using wax droplets was successful for determining if such an approach was feasible to obtain channels capable of supporting flow. Furthermore, this approach allowed very rapid prototyping for different designs of microfluidic devices. However, since the droplets deposited using the microdrop system are only ~0.06 mm in diameter, it took a relatively long time to print the wax and build-up the height of the devices reliably. Moreover, this method produced only temporary moulds and each printed design could only be used once because the wax was disrupted during removal of the PDMS. Therefore, the application of 3D printing moulds made from acrylic plastic for the preparation of PDMS microfluidic chips was tried.

7.2.2 Microfluidic devices prepared with 3D printed moulds

The design and fabrication of microfluidic chips using 3D printed acrylic moulds were a significant advancement for this study. They allowed more complex designs of channels with a higher accuracy. This approach still means that rapid modification and a versatile range of the devices can be designed and studied using ATR-FTIR spectroscopic imaging. Thus, unique microfluidic devices for the specific applications could be produced relatively quickly and inexpensively. Building upon knowledge learned from the devices made using wax moulds, all of the microfluidic chips designed to be made using 3D printed moulds were intended for use with the ZnSe imaging accessory. Some selected 3D printed moulds employed to create microfluidic devices capable of studying the dissolution of micro-formulations in this Chapter are shown in Figure 7.3.

Fabrication of the PDMS microfluidic chips in this study, for example, those shown in Figure 7.3, followed the same method as described in the previous Section. Since the inlets and outlets of these channels were designed to be in the same location, a Perspex top plate was custom built that allowed for the microfluidic chip to be held in place on the crystal, as shown in Figure 7.4. Figure 7.4 shows visible images and a schematic diagram of the different components used in the setup of the experiments. The tubing was attached to the top plate that was aligned with the inlet/outlets of the PDMS device. Thus, a controlled flow could be maintained through the channels using a syringe pump (Harvard Apparatus, USA).

The four different microfluidic devices that were used to obtain the results discussed in the following Sections of this Chapter are shown in Figure 7.5. Figure 7.5A–C show visible images of the microfluidic devices with multiple channels and dissolution chambers in which formulations can be placed. The width of the channels in these devices is 0.5 mm and the oval shaped dissolution chamber is 2 mm × 3 mm in size. Micro-formulations up to 1 mm in diameter could be studied within the microfluidic devices. The positioning of the dissolution

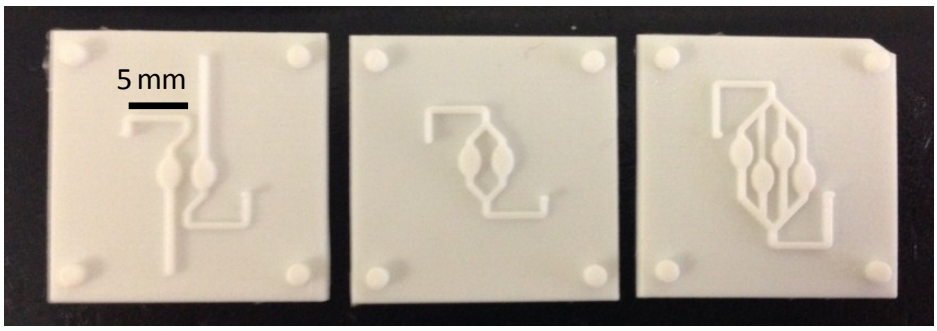


Figure 7.3 – Visible images of the 3D printed moulds for creating devices that can study the dissolution of micro-formulations.

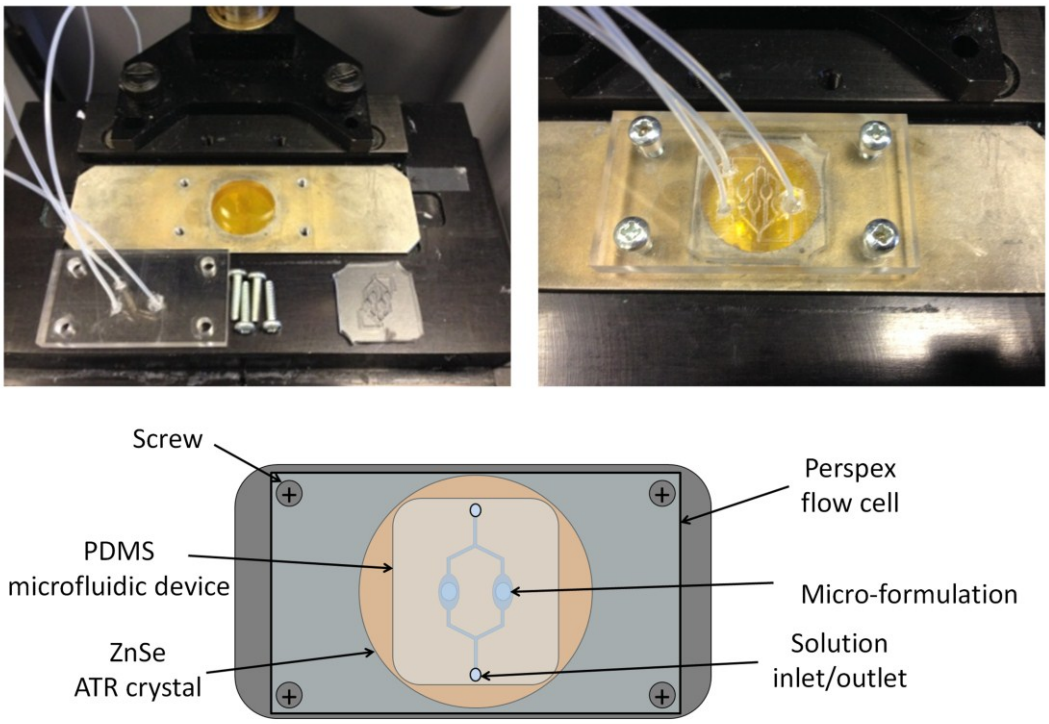


Figure 7.4 – Visible images showing the disassembled (top left) and assembled (top right) setup of the microfluidic device for ATR-FTIR spectroscopic imaging measurements using a ZnSe crystal. Below, is a schematic representation of the experimental setup.

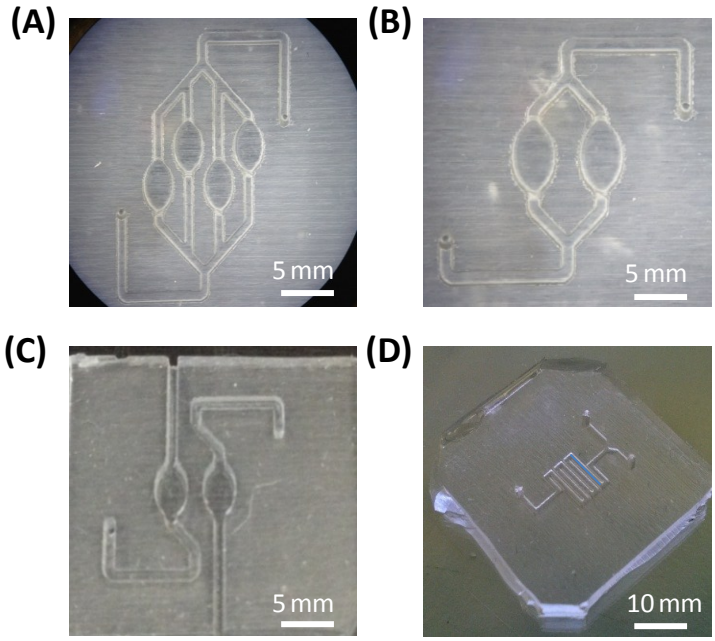


Figure 7.5 – Visible images of the four PDMS microfluidic devices that were used for the experiments in this work.

chambers in the device with four channels (Figure 7.5A) were offset to allow all of the chambers to be imaged in a single experiment. Figure 7.5C shows the microfluidic device used to investigate the flow of two solutions with different pH values simultaneously. By the use of two separate inlets, different dissolution media can flow through the channels. As a result of the versatility of these microfluidic devices; for instance, further work that has not been conducted in this thesis could investigate the effect of different flow rates on micro-formulations using this same device. Finally, Figure 7.5D shows the T-junction PDMS device that was used to investigate a dissolved drug mixing with a different pH medium. Here, the width and height of the channels are 0.5 mm and 1.5 mm, respectively. The serpentine channel after the T-junction was designed to record more information about the system by utilising the full imaged area observed in the measurements.

7.2.3 Functionalising PDMS devices for more efficient flow

Before the assessment of model pharmaceutical formulations, preliminary experiments were carried out to test the reliability of the devices and experimental setup. For these, PEG was deposited onto the ZnSe crystal and the dissolution in water was recorded. However, during the experiments, it was not possible to achieve flow of the water through all of the channels in the microfluidic chips. Problems with the flow of water were proposed to be caused as a result of the inherent hydrophobicity of pure PDMS. Figure 7.6A shows the results of attempting to flow water through the devices with four separate channels. The ATR-FTIR spectroscopic images showing the spatial distribution of water indicate that solution is only initially present in one of the channels, before eventually beginning to fill another channel. This is very problematic for the intended investigations of multiple dissolution experiments, making the simultaneous study of four channels impossible. Hence, a method to achieve flow through all of the channels at the same time was needed to be developed in order for this work to progress any further.

To prepare microfluidic devices where flow through all of the channels could be achieved poly(dimethylsiloxane-b-ethylene oxide polymeric) (PDMS-b-PEO) was added to the PDMS mixture during preparation, 1 % by weight. PDMS-b-PEO has been reported as an effective surfactant to add to pure PDMS to reduce its hydrophobicity (Yao and Fang, 2012). The modified PDMS was cast over the mould and cured under the same conditions as pure PDMS. However, the devices that were produced were much more hydrophilic in nature. Hence, as shown by the distribution of water in Figure 7.6B, the flow could be achieved in all four channels simultaneously. Subsequently, the PEG dissolved in all four channels at a

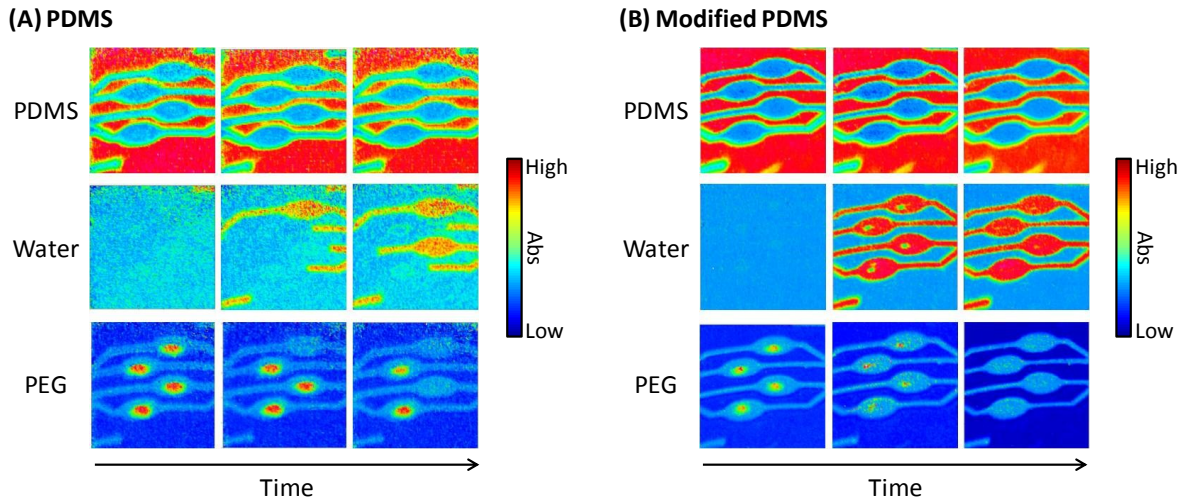


Figure 7.6 – ATR-FTIR spectroscopic images showing the results from the dissolution of PEG in (A) pure PDMS devices and (B) modified PDMS devices. The distribution of the PDMS, water and PEG have been shown as a function of time and the spectroscopic images were generated based on the integration of the unique bands between 1295–1240, 3600–3000 and 975–910 cm^{-1}, respectively. The image size is ~11.5 × 8 mm^2.

similar rate. This result was significant for advancing the application of PDMS devices for investigating the dissolution through multiple channels in ATR mode. The slight drawback of adding this PDMS-b-PEO surfactant to PDMS is that the final cured product loses some transparency.

7.3 Simultaneous screening of the dissolution of micro-formulations

Designing microfluidic devices where multiple dissolution experiments could be investigated simultaneously provided the opportunity to explore high-throughput screening *in situ*. This Section presents the results recorded using specifically designed microfluidic devices containing separate channels and tablet chambers that were studied using macro ATR-FTIR spectroscopic imaging to reveal information about the behaviour of drug release. The reliability and robustness of ATR-FTIR spectroscopic imaging for the study of pharmaceutical tablets and formulations have been well established in recent years, but this is the first time that micro-formulations have been investigated under flowing conditions (Ewing et al., 2015a, Ewing et al., 2015b, Kazarian and Ewing, 2013).

7.3.1 Materials

Ibuprofen and PEG (mw: 1000 $g.mol^{-1}$) were purchased from Sigma-Aldrich (UK) and used as received. Two different dissolution media were used in this investigation, a phosphate buffer (pH 7) and a 0.1 M HCl solution (pH 1). For the preparation of the phosphate buffer,

0.1 M sodium hydroxide solution was added to 0.1 M potassium dihydrogen phosphate solution in a 0.8:1.0 ratio. The 0.1 M HCl solution was prepared by diluting 8.30 mL of 12 M HCl in 1 L of deionised water.

7.3.2 ATR-FTIR spectroscopy and spectroscopic imaging

An Alpha FTIR spectrometer (Bruker, Germany) with a single element detector was used to measure the infrared spectra of the individual components for preliminary assessment in this investigation. ATR sampling mode utilising a diamond crystal was used to record the mid-infrared range across 4000–600 cm^{-1} with a resolution of 8 cm^{-1} and 64 co-added scans.

The ATR-FTIR spectroscopic imaging approach used a ZnSe crystal with a variable angle accessory (PIKE, Technologies). This ATR-FTIR accessory was placed in the macrochamber (IMAC) which is specifically designed for spectroscopic imaging applications. The macrochamber was fitted to an Equinox 55 FTIR spectrometer (Bruker, Germany) and an FPA detector to record spectroscopic images in the mid-IR region between 4000–900 cm^{-1}. OPUS software was used to record the spectral data at a resolution of 8 cm^{-1} and 16 co-added scans. The size of the FPA detector aligned for use with the ZnSe crystal in pixels was both 128 × 128 and 96 × 96 pixels dependent upon the microfluidic device used resulted in an image size of ~11.5 × 8 mm^2 and ~7.75 × 6 mm^2, respectively. The spectral band regions that were used to generate the spectroscopic images in this Section are the following: ibuprofen (1790–1695 cm^{-1}), PEG (1160–1045 cm^{-1}) and aqueous medium (3600–3000 cm^{-1}).

7.3.3 Preparation of the pharmaceutical micro-formulations

The micro-formulations investigated in this work were also prepared using the microdrop system. A different dispensing head was used where ibuprofen and PEG (mw: 1000 $g.mol^{-1}$) were combined in 1:3 weight ratio in the vessel and heated to 120 °C until both species had melted and mixed. Next, droplets of the formulation (~0.06 mm diameter with a volume of 113 pL) were dispensed directly onto the measured surface of the ZnSe crystal in specified locations that allowed the channels of the microfluidic devices to be placed and attached to the crystal around the micro-formulations. Micro-formulations were prepared by dispensing the droplets in an arrangement so that a total diameter of ~0.5 mm and a height of 0.06 mm, hence, this resulted in formulations with a total volume of approximately 12 nL.

7.3.4 High-throughput screening of micro-formulations under the same flowing conditions

The preparation of the formulations using the microdrop system is similar to that of a hot melt approach meaning that molecularly dispersed ibuprofen was obtained in the formulated mixture. Thus, the stability of this form could be investigated during the experiments. Proof of the molecularly dispersed form of ibuprofen is evident in the ATR-FTIR spectra shown in Figure 7.7. Figure 7.7 presents the ATR-FTIR spectrum of crystalline ibuprofen, PEG and the ibuprofen/PEG formulation (1:3 weight ratio). The appearance of ibuprofen in the molecularly dispersed form was confirmed in the ATR-FTIR spectrum of the formulation by the shift of the ν(C=O) absorption band from 1704 cm^{-1} (powdered form of ibuprofen) to 1730 cm^{-1} (when in the formulation). It has been reported in previous studies with ATR-FTIR spectroscopic imaging that structural changes from the molecularly dispersed to the crystalline form of ibuprofen can be characterised during release experiments (Kazarian and Chan, 2003). As a result, this is a suitable and reliable model system to demonstrate the potential of determining the behaviour of drugs using novel microfluidic devices.

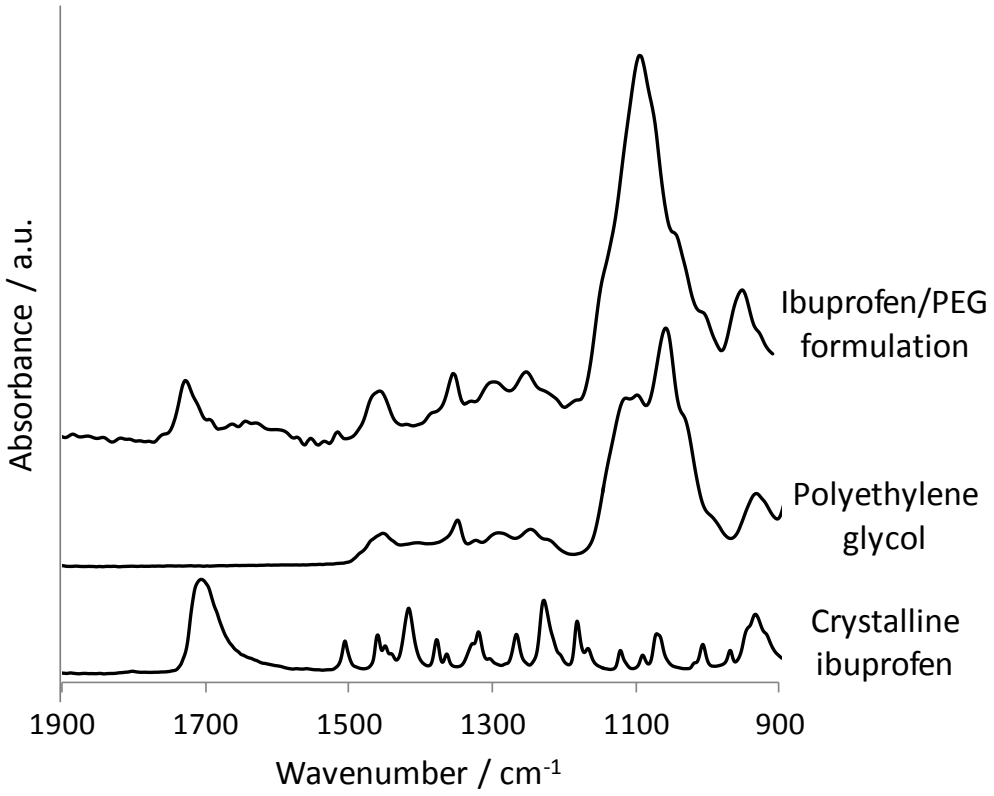


Figure 7.7 – ATR-FTIR spectra of the ibuprofen/PEG (1:3 weight ratio) formulation, polyethylene glycol (mw: 1000 $g.mol^{-1}$) and ibuprofen in the crystalline state.

The microfluidic devices were designed such that the full area of the FPA detector was utilised for analysis using ATR-FTIR spectroscopic imaging. Hence, 128 × 128 pixels were measured by placing the devices directly onto the measuring surface of ZnSe crystal in a commercial ATR-FTIR accessory (PIKE Technology). The size of the obtained spectroscopic images using this setup was approximately 11.5 × 8 mm^2 with a spatial resolution of ~150 µm. The spectroscopic images in Figure 7.8, demonstrate that it is possible to study four different channels simultaneously using the current design. However, it is feasible that further iterations can provide the opportunity to study more channels within this imaging field of view.

In these experiments, the dissolution of ibuprofen/PEG micro-formulations (1:3 weight ratio) in a solution of pH 7 were studied. The spectroscopic images presented in Figure 7.8 show the spatial distribution of ibuprofen, PEG and the aqueous medium during the experiment. One of the significant advantages of using the microfluidic devices is realised in these experiments as all four micro-formulations in the channels dissolve at the same rate. Thus, in a single experiment using this setup, it is possible to screen multiple formulations in high-throughput at the same time. Furthermore, complete release of ibuprofen in the pH 7 aqueous medium is observed after 20 min, and at a similar rate to the PEG excipient. The spectroscopic images show that this is coincident with the ingress of the aqueous medium

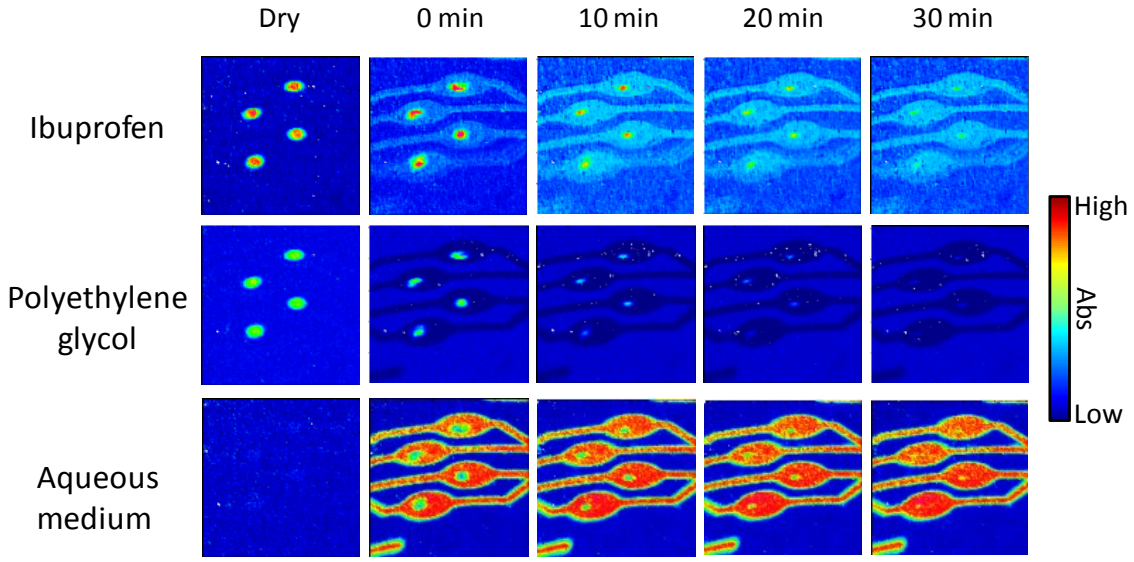


Figure 7.8 – ATR-FTIR spectroscopic images showing the simultaneous dissolution of four ibuprofen/PEG (1:3 weight ratio) formulations in neutral solution. The spatial distribution of PEG (top row), ibuprofen (middle row) and the aqueous solution (bottom row) have been presented. The dimensions of the images are ~11.5 × 8 mm^2.

towards the core of the formulations. As a result, the rate of ibuprofen drug release can be increased when it is in the molecularly dispersed form. Such results can have implications for the development of new delivery systems, for example, the design of micro-formulations or particles within capsules as an alternative method to solid tablet compacts.

Figure 7.9 shows the result of the same ibuprofen/PEG formulation as described above, but instead in the presence of an acidic solution. In this experiment, interesting observations relating to the behaviour of the formulation in the acidic solution under flow were identified. The ATR-FTIR spectroscopic images confirm that there is little dissolution of both the ibuprofen and the PEG from these micro-formulations during the experiment. The images recorded at 20 min show that there is still the presence of both the drug and excipient and more interestingly the solution has not penetrated into the tablet matrix after this time. In contrast, complete release and dissolution of the materials was observed after this period for the same micro-formulations in a neutral solution.

The reasons for the differences in the drug release behaviour can be revealed in the ATR-FTIR spectra that have been extracted from the formulations and are shown in Figure 7.9. The ibuprofen in the formulations before the introduction of the acidic solution is characterised to be in the molecularly dispersed form. As the experiment progressed, there is a shift in the ν(C=O) absorption band at 1730 cm^{-1} to a lower wavenumber at 1705 cm^{-1}. This change in band position is evidence of conversion back to the crystalline form induced

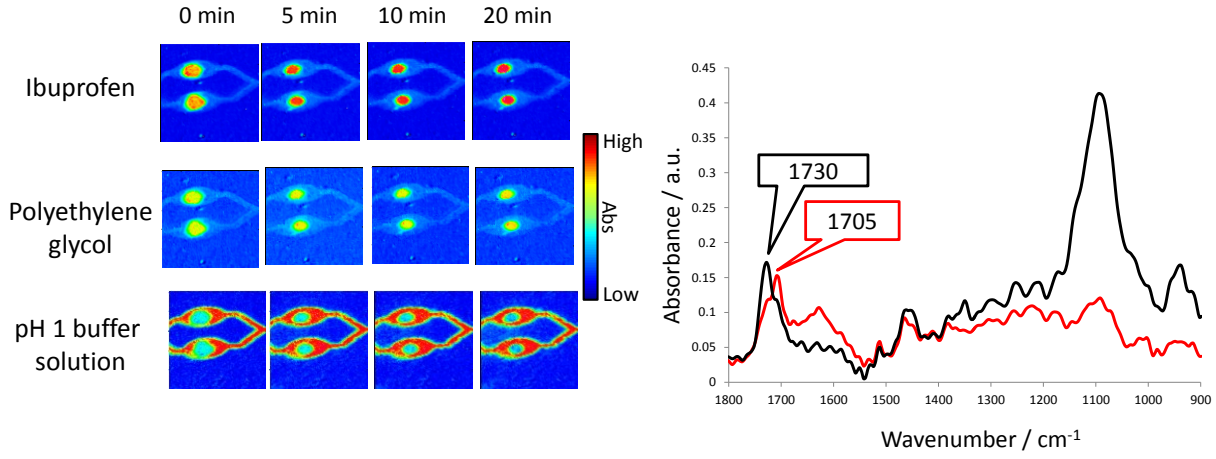


Figure 7.9 – (A) ATR-FTIR spectroscopic images showing the simultaneous dissolution of two ibuprofen/PEG formulations in acidic medium. The spatial distribution of, ibuprofen (top row) PEG (middle row) and the aqueous solution (bottom row) have been presented. The dimensions of the images are ~11.5 × 8 mm^2. (B) Extracted ATR-FTIR spectra taken from the centre of the formulation at 0 min (Black) and 20 min (Red).

upon contact with the acidic medium that dissolves more slowly than the molecularly dispersed form. In addition to slower drug release, it also appears that formation of the crystalline form also inhibits ingress of the solution into the micro-formulation that could be a reason for the reduced rate of dissolution. Therefore, it is possible to determine structural changes during the *in situ* experiment under flow in addition to spatial information about the different species. Due to the high-throughput nature of these investigations the reliability of the results can be compared in a single experiment meaning that rapid screening of multiple samples is possible.

7.3.5 Simultaneous screening of multiple formulations under flowing conditions in different pH environments

In addition to the microfluidic devices designed to study high-throughput dissolution behaviour of multiple micro-formulations, it has also been demonstrated that devices to simultaneously study the same formulations but under different flowing conditions can be produced. These microfluidic chips have multiple inlets and outlets. As shown in Figure 7.10, a device with two channels was studied that is capable of flowing two different media at the same time. Here, dissolution of the ibuprofen/PEG formulation in both the neutral and acidic solutions has been screened at the same time. The spectroscopic images and extracted spectra presented in Figure 7.10 show that there are obvious differences between the behaviour of the micro-formulation in the different aqueous media. Similarly, to the structural changes characterised in Figure 7.9, the appearance of the crystalline form of ibuprofen is observed in the acidic medium that inhibits the release of the drug and dissolution of the formulation (Figure 7.10C). On the other hand, in the neutral medium, no changes in structural form were observed and subsequently the drug was readily released into the surrounding solution.

One advantage of studying micro-formulations in microfluidic devices with two channels is that the sampling area of interest is smaller, thus, a smaller pixel array of the FPA detector can be used. While this does mean that reduced dimensions of the spectroscopic images are obtained, it allows for faster measurements to be recorded using the same number of co-added scans (16 scans) and spectral resolution (8 cm^{-1}). Figure 7.10 shows the results from the two channels devices where 96 × 96 pixels were measured which allowed a slightly reduced imaged area (7.75 × 6 mm^2) to be recorded. As a result of the faster measurement time, it was possible to record images in ~1 min and hence the data obtained from the first 5 min after introducing the different solutions have been presented. The spectroscopic images in Figure 7.10 determine that changes in the structural form of ibuprofen are apparent in the

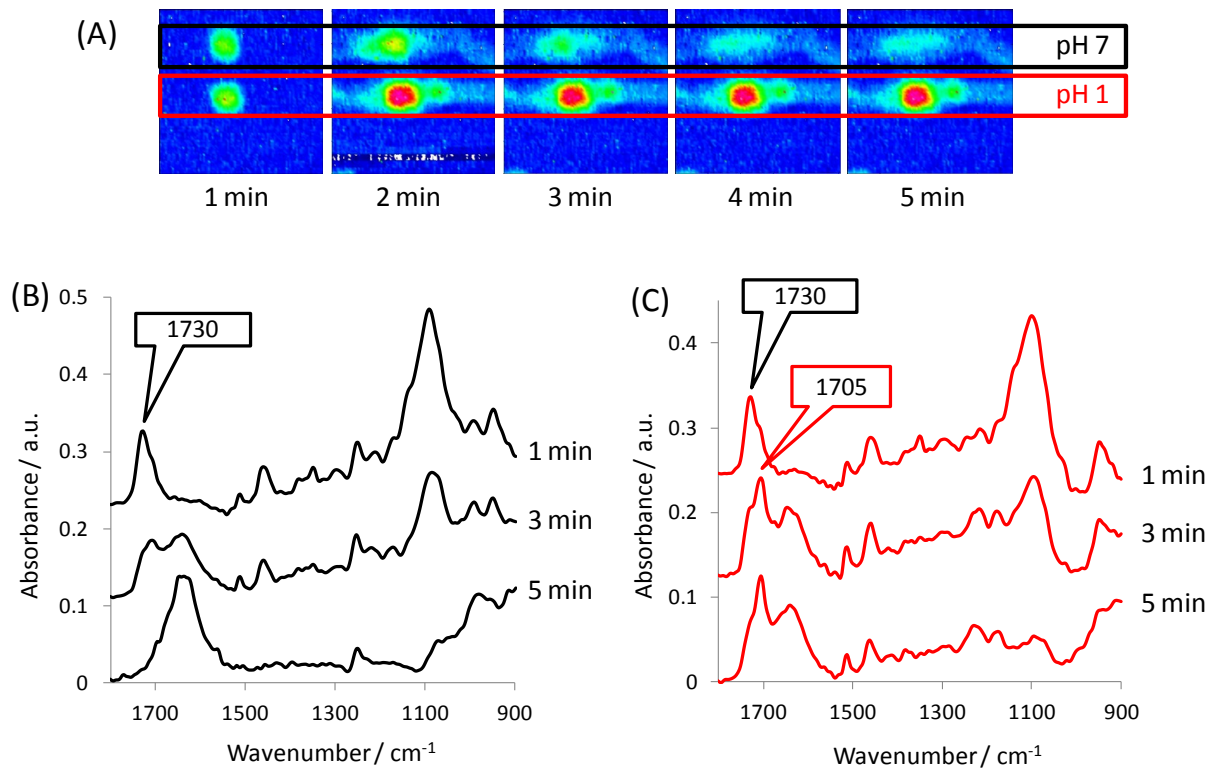


Figure 7.10 – (A) ATR-FTIR spectroscopic images showing the behaviour of ibuprofen during the simultaneous dissolution of two ibuprofen/PEG formulations (1:3 weight ratio) in different pH media. The size of the spectroscopic images is ~7.75 × 6 mm^2. Any structural changes of ibuprofen in the media during the experiment were shown in the extracted ATR-FTIR spectra, from the centre of the tablet in the pH 7 (B) and pH 1 (C) solution.

presented data immediately upon contact with the acidic medium. In contrast, dissolution of the micro-formulation in the neutral medium is fast and the ibuprofen appears to be near complete release after 5 min during these experiments. These results demonstrate the possibility of applying ATR-FTIR spectroscopic imaging to determine the behaviour of multiple formulations in different conditions at the same time. Moreover, the measurement settings of the spectrometer and the design of the microfluidic devices can be tuned and optimised depending upon the application.

Miniaturisation of formulations, for example, those studied in this work, could prove to be very useful for the screening newly developed delivery systems. Furthermore, the use of ATR-FTIR spectroscopic imaging is a powerful approach to reveal the inherent chemical specificity and allows one to detect changes in the structural from (e.g. from molecularly dispersed to crystalline) in real time. In these experiments, four micro-formulations have been investigated simultaneously under the same aqueous conditions under flow. However, it is conceivable that further modifications can be made to the devices whereby more channels

can be studied by reducing the channels width and formulation size. As a result, the combination of ATR-FTIR spectroscopic imaging with microfluidic devices, as presented here, is a flexible approach to study a range of formulations depending upon the problem of interest. The devices that have been shown in this work were used in high-throughput applications where the behaviour of several of the same ibuprofen/PEG formulations was monitored at the same time, thus avoiding the need for many repeat experiments. This approach may be particularly advantageous for rapid screening of large numbers of samples or where the amount of sample is limited.

7.4 Crystallisation of a dissolved drug in changing pH environments

The investigation into the recrystallisation of a model API, sodium ibuprofen, which was dissolved in a neutral solution and mixed with an acidic medium, has been studied. The motivation of such a study stems from the drive to improve the dissolution rates of drugs from tablet compacts in the field of pharmaceutical research, for example, the ionisation of drug candidates (Ewing et al., 2015b, Serajuddin, 2007). However, the behaviour of these drugs after they have been released from the tablet matrix and dissolved into the surrounding solution is actually of great importance. Subsequent effects such as localised areas of saturation and supersaturation can initiate recrystallisation and precipitation of the drug even after it has dissolved from the tablet.

7.4.1 Preparation of sodium ibuprofen solutions

Three different concentration solutions of sodium ibuprofen dissolved were studied in this investigation, 200 $mg.mL^{-1}$, 100 $mg.mL^{-1}$and 50 $mg.mL^{-1}$. 2 g, 1 g and 0.5 g of sodium ibuprofen were dissolved in 10 mL of phosphate buffer and stirred at room temperature until the solid had dissolved. The solutions were stored in sealed vessels until use.

7.4.2 ATR-FTIR spectroscopy and spectroscopic imaging

An Alpha FTIR spectrometer with a single element detector was used to measure the infrared spectra of the individual components for preliminary assessment in this investigation. ATR sampling mode utilising a diamond crystal was used to record the mid-infrared range across 4000–600 cm^{-1} with a spectral resolution of 8 cm^{-1} and 64 co-added scans.

The microfluidic devices were attached to a ZnSe crystal of the variable angle accessory (PIKE Technologies) for the ATR-FTIR spectroscopic imaging approach. The FPA detector was setup to record a pixel array size of 128 × 128 that produced an image size of ~11.5 × 8 mm^2. The spectral band regions used to generate the spectroscopic images in this

Section are the following: sodium ibuprofen (1580–1525 cm^{-1}), crystalline ibuprofen (1735–1680 cm^{-1}) and the aqueous medium (3600–3000 cm^{-1}).

7.4.3 Results of dissolved drug in changing pH conditions

In this study, a microfluidic device was designed to include two inlets that meet at a T-junction followed by a serpentine channel to monitor the behaviour of a dissolved drug upon mixing with a different solution (Figure 7.11). This microfluidic device was attached to the measuring surface a ZnSe crystal where the width and height of the channels was 0.5 mm and 1.5 mm, respectively. For these experiments, two different aqueous samples were injected into the separate inlets at a controlled flow rate (10 µL/min) at the same time where they mixed at the T-junction. Figure 7.11 presents the results of a 200 $mg.mL^{-1}$ solution of sodium ibuprofen dissolved in a neutral solution mixing with an acidic solution (pH 1, 0.1 M HCl acid). Previously, the effects of local areas of saturation outside of the tablet have been detected using macro ATR-FTIR spectroscopic imaging and shown to result in recrystallisation of the drug just outside of the tablet matrix (Punčochová et al., 2015).

The spectroscopic images in Figure 7.11 reveal the spatial distribution of the sodium ibuprofen, crystalline ibuprofen and aqueous medium respectively. In the spectroscopic images, it is possible to characterise and determine regions of the conversion of ibuprofen from the ionised structure to the solid crystalline form. Structural changes began to initiate after 2 min and as the experiment progressed the extent of this conversion continued to increase. As highlighted in the spectroscopic images by the increasing relative absorbance of

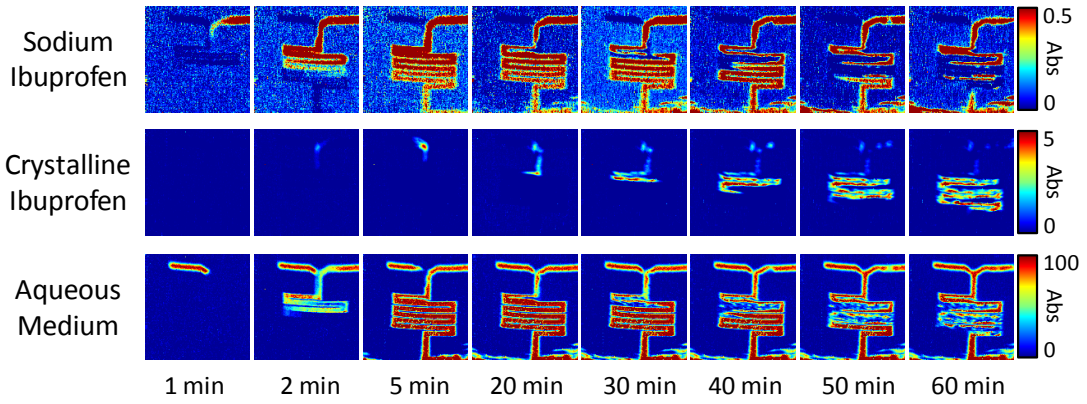


Figure 7.11 – ATR-FTIR spectroscopic images showing the precipitation of crystalline ibuprofen crystals upon contact and mixing of a sodium ibuprofen solution (2 $mg.mL^{-1}$) with a pH 1 solution. The spatial distribution of sodium ibuprofen (top row), crystalline ibuprofen (middle row) and aqueous solution (bottom row) are presented. The size of the image is ~11.5 × 8 mm^2.

the crystalline ibuprofen in the channel during the experiment. Conversely, at the same time, the concentration of the sodium ibuprofen decreases as a result of the changing structural form.

Furthermore, the ATR-FTIR spectroscopic images of all components present allow conclusions about the behaviour of the materials within the channels to be determined. The ATR-FTIR images representing the distribution of the aqueous solution show that as crystalline ibuprofen was formed, it was displaced from the surface of the ZnSe crystal. This result is an example where ATR-FTIR imaging can be a valuable tool for pharmaceutical research as it measures the first few micrometres in contact with the crystal. Significantly, it is widely reported that NSAIDs, such as ibuprofen, can have problematic effect in the digestive system when there is a build-up of crystalline material on the lining of the gastrointestinal tract. Here we present evidence that the formation of crystalline ibuprofen can result in the drug settling upon the lower surface in the channel even under flowing conditions.

The fast dynamic measurements in these experiments demonstrate that there is the appearance of a higher concentration of crystalline ibuprofen as the experiment progressed as a function of time. Also, the ability to monitor the behaviour and characterise different phases present in the channels in real time has been demonstrated in these experiments by extraction of ATR-FTIR spectra shown in Figure 7.12. The formation of crystalline ibuprofen in a solid state from an aqueous solution is detected and spatially resolved in the ATR-FTIR spectroscopic images. The high sensitivity and chemical specificity of ATR-FTIR spectroscopic imaging mean that it was possible to detect the presence of the sodium ibuprofen dissolved in solution. The extracted spectra are shown in Figure 7.12. Additionally, it is possible to monitor specific pixels from the FPA detector in the different time-resolved images. Figure 7.12 shows the changes in the extracted spectra taken from a bend in the serpentine channel as the experiment progressed.

The ATR-FTIR spectra from these particular pixels display obvious changes, such as the increase in the absorbance of the spectral bands associated with crystalline ibuprofen. Unique absorbance bands, for example, those with the peak at 1705, 1320 and 1230 cm^{-1} increase during the experiment. In contrast, the images that are associated with the sodium ibuprofen solution, specifically the bands with the peaks at 1542, 1397 and 1365 cm^{-1}, consequently decrease in absorbance. Complementary information about the aqueous medium can also be revealed in the spectroscopic images. The behaviour of the aqueous medium is highlighted by the decrease and then the absence of the spectral band associated with the bending mode of

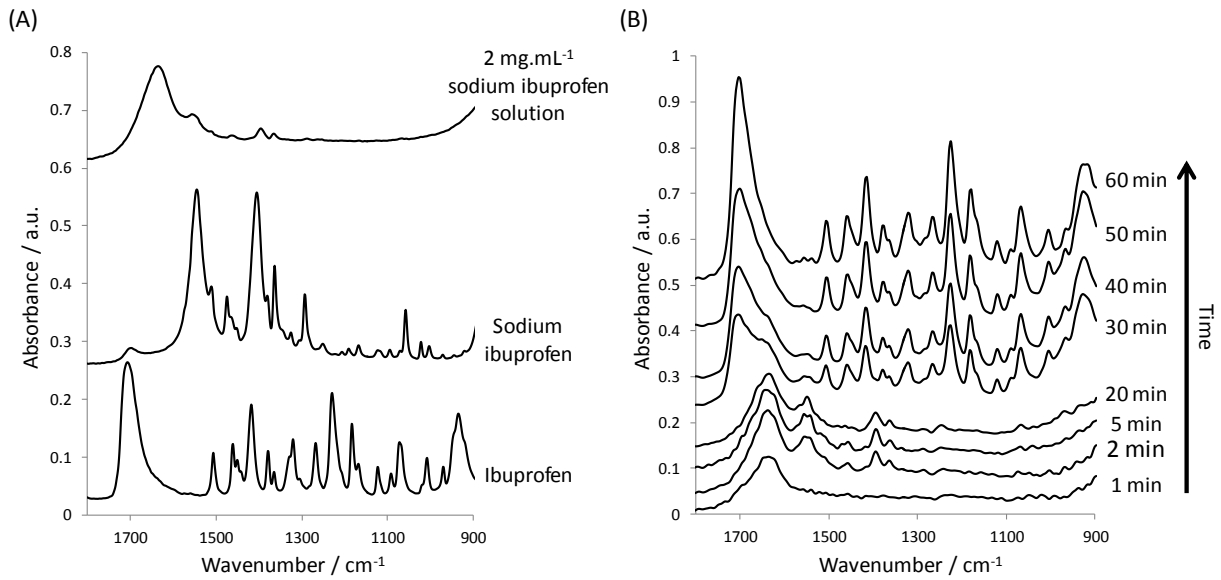


Figure 7.12 – (A) ATR-FTIR spectra recorded for the pure 2 mg.mL^{-1} sodium ibuprofen solution, sodium ibuprofen and crystalline ibuprofen. (B) Extracted spectra from the 2 mg.mL^{-1} sodium ibuprofen solution experiment. The spectra were extracted from a bend in the serpentine channel as the experiment proceeded.

water with a peak at 1635 cm^{-1}. The disappearance of this spectral band is evidence of the solution being displaced from the measured surface of the crystal, which is thus determined in the spectroscopic images in Figure 7.11. The extracted spectra presented in Figure 7.12 reveal chemically specific information about the systems while the spectroscopic images reveal the spatial distribution of these species. Hence, a wealth of information can be gained from such experiments where not only can structural changes be characterised but the extent of conversion and the behaviour of the materials under flow can be assessed.

Figure 7.13 presents the distribution of crystalline ibuprofen as a function of time for experiments where different concentration solutions of sodium ibuprofen were studied. Here, it can be seen that the relative amount of crystalline ibuprofen that was formed during the experiment is dependent upon the initial concentration of the drug in solution. Nevertheless, there is the presence of crystalline ibuprofen in all of the experiments. In general, the trend relating to the formation of the solid crystalline ibuprofen is that the higher the concentration of the sodium ibuprofen solution, the greater the extent of crystallisation. The ATR-FTIR spectroscopic images recorded for the 200 mg.mL^{-1} sodium ibuprofen solution show that crystalline ibuprofen is present within the entire serpentine channel at around 60 min. Whereas, the 100 mg.mL^{-1} sodium ibuprofen solutions show that crystalline ibuprofen was formed but to a lesser degree. In these images (middle row Figure 7.13), there tends to be an

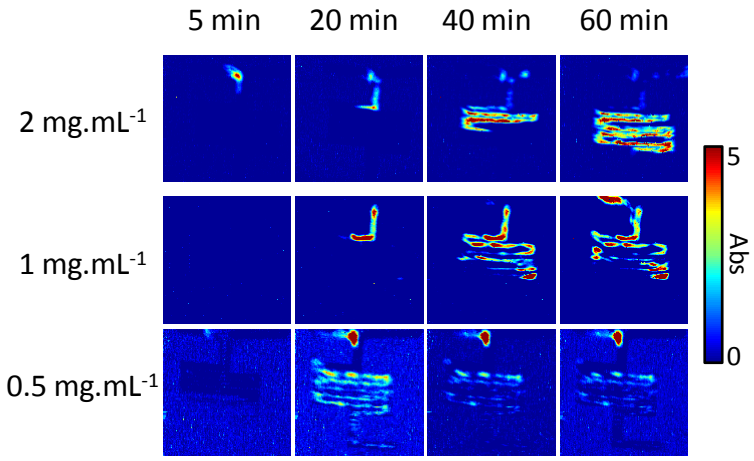


Figure 7.13 – ATR-FTIR spectroscopic images showing the precipitation of crystalline ibuprofen crystals from sodium ibuprofen solutions with different concentrations upon mixing with a pH 1 solution. The spatial distribution of crystalline ibuprofen is shown in the 2 mg.mL^{-1} (top row), 1 mg.mL^{-1} (middle row) and 0.5 mg.mL^{-1} (bottom row) experiments. The size of the images is ~11.5 × 8 mm^2.

aggregation of the crystalline ibuprofen at predominantly the bends in the channel. Finally, the results from the 50 mg.mL^{-1} sodium ibuprofen solution demonstrate the lowest amount of crystalline ibuprofen formation. Importantly, however, it is possible to characterise and detect the phase separation at the T-junction in the device. In the images recorded for these experiments (bottom row Figure 7.13), such as the spectroscopic image recorded at 20 min, crystalline ibuprofen is present but in a low concentration throughout the device. Interestingly, agglomeration of the particles is not seen to occur. One possible explanation is that the flowing solution could carry the particles through the channels but since the relative concentration of crystalline ibuprofen is low, there is no accumulation of the precipitates within the channel.

These results have shown that the behaviour of a dissolved drug in solutions with different concentrations can be effectively studied. Not only can the recrystallisation of drug from the solutions can be characterised and spatially resolved using ATR-FTIR spectroscopic imaging, but the extent of crystallisation from different solutions can be assessed. Comparisons of various experiments can prove very powerful when information about the behaviour of drug solutions is of interest. Similarly to the dissolution of micro-formulations, it is feasible that novel devices can be created to study these systems developed for high-throughput analysis. Thus, an opportunity exists to utilise this approach as a platform to determine specific concentrations where crystallisation can occur and a wide range of experiments can be designed to investigate such systems thoroughly.

7.5 Conclusions

Microfluidic devices specifically designed for use with macro ATR-FTIR spectroscopic imaging have been developed and the ability to study the behaviour of model systems with relevance to drug release has been reported. Firstly, many micro-formulations under flow were investigated and the effect of different aqueous solutions on the dissolution of the formulations was explored in a high-throughput manner using spectroscopic imaging combined with microfluidics for the first time. It was seen that the acidic medium inhibited release of ibuprofen as a result of conversion from the molecularly dispersed form to crystalline ibuprofen. These structural changes were characterised in the extracted ATR-FTIR spectra. Furthermore, microfluidic devices that allowed micro-formulations to be exposed to different aqueous conditions simultaneously were investigated and have been shown as an effective approach to screen multiple micro-formulations in a single experiment.

This work also highlights the importance of studying the behaviour of the drug after it has been released, i.e. recrystallisation of the drug from solution. Ibuprofen was characterised to recrystallise from a sodium ibuprofen solution upon contact and mixing with an acidic medium. A unique microfluidic device with a T-junction and serpentine channel arrangement allowed the entire field of view of the imaging system to be utilised. These results have shown a clear phase transition from sodium ibuprofen that was dissolved in a neutral solution converting to solid crystalline ibuprofen. Proof of this was determined by analysis of the macro ATR-FTIR spectroscopic imaging data. The collected data also provided further scope to explore the extent of crystallisation from different solutions of dissolved drug under flow. The behaviour of the solid particles was determined where accumulation and the subsequent build-up of the precipitation were spatially resolved.

The combined approach of using macro ATR-FTIR spectroscopic imaging with microfluidic devices could prove to be a very useful high-throughput analytical method to analyse drug release and the behaviour of the materials *in situ* under flowing conditions. The success of combining microfluidics with spectroscopic imaging to study pharmaceutical formulations under flow will impact applications in the fields of pharmaceutical science, biological chemistry and medicine. Further development of this approach can potentially establish this experimental setup as a reliable and robust method for studying a range of formulations and solutions in the future. Especially since innovative technologies for high-throughput analysis of formulations are of great interest for pharmaceutical formulation development.

8 Conclusions and Future Work

8.1 Overall summary

In this thesis, ATR-FTIR spectroscopy and spectroscopic imaging have been successfully applied to study the stability and dissolution behaviour of several different pharmaceutical formulations. *In situ* tablet dissolution experiments allowed the behaviour of amorphous solid dispersions (ASDs), the effect of drug carriers, and ionised drug forms to be monitored. In all of these investigations, the spatial distribution and chemical information revealed by macro ATR-FTIR spectroscopic imaging measurements were essential for determining the processes and mechanisms that affected drug release. Furthermore, the development of specifically designed microfluidic devices that can be studied using macro ATR-FTIR spectroscopic imaging has been reported. The results presented in this thesis have demonstrated that macro ATR-FTIR spectroscopic imaging has great potential to be employed for the assessment of pharmaceutical systems that can aid the development and design of novel formulations.

8.1.1 Drug release from tablet compacts monitored by macro ATR-FTIR spectroscopic imaging

The application of macro ATR-FTIR spectroscopic imaging to investigate the drug release from ASDs was demonstrated using indomethacin as a model drug. Two formulations of indomethacin with different polymer excipients, PEG and HPMC, were studied in this work. The significance of these results was to determine the stability of the amorphous form of the drug within the solid dispersions before and during tablet dissolution experiments. ASDs containing indomethacin and HPMC were successful in achieving an increased stability of amorphous indomethacin. As a result, a faster rate of drug release was observed in the chemical images recorded during tablet dissolution experiments. The increased stability was proposed to be a result of inhibited mobility of the drug in the formulation. Conversely, the amorphous form of indomethacin in ASDs formulated with PEG was not stable for long periods after preparation. ATR-FTIR spectroscopy clearly characterised structural changes of amorphous indomethacin crystallising to the γ form. Furthermore, macro ATR-FTIR spectroscopic imaging was used to study the interface between the amorphous indomethacin and molten PEG, which indicated that mobility through this polymer is possible. During cooling, changes from the amorphous form to the γ form, via the metastable α intermediate

were detected. Crystallisation from amorphous to γ indomethacin was also detected during tablet dissolution experiments in real time which significantly inhibited dissolution. The results from this study were successful in determining the stability of amorphous indomethacin in different solid dispersions. Thus, the importance of selecting the most appropriate excipients to stabilise the drug has been highlighted. Macro ATR-FTIR spectroscopic imaging was a valuable tool for detecting crystallisation; hence, this approach has been demonstrated to have great potential for monitoring changes in structural forms of the drug during storage and release.

Macro ATR-FTIR spectroscopic imaging was used with parallel UV detection to determine the influence of carriers for improving the dissolution of a poorly aqueous soluble drug. Firstly, formulations containing indomethacin as a poorly water-soluble drug and nicotinamide as a readily water-soluble carrier were investigated. The amount of indomethacin dissolved from different tablet compacts made from indomethacin/ nicotinamide formulations in varying weight ratios was compared. This is the first example where macro ATR-FTIR spectroscopic imaging was used to study interactions between two APIs in a single tablet compact. H-bonded interactions between indomethacin and nicotinamide were detected by the appearance of absorption bands at 1624 and 1114 cm^{-1}. The amount of indomethacin dissolved from the tablets increased for all of the formulations containing nicotinamide compared to pure indomethacin tablets. However, this effect was seen to be optimal for certain formulations where the H-bonding was maintained during the tablet dissolution experiment. As a result, two different mechanisms of dissolution were determined by analysis of the measured data. (1) The formation of H-bonded interactions between indomethacin and nicotinamide resulted in the poorly water-soluble drug being carried into the solution and thus dissolving faster. (2) The disintegration of the tablet matrix by dissolution of the more readily soluble carrier that increased the surface area of the compact available for dissolution. These proposed mechanisms were validated by studying tablets formulated with indomethacin with added urea and mannitol. These were selected as urea was reported to form interactions with indomethacin while mannitol was not. The release and dissolution of indomethacin from these formulations were consistent with the mechanisms observed from the indomethacin/nicotinamide tablets. As a result, the combination of macro ATR-FTIR spectroscopic imaging with UV detection was effective for the comprehensive assessment of quantifying determining drug release mechanisms during dissolution experiments. Detecting the intermolecular interactions between indomethacin and nicotinamide was essential to propose the mechanisms of drug release since a significant

decrease in the rate of dissolution was recorded in the UV dissolution profiles when these interactions were no longer present within the tablets. The use of ATR-FTIR spectroscopic imaging with conventional dissolution apparatus can reveal further information about the measured formulation that is not possible by employing a single analytical approach.

Finally, the effect of different aqueous pH environments on the stability and drug release of tablet compacts containing an ionised API were studied. Here, macro ATR-FTIR spectroscopic imaging and Raman mapping were used to assess the behaviour of the ionised form of the drug during *in situ* dissolution experiments. Complete release of the ionised API was observed in the spectroscopic images and maps from the experiments in the neutral dissolution medium. However, in the acidic medium, the formation of the free acid form of the drug was detected immediately upon contact with the aqueous solution. Initially, this occurred around the edge of the tablet which slowed ingress of the solution. Although, as the aqueous solution did slowly ingress towards the core of the tablet, conversion from the ionised API to the free acid form of the drug continued until eventually it was observed throughout the whole tablet. Consequently, the drug did not dissolve from these tablet compacts. This work has successfully demonstrated the application of using macro ATR-FTIR spectroscopic imaging and Raman mapping to monitor the same tablets compacts where each approach provided complementary information from different samples. Moreover, ATR-FTIR spectroscopic imaging has been employed to assess the behaviour of a developmental drug in the industrial pipeline that suggests that this approach has great potential for further industrial applications.

To conclude, macro ATR-FTIR spectroscopic imaging was successfully utilised to reveal valuable information about the behaviour of drugs in a range of tablet compacts. When necessary to complement the results recorded by macro ATR-FTIR spectroscopic imaging, alternative analytical approaches were used to provide additional information about the delivery systems. Hence, the results presented in this thesis have demonstrated further development of macro ATR-FTIR spectroscopic imaging for the study of tablet compacts.

8.1.2 Development of microfluidic devices for screening dissolution of pharmaceutical formulations with macro ATR-FTIR spectroscopic imaging

The work undertaken in this project has also explored the use of macro ATR-FTIR spectroscopic imaging to study pharmaceutical systems in microfluidic devices. New microfluidic devices were designed that could be attached to the measuring surface of a ZnSe crystal to achieve successful results in this work. Firstly, devices capable of assessing the

behaviour of multiple formulations simultaneously were made using modified PDMS. It was possible to achieve flow of aqueous solutions through all of the channels meaning that behaviour of several micro-formulations (0.5 mm diameter) could be monitored in solutions with different pH values. The acidic medium was detected to decrease the rate of drug release from model ibuprofen/PEG formulations by initiating a form change from molecularly dispersed ibuprofen to its crystalline form. These structural changes were clearly distinguishable in the extracted FTIR spectra from the spectroscopic imaging data. Further designs of the microfluidic devices allowed different solutions to flow through the individual channels at the same time. Hence, the stability and behaviour of the same micro-formulation were assessed in various conditions in a single experiment.

Monitoring the drug after it has been released from a tablet or dissolved in the solution is relatively unexplored but nonetheless, can have implications for drug delivery. For example, local areas of supersaturation can initiate precipitation from solution. Thus, microfluidic devices with a T-junction were created where a solution of dissolved drug could contact a solution with a different pH value. Here, different solutions of a model ionised drug, sodium ibuprofen, dissolved in a neutral solution were studied upon contact with an acidic medium. A clear phase transition was detected and characterised as precipitates of the non-ionised crystalline form of ibuprofen. Subsequently, there was the agglomeration of the precipitates in the microfluidic channel that was spatially resolved in the spectroscopic images.

The combined use of macro ATR-FTIR spectroscopic imaging to study pharmaceutical systems in microfluidic channels has been demonstrated and these preliminary investigations could provide a platform for further development of this approach in the future. Particularly since novel approaches for high-throughput screening of formulations are of interest to the pharmaceutical industry.

8.2 Recommendations for future work

The main aim of this thesis is to demonstrate further the use of macro ATR-FTIR spectroscopic imaging as a valuable analytical approach to assess pharmaceutical systems, be it from dissolving tablet compacts or in microfluidic channels. It is hoped that this work can be a useful platform for the continued development of ATR-FTIR spectroscopic imaging in the future. Investigations of novel formulations can aid the design of more efficient pharmaceutical products which can establish this approach as a reliable technique for industrial applications.

Exciting opportunities exist for the development of the work presented in this thesis. Some ideas for future investigations are summarised in the following points:

1) A logical continuation of the work relating to the use of ATR-FTIR spectroscopic imaging for the detection of structural or chemical changes could be to differentiate between hydrates and anhydrates of pharmaceutical materials. A hydrate is a solid material that contains the parent anhydrate compound and water. The presence of water in a pharmaceutical hydrate can influence characteristics such as the dissolution rate, bioavailability and solubility of the material. Hence, maintaining the desired form of the drug is important for controlling drug delivery. As a result of the expected changes in the FTIR spectrum between the different forms, ATR-FTIR spectroscopic imaging can be used to determine the structure of the hydrates or assess the behaviour of the materials in different environments or solutions.

2) Co-crystals can be used as a means to enhance the bioavailability and dissolution rate of poorly water-soluble drugs by formation of a single crystalline phase between two or more pharmaceutically approved molecules, including an API. ATR-FTIR spectroscopic imaging has the potential to be a useful approach to detect the formation of co-crystals by the appearance of new spectral bands in the FTIR spectrum. Hence, the stability of the co-crystals in tablet compacts during *in situ* dissolution studies can be investigated. Furthermore, the influence of high temperature and/or humidity environments on maintaining the co-crystal structures can be explored.

3) Another potential development that builds on the work presented in this thesis is to design novel microfluidic devices capable of high-throughput assessment of many formulations under flow. It is feasible, based on the devices presented in this work that microfluidic chips with smaller channels could be created that can monitor up to ten

micro-formulations in a single experiment. Microfluidic devices where the conditions, such as flow rate and pH medium, can be changed, for example, by adding another inlet for an additional solution downstream could produce some interesting results into the effect of different aqueous conditions on formulations.

4) 3D information from the samples can be collected using ATR-FTIR spectroscopic imaging by changing the angle of incidence of the incoming IR beam to the ATR crystal. Thus, information from different depths within the sample can be collected. The principle of this approach has been demonstrated by varying the angle of incidence by the use of apertures and has been reported for the study of layered polymer samples (Wrobel et al., 2015, Frosch et al., 2010). However, this approach has not yet been applied for the ATR-FTIR spectroscopic imaging studies of pharmaceutical systems. There is potential that this can be used to determine the quality of coatings or detect the thickness of layers in multi-layered tablets.

5) ATR-FTIR spectroscopic imaging can be useful for the determining interactions between different drugs in individual layers in the bilayer or multi-layered tablets. Any interactions could result in diffusion of the drugs between the layers that can affect drug release. Such research can potentially have a great impact due to the increasing number of drug delivery systems containing more than one API. Furthermore, experimental data from spectroscopic imaging could be used in combination with mathematical models (Kimber et al., 2012) to predict the diffusion or interactions between the drugs at this interface.

6) Finally, the use of ATR-FTIR spectroscopic imaging with other analytical methods could aid the development of novel pharmaceutical delivery systems. Comparing the results from this approach with other established analytical approaches such as differential scanning calorimetry, MRI and X-ray diffraction can mean that a wealth of information can be recorded about the formulations.

References

ABDALLAH, D. M. 2010. Nicotinamide alleviates indomethacin-induced gastric ulcers: a novel antiulcer agent. *European Journal of Pharmacology,* 627**,** 276–280.

AGUIAR, A. J. & ZELMER, J. E. 1969. Dissolution behavior of polymorphs of chloramphenicol palmitate and mefenamic acid. *Journal of Pharmaceutical Sciences,* 58**,** 983–987.

AHLNECK, C. & ALDERBORN, G. 1989. Moisture adsorption and tabletting. II. The effect on tensile strength and air permeability of the relative humidity during storage of tablets of 3 crystalline materials. *International journal of pharmaceutics,* 56**,** 143-150.

AHLNECK, C. & ZOGRAFI, G. 1990. The molecular basis of moisture effects on the physical and chemical stability of drugs in the solid state. *International Journal of Pharmaceutics,* 62**,** 87–95.

AHUJA, N., KATARE, O. P. & SINGH, B. 2007. Studies on dissolution enhancement and mathematical modeling of drug release of a poorly water-soluble drug using water-soluble carriers. *European Journal of Pharmaceutics and Biopharmaceutics,* 65**,** 26–38.

AINA, A., HARGREAVES, M. D., MATOUSEK, P. & BURLEY, J. C. 2010. Transmission Raman spectroscopy as a tool for quantifying polymorphic content of pharmaceutical formulations. *Analyst,* 135**,** 2328–2333.

ALANAZI, F. K. 2007. Evaluation of spray and freeze-dried excipient bases containing disintegration accelerators for the formulation of metoclopramide orally disintegrating tablets. *Saudi Pharmaceutical Journal,* 15**,** 105–119.

ALONZO, D. E., ZHANG, G. G., ZHOU, D., GAO, Y. & TAYLOR, L. S. 2010. Understanding the behavior of amorphous pharmaceutical systems during dissolution. *Pharmaceutical Research,* 27**,** 608–618.

AMIGO, J. M. 2010. Practical issues of hyperspectral imaging analysis of solid dosage forms. *Analytical and Bioanalytical Chemistry,* 398**,** 93-109.

ANDRONIS, V., YOSHIOKA, M. & ZOGRAFI, G. 1997. Effects of sorbed water on the crystallization of indomethacin from the amorphous state. *Journal of Pharmaceutical Sciences,* 86**,** 346–351.

ASO, Y., YOSHIOKA, S. & KOJIMA, S. 2004. Molecular mobility-based estimation of the crystallization rates of amorphous nifedipine and phenobarbital in poly (vinylpyrrolidone) solid dispersions. *Journal of Pharmaceutical Sciences,* 93**,** 384–391.

ATKINS, P. & DE PAULA, J. 2005. *Elements of Physical Chemistry,* Oxford, Oxford University Press.

AVDEEF, A., TSINMAN, K., TSINMAN, O., SUN, N. & VOLOBOY, D. 2009. Miniaturization of powder dissolution measurement and estimation of particle size. *Chemistry & Biodiversity,* 6**,** 1796–1811.

BAKER, M. J., TREVISAN, J., BASSAN, P., BHARGAVA, R., BUTLER, H. J., DORLING, K. M., FIELDEN, P. R., FOGARTY, S. W., FULLWOOD, N. J. & HEYS, K. A. 2014. Using Fourier transform IR spectroscopy to analyze biological materials. *Nature Protocols,* 9**,** 1771–1791.

BATES, T. R. 1969. Dissolution characteristics of reserpine-polyvinylpyrrolidone co-precipitates. *Journal of Pharmacy and Pharmacology,* 21**,** 710–712.

BEEBE, D. J., MENSING, G. A. & WALKER, G. M. 2002. Physics and applications of microfluidics in biology. *Annual Review of Biomedical Engineering,* 4**,** 261–286.

BETTINI, R., CATELLANI, P. L., SANTI, P., MASSIMO, G., PEPPAS, N. A. & COLOMBO, P. 2001. Translocation of drug particles in HPMC matrix gel layer: effect of drug solubility and influence on release rate. *Journal of Controlled Release,* 70**,** 383-391.

BHARGAVA, R., FERNANDEZ, D. C., HEWITT, S. M. & LEVIN, I. W. 2006. High throughput assessment of cells and tissues: Bayesian classification of spectral metrics from infrared vibrational spectroscopic imaging data. *Biochimica et Biophysica Acta-Biomembranes,* 1758**,** 830–845.

BLACK, D. B. & LOVERING, E. G. 1977. Estimation of Degree of Crystallinity in Digoxin by X-ray and IR Methods. *Journal of Pharmacy and Pharmacology,* 29**,** 684-687.

BOGDANOVA, S., SIDZHAKOVA, D., KARAIVANOVA, V. & GEORGIEVA, S. 1998. Aspects of the interactions between indomethacin and nicotinamide in solid dispersions. *International Journal of Pharmaceutics,* 163**,** 1–10.

BORKA, L. 1974. Polymorphism of indomethacin - New modifications, their melting behaviour and solubility. *Acta Pharmaceutica Suecica,* 11**,** 295–303.

BOULET-AUDET, M., BYRNE, B. & KAZARIAN, S. G. 2015. Cleaning-in-place of immunoaffinity resins monitored by in situ ATR-FTIR spectroscopy. *Analytical and Bioanalytical Chemistry,* 407**,** 7111–7122.

BRAUNS, E. B. 2014. Mid-infrared diffuse reflection on ultrafast time scales. *Applied Spectroscopy,* 68**,** 1–4.

BREITENBACH, J. 2002. Melt extrusion: from process to drug delivery technology. *European Journal of Pharmaceutics and Biopharmaceutics,* 54**,** 107–117.

BREITENBACH, J., SCHROF, W. & NEUMANN, J. 1999. Confocal Raman-spectroscopy: analytical approach to solid dispersions and mapping of drugs. *Pharmaceutical Research,* 16**,** 1109–1113.

BRITS, M., LIEBENBERG, W. & DE VILLIERS, M. M. 2010. Characterization of Polymorph Transformations That Decrease the Stability of Tablets Containing the WHO Essential Drug Mebendazole. *Journal of Pharmaceutical Sciences,* 99**,** 1138–1151.

BROUWERS, J., TACK, J. & AUGUSTIJNS, P. 2007. In vitro behavior of a phosphate ester prodrug of amprenavir in human intestinal fluids and in the Caco-2 system: illustration of intraluminal supersaturation. *International Journal of Pharmaceutics,* 336**,** 302–309.

BUGAY, D. E. & BRITTAIN, H. G. 2006a. Infrared absorption spectroscopy. *In:* BRITTAIN, H. G. (ed.) *Spectroscopy of Pharmaceutical Solids.* Milford, New Jersey, USA: Taylor & Francis.

BUGAY, D. E. & BRITTAIN, H. G. 2006b. Raman spectroscopy. *In:* BRITTAIN, H. G. (ed.) *Spectroscopy of Pharmaceutical Solids.* Milford, New Jersey, USA: Taylor & Francis.

CABRI, W., GHETTI, P., POZZI, G. & ALPEGIANI, M. 2007. Polymorphisms and patent, market, and legal battles: Cefdinir case study. *Organic Process Research & Development,* 11**,** 64-72.

CESCHAN, N. E., BUCALÁ, V. & RAMÍREZ-RIGO, M. V. 2015. Polymeric microparticles containing indomethacin for inhalatory administration. *Powder Technology,* 285**,** 51–61.

CHAN, K. L. A., ELKHIDER, N. & KAZARIAN, S. G. 2005a. Spectroscopic imaging of compacted pharmaceutical tablets. *Chemical Engineering Research & Design,* 83**,** 1303-1310.

CHAN, K. L. A., FLEMING, O. S., KAZARIAN, S. G., VASSOU, D., CHRYSSIKOS, G. D. & GIONIS, V. 2004. Polymorphism and devitrification of nifedipine under

controlled humidity: a combined FT-Raman, IR and Raman microscopic investigation. *Journal of Raman Spectroscopy,* 35**,** 353–359.

CHAN, K. L. A., GULATI, S., EDEL, J. B., DE MELLO, A. J. & KAZARIAN, S. G. 2009. Chemical imaging of microfluidic flows using ATR-FTIR spectroscopy. *Lab on a Chip,* 9**,** 2909–2913.

CHAN, K. L. A., HAMMOND, S. V. & KAZARIAN, S. G. 2003. Applications of attenuated total reflection infrared spectroscopic imaging to pharmaceutical formulations. *Analytical Chemistry,* 75**,** 2140–2146.

CHAN, K. L. A. & KAZARIAN, S. G. 2003. New opportunities in micro- and macro-attenuated total reflection infrared spectroscopic imaging: Spatial resolution and sampling versatility. *Applied Spectroscopy,* 57**,** 381-389.

CHAN, K. L. A. & KAZARIAN, S. G. 2004. FTIR spectroscopic imaging of dissolution of a solid dispersion of nifedipine in poly(ethylene glycol). *Molecular Pharmaceutics,* 1**,** 331-335.

CHAN, K. L. A. & KAZARIAN, S. G. 2005. Fourier transform infrared imaging for high-throughput analysis of pharmaceutical formulations. *Journal of Combinatorial Chemistry,* 7**,** 185-189.

CHAN, K. L. A. & KAZARIAN, S. G. 2006a. ATR-FTIR spectroscopic imaging with expanded field of view to study formulations and dissolution. *Lab on a Chip,* 6**,** 864–870.

CHAN, K. L. A. & KAZARIAN, S. G. 2006b. ATR-FTIR spectroscopic imaging with expanded field of view to study formulations and dissolution. *Lab on a Chip,* 6**,** 864-870.

CHAN, K. L. A. & KAZARIAN, S. G. 2006c. High-throughput study of poly (ethylene glycol)/ibuprofen formulations under controlled environment using FTIR imaging. *Journal of Combinatorial Chemistry,* 8**,** 26–31.

CHAN, K. L. A. & KAZARIAN, S. G. 2007. Attenuated total reflection Fourier transform infrared imaging with variable angles of incidence: A three-dimensional profiling of heterogeneous materials. *Applied Spectroscopy,* 61**,** 48-54.

CHAN, K. L. A. & KAZARIAN, S. G. 2013a. Aberration-free FTIR spectroscopic imaging of live cells in microfluidic devices. *Analyst,* 138**,** 4040–4047.

CHAN, K. L. A. & KAZARIAN, S. G. 2013b. Label-free chemical detection in microfabricated devices using FT-IR spectroscopic imaging. *Spectroscopy***,** 22–27.

CHAN, K. L. A., KAZARIAN, S. G., MAVRAKI, A. & WILLIAMS, D. R. 2005b. Fourier transform infrared imaging of human hair with a high spatial resolution without the use of a synchrotron. *Applied Spectroscopy,* 59**,** 149-155.

CHAN, K. L. A., KAZARIAN, S. G., VASSOU, D., GIONIS, V. & CHRYSSIKOS, G. D. 2007a. In situ high-throughput study of drug polymorphism under controlled temperature and humidity using FT-IR spectroscopic imaging. *Vibrational Spectroscopy,* 43**,** 221-226.

CHAN, K. L. A., KAZARIAN, S. G., VASSOU, D., GIONIS, V. & CHRYSSIKOS, G. D. 2007b. In situ high-throughput study of drug polymorphism under controlled temperature and humidity using FT-IR spectroscopic imaging. *Vibrational Spectroscopy,* 43**,** 221–226.

CHAN, K. L. A., NIU, X., DE MELLO, A. J. & KAZARIAN, S. G. 2010. Rapid prototyping of microfluidic devices for integrating with FT-IR spectroscopic imaging. *Lab on a Chip,* 10**,** 2170–2174.

CHAN, K. L. A., NIU, X., DEMELLO, A. J. & KAZARIAN, S. G. 2011. Generation of chemical movies: FT-IR spectroscopic imaging of segmented flows. *Analytical Chemistry,* 83**,** 3606–3609.

CHAN, K. L. A., TAY, F. H., POULTER, G. & KAZARIAN, S. G. 2008a. Chemical imaging with variable angles of incidence using a diamond attenuated total reflection accessory. *Applied Spectroscopy,* 62**,** 1102-1107.

CHAN, K. L. A., TAY, F. H., TAYLOR, C. & KAZARIAN, S. G. 2008b. A novel approach for study of in situ diffusion in human hair using Fourier transform infrared spectroscopic imaging. *Applied Spectroscopy,* 62**,** 1041-1044.

CHANDRAN, S., GESENBERG, C., LEVONS, J., HUBERT, M. & RAGHAVAN, K. 2011. A high-throughput spectrophotometric approach for evaluation of precipitation resistance. *Journal of Pharmaceutical and Biomedical Analysis,* 56**,** 698–704.

CHEN, Y. Y., HUGHES, L. P., GLADDEN, L. F. & MANTLE, M. D. 2010. Quantitative ultra-fast MRI of HPMC swelling and dissolution. *Journal of Pharmaceutical Sciences,* 99**,** 3462–3472.

CHENG, W. C., HE, Y., CHANG, A. Y. & QUE, L. 2013. A microfluidic chip for controlled release of drugs from microcapsules. *Biomicrofluidics,* 7**,** 1–10.

CHIOU, W. L. & RIEGELMAN, S. 1969. Preparation and dissolution characteristics of several fast-release solid dispersions of griseofulvin. *Journal of Pharmaceutical Sciences,* 58**,** 1505–1510.

CHIOU, W. L. & RIEGELMAN, S. 1971. Pharmaceutical applications of solid dispersion systems. *Journal of Pharmaceutical Sciences,* 60**,** 1281-1302.

CHOWHAN, Z. T. & CHI, L. H. 1986. DRUG EXCIPIENT INTERACTIONS RESULTING FROM POWDER MIXING .3. SOLID-STATE PROPERTIES AND THEIR EFFECT ON DRUG DISSOLUTION. *Journal of Pharmaceutical Sciences,* 75**,** 534-541.

CHRISTENSEN, N. P. A., NIELSEN, S., RANTANEN, J., CORNETT, C. & BERTELSEN, P. 2014. Processing-induced salt formation of two oxicams in solid dosage forms affects dissolution behavior and chemical degradation. *Powder Technology,* 266**,** 175–182.

CHRISTENSEN, N. P. A., RANTANEN, J., CORNETT, C. & TAYLOR, L. S. 2012. Disproportionation of the calcium salt of atorvastatin in the presence of acidic excipients. *European Journal of Pharmaceutics and Biopharmaceutics,* 82**,** 410–416.

CLARKE, F. C., HAMMOND, S. V., JEE, R. D. & MOFFAT, A. C. 2002. Determination of the information depth and sample size for the analysis of pharmaceutical materials using reflectance near-infrared microscopy. *Applied Spectroscopy,* 56**,** 1475–1483.

CLARKE, F. C., JAMIESON, M. J., CLARK, D. A., HAMMOND, S. V., JEE, R. D. & MOFFAT, A. C. 2001. Chemical image fusion. The synergy of FT-NIR and Raman mapping microscopy to enable a move complete visualization of pharmaceutical formulations. *Analytical Chemistry,* 73**,** 2213–2220.

COHEN, J. L., HUBERT, B. B., LEESON, L. J., RHODES, C. T., ROBINSON, J. R., ROSEMAN, T. J. & SHEFTER, E. 1990. The development of USP dissolution and drug release standards. *Pharmaceutical Research,* 7**,** 983-987.

COLLEY, C. S., KAZARIAN, S. G., WEINBERG, P. D. & LEVER, M. J. 2004. Spectroscopic imaging of arteries and atherosclerotic plaques. *Biopolymers,* 74**,** 328-335.

COLOMBO, P. 1993. Swelling-controlled release in hydrogel matrices for oral route. *Advanced drug delivery reviews,* 11**,** 37-57.

COLOMBO, P., BETTINI, R., SANTI, P. & PEPPAS, N. A. 2000. Swellable matrices for controlled drug delivery: gel-layer behaviour, mechanisms and optimal performance. *Pharmaceutical science & technology today,* 3**,** 198-204.

CONTE, U. & MAGGI, L. 1996. Modulation of the dissolution profiles from Geomatrix® multi-layer matrix tablets containing drugs of different solubility. *Biomaterials,* 17**,** 889–896.

COOPER, A. I., KAZARIAN, S. G. & POLIAKOFF, M. 1993. Supercritical fluid impregnation of polyethylene films, a new approach to studying equilibria in matrices; the hydrogen bonding of fluoroalcohols to (η5-C5Me5)Ir(CO)2 and the effect on C-H activation. *Chemical Physics Letters,* 206**,** 175-180.

COUTTS-LENDON, C. A., WRIGHT, N. A., MIESO, E. V. & KOENIG, J. L. 2003. The use of FT-IR imaging as an analytical tool for the characterization of drug delivery systems. *Journal of Controlled Release,* 93**,** 223-248.

CROWLEY, M. M., ZHANG, F., REPKA, M. A., THUMMA, S., UPADHYE, S. B., KUMAR BATTU, S., MCGINITY, J. W. & MARTIN, C. 2007. Pharmaceutical applications of hot-melt extrusion: part I. *Drug Development and Industrial Pharmacy,* 33**,** 909–926.

CUNNINGHAM, J., SINKA, I. & ZAVALIANGOS, A. 2004. Analysis of tablet compaction. I. Characterization of mechanical behavior of powder and powder/tooling friction. *Journal of pharmaceutical sciences,* 93**,** 2022-2039.

DAI, W.-G., POLLOCK-DOVE, C., DONG, L. C. & LI, S. 2008. Advanced screening assays to rapidly identify solubility-enhancing formulations: high-throughput, miniaturization and automation. *Advanced Drug Delivery Reviews,* 60**,** 657–672.

DAI, W. G. 2010. In vitro methods to assess drug precipitation. *International Journal of Pharmaceutics,* 393**,** 1–16.

DANESH, A., CHEN, X., DAVIES, M. C., ROBERTS, C. J., SANDERS, G. H. W., TENDLER, S. J. B., WILLIAMS, P. M. & WILKINS, M. J. 2000. Polymorphic discrimination using atomic force microscopy: distinguishing between two polymorphs of the drug cimetidine. *Langmuir,* 16**,** 866–870.

DAVID, S. E., TIMMINS, P. & CONWAY, B. R. 2012. Impact of the counterion on the solubility and physicochemical properties of salts of carboxylic acid drugs. *Drug Development and Industrial Pharmacy,* 38**,** 93–103.

DE BOER, A. H., BOLHUIS, G. K. & LERK, C. F. 1978. Bonding characteristics by scanning electron microscopy of powders mixed with magnesium stearate. *Powder Technology,* 20**,** 75–82.

DING, Y. Z., LI, J. N., XIAO, W. W., XIAO, K., LEE, J., BHARDWAJ, U., ZHU, Z. J., DIGIGLIO, P., YANG, G. M., LAM, K. S. & PAN, T. R. 2015. Microfluidic-enabled print-to-screen platform for high-throughput screening of combinatorial chemotherapy. *Analytical Chemistry,* 87**,** 10166–10171.

DOCOSLIS, A., HUSZARIK, K. L., PAPAGEORGIOU, G. Z., BIKIARIS, D., STERGIOU, A. & GEORGARAKIS, E. 2007. Characterization of the distribution, polymorphism, and stability of nimodipine in its solid dispersions in polyethylene glycol by micro-Raman spectroscopy and powder X-ray diffraction. *The AAPS Journal,* 9**,** 361–370.

DUFFY, D. C., MCDONALD, J. C., SCHUELLER, O. J. & WHITESIDES, G. M. 1998. Rapid prototyping of microfluidic systems in poly (dimethylsiloxane). *Analytical Chemistry,* 70**,** 4974–4984.

ELDER, D. P., HOLM, R. & DE DIEGO, H. L. 2013. Use of pharmaceutical salts and cocrystals to address the issue of poor solubility. *International Journal of Pharmaceutics,* 453**,** 88–100.

ELKHIDER, N., CHAN, K. L. A. & KAZARIAN, S. G. 2007. Effect of moisture and pressure on tablet compaction studied with FTIR spectroscopic imaging. *Journal of Pharmaceutical Sciences,* 96**,** 351-360.

EVERALL, N. J., PRIESTNALL, I. M., CLARKE, F., JAYES, L., POULTER, G., COOMBS, D. & GEORGE, M. W. 2009. Preliminary Investigations into Macroscopic Attenuated Total Reflection. Fourier Transform Infrared Imaging of Intact Spherical Domains: Spatial Resolution and Image Distortion. *Applied Spectroscopy,* 63**,** 313-320.

EWING, A. V., BIGGART, G. D., HALE, C. R., CLARKE, G. S. & KAZARIAN, S. G. 2015a. Comparison of pharmaceutical formulations: ATR-FTIR spectroscopic imaging to study drug-carrier interactions. *International Journal of Pharmaceutics,* 495**,** 112–121.

EWING, A. V., CLARKE, G. S. & KAZARIAN, S. G. 2014. Stability of indomethacin with relevance to the release from amorphous solid dispersions studied with ATR-FTIR spectroscopic imaging. *European Journal of Pharmaceutical Sciences,* 60**,** 64–71.

EWING, A. V., WRAY, P. S., CLARKE, G. S. & KAZARIAN, S. G. 2015b. Evaluating drug delivery with salt formation: drug disproportionation studied in situ by ATR-FTIR imaging and Raman mapping. *Journal of Pharmaceutical and Biomedical Analysis,* 111**,** 248–256.

FAGERBERG, J. H., TSINMAN, O., SUN, N., TSINMAN, K., AVDEEF, A. & BERGSTRÖM, C. A. 2010. Dissolution rate and apparent solubility of poorly soluble drugs in biorelevant dissolution media. *Molecular Pharmaceutics,* 7**,** 1419–1430.

FAURE, A., YORK, P. & ROWE, R. C. 2001. Process control and scale-up of pharmaceutical wet granulation processes: a review. *European Journal of Pharmaceutics and Biopharmaceutics,* 52**,** 269–277.

FLEMING, O. S., CHAN, K. L. A. & KAZARIAN, S. G. 2004. FT-IR imaging and Raman microscopic study of poly(ethylene terephthalate) film processed with supercritical CO2. *Vibrational Spectroscopy,* 35**,** 3-7.

FORD, J. L. & RUBINSTEIN, M. H. 1978. Phase equilibria and dissolution rates of indomethacin-polyethylene glycol 6000 solid dispersions. *Pharmaceutica Acta Helvetiae,* 53**,** 327–332.

FORD, J. L., RUBINSTEIN, M. H., MCCAUL, F., HOGAN, J. E. & EDGAR, P. J. 1987. Importance of drug type, tablet shape and added diluents on drug release kinetics from hydroxypropylmethylcellulose matrix tablets. *International Journal of Pharmaceutics,* 40**,** 223–234.

FRIEND, D. R. 2005. New oral delivery systems for treatment of inflammatory bowel disease. *Advanced Drug Delivery Reviews,* 57**,** 247–265.

FROSCH, T., CHAN, K. L. A., WONG, H. C., CABRAL, J. O. T. & KAZARIAN, S. G. 2010. Nondestructive Three-Dimensional Analysis of Layered Polymer Structures with Chemical Imaging. *Langmuir,* 26**,** 19027-19032.

FUJIMAKI, Y., MATSUBARA, T., SAKAMOTO, T., SASAKURA, D., MIURA, T., TAKEKAWA, M. & HIYAMA, Y. 2009. Distribution of ethenzamide and other ingredients on granule surfaces studied by Raman microspectroscopy and mapping. *Die Pharmazie-An International Journal of Pharmaceutical Sciences,* 64**,** 316–322.

FYFE, C. A., GRONDEY, H., BLAZEK-WELSH, A. I., CHOPRA, S. K. & FAHIE, B. J. 2000. NMR imaging investigations of drug delivery devices using a flow-through USP dissolution apparatus. *Journal of Controlled Release,* 68**,** 73-83.

GABRIENKO, A. A., MARTYANOV, O. N. & KAZARIAN, S. G. 2015a. Effect of temperature and composition on the stability of crude oil blends studied with chemical imaging in situ. *Energy & Fuels,* 29**,** 7114–7123.

GABRIENKO, A. A., MOROZOV, E. V., SUBRAMANI, V., MARTYANOV, O. N. & KAZARIAN, S. G. 2015b. Chemical visualization of asphaltenes aggregation

processes studied in situ with ATR-FTIR spectroscopic imaging and NMR imaging. *Journal of Physical Chemistry C,* 119**,** 2646–2660.

GAO, P. & MEURY, R. H. 1996. Swelling of hydroxypropyl methylcellulose matrix tablets. 1. Characterization of swelling using a novel optical imaging method. *Journal of Pharmaceutical Sciences,* 85**,** 725-731.

GARDNER, C. R., ALMARSSON, O., CHEN, H., MORISSETTE, S., PETERSON, M., ZHANG, Z., WANG, S., LEMMO, A., GONZALEZ-ZUGASTI, J. & MONAGLE, J. 2004. Application of high throughput technologies to drug substance and drug product development. *Computers & Chemical Engineering,* 28**,** 943–953.

GENINA, N., HOLLÄNDER, J., JUKARAINEN, H., MÄKILÄ, E., SALONEN, J. & SANDLER, N. 2015. Ethylene vinyl acetate (EVA) as a new drug carrier for 3D printed medical drug delivery devices. *European Journal of Pharmaceutical Sciences***,** in press.

GLASSFORD, S., CHAN, K. L. A., BYRNE, B. & KAZARIAN, S. G. 2012a. Chemical Imaging of Protein Adsorption and Crystallization on a Wettability Gradient Surface. *Langmuir,* 28**,** 3174-3179.

GLASSFORD, S. E., GOVADA, L., CHAYEN, N. E., BYRNE, B. & KAZARIAN, S. G. 2012b. Micro ATR FTIR imaging of hanging drop protein crystallisation. *Vibrational Spectroscopy,* 63**,** 492-498.

GOLDBERG, A. H., GIBALDI, M., KANIG, J. L. & MAYERSOHN, M. 1966. Increasing dissolution rates and gastrointestinal absorption of drugs via solid solutions and eutectic mixtures IV: Chloramphenicol—urea system. *Journal of Pharmaceutical Sciences,* 55**,** 581–583.

GORDON, K. C. & MCGOVERIN, C. M. 2011. Raman mapping of pharmaceuticals. *International Journal of Pharmaceutics,* 417**,** 151–162.

GOVINDARAJAN, R., ZINCHUK, A., HANCOCK, B., SHALAEV, E. & SURYANARAYANAN, R. 2006. Ionization states in the microenvironment of solid dosage forms: effect of formulation variables and processing. *Pharmaceutical Reserach,* 23**,** 2454–2468.

GUERRIERI, P., JARRING, K. & TAYLOR, L. S. 2010. Impact of counterion on the chemical stability of crystalline salts of procaine. *Journal of Pharmaceutical Sciences,* 99**,** 3719–3730.

GUERRIERI, P. & TAYLOR, L. S. 2009. Role of salt and excipient properties on disproportionation in the solid-state. *Pharmaceutical Research,* 26**,** 2015–2026.

GUPPER, A. & KAZARIAN, S. G. 2005. Study of solvent diffusion and solvent-induced crystallization in syndiotactic polystyrene using FT-IR spectroscopy and imaging. *Macromolecules,* 38**,** 2327-2332.

GUPPER, A., WILHELM, P., SCHMIED, M., KAZARIAN, S. G., CHAN, K. L. A. & REUßNER, J. 2002. Combined Application of Imaging Methods for the Characterization of a Polymer Blend. *Appl. Spectrosc.,* 56**,** 1515-1523.

HANCOCK, B. C. & PARKS, M. 2000. What is the true solubility advantage for amorphous pharmaceuticals? *Pharmaceutical Research,* 17**,** 397–404.

HANCOCK, B. C. & ZOGRAFI, G. 1997. Characteristics and significance of the amorphous state in pharmaceutical systems. *Journal of Pharmaceutical Sciences,* 86**,** 1–12.

HARRICK, N. J. & DU PRÉ, F. K. 1966. Effective Thickness of Bulk Materials and of Thin Films for Internal Reflection Spectroscopy. *Applied Optics,* 5**,** 1739-1743.

HEIKKILA, T., PELTONEN, L., TASKINEN, S., LAAKSONEN, T. & HIRYONEN, J. 2008. 96-well plate surface tension measurements for fast determination of drug solubility. *Letters in Drug Design & Discovery,* 5**,** 471–476.

HEINZ, A., SAVOLAINEN, M., RADES, T. & STRACHAN, C. J. 2007. Quantifying ternary mixtures of different solid-state forms of indomethacin by Raman and near-infrared spectroscopy. *European Journal of Pharmaceutical Sciences,* 32**,** 182–192.

HIGUCHI, W. I., HAMLIN, W. E. & MEHTA, S. C. 1969. Infrared attenuated total reflectance (ATR) method for observing the water-mediated surface phase reversion of methylprednisolone II to I during dissolution. *Journal of Pharmaceutical Sciences,* 58**,** 1145-1146.

HOGAN, J. 1989. Hydroxypropylmethylcellulose sustained release technology. *Drug Development and Industrial Pharmacy,* 15**,** 975-999.

HOOTON, J. C., GERMAN, C. S., ALLEN, S., DAVIES, M. C., ROBERTS, C. J., TENDLER, S. J. B. & WILLIAMS, P. M. 2004. An atomic force microscopy study of the effect of nanoscale contact geometry and surface chemistry on the adhesion of pharmaceutical particles. *Pharmaceutical Research,* 21**,** 953–961.

HSIEH, Y. L. & TAYLOR, L. S. 2015. Salt stability-effect of particle size, relative humidity, temperature and composition on salt to free base conversion. *Pharmaceutical Reserach,* 32**,** 549–561.

HSU, M. N., LUO, R., KWEK, K. Z., POR, Y. C., ZHANG, Y. & CHEN, C.-H. 2015. Sustained release of hydrophobic drugs by the microfluidic assembly of multistage microgel/poly (lactic-co-glycolic acid) nanoparticle composites. *Biomicrofluidics,* 9**,** 1–7.

HUANG, X. & BRAZEL, C. S. 2001. On the importance and mechanisms of burst release in matrix-controlled drug delivery systems. *Journal of Controlled Release,* 73**,** 121–136.

HULSE, W. L., GRAY, J. & FORBES, R. T. 2012. A discriminatory intrinsic dissolution study using UV area imaging analysis to gain additional insights into the dissolution behaviour of active pharmaceutical ingredients. *International Journal of Pharmaceutics,* 434**,** 133–139.

IFPMA 2015. *The pharmaceutical industry and global health: facts and figures 2015*.

JAIN, A. K. 2008. Solubilization of indomethacin using hydrotropes for aqueous injection. *European Journal of Pharmaceutics and Biopharmaceutics,* 68**,** 701–714.

JIVRAJ, M., MARTINI, L. G. & THOMSON, C. M. 2000. An overview of the different excipients useful for the direct compression of tablets. *Pharmaceutical science & technology today,* 3**,** 58-63.

KANENIWA, N., OTSUKA, M. & HAYASHI, T. 1985. Physicochemical characterization of indomethacin polymorphs and the transformation kinetics in ethanol. *Chemical & Pharmaceutical Bulletin,* 33**,** 3447–3455.

KANG, L., CHUNG, B. G., LANGER, R. & KHADEMHOSSEINI, A. 2008. Microfluidics for drug discovery and development: From target selection to product lifecycle management. *Drug Discovery Today,* 13**,** 1–13.

KANIG, J. L. 1964. Properties of fused mannitol in compressed tablets. *Journal of Pharmaceutical Sciences,* 53**,** 188–192.

KAO, J. Y., MCGOVERIN, C. M., GRAESER, K. A., RADES, T. & GORDON, K. C. 2012. Measurement of amorphous indomethacin stability with NIR and Raman spectroscopy. *Vibrational Spectroscopy,* 58**,** 19–26.

KASIM, N. A., WHITEHOUSE, M., RAMACHANDRAN, C., BERMEJO, M., LENNERNAS, H., HUSSAIN, A. S., JUNGINGER, H. E., STAVCHANSKY, S. A., MIDHA, K. K., SHAH, V. P. & AMIDON, G. L. 2004. Molecular properties of WHO essential drugs and provisional biopharmaceutical classification. *Molecular Pharmaceutics,* 1**,** 85–96.

KAUSHAL, A. M., GUPTA, P. & BANSAL, A. K. 2004. Amorphous drug delivery systems: molecular aspects, design, and performance. *Critical Reviews in Therapeutic Drug Carrier Systems,* 21**,** 133–93.

KAWABATA, Y., WADA, K., NAKATANI, M., YAMADA, S. & ONOUE, S. 2011. Formulation design for poorly water-soluble drugs based on biopharmaceutics classification system: basic approaches and practical applications. *International Journal of Pharmaceutics,* 420**,** 1–10.

KAZARIAN, S. 2000. Polymer processing with supercritical fluids. *Polymer Science Series,* 42**,** 78-101.

KAZARIAN, S. G. 2002. Polymers and supercritical fluids: Opportunities for vibrational spectroscopy. *Macromolecular Symposia,* 184**,** 215-228.

KAZARIAN, S. G. 2007. Enhancing high-throughput technology and microfluidics with FTIR spectroscopic imaging. *Analytical and Bioanalytical Chemistry,* 388**,** 529–532.

KAZARIAN, S. G. & CHAN, K. L. A. 2003. "Chemical photography" of drug release. *Macromolecules,* 36**,** 9866–9872.

KAZARIAN, S. G. & CHAN, K. L. A. 2006a. Applications of ATR-FTIR spectroscopic imaging to biomedical samples. *Biochimica Et Biophysica Acta-Biomembranes,* 1758**,** 858-867.

KAZARIAN, S. G. & CHAN, K. L. A. 2006b. Sampling approaches in Fourier transform infrared imaging applied to polymers. *In:* GRUNDKE, K., STAMM, M. & ADLER, H. J. (eds.) *Characterization of Polymer Surfaces and Thin Films.*

KAZARIAN, S. G. & CHAN, K. L. A. 2013a. ATR-FTIR spectroscopic imaging: recent advances and applications to biological systems. *Analyst,* 138**,** 1940-1951.

KAZARIAN, S. G. & CHAN, K. L. A. 2013b. ATR-FTIR spectroscopic imaging: recent advances and applications to biological systems. *Analyst,* 138**,** 1940–1951.

KAZARIAN, S. G., CHAN, K. L. A. & TAY, F. H. 2009. ATR FT-IR Imaging for Pharmaceutical and Polymeric Materials: From Micro and Macro Approaches. *In:* SALZER, R. & SIESLER, H. W. (eds.) *Infrared and Raman Spectroscopic Imaging.* Wiley-VCH Verlag GmbH & Co. KGaA.

KAZARIAN, S. G. & EWING, A. V. 2013. Applications of Fourier transform infrared spectroscopic imaging to tablet dissolution and drug release. *Expert Opinion on Drug Delivery,* 10**,** 1207–1221.

KAZARIAN, S. G. & MARTIROSYAN, G. G. 2002. Spectroscopy of polymer/drug formulations processed with supercritical fluids: In situ ATR-IR and Raman study of impregnation of ibuprofen into PVP. *International Journal of Pharmaceutics,* 232**,** 81-90.

KAZARIAN, S. G. & VAN DER WEERD, J. 2008. Simultaneous FTIR spectroscopic imaging and visible photography to monitor tablet dissolution and drug release. *Pharmaceutical Research,* 25**,** 853-860.

KAZARIAN, S. G., VINCENT, M. F., BRIGHT, F. V., LIOTTA, C. L. & ECKERT, C. A. 1996. Specific intermolecular interaction of carbon dioxide with polymers. *Journal of the American Chemical Society,* 118**,** 1729–1736.

KHADKA, P., RO, J., KIM, H., KIM, I., KIM, J. T., KIM, H., CHO, J. M., YUN, G. & LEE, J. 2014. Pharmaceutical particle technologies: An approach to improve drug solubility, dissolution and bioavailability. *Asian Journal of Pharmaceutical Sciences,* 9**,** 304–316.

KHALED, S. A., BURLEY, J. C., ALEXANDER, M. R. & ROBERTS, C. J. 2014. Desktop 3D printing of controlled release pharmaceutical bilayer tablets. *International Journal of Pharmaceutics,* 461**,** 105–111.

KHALED, S. A., BURLEY, J. C., ALEXANDER, M. R., YANG, J. & ROBERTS, C. J. 2015. 3D printing of five-in-one dose combination polypill with defined immediate and sustained release profiles. *Journal of Controlled Release,* 217**,** 308–314.

KHANDARE, J. & MINKO, T. 2006. Polymer–drug conjugates: progress in polymeric prodrugs. *Progress in Polymer Science,* 31**,** 359–397.

KIMBER, J. A., GERST, M. & KAZARIAN, S. G. 2014. Fast drying and film formation of latex dispersions studied with FTIR spectroscopic imaging. *Langmuir,* 30**,** 13588–13595.

KIMBER, J. A., KAZARIAN, S. G. & ŠTĚPÁNEK, F. 2012. Modelling of pharmaceutical tablet swelling and dissolution using discrete element method. *Chemical Engineering Science,* 69**,** 394-403.

KIMBER, J. A., KAZARIAN, S. G. & ŠTĚPÁNEK, F. 2013. Formulation design space analysis for drug release from swelling polymer tablets. *Powder Technology,* 236**,** 179-187.

KOENIG, J. L. 1998. *Microscopic Imaging of Polymers,* Washington, DC, USA, American Chemical Society.

KOENIG, J. L. & BOBIAK, J. P. 2007. Raman and Infrared Imaging of Dynamic Polymer Systems. *Macromolecular Materials and Engineering,* 292**,** 801-816.

KONNO, H., HANDA, T., ALONZO, D. E. & TAYLOR, L. S. 2008. Effect of polymer type on the dissolution profile of amorphous solid dispersions containing felodipine. *European Journal of Pharmaceutics and Biopharmaceutics,* 70**,** 493–499.

KOTTKE, M. K. & RUDNIC, E. M. 2002. Tablet dosage forms. *In:* BANKER, G. S., SIEPMANN, J. & RHODES, C. T. (eds.) *Modern Pharmaceutics*. 4 ed.

KRAFFT, C., SHAPOVAL, L., SOBOTTKA, S. B., GEIGER, K. D., SCHACKERT, G. & SALZER, R. 2006. Identification of primary tumors of brain metastases by SIMCA classification of IR spectroscopic images. *Biochimica et Biophysica Acta (BBA)-Biomembranes,* 1758**,** 883-891.

KRISTENSEN, H. G. & SCHAEFER, T. 1987. Granulation: A review on pharmaceutical wet-granulation. *Drug Development and Industrial Pharmacy,* 13**,** 803–872.

KUENTZ, M. 2015. Analytical technologies for real-time drug dissolution and precipitation testing on a small scale. *Journal of Pharmacy and Pharmacology,* 67**,** 143–159.

KUIMOVA, M. K., CHAN, K. L. A. & KAZARIAN, S. G. 2009. Chemical imaging of live cancer cells in the natural aqueous environment. *Applied Spectroscopy,* 63**,** 164-171.

LANGER, R. & PEPPAS, N. 1983. Chemical and physical structure of polymers as carriers for controlled release of bioactive agents: A review. *Journal of Macromolecular Science-Reviews in Macromolecular Chemistry and Physics,* 23**,** 61-126.

LANZA, F. L., ROYER, G. L., NELSON, R. S., CHEN, T. T., SECKMAN, C. E. & RACK, M. F. 1979. The effects of ibuprofen, indomethacin, aspirin, naproxen, and placebo on the gastric mucosa of normal volunteers. *Digestive Diseases and Sciences,* 24**,** 823-828.

LARKIN, P. J., WASYLYK, J. & RAGLIONE, M. 2015. Application of low-and mid-frequency Raman spectroscopy to characterize the amorphous-crystalline transformation of indomethacin. *Applied Spectroscopy,* 69**,** 1217–1228.

LEUNER, C. & DRESSMAN, J. 2000. Improving drug solubility for oral delivery using solid dispersions. *European Journal of Pharmaceutics and Biopharmaceutics,* 50**,** 47–60.

LEVIS, K. A., LANE, M. E. & CORRIGAN, O. I. 2003. Effect of buffer media composition on the solubility and effective permeability coefficient of ibuprofen. *International Journal of Pharmaceutics,* 253**,** 49-59.

LEWIS, E. N., TREADO, P. J., REEDER, R. C., STORY, G. M., DOWREY, A. E., MARCOTT, C. & LEVIN, I. W. 1995. Fourier transform spectroscopic imaging using an infrared focal-plane array detector. *Analytical Chemistry,* 67**,** 3377-3381.

LIN, S. Y. 1992. Isolation and solid-state characteristics of a new crystal from of indomethacin. *Journal of Pharmaceutical Sciences,* 81**,** 572–576.

LINDENBERG, M., KOPP, S. & DRESSMAN, J. B. 2004. Classification of orally administered drugs on the World Health Organization Model list of Essential Medicines according to the biopharmaceutics classification system. *European Journal of Pharmaceutics and Biopharmaceutics,* 58**,** 265–278.

LIVERSIDGE, G. G. & CONZENTINO, P. 1995. Drug particle size reduction for decreasing gastric irritancy and enhancing absorption of naproxen in rats. *International Journal of Pharmaceutics,* 125**,** 309–313.

LOBENBERG, R. & AMIDON, G. L. 2000. Modern bioavailability, bioequivalence and biopharmaceutics classification system. New scientific approaches to international regulatory standards. *European Journal of Pharmaceutics and Biopharmaceutics,* 50**,** 3–12.

LÖBMANN, K., LAITINEN, R., GROHGANZ, H., GORDON, K. C., STRACHAN, C. & RADES, T. 2011. Coamorphous drug systems: enhanced physical stability and dissolution rate of indomethacin and naproxen. *Molecular Pharmaceutics,* 8**,** 1919–1928.

LOPES, C. M., LOBO, J. M. S., PINTO, J. F. & COSTA, P. C. 2007. Compressed matrix core tablet as a quick/slow dual-component delivery system containing ibuprofen. *AAPS PharmSciTech,* 8**,** 195–202.

LÓPEZ-PERIAGO, A. M., VEGA, A., SUBRA, P., ARGEMÍ, A., SAURINA, J., GARCÍA-GONZÁLEZ, C. A. & DOMINGO, C. 2008. Supercritical CO2 processing of polymers for the production of materials with applications in tissue engineering and drug delivery. *Journal of Materials Science,* 43**,** 1939–1947.

LYON, R. C., LESTER, D. S., LEWIS, E. N., LEE, E., LAWRENCE, X. Y., JEFFERSON, E. H. & HUSSAIN, A. S. 2002. Near-infrared spectral imaging for quality assurance of pharmaceutical products: analysis of tablets to assess powder blend homogeneity. *AAPS PharmSciTech,* 3**,** 1–15.

MAJUMDER, M., BUCKTON, G., RAWLINSON-MALONE, C. F., WILLIAMS, A. C., SPILLMAN, M. J., PIDCOCK, E. & SHANKLAND, K. 2013. Application of hydrogen-bond propensity calculations to an indomethacin–nicotinamide (1: 1) co-crystal. *CrystEngComm,* 15**,** 4041–4044.

MARUYOSHI, K., IUGA, D., ANTZUTKIN, O. N., ALHALAWEH, A., VELAGA, S. P. & BROWN, S. P. 2012. Identifying the intermolecular hydrogen-bonding supramolecular synthons in an indomethacin–nicotinamide cocrystal by solid-state NMR. *Chemical Communications,* 48**,** 10844–10846.

MATSUMOTO, T. & ZOGRAFI, G. 1999. Physical properties of solid molecular dispersions of indomethacin with poly (vinylpyrrolidone) and poly (vinylpyrrolidone-co-vinyl-acetate) in relation to indomethacin crystallization. *Pharmaceutical Research,* 16**,** 1722–1728.

MERISKO-LIVERSIDGE, E., LIVERSIDGE, G. G. & COOPER, E. R. 2003. Nanosizing: a formulation approach for poorly-water-soluble compounds. *European Journal of Pharmaceutical Sciences,* 18**,** 113–120.

MERRITT, J. M., VISWANATH, S. K. & STEPHENSON, G. A. 2013. Implementing quality by design in pharmaceutical salt selection: a modeling approach to understanding disproportionation. *Pharmaceutical Reserach,* 30**,** 203–217.

MIKAC, U., KRISTL, J. & BAUMGARTNER, S. 2011. Using quantitative magnetic resonance methods to understand better the gel-layer formation on polymer-matrix tablets. *Expert Opinion on Drug Delivery,* 8**,** 677-692.

MILLAN, M., CARABALLO, I. & RABASCO, A. M. 1998. The role of the drug/excipient particle size ratio in the percolation model for tablets. *Pharmceutical Research,* 15**,** 216–220.

NANUBOLU, J. B. & BURLEY, J. C. 2012. Investigating the recrystallization behavior of amorphous paracetamol by variable temperature Raman studies and surface Raman mapping. *Molecular Pharmaceutics,* 9**,** 1544–1558.

NEWMAN, A., KNIPP, G. & ZOGRAFI, G. 2012. Assessing the performance of amorphous solid dispersions. *Journal of Pharmaceutical Sciences,* 101**,** 1355–1377.

NOYES, A. A. & WHITNEY, W. R. 1897. The rate of solution of solid substances in their own solutions. *Journal of the American Chemical Society,* 19**,** 930–934.

ØSTERGAARD, J., MENG-LUND, E., LARSEN, S. W., LARSEN, C., PETERSSON, K., LENKE, J. & JENSEN, H. 2010a. Real-time UV imaging of nicotine release from transdermal patch. *Pharmaceutical Research,* 27**,** 2614-2623.

ØSTERGAARD, J., MENG-LUND, E., LARSEN, S. W., LARSEN, C., PETERSSON, K., LENKE, J. & JENSEN, H. 2010b. Real-time UV imaging of nicotine release from transdermal patch. *Pharmaceutical Research,* 27**,** 2614–2623.

ØSTERGAARD, J., YE, F., RANTANEN, J., YAGHMUR, A., LARSEN, S. W., LARSEN, C. & JENSEN, H. 2011. Monitoring lidocaine single-crystal dissolution by ultraviolet imaging. *Journal of Pharmaceutical Sciences,* 100**,** 3405–3410.

PAJANDER, J., BALDURSDOTTIR, S., RANTANEN, J. & ØSTERGAARD, J. 2012. Behaviour of HPMC compacts investigated using UV-imaging. *International Journal of Pharmaceutics,* 427**,** 345–353.

PALOMBO, F., CREMERS, S. G., WEINBERG, P. D. & KAZARIAN, S. G. 2009. Application of Fourier transform infrared spectroscopic imaging to the study of effects of age and dietary l-arginine on aortic lesion composition in cholesterol-fed rabbits. *Journal of The Royal Society Interface,* 6**,** 669-680.

PATRA, C., KUMAR, A., PANDIT, H., SINGH, S. & DEVI, M. 2007. Design and evaluation of sustained release bilayer tablets of propranolol hydrochloride. *Acta Pharmaceutica,* 57**,** 479–489.

PATTERSON, B. M. & HAVRILLA, G. J. 2006. Attenuated total internal reflection infrared microspectroscopic imaging using a large-radius germanium internal reflection element and a linear array detector. *Applied Spectroscopy,* 60**,** 1256–1266.

PATTERSON, J. E., JAMES, M. B., FORSTER, A. H., LANCASTER, R. W., BUTLER, J. M. & RADES, T. 2005. The influence of thermal and mechanical preparative techniques on the amorphous state of four poorly soluble compounds. *Journal of Pharmaceutical Sciences,* 94**,** 1998–2012.

PEPPAS, N., BURES, P., LEOBANDUNG, W. & ICHIKAWA, H. 2000. Hydrogels in pharmaceutical formulations. *European journal of pharmaceutics and biopharmaceutics,* 50**,** 27-46.

PEPPAS, N. A. 1985. Analysis of Fickian and non-Fickian drug release from polymers. *Pharmaceutica Acta Helvetiae,* 60**,** 110–111.

PHAM, A. T. & LEE, P. I. 1994. Probing the mechanisms of drug release from hydroxypropylmethyl cellulose matrices. *Pharmaceutical research,* 11**,** 1379-1384.

PIFFERI, G., SANTORO, P. & PEDRANI, M. 1999. Quality and functionality of excipients. *Farmaco,* 54**,** 1-14.

PILETSKA, E. V., ABD, B. H., KRAKOWIAK, A. S., PARMAR, A., PINK, D. L., WALL, K. S., WHARTON, L., MOCZKO, E., WHITCOMBE, M. J., KARIM, K. &

PILETSKY, S. A. 2015. Magnetic high throughput screening system for the development of nano-sized molecularly imprinted polymers for controlled delivery of curcumin. *Analyst,* 140**,** 3113–3120.

PRATI, S., JOSEPH, E., SCIUTTO, G. & MAZZEO, R. 2010. New advances in the application of FTIR microscopy and spectroscopy for the characterization of artistic materials. *Accounts of Chemical Research,* 43**,** 792–801.

PRIEMEL, P. A., GROHGANZ, H., GORDON, K. C., RADES, T. & STRACHAN, C. J. 2012. The impact of surface- and nano-crystallisation on the detected amorphous content and the dissolution behaviour of amorphous indomethacin. *European Journal of Pharmaceutics and Biopharmaceutics,* 82**,** 187–193.

PRIEMEL, P. A., LAITINEN, R., BARTHOLD, S., GROHGANZ, H., LEHTO, V.-P., RADES, T. & STRACHAN, C. J. 2013. Inhibition of surface crystallisation of amorphous indomethacin particles in physical drug–polymer mixtures. *International Journal of Pharmaceutics,* 456**,** 301–306.

PUCHERT, T., LOCHMANN, D., MENEZES, J. C. & REICH, G. 2010. Near-infrared chemical imaging (NIR-CI) for counterfeit drug identification—a four-stage concept with a novel approach of data processing (Linear Image Signature). *Journal of Pharmaceutical and Biomedical Analysis,* 51**,** 138–145.

PUDLAS, M., KYEREMATENG, S. O., WILLIAMS, L. A., KIMBER, J. A., VAN LISHAUT, H., KAZARIAN, S. G. & WOEHRLE, G. H. 2015. Analyzing the impact of different excipients on drug release behavior in hot-melt extrusion formulations using FTIR spectroscopic imaging. *European Journal of Pharmaceutical Sciences,* 67**,** 21–31.

PUNČOCHOVÁ, K., EWING, A. V., GAJDOŠOVÁ, M., SARVAŠOVÁ, N., KAZARIAN, S. G., BERÁNEK, J. & ŠTĚPÁNEK, F. 2015. Identifying the mechanisms of drug release from amorphous solid dispersions using MRI and ATR-FTIR spectroscopic imaging. *International Journal of Pharmaceutics,* 483**,** 256–267.

QIAO, N., WANG, K., SCHLINDWEIN, W., DAVIES, A. & LI, M. 2013. In situ monitoring of carbamazepine–nicotinamide cocrystal intrinsic dissolution behaviour. *European Journal of Pharmaceutics and Biopharmaceutics,* 83**,** 415–426.

QURESHI, S. A. & SHABNAM, J. 2001. Cause of high variability in drug dissolution testing and its impact on setting tolerances. *European Journal of Pharmaceutical Sciences,* 12**,** 271-276.

RAJABI-SIAHBOOMI, A. R., BOWTELL, R. W., MANSFIELD, P., HENDERSON, A., DAVIES, M. C. & MELIA, C. D. 1994. Structure and behaviour in hydrophilic matrix sustained release dosage forms: 2. NMR-imaging studies of dimensional changes in the gel layer and core of HPMC tablets undergoing hydration. *Journal of Controlled Release,* 31**,** 121-128.

REPKA, M. A., BATTU, S. K., UPADHYE, S. B., THUMMA, S., CROWLEY, M. M., ZHANG, F., MARTIN, C. & MCGINITY, J. W. 2007. Pharmaceutical applications of hot-melt extrusion: Part II. *Drug Development and Industrial Pharmacy,* 33**,** 1043–1057.

RICCI, C., BLEAY, S. & KAZARIAN, S. G. 2007a. Spectroscopic Imaging of latent fingermarks collected with the aid of a gelatin tape. *Analytical Chemistry,* 79**,** 5771-5776.

RICCI, C., BLOXHAM, S. & KAZARIAN, S. G. 2007b. ATR-FTIR imaging of albumen photographic prints. *Journal of Cultural Heritage,* 8**,** 387-395.

RICCI, C., ELIASSON, C., MACLEOD, N. A., NEWTON, P. N., MATOUSEK, P. & KAZARIAN, S. G. 2007c. Characterization of genuine and fake artesunate anti-malarial tablets using Fourier transform infrared imaging and spatially offset Raman

spectroscopy through blister packs. *Analytical and Bioanalytical Chemistry,* 389**,** 1525–1532.

RICHARDSON, J. C., BOWTELL, R. W., MÄDER, K. & MELIA, C. D. 2005. Pharmaceutical applications of magnetic resonance imaging (MRI). *Advanced Drug Delivery Reviews,* 57**,** 1191-1209.

ROHRS, B. R., AMIDON, G. E., MEURY, R. H., SECREAST, P. J., KING, H. M. & SKOUG, C. J. 2006. Particle size limits to meet USP content uniformity criteria for tablets and capsules. *Journal of Pharmaceutical Sciences,* 95**,** 1049–1059.

ROHRS, B. R., THAMANN, T. J., GAO, P., STELZER, D. J., BERGREN, M. S. & CHAO, R. S. 1999. Tablet dissolution affected by a moisture mediated solid-state interaction between drug and disintegrant. *Pharmaceutical Reserach,* 16**,** 1850–1856.

RUMONDOR, A. C. F., MARSAC, P. J., STANFORD, L. A. & TAYLOR, L. S. 2009. Phase behavior of poly(vinylpyrrolidone) containing amorphous solid dispersions in the presence of moisture. *Molecular Pharmaceutics,* 6**,** 1492–1505.

SALAZAR, J., MULLER, R. H. & MOSCHWITZER, J. P. 2013. Application of the combinative particle size reduction technology H 42 to produce fast dissolving glibenclamide tablets. *European Journal of Pharmaceutics and Biopharmaceutics,* 49**,** 565–577.

SANZ, G. & FUSTER, V. 2009. Fixed-dose combination therapy and secondary cardiovascular prevention: rationale, selection of drugs and target population. *Nature Clinical Practice Cardiovascular Medicine,* 6**,** 101–110.

ŠAŠIĆ, S. & OZAKI, Y. 2010. *Raman, Infrared, and Near-Infrared Chemical Imaging,* Hoboken, NJ, USA, John Wiley & Sons, Ltd.

SASTRY, S. V., NYSHADHAM, J. R. & FIX, J. A. 2000. Recent technological advances in oral drug delivery – a review. *Pharmaceutical Science & Technology Today,* 3**,** 138–145.

SAVJANI, K. T., GAJJAR, A. K. & SAVJANI, J. K. 2012. Drug solubility: importance and enhancement techniques. *ISRN pharmaceutics,* 2012**,** 1–10.

SAVOLAINEN, M., HEINZ, A., STRACHAN, C., GORDON, K. C., YLIRUUSI, J., RADES, T. & SANDLER, N. 2007. Screening for differences in the amorphous state of indomethacin using multivariate visualization. *European Journal of Pharmaceutical Sciences,* 30**,** 113–123.

SAVOLAINEN, M., KOGERMANN, K., HEINZ, A., AALTONEN, J., PELTONEN, L., STRACHAN, C. & YLIRUUSI, J. 2009. Better understanding of dissolution behaviour of amorphous drugs by *in situ* solid-state analysis using Raman spectroscopy. *European Journal of Pharmaceutics and Biopharmaceutics,* 71**,** 71–79.

SEBHATU, T., AHLNECK, C. & ALDERBORN, G. 1997. The effect of moisture content on the compression and bond-formation properties of amorphous lactose particles. *International Journal of Pharmaceutics,* 146**,** 101–114.

SERAJUDDIN, A. 1999. Solid dispersion of poorly water-soluble drugs: early promises, subsequent problems, and recent breakthroughs. *Journal of Pharmaceutical Sciences,* 88**,** 1058–1066.

SERAJUDDIN, A. T. M. 2007. Salt formation to improve drug solubility. *Advanced Drug Delivery Reviews,* 59**,** 603–616.

SHAH, S. M., JAIN, A. S., KAUSHIK, R., NAGARSENKER, M. S. & NERURKAR, M. J. 2014. Preclinical formulations: insight, strategies, and practical considerations. *AAPS Pharmscitech,* 15**,** 1307–1323.

SHENDE, P. K., VELLODY, V. V. & GAUD, R. 2013. Tab-in-tab formulation of ramipril and nifedipine for effective anti-hypertensive activity. *Journal of Pharmaceutical Reserach,* 6**,** 656–662.

SHIKO, G., GLADDEN, L. F., SEDERMAN, A. J., CONNOLLY, P. C. & BUTLER, J. M. 2011. MRI studies of the hydrodynamics in a USP 4 dissolution testing cell. *Journal of Pharmaceutical Sciences,* 100**,** 976–991.

SHINZAWA, H., AWA, K., KANEMATSU, W. & OZAKI, Y. 2009a. Multivariate data analysis for Raman spectroscopic imaging. *Journal of Raman Spectroscopy,* 40**,** 1720–1725.

SHINZAWA, H., AWA, K. & OZAKI, Y. 2011. Compression-induced morphological and molecular structural changes of cellulose tablets probed with near infrared imaging. *Journal of near Infrared Spectroscopy,* 19**,** 15-22.

SHINZAWA, H., AWA, K., OZAKI, Y. & SATO, H. 2009b. Near-Infrared Imaging Analysis of Cellulose Tablets by a Band Position Shift. *Applied Spectroscopy,* 63**,** 974-977.

SIEPMANN, J., KRANZ, H., BODMEIER, R. & PEPPAS, N. 1999. HPMC-matrices for controlled drug delivery: a new model combining diffusion, swelling, and dissolution mechanisms and predicting the release kinetics. *Pharmaceutical research,* 16**,** 1748-1756.

SIEPMANN, J. & PEPPAS, N. 2001. Modeling of drug release from delivery systems based on hydroxypropyl methylcellulose (HPMC). *Advanced Drug Delivery Reviews,* 48**,** 139-157.

SIEWERT, M., DRESSMAN, J., BROWN, C. K., SHAH, V. P., AIACHE, J.-M., AOYAGI, N., BASHAW, D., BROWN, C., BROWN, W. & BURGESS, D. 2003. FIP/AAPS guidelines to dissolution/in vitro release testing of novel/special dosage forms. *AAPS PharmSciTech,* 4**,** 43-52.

SIX, K., VERRECK, G., PEETERS, J., BREWSTER, M. & MOOTER, G. V. D. 2004. Increased physical stability and improved dissolution properties of itraconazole, a class II drug, by solid dispersions that combine fast-and slow-dissolving polymers. *Journal of Pharmaceutical Sciences,* 93**,** 124–131.

SKRDLA, P. J. & ZHANG, D. 2014. Disproportionation of a crystalline citrate salt of a developmental pharmaceutical compound: Characterization of the kinetics using pH monitoring and online Raman spectroscopy plus quantitation of the crystalline free base form in binary physical mixtures using FT-Raman, XRPD and DSC. *Journal of Pharmaceutical and Biomedical Analysis,* 90**,** 186–191.

SOMMER, A. J., TISINGER, L. G., MARCOTT, C. & STORY, G. M. 2001. Attenuated total internal reflection infrared mapping microspectroscopy using an imaging microscope. *Applied Spectroscopy,* 55**,** 252-256.

SONG, Y., YANG, X., CHEN, X., NIE, H., BYRN, S. & LUBACH, J. W. 2015. Investigation of drug-excipient interactions in lapatinib amorphous solid dispersions using solid-state NMR spectroscopy. *Molecular Pharmaceutics,* 12**,** 857–866.

SPRING, M., RICCI, C., PEGGIE, D. A. & KAZARIAN, S. G. 2008. ATR-FTIR imaging for the analysis of organic materials in paint cross sections: case studies on paint samples from the National Gallery, London. *Analytical and Bioanalytical Chemistry,* 392**,** 37-45.

SROKA-BARTNICKA, A., KIMBER, J. A., BORKOWSKI, L., PAWLOWSKA, M., POLKOWSKA, I., KALISZ, G., BELCARZ, A., JOZWIAK, K., GINALSKA, G. & KAZARIAN, S. G. 2015. The biocompatibility of carbon hydroxyapatite/beta-glucan composite for bone tissue engineering studied with Raman and FTIR spectroscopic imaging. *Analytical and Bioanalytical Chemistry,* 407**,** 7775–7785.

STADLER, B. 2015. Preface to special topic: microfluidics in drug delivery. *Biomicrofluidics,* 9**,** 052501.

STAVITSKI, E. & WECKHUYSEN, B. M. 2010. Infrared and Raman imaging of heterogeneous catalysts. *Chemical Society Reviews,* 39**,** 4615–4625.

STEPHENSON, G. A., ABURUB, A. & WOODS, T. A. 2011. Physical stability of salts of weak bases in the solid-state. *Journal of Pharmaceutical Sciences,* 100**,** 1607–1617.

STUART, B. H. 2004. *IR Spectroscopy: Fundamentals and Applications–Analytical Techniques in the Sciences*, New York: John Wiley & Sons Ltd.

SUN, C. C. 2008. Mechanism of moisture induced variations in true density and compaction properties of microcrystalline cellulose. *International Journal of Pharmaceutics,* 346**,** 93–101.

SUNG, K., NIXON, P. R., SKOUG, J. W., JU, T. R., GAO, P., TOPP, E. & PATEL, M. 1996. Effect of formulation variables on drug and polymer release from HPMC-based matrix tablets. *International journal of pharmaceutics,* 142**,** 53-60.

SURWASE, S. A., BOETKER, J. P., SAVILLE, D., BOYD, B. J., GORDON, K. C., PELTONEN, L. & STRACHAN, C. J. 2013. Indomethacin: new polymorphs of an old drug. *Molecular Pharmaceutics,* 10**,** 4472–4480.

TALUKDAR, M. M. & KINGET, R. 1995. Swelling and drug release behaviour of xanthan gum matrix tablets. *International Journal of Pharmaceutics,* 120**,** 63–72.

TAY, F. H. & KAZARIAN, S. G. 2009. Study of Petroleum Heat-exchanger Deposits with ATR-FTIR Spectroscopic Imaging. *Energy & Fuels,* 23**,** 4059-4067.

TAYLOR, L. S. & LANGKILDE, F. W. 2000. Evaluation of solid-state forms present in tablets by Raman spectroscopy. *Journal of Pharmaceutical Sciences,* 89**,** 1342–1353.

TAYLOR, L. S. & ZOGRAFI, G. 1997a. Spectroscopic characterization of interactions between PVP and indomethacin in amorphous molecular dispersions. *Pharmaceutical Research,* 14**,** 1691-1698.

TAYLOR, L. S. & ZOGRAFI, G. 1997b. Spectroscopic characterization of interactions between PVP and indomethacin in amorphous molecular dispersions. *Pharmaceutical Research,* 14**,** 1691–1698.

THAKRAL, N. K., MOHAPATRA, S., STEPHENSON, G. A. & SURYANARAYANAN, R. 2015. Compression-induced crystallization of amorphous indomethacin in tablets: characterization of spatial heterogeneity by two-dimensional X-ray diffractometry. *Molecular Pharmaceutics,* 12**,** 253–263.

TONG, P. & ZOGRAFI, G. 1999. Solid-state characteristics of amorphous sodium indomethacin relative to its free acid. *Pharmaceutical Research,* 16**,** 1186-1192.

TRAFFORD, A. D., JEE, R. D., MOFFAT, A. C. & GRAHAM, P. 1999. A rapid quantitative assay of intact paracetamol tablets by reflectance near-infrared spectroscopy. *Analyst,* 124**,** 163–167.

TSINMAN, K., AVDEEF, A., TSINMAN, O. & VOLOBOY, D. 2009. Powder dissolution method for estimating rotating disk intrinsic dissolution rates of low solubility drugs. *Pharmaceutical Research,* 26**,** 2093–2100.

UHRICH, K. E., CANNIZZARO, S. M., LANGER, R. S. & SHAKESHEFF, K. M. 1999. Polymeric systems for controlled drug release. *Chemical Reviews,* 99**,** 3181.

VAJNA, B., FARKAS, I., FARKAS, A., PATAKI, H., NAGY, Z., MADARÁSZ, J. & MAROSI, G. 2011a. Characterization of drug–cyclodextrin formulations using Raman mapping and multivariate curve resolution. *Journal of Pharmaceutical and Biomedical Analysis,* 56**,** 38–44.

VAJNA, B., PATAKI, H., NAGY, Z., FARKAS, I. & MAROSI, G. 2011b. Characterization of melt extruded and conventional Isoptin formulations using Raman chemical imaging and chemometrics. *International Journal of Pharmaceutics,* 419**,** 107–113.

VALIZADEH, H., NOKHODCHI, A., QARAKHANI, N., ZAKERI-MILANI, P., AZARMI, S., HASSANZADEH, D. & LOBENBERG, R. 2004. Physicochemical

characterization of solid dispersions of indomethacin with PEG 6000, Myrj 52, lactose, sorbitol, dextrin, and Eudragit (R) E100. *Drug Development and Industrial Pharmacy,* 30**,** 303–317.

VAN DER WEERD, J., CHAN, K. L. A. & KAZARIAN, S. G. 2004. An innovative design of compaction cell for in situ FT-IR imaging of tablet dissolution. *Vibrational Spectroscopy,* 35**,** 9-13.

VAN DER WEERD, J. & KAZARIAN, S. G. 2004a. Combined approach of FTIR imaging and conventional dissolution tests applied to drug release. *Journal of Controlled Release,* 98**,** 295–305.

VAN DER WEERD, J. & KAZARIAN, S. G. 2004b. Combined approach of FTIR imaging and conventional dissolution tests applied to drug release. *Journal of Controlled Release,* 98**,** 295-305.

VAN DER WEERD, J. & KAZARIAN, S. G. 2004c. Validation of macroscopic attenuated total reflection-Fourier transform infrared imaging to study dissolution of swelling pharmaceutical tablets. *Applied Spectroscopy,* 58**,** 1413–1419.

VAN DER WEERD, J. & KAZARIAN, S. G. 2005. Release of poorly soluble drugs from HPMC tablets studied by FTIR imaging and flow-through dissolution tests. *Journal of Pharmaceutical Sciences,* 94**,** 2096–2109.

VAN EERDENBRUGH, B. & TAYLOR, L. S. 2010. Small scale screening to determine the ability of different polymers to inhibit drug crystallization upon rapid solvent evaporation. *Molecular Pharmaceutics,* 7**,** 1328–1337.

VAN EERDENBRUGH, B. & TAYLOR, L. S. 2011. Application of mid-IR spectroscopy for the characterization of pharmaceutical systems. *International Journal of Pharmaceutics,* 417**,** 3-16.

VAN HOOGEVEST, P., LIU, X. & FAHR, A. 2011. Drug delivery strategies for poorly water-soluble drugs: the industrial perspective. *Expert Opinion on Drug Delivery,* 8**,** 1481–1500.

VASCONCELOS, T., SARMENTO, B. & COSTA, P. 2007. Solid dispersions as strategy to improve oral bioavailability of poor water soluble drugs. *Drug discovery today,* 12**,** 1068–1075.

VELASCO, D., DANOUX, C. B., REDONDO, J. A., ELVIRA, C., SAN ROMAN, J., WRAY, P. S. & KAZARIAN, S. G. 2011. pH-sensitive polymer hydrogels derived from morpholine to prevent the crystallization of ibuprofen. *Journal of Controlled Release,* 149**,** 279-288.

VUEBA, M., BATISTA DE CARVALHO, L., VEIGA, F., SOUSA, J. & PINA, M. 2006. Influence of cellulose ether mixtures on ibuprofen release: MC25, HPC and HPMC K100M. *Pharmaceutical development and technology,* 11**,** 213-228.

WALD, N. J. & LAW, M. R. 2003. A strategy to reduce cardiovascular disease by more than 80%. *British Medical Journal,* 326**,** 1419–1423.

WALSH, M. J., HOLTON, S. E., KAJDACSY-BALLA, A. & BHARGAVA, R. 2012. Attenuated total reflectance Fourier-transform infrared spectroscopic imaging for breast histopathology. *Vibrational Spectroscopy,* 60**,** 23–28.

WARDROP, J., JABER, A. B. & AYRES, J. W. 1998. Multiple-layer compression-coated tablets: Formulation and humidity studies of novel chewable amoxicillin/clavulanate tablet formulations. *Drug Development and Industrial Pharmacy,* 24**,** 729–736.

WATANABE, T., HASEGAWA, S., WAKIYAMA, N., KUSAI, A. & SENNA, M. 2003. Comparison between polyvinylpyrrolidone and silica nanoparticles as carriers for indomethacin in a solid state dispersion. *International Journal of Pharmaceutics,* 250**,** 283–286.

WESSEL, E., VOGEL, C., KOLOMIETS, O., HOFFMANN, U. & SIESLER, H. W. 2009. FT-IR and NIR Spectroscopic Imaging: Principals, Practical Aspects and Applications in Material and Pharmaceutical Sciences. *In:* SALZER, R. & SIESLER, H. W. (eds.) *Infrared and Raman Spectroscopic Imaging.* Wiley-VCH Verlag GmbH & Co. KGaA.

WHITESIDES, G. M. 2006. The origins and the future of microfluidics. *Nature,* 442**,** 368–373.

WILLIAMS, H. D., TREVASKIS, N. L., CHARMAN, S. A., SHANKER, R. M., CHARMAN, W. N., POUTON, C. W. & PORTER, C. J. 2013a. Strategies to address low drug solubility in discovery and development. *Pharmacological reviews,* 65**,** 315-499.

WILLIAMS, H. D., TREVASKIS, N. L., CHARMAN, S. A., SHANKER, R. M., CHARMAN, W. N., POUTON, C. W. & PORTER, C. J. H. 2013b. Strategies to address low drug solubility in discovery and development. *Pharmacological Reviews,* 65**,** 315–499.

WINDBERGS, M., JURNA, M., OFFERHAUS, H. L., HEREK, J. L., KLEINEBUDDE, P. & STRACHAN, C. J. 2009. Chemical imaging of oral solid dosage forms and changes upon dissolution using coherent anti-Stokes Raman scattering microscopy. *Analytical Chemistry,* 81**,** 2085-2091.

WINDBERGS, M. & WEITZ, D. A. 2011. Drug Dissolution Chip (DDC): a microfluidic approach for drug release. *Small,* 7**,** 3011–3015.

WRAY, P., LI, J., LI, L. Q. & KAZARIAN, S. G. 2014. Combined study of biphasic and zero-order release formulations with dissolution tests and ATR–FTIR spectroscopic imaging. *Journal of Pharmaceutical Sciences,* 103**,** 1995–2004.

WRAY, P. S., CLARKE, G. S. & KAZARIAN, S. G. 2011. Application of FTIR Spectroscopic Imaging to Study the Effects of Modifying the pH Microenvironment on the Dissolution of Ibuprofen from HPMC Matrices. *Journal of Pharmaceutical Sciences,* 100**,** 4745-4755.

WRAY, P. S., CLARKE, G. S. & KAZARIAN, S. G. 2013. Dissolution of tablet-in-tablet formulations studied with ATR-FTIR spectroscopic imaging. *European Journal of Pharmaceutical Sciences,* 48**,** 748–757.

WRAY, P. S., SINCLAIR, W. E., JONES, J. W., CLARKE, G. S. & BOTH, D. 2015. The use of in situ near infrared imaging and Raman mapping to study the disproportionation of a drug HCl salt during dissolution. *International Journal of Pharmaceutics,* 493**,** 198–207.

WROBEL, T. P., VICHI, A., BARANSKA, M. & KAZARIAN, S. G. 2015. Micro-attenuated total reflection Fourier transform infrared (micro ATR FT-IR) spectroscopic imaging with variable angles of incidence. *Applied Spectroscopy,* 69**,** 1170–1174.

WURSTER, D. E., BURAPHACHEEP, V. & PATEL, J. M. 1993. The determination of diffusion coefficients in semisolids by Fourier transform infrared (FT-IR) spectroscopy. *Pharmaceutical Research,* 10**,** 616-620.

YAO, M. & FANG, J. 2012. Hydrophilic PEO-PDMS for microfluidic applications. *Journal of Micromechanics and Microengineering,* 22**,** 025012.

YE, F., YAGHMUR, A., JENSEN, H., LARSEN, S. W., LARSEN, C. & ØSTERGAARD, J. 2011. Real-time UV imaging of drug diffusion and release from Pluronic F127 hydrogels. *European Journal of Pharmaceutical Sciences,* 43**,** 236–243.

ZANNOU, E. A., JI, Q., JOSHI, Y. M. & SERAJUDDIN, A. 2007. Stabilization of the maleate salt of a basic drug by adjustment of microenvironmental pH in solid dosage form. *International Journal of Pharmaceutics,* 337**,** 210–218.

ZELKÓ, R., BUDAVÁRI, Z., MARTON, S. & RÁCZ, I. 1999. The effect of solid/liquid interactions on the migration of riboflavin in tray-dried granule beds. *S.T.P. Pharma Sciences,* 9**,** 215–217.

ZHANG, G., SENAK, L. & MOORE, D. J. 2011. Measuring changes in chemistry, composition, and molecular structure within hair fibers by infrared and Raman spectroscopic imaging. *Journal of biomedical optics,* 16**,** 056009-056009.

ZHANG, L., HENSON, M. J. & SEKULIC, S. S. 2005. Multivariate data analysis for Raman imaging of a model pharmaceutical tablet. *Analytica Chimica Acta,* 545**,** 262–278.

ZHANG, S. W., YU, L., HUANG, J., HUSSAIN, M. A., DERDOUR, L., QIAN, F. & DE VILLIERS, M. M. 2014. A method to evaluate the effect of contact with excipients on the surface crystallization of amorphous drugs. *AAPS PharmSciTech,* 15**,** 1516–1526.

ZHANG, Y. & MCGEORGE, G. 2015. Quantitative analysis of pharmaceutical bilayer tablets using transmission Raman spectroscopy. *Journal of Pharmaceutical Innovation,* 10**,** 269–280.